Palacký University
Olomouc

Self-organized biopolymer layers and coatings with mineral fillers for special applications

MSc. Yousef Murtaja

Dissertation of Doctorate in Nanomaterials Chemistry

Supervisor: prof. Ing. Lubomír Lapčík, Ph.D.

Department of Physical Chemistry

Olomouc 2023

Faculty
of Science

Palacký University
Olomouc

Contents

Author's statement

I affirm that I have submitted the given dissertation on the subject (Self-organized biopolymer layers and coatings with mineral fillers for special applications), with the guidance of my supervisor prof. Ing. Lubomír Lapčík, Ph.D., and all references to the literature used are accurately cited. The experimental aspect of the study relies on findings that have been published in well-regarded professional journals. The papers that I have written as the primary author or co-author are included as appendices in this thesis.

In Olomouc on

MSc. Yousef Murtaja

Acknowledgments

During my academic pursuits and research, I've been fortunate adequate to receive aid and encouragement from numerous individuals within my professional network of mine as well as from members of my community. I'm grateful to my supervisor prof. Ing. Dr. Lubomír Lapčík, a professor at the University of Olomouc, Faculty of Science, Department of Physical Chemistry for his unwavering support during my research. I couldn't have finished this dissertation without his academic assistance, helpful insights, along with regular monitoring of the progress of mine. The lab staff members at my university continue to be a good assistance to me all of the time and I owe them a debt of thankfulness. I express my acknowledgment to the faculty community, such as my teachers, and colleagues in research, for their constant support. Finally, I'd love to come across my gratitude towards my family, especially my mom, whose support and well wishes were crucial in allowing me to finish my dissertation in the specified timeframe.

Bibliographical identification

Author:	MSc. Yousef Murtaja
Tittle:	Self-organized biopolymer layers and coatings with mineral fillers for special applications
Type:	Dissertation
Department:	Department of physical chemistry
Supervisor:	prof. Ing. Lubomír Lapčík, Ph.D.
Year of publishing:	2023
Number of Pages:	144 (Appendices including)
Appendices:	5
Language:	English

Abstract

This dissertation emphasizes the application of mineral fillers in natural biopolymer layers for specific purposes, polymer composites, and nanofillers and their properties. The thesis is presented as a collection of scientific research in the form of thematically arranged published papers, supported by an annotated theoretical framework. Alternatives to artificial coatings are available in natural biopolymers with added mineral fillers, which are environmentally friendly and sustainable in the long term. Integrating mineral fillers into these coatings can improve their properties to meet specific application requirements. Nanofillers added to polymer composites can improve mechanical strength and resistance to high temperatures without any degradation effect.

The first research paper confirms that perlite plays a key role in the thermal and mechanical properties of HDPE-based nanocomposite materials. Young's tensile modulus increases with increasing filler material concentration, leading to an increase in stiffness. The degree of fracture toughness decreases with increasing concentration of perlite at brittle fracture. However, higher concentrations of filler material are also associated with the measured ductile fracture behavior. SEM analysis confirms the strong bonding between the polymer matrix chains and the filler particle.

Further research revealed the effect of two different types of inorganic mineral fillers, calcium carbonate nanoparticles, and mineral nano silicates (nano clay), on the mechanical behavior of HDPE nanocomposite polymers in a semi-operational test. The study focuses on the characterization of fillers uniformly dispersed in the samples using SEM imaging techniques, X-ray analysis of dispersion spectra, and the TEM method. However, the addition of these fillers improves the technical properties of the polymer composites as shown by the combination of the elastic modulus and the microhardness observed. The amount and extent of fillers in the composites determine their elastic mechanical behavior and plasticity.

The technical properties of epoxy/HNTs & GnPs composites are the focus of the third research study. These shows that planar particles exhibit mutual sliding during mechanical testing, thereby reducing the overall stiffness of GnPs nanocomposites and increasing their ductility and plasticity. The stiffness of epoxy/HNT composites decreases with the addition of nanofiller, as indicated by the observed lower Young's modulus in tension. The study reveals the different mechanical responses of the tested materials due to the ductile and brittle fracture processes occurring.

In addition, the resistance of polyurethane foams to thermal degradation, including thermal stress-induced changes in their mechanical properties, is studied using selected physicochemical methods. The effect of increased relative humidity on degradation, leading to a decrease in stiffness and permanent deformation, was also found. In addition, the dynamic-mechanical properties of the studied composite materials were investigated by measuring the vibration damping excited by a single degree of freedom oscillatory system (SDOF). In this way, the changes in elasticity caused by different conditioning of the studied samples, which led to progressive degradation and loss of thermal stability, were monitored.

In summary, this dissertation provides valuable insights into the latest research trends and developments in natural biopolymer films with mineral fillers, their properties, and potential applications. The results of the studies in this dissertation provide important data for the design of sustainable and environmentally friendly materials for specific needs and offer possible directions for scientific developments in the field of polymer composites and nanofillers.

Bibliografická identifikace

Autor:	MSc. Yousef Murtaja
Název:	Samoorganizované biopolymerní vrstvy a povlaky s minerálními plnivy pro speciální aplikace
Typ:	Disertační
Oddělení:	Katedra fyzikální chemie
Dozorce:	prof. Ing. Lubomír Lapčík, Ph.D.
Rok vydání:	2023
Počet stran:	144 (Včetně dodatky)
Dodatky:	5
Jazyk:	Angličtina

Abstrakt

Disertační práce klade důraz na aplikaci minerálních plniv do přírodních biopolymerních vrstev pro specifické účely, dále na polymerní kompozity a nanoplniva a také na jejich vlastnosti. Práce je prezentována jako souhrn vědeckého výzkumu formou tematicky uspořádaných publikovaných odborných článků, podpořených komentovaným teoretickým rámcem. Alternativy k umělým nátěrům jsou dostupné v přírodních biopolymerech s přísadami minerálních plniv, které jsou šetrné k životnímu prostředí a dlouhodobě udržitelné. Integrace minerálních plniv do těchto nátěrů může zlepšit jejich vlastnosti, aby vyhovovaly specifickým aplikačním požadavkům. Nanoplniva přidaná do polymerního kompozitu mohou zlepšit mechanickou pevnost a odolnost vůči vysokým teplotám bez jakéhokoli degradačního účinku.

První výzkumný článek potvrzuje, že perlit hraje klíčovou roli v tepelných a mechanických vlastnostech nanokompozitních materiálů na bázi HDPE. Youngův modul pružnosti v tahu se zvyšuje s rostoucí koncentrací výplňového materiálu, což vede ke zvýšení tuhosti. Stupeň lomové houževnatosti klesá s rostoucí koncentrací perlitu při křehkém lomu. Nicméně vyšší koncentrace plniva jsou také spojeny s naměřeným průběhem tvárného lomu. Analýza SEM potvrzuje silnou vazbu mezi řetězci polymerní matrice a částicí plniva.

Další výzkum odhalil vliv dvou různých typů anorganických minerálních plniv, nanočástic uhličitanu vápenatého a minerálních nanosilikátů na mechanické chování nanokompozitních polymerů HDPE v poloprovozním testu. Studie se zaměřuje na charakterizaci plniv rovnoměrně rozptýlených ve vzorcích pomocí zobrazovacích technik SEM, RTG analýzou disperzních spekter a metodou TEM. Přidání těchto plniv však zlepšuje technické vlastnosti polymerních kompozitů, jak ukazuje kombinace modulu pružnosti a zjištěné mikrotvrdosti. Množství a rozsah plniv v kompozitech určují jejich elastické mechanické chování a plasticitu.

Technické vlastnosti epoxidových/HNTs & GnPs kompozitů jsou středem zájmu třetí výzkumné studie. Tato ukazuje, že planární částice vykazují vzájemné klouzání v průběhu mechanického testování a tím snižují celkovou tuhost GnPs nanokompozitů a zvyšují jejich tažnost a plasticitu. Tuhost epoxidových/HNT kompozitů klesá přídavkem nanoplniva, což naznačuje zjištěný nižší Youngův modul pružnosti v tahu. Studie odhaluje různé mechanické odezvy zkoušených materiálů v důsledku vznikajících tvárných i křehkých lomových dějů.

Dále je pomocí vybraných fyzikálně-chemických metod studována odolnost polyuretanových pěn vůči tepelné degradaci včetně změn jejich mechanických vlastností indukovaných tepelným namáháním. Byl zjištěn také vliv zvýšené relativní vlhkosti na degradaci, vedoucí ke snížení tuhosti a permanentní deformace. Dále byly proměřeny dynamicko-mechanické vlastnosti studovaných kompozitních materiálů metodou měření útlumu vibrací vybuzených oscilačním systémem o jednom stupni volnosti (SDOF). Tímto způsobem byly sledovány změny elasticity způsobené různým kondicionováním studovaných vzorků, které vedly k postupné degradaci a ztrátě tepelné stability.

V souhrnu, tato disertační práce poskytuje cenné poznatky o nejnovějších výzkumných trendech a vývoji v oblasti přírodních biopolymerních vrstev s minerálními plnivy, jejich vlastnostech a potenciálních aplikacích. Výsledky studií této disertační práce poskytují důležitá data pro tvorbu udržitelných a ekologicky šetrných materiálů pro specifické potřeby a nabízí možné směry vědeckého vývoje v oblasti polymerních kompozitů a nanoplniv.

List of figures

List of tables

List of abbreviations

BSE	Back Scattered Electrons
CMC	Carboxy Methyl Cellulose
CTAC	Cetyl Trimethyl Ammonium Chloride
CTBN	Carboxyl Terminated Butadiene Acrylonitrile
DGEBA	Di Glycidyl Ether of Bisphenol A
DOS	Dioctyl Sodium Sulfosuccinate
DSC	Differential Scanning Calorimetry
DTA	Differential Thermal Analysis
DVS	Di Vinyl Sulfone
EDS	Energy Dispersive Spectroscopy
GNPs	Graphene Nano Platelets
HDPE	High Density Polyethylene
HEC	Hydroxy Ethyl Cellulose
HIT	Hardness Indentation
HNTs	Halloysite Nano Tubes
LDPE	Low Density Poly Ethylene
LLDPE	Linear Low Density Poly Ethylene
NaCMC	Sodium Carboxy Methyl Cellulose
NC	Nitro Cellulose
OC	Oxy Cellulose
PAN	Poly Acryl Nitrile
PHA	Poly Hydroxy Alkynoate
PLA	Polylactic Acid
PU	Poly Urethane
RH	Relative Humidity
SDG	Sodium Decyl Galacturonate.
SDOF	Single Degree of Freedom
SDS	Sodium Dodecyl Sulfate

SE	Secondary Electron Mode
SEM	Scanning Electron Microscopy
SFE	Surface Free Energy
SSL	Surface Swollen Layer
TEM	Transmission Electron Microscopy
TG	Thermo Gravimetry
TS	Tensile Strength
TTAB	Tetradecyl Trimethyl Ammonium Bromide
VLDPE	Very Low Density PolyEthylene
VLPs	Virus Like Particles

1. Introduction

All-natural biopolymers are now a promising solution for satisfying the increasing need for polymeric materials and also addressing environmental issues. Natural biopolymers are employed in daily life and many industries including engineering and medicine, defense, and cars, allowing them to cross-link and produce lasting and revolutionary components. With decreased economic variability, light polymer composites can tackle power use and high price concerns in industries heavily reliant on heavy building materials. Furthermore, substantial research is performed to enhance the qualities of biopolymers to minimize waste as well as carbon emissions in materials-based industries. Biopolymers derived from natural sources possess specific qualities because they can naturally appear inside living organisms, call for no extra treatment just before use, happen in different physical forms solid, solution, semi-solid, and are capable to make thin layers on solid surfaces. These characteristics render them appropriate for utilization in the region of printing arts, the packaging market, the textile market, and other industries. (1-3). Natural, renewable, and plentiful, cellulose is a complex polymer with linear glucose-built alongside polysaccharides (Figure 1.a). It also offers nourishment to numerous organisms such as Algae, bacteria, and plant cells. During the 1920s, carboxymethyl cellulose (CMC) (Figure 1.b) acquired considerable manufacturing significance. Its discovery exposed its enormous potential in different industries like food industries, textiles, paper, and drug sectors largely because of its economical manufacturing process and high effectiveness. Nitrocellulose (NC) is a rich natural cellulose derivative employed in printing inks, coatings, filter media, and biochemistry (5-7). Oxycellulose (OC) is a chemically risk-free organic polymer that breaks down easily and is compatible biologically (8,9). It finds application in surgical operations (10). The chemical substance hydroxyethyl cellulose (HEC) (another derivative of cellulose) is a well-known component of pharmaceuticals, skin care products as well as food businesses (Figure 1.c). It isn't toxic, non-ionic, or hydrophilic (11,12).

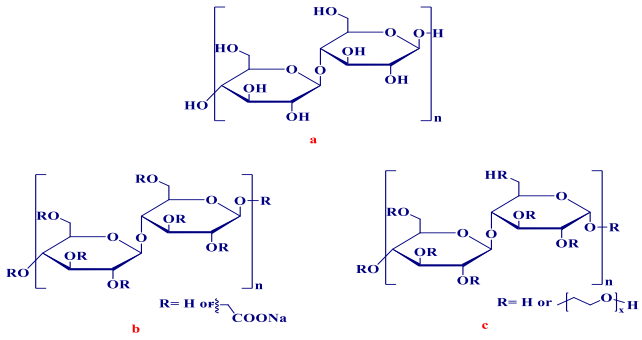

Figure 1. *(a) The structural formula of cellulose (b) The material configuration of carboxymethyl cellulose together with sodium salt (c) The composition structural of hydroxyethyl cellulose.*

HEC coatings possess the superior capability to form a film, and their ability to break down naturally and harmonize with biological systems makes them suitable for various biomedical uses. (13) Therefore, thoroughly examining diffusion and diffusion aspects of swelling and dissolution in the biopolymers mentioned above, specifically CMC and also HEC, can contribute to advancing the growth of contemporary industries that heavily rely on these biopolymers. Poly(ethylene) is a popular semicrystalline polymer that is extensively utilized because of its affordable price and distinctive physiochemical characteristics. The HDPE nanocomposites demonstrate significant strength in their overall mechanical properties. The

difference in elasticity modulus between the filler nanoparticles and polymer matrix results in a much better likelihood of cavity formation (14-18). The usage of inorganic mineral nano-fillers is growing in popularity to enhance the performance of polymers like HDPE, particularly in terms of their ability to withstand wear and tear (19,20). The inclusion of these additives can alter the physiochemical behaviors of polymers, impacting their ability to wear durability wear and rupture, their surface strength, and their resilience and ductility (20). The addition of tiny particles to thermoplastic polymers resulted in enhancements in characteristics such as air permeability, elasticity, mechanical strength, rigidity, and stiffness (21-24). Mineral fillers like perlite have been found to enhance the thermal stability and sound absorption aspects of polyesters (25-28). It is essential to comprehend how the performance of composites in consumer products and industries is affected by the polymer matrix and filler particles (28,29). The semi-crystalline polymers contain interconnected spherulites that make up the crystalline portion (30). Current studies suggest that the properties of thermoplastic polymer materials, including their mechanical characteristics and the mechanism they melt and crystallize, are greatly affected by the type, shape, and size of mineral fillers (31). According to reference (32), the overall effectiveness of mineral fillers in composite applications is impacted by factors such as the size, shape, and dispersion of the filler particles. To ensure a high level of consistency in producing biopolymer composites, it might be essential to perform mechanical evaluations on the materials obtained from commercially available fillers. The incorporation of nanofillers like GnPs and HNPs, along with an appropriate polymer matrix, can greatly enhance the durability (toughness) of the substances (33,34). Polymer composites such as polyester, polyurethane, and epoxy were recognized for their extraordinary mechanical strength and ability to absorb moisture, as well as their minimal shrinkage and reduced emission of toxic substances during the treating process (35-37). Although the tribological characteristics of epoxy resin are restricted, its influence on mechanical durability has made it a favored option in industrial settings. In biopolymers with differing properties, HNTs and GnPs function as highly effective nanofillers. GnPs possess excellent thermal stability, conductivity, fracture toughness, as well as enhance lubrication. On the other hand, HNTs exhibit a greater dispersion ratio and have surface hydroxyl groups with low density, leading to effortless diffusion and reduced aggregation. Incorporating HNTs and GnPs nanofillers into epoxy matrix composites produces a positive effect on the plasticity, mechanical strength, heat resistance, and longevity of the material. Further investigation is needed to determine the individual impacts of HNTs and GnPs as separate nanofillers (36-39).

2. Biopolymers

The amazing flexibility of intelligent materials has revolutionized sustainable product development. The capability to respond to outside stimuli and change with it their surroundings has made them desirable for applications in engineering, defense, medicine, and automobile manufacturing. Memory alloys, hydrogels, pigments with color changing with light or temperature, and polymers which can recall and return to their initial form are examples of smart materials (40). Smart materials provide a major benefit in that they can be personalized to fit a certain usage, leading to a diverse array of physical, chemical, and biological attributes. The trend has presented engineers as well as researchers with stimulating opportunities to produce sophisticated single and combined systems that adjust to industry requirements. The development of science and engineering has resulted in a need for extremely innovative and environment-friendly materials which meet the requirements of contemporary industries. Engineers specialized in materials are always exploring methods to utilize the distinct features of intelligent materials in an attempt to develop environmentally

friendly and inventive goods which fulfill the demands of contemporary society (41). Heavy construction materials, in particular in transportation, are costly and call for a higher energy level, which produces considerable problems in the materials industry for handling and production. This has led scientists to research simple and cost-effective ways of producing lightweight and strong mechanically absorbing polymer composites. Additionally, because green waste is lowering and carbon emissions rising, biopolymers are now being redesigned to enhance their properties and properties. Research into different biopolymers including Polylactic acid (PLA), polyhydroxyalkanoates (PHA) (42) starch, cellulose, pectin as well as chitosan has produced a selection of biopolymers and bio composites which share qualities with standard bio-packaging (43). Lightweight biopolymer composites should see automobiles dropping in weight by 50% within the next ten years, meaning a 50% decrease in gas use. The features of polymer composites and polymer-based ceramics might be utilized to develop as well as make innovative lightweight engines. Natural biopolymers possess many benefits, including their deliberate formation inside living organisms, their mixed properties in solid, semi-solid, and liquid forms, and their potential to be used with no further treatment, which is creating growing interest. In addition to that, they enable the easy development of thin coatings on solid surfaces, which happens to be a method of industries like printing arts, textiles, and packaging components (1,2). The surfaces are made more water-repellent and water-attracting by this technique. Contact lens surface enhancement has been discovered by utilizing cross-linked hydrogel coatings (44,45). Written works are examined principally as carbon-based polymers (nanoscale fibers & dispersions, cyclic fullerenes) and polymers made of boron and silicon. This considerable thesis has emphasized biopolymers such as cellulose and its variations, such as Nitrocellulose, hydroxyethyl cellulose, carboxymethyl cellulose, along with oxycellulose. In (Figure 1) we see cellulose placed like a linear polysaccharide of glucose (46) which offers mechanical support for plant life, algae, fungi, and bacteria. Probably the most abundant and renewable resource on earth is cellulose, an all-natural polymer. The annual production of cellulose is thought to be 75 to 100 billion tons (3) (A number which has developed since 1912). It's generally obtained as pulp or extracted from organic sources such as cotton, bark, wood, jute, leaves, and timber. As a derivative of cellulose, CMC received significance for commerce and industry during the 1920s because of its easy production procedure as well as cost-efficient parts. CMC finds application in different industries including food, beauty products, pharmaceuticals, paper & textiles. Much like cellulose, the substance derivative nitrocellulose (NC) is commonly used in industries like coatings, varnishing, filtration membranes, printing inks, and numerous other purposes. Its content a nitrogen-based (5,7,47) determines its useability for various uses. The creation of NC aerogel is growing its usage in purification science, separations, and biomedical applications (48). Oxycellulose (OC) is a non-toxic polymer that can degrade effortlessly over time to be employed in surgeries. It’s suitable for living organisms and may be utilized to avoid bleeding and tissue adhesion. The market provides the product in two forms - knitted fabric or staple fiber. HEC is a kind of cellulose that has no taste, is edible and has a strong water sensitivity. It's extensively used in the pharmaceutical, cosmetic, and food industries as depicted in (Figure 1.c) (11,12). HEC offers qualities including biocompatibility, biodegradability, and film-forming capabilities which cause it to be extremely appropriate to be utilized in biomedical methods (48). Food packaging materials are produced using aluminosilicates combined with natural biopolymers (49). This dissertation is designed to examine different biopolymers with a particular focus on cellulose derivatives like hydroxyethyl cellulose as well as

carboxymethyl cellulose. The biopolymers discussed previously are graphically shown in (Figure 1). The thesis will concentrate on the investigation of different polymer aspects including their spreading or diffusion, swelling phenomena, and breaking down operations, surface force, strength, and behavior of diffusion (50). The assessment (51-53) will focus on industrial additives employed in the printing as well as textile industries. These additives are utilized for several functions including safeguarding printing plates from dampness, protecting printing plates, and enhancing textile coloration. The areas of biopolymer cross-link and diffusion coefficient will also be discussed. I will initially look at nanomaterials, polymers composites, polymer nano composites, and nanofillers, and any configurations of the polymers and their characteristics before proceeding to the characteristics of biopolymers.

3. Nanomaterials

Nanotechnology describes a scientific area and technological advancement wherein structures and devices are controlled as well as examined at incredibly small scales, including atomic, molecular, along with macromolecular levels. Scales generally measure between 1 to 100 nanometers (54). The word "nanotechnology" is believed to have its origins in (Japan), where Taniguchi (55) coined it. The importance of dimensions of roughly 1 billionth of a meter is particularly dealt with in this specific branch of manufacturing. Nanoparticles have been found to have advantages over bigger than microspheres as demonstrated by research (56). In addition, biological nanoparticles have mainly been created for drug delivery purposes as an alternative to liposome technology (57). The objective of this particular method is to tackle worries regarding the durability of liposomes in biological fluids while being kept. Nanoparticle technology is a brand-new advancement that could boost the effectiveness of medication. Colloidal drug delivery methods could include nanoparticles, therefore enabling modified body distribution for specific drug delivery (58). Additionally, they might improve the absorption of compounds into cells (59), which decreases the harmful and negative consequences of unbound medicines (60). Nanoparticles may be carried from the bloodstream to several locations within the entire body, facilitating treatments that target the whole system (61). It's possible to produce nanoparticles utilizing different materials including proteins and artificial polymers. The selection of materials for nanoparticles is determined by numerous elements, including their size and structure, area charge, flexibility, compatibility and biodegradability with living organisms, possible toxicity, and preferred drug release profile (62,63).

4. Biopolymer nanoparticles

For The first time, albumin (64) and non-biodegradable artificial polymers like polyacrylamide and poly (methyl acrylate) were utilized to develop biopolymer nanoparticles (65,66). The danger of extended harm resulting from the build-up of biodegradable polymers inside cells or tissues has become a significant obstacle to their application as a systemic therapy for human beings. The main focus was moved to nanoparticles created from man-made bio-degradable polymers including poly alkyl cyanoacrylate, poly (lactic-co-glycolic acid) and polyanhydride (67-70). The literature presents substantial exploration from several directions (71-76) on possible therapeutic uses of biodegradable colloid systems. Nevertheless, earlier studies (77,78) have cautioned these systems might encounter toxicological difficulties. Additionally, the hydrophobic qualities of the polymers utilized in

bio nanoparticle-based delivery methods exert a constraint on effectiveness in supplying hydrophilic substances like nucleic acids, proteins, and peptides (such as genes and oligonucleotides). The process of enclosing and shielding the drug against enzyme breakdown could be inefficient (75-79). Thus, scientists have looked at using naturally occurring materials that possess a greater water affinity for nanoparticle manufacturing (80-82). It had been recognized several years back those biodegradable nanoparticles are necessary for their usage as drug carriers (83). Liposomes, virus-like particles (VLPs), in addition to proteins, are biopolymer nanoparticles that possess a variety of benefits, including their simplicity of generating from obviously degradable polymers and their enhanced stability in natural fluids and storage (84). A report (85.) proposes that proteins and polysaccharides might be blended to make biodegradable nanoparticles that may deliver standardized, sustained, and targeted drugs. This delivery technique has demonstrated promising accomplishments in improving the therapeutic effects of drugs while lessening their negative effects.

5. Polymer composite and nanocomposite

PMCs and PNCs (Polymer composite & nanocomposite) consist of a Polymer element and additives including inorganic fillers which improve the structure and the function when used. Or alternatively, polymer nanocomposites (PNCs) include molecules and fibers/films which measure somewhere between 5 and 100 nanometers in dimension, with no less than 1 nm of those elements contained. PCMs and PNCs are made and formed by utilizing both synthetic and natural polymers as matrices. The thermoplastic materials used in these methods can undergo reversible viscous flow upon heating or a curing agent when exposed to heat or a curing agent. Harito and colleagues (86) concluded that polymer nanocomposites (PNCs) are matrices of polymer or copolymer-containing nanomaterials or even nanofillers. Fillers containing at least 1 dimension measuring between 1 and 50 nm are specified. PNCs have applications in electronics, structural, biomedicine, and optics. Hashim et al. pointed to polymer thin films as crucial to a range of technical uses, which include adhesives and coatings, and natural products. (87). Redondo and colleagues, based on (88), the existing research emphasis is on adjusting the attributes of materials in polymer nanocomposites by altering the size as well as the number of nanoparticles. Nevertheless, the difficulty is based on effectively dispersing PNCs films or coatings. The polymer structure has nanoscale particles but with increasing amounts of particles, dispersion becomes problematic because of their tendency to aggregate together. To handle this specific issue, nanoparticles may have chemically altered the surfaces to create a consistent dispersion. Complex and costly fabrication methods might be created, possibly due to this (89). The function of the interface between nanoparticles along with polymers is incredibly important in identifying the physical, chemical, and as well mechanical engineering attributes of polymer nanocomposites. (90). In traditional polymer composites, a particular filler could affect other significant qualities by impacting their general quality. A rise in stiffness of materials which block or hold off flames can reduce durability, see-through ability, or mechanical characteristics. Individually tailored nanoparticles can possibly reverse or eliminate specific properties declining while concurrently improving numerous desirable advantages within nanoparticles. (91). My studies suggest that perlite mineral filler plays a crucial part in the thermal and mechanical properties of HDPE polymer nanocomposites. The Young's modulus progressively increased with better filler concentration; break elongation decreased. Perlite concentration of 15 wt.% exhibited a 37 wt.% increase in Young's modulus of elasticity compared to pure HDPE. The stress-strain curve (Figure 2) was utilized to analyze all these factors. Non-destructive vibration analysis (displacement transmissibility measurements) confirmed the improved stiffness in uniaxial tensile mechanical strength experiments, which revealed a change in the original peak frequency direction (position) towards higher degrees

of excitation. The toughness against fractures reduced with increasing perlite content, suggesting the fractures were much more likely to be brittle fracture. However, SEM pictures showed places in which the fractures had been ductile-indicating greater filler levels-after examination of the material. Perlite particles added stress concentration to the composite matrix. The increased filler concentration was related to a modest temperature rise which was linked with melting, suggesting a stronger link between the particles of filler and the chains of the polymer. Another study investigated the structural characteristics of epoxy resin nanocomposites containing nanoscale graphene nanoplatelets (GnPs) along with halloysite nanotubes (HNTs) as fillers. The experiment found that the modulus of elasticity of Young was altered nonlinearly by the inclusion of GnPs fillers. The nanocomposites experienced greater ductility when the GnPs nanofiller was between 1 and 0 wt.%. The reason for this might be the movement between specific GnPs, nanoparticles that have been separated into the matrix. Nevertheless, once HNTs fillers have been included, Young's modulus of elasticity remained fairly consistent. The HNTs nanoparticles were caught inside the surrounding material during mechanical tests and their movement was severely limited. The SSC plot results (Figure 2) demonstrated that the more rigidity epoxy/HNTs nanocomposites had greater fracture stiffness values at reduced filler levels than the epoxy/GnPs nanocomposite. The GnPs filler does this mainly because of its gliding dissipative effect. Elongation at break dimensions demonstrates the special epoxy/GnPs nanocomposite combinations become more plastic and ductile as the GnPs filler quantity increases. epoxy/GnPs nanocomposites showed a lower indentation modulus than ethylene HNTs nanocomposites based on micro-hardness assessments. The very first one shows more mechanical dissipation (the friction from the GnPs filler during a glide is in excess than the epoxy/HNTs. The research utilized a non-destructive mechanical damping technique for forced oscillations at a reduced frequency of 2-3,200 Hz to determine mechanical qualities by locating the first resonance frequency peak. The verification of this effect has established the plasticization effect in epoxy/GnPs nanocomposites. The epoxy/HNTs nanocomposites had a considerably greater peak position for 1st resonance frequency than some other components, indicating superior overall performance. The incorporation of little fillers including carbon nanotubes, nitrocellulose and carbon graphene makes it easier to manage and enhance polymer nanocomposites (86).

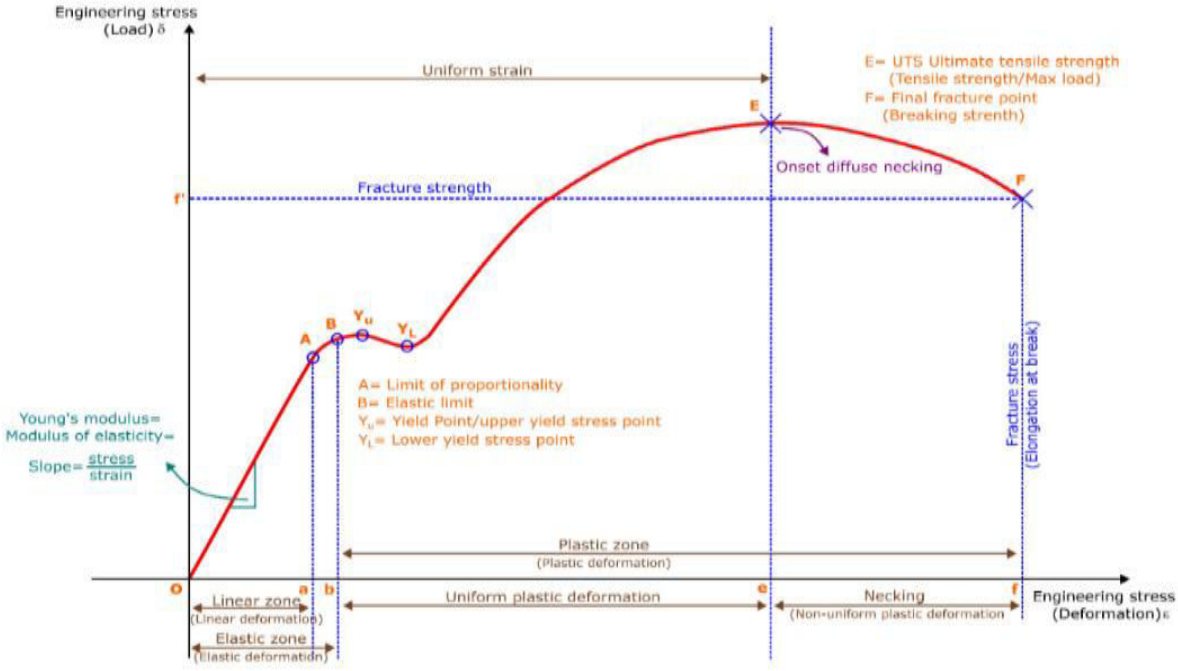

Figure 2. *A stress-strain curve (SSC).*

6. Nanofillers

Nanofillers, especially those made of clays and carbon nanotubes, have received a lot of attention in recent years. The widely accepted definition of nanoparticles requires that they have at least one measurement between 1 and 100 nm and that their remaining dimensions exceed 100 nm. It is feasible to classify these particles into more specific groups, depending on the number of dimensions they possess within the nanometer scale. Nanoparticles are zero-dimensional particles, nanofibers are one-dimensional particles, and nanoplates are two-dimensional particles. To begin with, it should be noted that nanofillers aren't a new concept; in fact, nanoparticle fillers are well-established on the market. The substances mentioned above consist of calcium carbonates, fumed and precipitated silicas, and carbon blacks. Synthetic polymer nanoparticles are also becoming popular. Our research studies investigate precisely how the mechanical and structural properties of HDPE composites, manufactured in a test facility, are influenced by the addition of nano-sized mineral fillers such as nano $CaCO_3$ and nano clay. The findings indicated that the inclusion of fillers had a notable positive impact on the mechanical properties of the composites. This was evident through an increase in both the elastic and indentation modulus. As an illustration, the HDPE's elasticity modulus rose by 51.5% to 1470.0 ± 54.7 MPa when 5% of nano $CaCO_3$ filler was added by approximately 34.5% to 1304.9 ± 83.7 MPa when 4% of nanoclay filler was added. The type of amount of filler used in addition influenced the plastic-elastic mechanical properties of the materials. This was evident from the materials' decreased ability to stretch before breaking and increased area under the stress-strain curve at higher filler concentrations. The optimal filler concentration for both composite types was discovered to be 5%. Furthermore, the thermal stability of both nanocomposites was higher than that of pure HDPE, suggesting a far more robust bond with the HDPE matrix. These results indicate that nanocomposites have the potential to be beneficial in complicated product designs as they possess both elastoplastic mechanical properties across a variety of deformation rates and increased stability in terms of heat. Although nanofillers have been receiving a great deal of attention lately, it is crucial to keep in mind that the concept is not new. Nanoparticulate material fillers have been on the market for quite some time and are widely recognized. Examples of these kinds of materials are carbon blacks, fumed silicas, and precipitated calcium carbonates. Thus, a significant portion of the potential nanoparticle market is currently content. The discovery is likely to manifest itself as nanoplates as well as nanofibers. In this specific context, nanoparticles are described as having at least one measurement that ranges from 1-100 nm, except for flat substances such as graphene that could potentially have a thickness smaller than one nm. In the absence of porosity effects, the own surface area of the nanoparticles can range from 25 to much more than 750 m^2/g, which can be used to steer their movement. The mentioned trait is able to change depending on the specific weight and might display an unforeseen variation. When there is high density, a specific measurement decreases in its magnitude. Particles that have three dimensions at the nano scale are categorized as nanoparticles, whereas particles with one and two dimensions are known as nanofibers and nanoplates, respectively. This is depicted in (Figure 3).

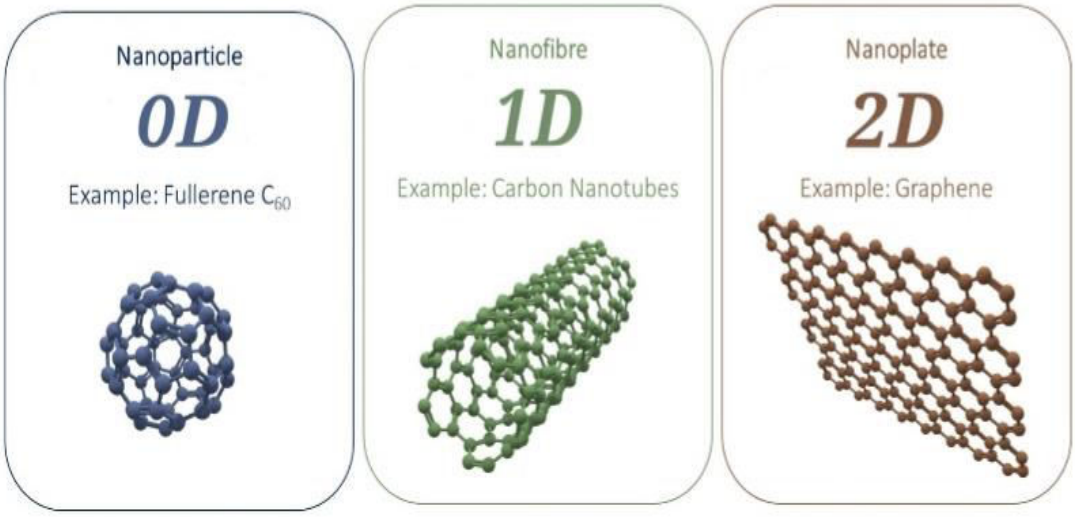

Figure 3. Nanoparticles, nanofibers, as well as nanoplates may be differentiated by the number of external measurements they possess on a nanoscale domain. Reproduced from (92).

7. Properties of biopolymer

Biopolymers are polymers accessible naturally and are from living organisms. The source of a substance might distinguish between various classes including polyesters, nucleic acids, proteins, and carbohydrates. Biopolymers are appealing for different uses because of their diverse characteristics (ability to decompose effortlessly, compatibility with living organisms, replenishment, and long-term viability) (93). Biopolymers are very appreciated for their capability to biodegrade, meaning they could be naturally decomposed by bacteria, and enzymes, together with various other all-natural mechanisms. Biopolymers are sustainable and may be utilized in areas involving reduced waste and pollution. Biopolymers aren't harmful and are compatible with living tissue or fluids. This distinctive property makes it ideal for biomedical uses like drug delivery methods and tissue engineering. Biopolymers tend to be inexhaustible and might be created by using sustainable energy sources like animals and plants, therefore permitting large-scale production without consuming natural resources. They are especially ideal for environmentally friendly and sustainably demanding applications because of this unique feature. Ultimately, biopolymers possess a different set of chemical and physical attributes which could be adjusted either by chemical alteration or by combining them with various polymers. For example, they possess great strength and durability, together with thermal stability, making them perfect for applications that require robust packaging materials together with some other uses where strength and longevity are essential. Biopolymers are appealing substances for different applications because of their assortment of distinct qualities, which include medicine, agriculture, packaging, along with various other sectors. While scientists continue to do research, they're finding new sources as well as strategies for creating biopolymers, which might have a wider utility scope.

7.1 Biological routes

Balaji et al. (93) highlighted the usage of natural substances as coating substitutes for enhancing the biocompatibility of polymers. In the latest analysis of covering techniques. Several surface modification methods are continuously evolving to customize polymers' biocompatibility and improve their interaction with the natural environment which is usually known as biofunctionalization methods. The regular goal of these different techniques, discussed in detail and depicted in (Figure 4). It is adapting the surface qualities related to a certain polymer to direct its cellular interactions for the consider site where its application is focused. Though diverse biofunctionalization techniques are obtainable, the thought of utilizing natural materials for bettering biocompatibility appears effective and rational because of the biofriendly exterior in which they're offered that's closer to imitating the innate environment. Certain commonly found biomolecules, which include proteins, carbohydrates, and peptides, have gained popularity on valuable items through innovative methods.

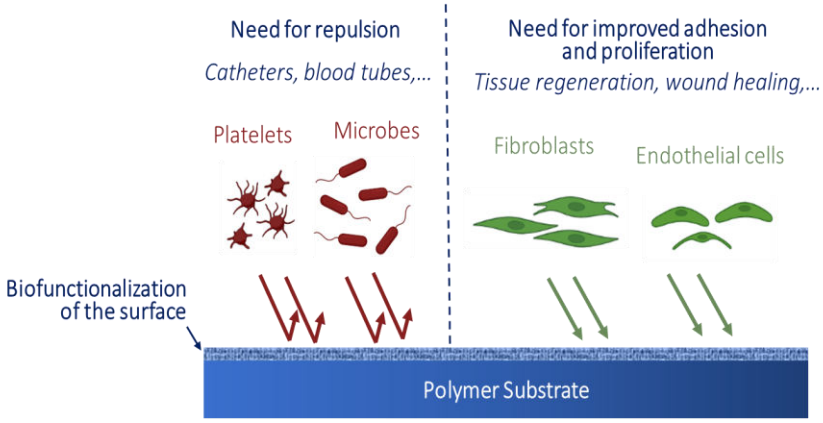

Figure 4. *The objective of biofunctionalization in relation to biomedical devices is to achieve specific goals. Reproduced from (93).*

According to current scientific studies, biological substances are attracting increasing scientific interest because of their nontoxic characteristics, compatibility with organic organisms, ability to replicate natural conditions, wide accessibility, and capability to prevent detrimental reactions related to synthetic polymer surfaces, like inflammation and the adherence of platelets. Biomaterials applied to a surface might induce cellular attachment, development as well as specialization leading to an advantageous impact on wound healing and tissue regeneration. Biochemical methods entail the transfer of substances including lipids, medications, receptors, drugs, ligands, and peptides of proteins upon material surfaces through bodily adsorption, and chemical or self-cross-linking conjugation. Integrating environmentally friendly materials in biological techniques and eliminating damaging materials make them more appealing for enhancing the compatibility of polymers with living organisms. Surface chemistry is crucial for different biomedical applications because of its ability to adhere or react chemically, as is surface morphology like roughness or texture. There are situations where these requirements oppose one another for a specific material. The utilization of silicones in cardiovascular implants might require the promotion of advantageous cell attachment to facilitate the correct integration and connection of the synthetic unit at the implantation area. On the other hand, some catheter silicones might prevent cell adhesion to lessen contamination and blockage of the tube.

8. Characterization of biopolymers

Table 1 presents the evaluation of the characterization of HEC and CMC according to their solid or crystal state and their liquid or cross-linked state. The movement of the macromolecular chain was analyzed using temperature-dependent dielectric spectra within the frequency range of 20 Hz to 1 MHz (94).

Parameter	**Compound**	
	CMC	**HEC**
10^3 (ε_s - ε_∞)	37.60	2.28
	2.18	
α	0.0598	0.676
	0.970	
β	1.000	1.000
	1.000	
10^{-3} τ_0/s	68.100	5.120
	3.810	
A'	2.48×10^{-19}	1.08×10^{-18}
n	0.700	0.535

Table 1. *The sample's optical permittivity is represented by ε_∞, while its static permittivity is represented by ε_s. The difference between these two values, (ε_s-ε_∞), represents the relaxation strength. The position of the relaxation on the same axis is represented by τ_0, and the slant of the low-frequency part of the relaxation curve is represented by α. The product of $\alpha \times \beta$ and characterizes the slope of the high-frequency part of the relaxation curve. A' represents the sample surface area, and n represents a mechanism of purely D.C. conductivity (94).*

Additionally, (Table 2) presents an overview of the analysis of CMC using corn starch, including details on crystallinity, average length, purity percentage, and average width (95). The information presented in the data clearly shows that CMC biopolymer has a wide range of uses as a stabilizer, emulsion binder, and thickener in various sectors (96,97). These industries include detergent, cosmetics (98), drilling, pharmaceutical, food, and textile (99). Furthermore, within the pharmaceutical field, CMC could function as a cohesive agent, aiding in the formation of drug tablets. It is worth pointing out that the level of substitution of CMC does not impact the purity percentage. The average width (100) has an inverse relationship with the percentage of crystallinity. In the same way, HEC, which is a type of cellulose ether that does not have an electrical charge, has beneficial properties when dissolve in water and is able to be applied in a few industries (101) like pharmaceuticals, food, and manufacturing. It could function as a thickener, stabilizer, binding agent, protective agent, along with suspending agent in several industrial processes (102).

Degrees of substitution (DS)	Mean length (mm)	Mean width (μm)	Percentage crystallinity (%)	Purity (%)
0.75	2.28	48.1	18.03	95
0.76	2.13	55.7	19.60	95
0.80	1.94	52.8	23.51	95
0.73	1.43	51.7	25.85	95

Table 2. *The attributes of the CMC sample vary (Adapted from reference 95). Bioresources from North Carolina State University provided the courtesy.*

The most commonly utilized CMC polymer is NaCMC, which is analyzed through rheology to figure out its flow characteristics, with the DS serving as the basis for the analysis. Samples of NaCMC with a variety of substitutions, when present in greater concentrations, can easily create gel-like structures (103) and also might display either thixotropic or shear aging characteristics (103,104). The reason behind the thixotropic and gelling characteristics of NaCMC with low substitution levels (103-107) is the formation of interchain aggregates and fringed micelles with a crystallized core. These occur when the degree of substitution drops below a particular threshold of around (0.9). The rheological properties of physical gels made from CMC with no cross-linking agents are due to the hydrophobic interactions that occur between the individual macromolecular chains (108-110). The research being discussed showed that CMC samples with DS ≈ 0.7 - 0.8 could be divided into two parts through the process of centrifugation. Fraction A displayed a pseudoplastic behavior, which means it thinned out when subjected to stress, and it did not exhibit thixotropic or gelling properties in a salt-free water solution. On the other hand, fraction B had limited solubility in water but readily dissolved in concentrated NaOH. At higher concentrations, fraction B's uneven distribution of substituents caused the formation associated with a thixotropic gel through hydrophobic associations between chains. The qualities of the HEC (111) water-based mixture can be altered by changes to the side chains, such as the addition of hydrophobic or ionic structures, or by modifying the polymer backbone. In HEC with hydrophobic adjustments, the thickening process occurs as the hydrophobic side chains combine to form a temporary intermolecular network. The HEC that has been altered in a catatonic manner (112-114) exhibits similar behavior as regular polyelectrolytes (115). The increase in viscosity is a result of the charged groups on the chain repelling each other, causing the macromolecule to expand. When the amount of surfactant increases, the micelles have fewer side chains, which eventually prevents the polymer molecules from forming intermolecular associations because the attached micellar aggregates repel each other due to electrostatic forces. As a result, the viscosity of the solution gets to its highest point and subsequently decreases as more surfactant is added (116,117). The suppression of intermolecular connections by hydrophobic side chains could potentially result in a viscosity that is much less than that of the unpolluted polymer solution. Equation (7) calculates the diffusion coefficient *(S)* based on the changes in surface tensions of the foamy medium *(f)* and the defoamer *(d)*, in addition to the interfacial tension between the two phases df. The TS values of CMC films (118) may differ based on the CMC ratio utilized and the existence of a substrate. The research conducted on CMC films made with sodium monochloroacetate and various levels of sodium hydroxide revealed that the tensile strength of the films rose when NaOH concentrations were at 20 and 30 g/100 mL. However, the strength decreased when the concentration exceeded 30 g/100 mL, as shown in (Table 3) (118). The level of substitution of the CMC DS was observed to have a direct correlation with the TS, because a higher level of substitution led to increased intermolecular forces between polymer chains, resulting in greater strength.

Types of film	Tensile strength (MPa)	Elongation at break (%)
20g/100mL NaOH-CMC	141.16 ± 8.32	2.32 ± 0.26
30g/100mL NaOH-CMC	255.54 ± 4.13	2.20 ± 0.81
40g/100mL NaOH-CMC	140.77 ± 14.43	2.07 ± 0.50
50g/100mL NaOH-CMC	53.42 ± 8.21	2.95 ± 1.13
60g/100mL NaOH-CMC	79.62 ± 9.76	2.28 ± 0.98

Table 3. *The mechanical characteristics of CMC films produced with different concentrations of NaOH at a temperature of 25C and relative humidity of 75 % are presented in this article, with the authorization of Elsevier. (Reproduced from reference 118) ID number 60075084 has been requested.*

Studies on the production of CMC corn starch films yielded comparable findings. The highest TS was obtained by combining four grams of CMC with no corn starch, according to the findings. Additionally, a ratio of 3:1 of CMC to corn starch is based on the findings. The lowest total score (TS) was achieved when corn starch was dissolved in a 1:1 ratio of CMC, as shown in (Figure 5). Lower concentrations of CMC corn starch led to an increase in the percentage of elongation at break, and also TS decreased in general with an increasing percentage of elongation at break (119).

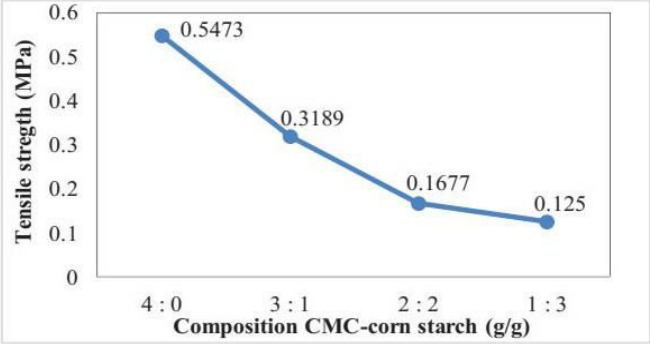

Figure 5. *The mechanical tensile strength was checked out (Derived and reproduced from reference 119). The American Institute of Physics has granted permission under license No. 5270921480448.*

The tensile strength and stretching capability until fracture of HEC films were also assessed. The addition of 4% CNC to HEC films that contain cellulose nanocrystals resulted in a 120.2 % increase in the TS, as shown in (Figure 6). However, the increase was restricted to no more than 8%. (120) The elongation at the point of fracture reduced by 95.6% when compared to films made of pure HEC. The incorporation of CNC has the potential to improve the tensile strength of HEC films, but as soon as a certain threshold is reached, the elongation at break starts to decline (120-122).

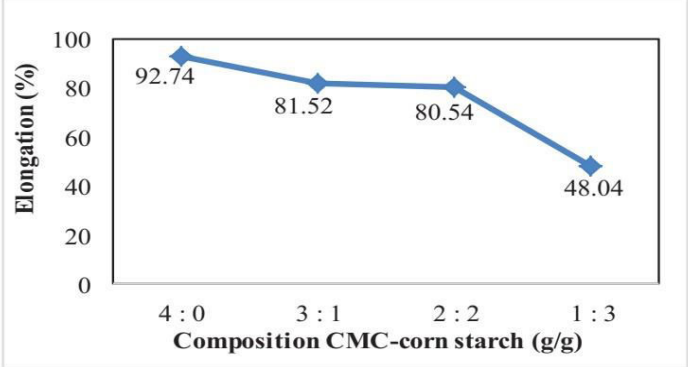

Figure 6. *The determination of the elongation ratio had been done (According to reference 119). The American Institute of Physics has approved and granted License No.5270921480448, which authorizes permission.*

(Table 3) and (Figure 5) (119) are relevant to the discussion of CMC-corn starch films, and (Figure 6) (120) is relevant to the discussion of HEC films with CNC.

9. Diffusion of polymers and surface tension

The transportation of substances is referred to as diffusion due to variations in chemical potential that can be affected by factors such as temperature, electric potential, pressure, and magnetic field. Many writers (97,123,124) have conducted thorough research on this subject. Fick's principles describe two distinct connections that elucidate the occurrence of diffusion. The one-dimensional diffusion laws of Fick can be used for a binary system:

i. Flick's law : $J_i = -D_i \frac{\delta c_i}{\delta x}$ (1)

ii. Flick's law : $\frac{\delta c_i}{\delta t} = \frac{\delta}{\delta x}\left(D_i \frac{\delta c_i}{\delta x}\right)$ (2)

The laws give a fundamental introduction to diffusion phenomena and also have wide potential applications in chemistry, physics, and engineering. Low molecular weight polymers usually have a diffusion coefficient within the range 10^{-5} to 10^{-14} cm^2 s^{-1}. Research by R.M. Barrer as well as colleagues have classified Polymer-permeate to (125):

a) $\frac{\partial c}{\partial t} = D\frac{\partial^2 c}{\partial x^2}$ $D = const. c = k.c$, (3)

b) $\frac{\partial c}{\partial t} = \frac{\partial}{\partial x}\left[D(c)\frac{\partial c}{\partial x}\right]$ $D = f(c)$ $c = k.c$, (4)

c) $\frac{\partial c}{\partial t} = \frac{\partial}{\partial x}\left[D(c)\frac{\partial c}{\partial x}\right]$ $D = f(c)$ $c = f'(c,)$ (5)

(3)

d) $\frac{\partial C}{\partial t} = \frac{\partial}{\partial x}\left[D(c)\frac{\partial C}{\partial x}\right]$ $D = f(c,t)$ $c = f'(c,)$ (6)

Different kinds of diffusion in polymers and hydrocarbon systems are described by categories a, b, c, and d. Category a is commonly associated with the dispersion of uncommon and largely two-atom gases in viscoelastic polymer states, whereas category b pertains to the dispersion in rubber and hydrocarbon systems with paraffin. The diffusion of heavy hydrocarbons within rubber layers can be described by category c, while category d is frequently used and has a diffusion coefficient that changes depending on the concentration and duration. In this instance, the strong interactions between the molecules of the chain as well as the penetrant cause the crystalline polymer to experience a gradual relaxation process.

Surfactant	CMC (g/litre)	Equilibrium/surface tension at CM conc × 10 (mN/m)
NPOEOP	0.06	36.9
C13OE18	0.08	27.7
Silvett L77	0.10	20.4
C10OE6	0.80	26.1
TTAB	1.18	37.2
CTAC	0.42	34
DOS	0.92	27
SDS	2.38	36.5
SDG	0.60	25

Table 4. *Surfactant solutions: Characteristics of the surfactant solutions. The critical micellar concentration will be the point at which the equilibrium surface tension reaches a certain value, which is multiplied by 10. This information is reproduced from reference 126. Academic Press, Elsevier Science has granted a license 5270931090431.*

Where: NPOEOP is polyoxypropylene with nonylphenyl group attached. C13OE18 is polyoxyethylene with isodecyl. The Silvett L77 is trisiloxane, oxypropylene, and polyoxyethylene. C10OE6 is polyoxyethylene with isodecyl. TTAB is tetradecyl trimethylammonium bromide CTAC is chloride ccetyltrimethylammonium. DOSis is a compound known as sodium bis(2-ethylhexyl) sulfosuccinate. SDS: sodium dodecyl sulfate. SDG is Decyl galacturonate of sodium. It is essential in various technological areas to comprehend how the interaction between solid and liquid interfaces impacts the ultimate dispersion of liquid droplets. An investigation was conducted to check out the actions of surfactant solutions once they reached a critical micellar concentration multiple of 10 (Figure 7) (126) and the actions of water droplets from the point of impact until one second later (Table 4) (126). All the solutions went through the same spreading process. The diffusion coefficient for spread, as demonstrated in Equation (7), is determined by multiplying the surface tension of the foaming phase as well as the surface tension of the defoamer phase, as well as the interfacial tension of both substances (df).

$$S = \sigma_f - \sigma_d - \sigma_{df} \tag{7}$$

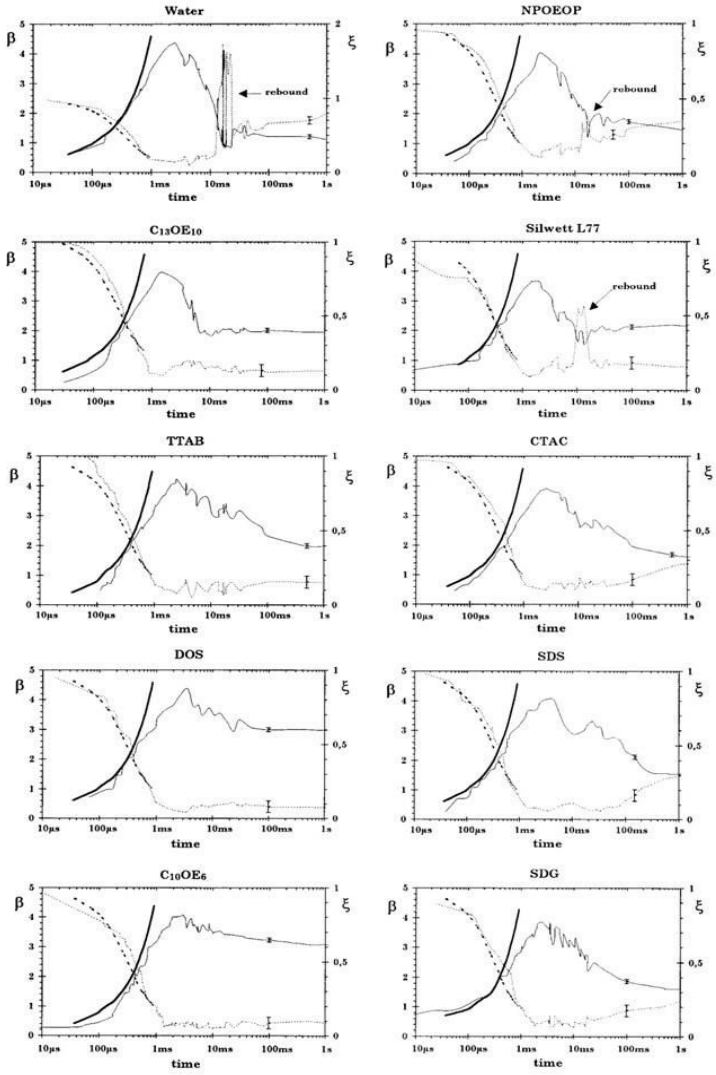

Figure 7. *The figure referenced gives instructions on determining the spreading factor of water and surfactants through the use of a CMC multiplier of 10 throughout a certain period. (Reproduced from ref.126) Elsevier Science has authorized Academic Press to grant permission no. 5270931090431.*

As the surface tension of a defoamer decreases, its spreading coefficient becomes more positive, which suggests a thermodynamic inclination towards defoaming. Equation (7) is specifically relevant to defoamers that are bulk liquid cannot be dissolved, but some hydrophobic solids that are dispersed may increase the efficiency of defoaming. Surfactants have a significant impact on the spreading process.

10. Diffuse process of swelling and dissolution of polymers

10.1 Diffuse process of swelling

Whenever rigid polymers are transformed at temperatures less than the second order turning point (T_g), into liquid phase, it consists of both swelling and dissolution procedures. The process of becoming swollen. The strong polymeric phase is expanded in the fluid stage by the addition of solvents, resulting in a broader solid surface. This occurrence, called Kirkendahl's effect (127), causes the polymer building to become less rigid and encourages the motion of large molecular chains. Thus, the system experiences a rise in the activity of free volume, leading to the substitution of contacts between polymers with contacts between the polymer and solvent. As a result, a layer on the surface is formed that is both enlarged and has a particular structure and thickness (128). Comprehending the swelling mechanism is dependent on comprehending the behavior of the stage interface, that is the boundary between the expanded layer as well as the fluid solvent. Based on Lapik and Valko's study (129), they examined how polymers dissolve through diffusion and determined that it is possible to assess the diffusion of liquid solvents into polymer foils by using certain parameters that depict the development of a surface area diffusion layer. The polymer matrix swells because of the solvent impact, leading to the formation of a surface area diffusion layer called a surface swollen layer (SSL) (130). The swelling process is naturally unstable and leads to the creation of a surface area layer that is swollen.

10.2 Swollen surface layer

The semi permeable surface layer (SSL) in a polymer is an indication of the resistance at the interphase, which impacts the movement of substances in both directions at a specific level. It consists of intricate formations that are typically present at temperatures lower than T_g. The thickness of this structure is mainly influenced by the molecular weight, temperature, and kinetic thermodynamic exercise of the solvent. Additionally, the historical past of polymer samples has a slight impact on it. As reported by Ueberreiter K. and Asmussen F. (130-136) SSL is made up of 4 layers (Figure 8). The first layer δ_1, is a liquid layer formed by solvent molecules that have been adsorbed onto the surface of polymeric substances. The second layer δ_2, is a rubber-like layer that has a fixed structure and contains many solvent molecules. The third layer δ_3, is a firm swollen layer that consists of a continuous liquid phase with a dispersed polymer that has a gel-like quality. Finally, the permeation is the fourth layer δ_4, If the temperature drops below T_{gel} ($T_L<T<T_{gel}$), δ_2 disappears and only layers 1,3, and 4 maintained. In the event the temperature drops below T_L ($T<T_L$), layers 1 and 3 aren't present, and only layer 4 forms the SSL. The thickness of every layer varies, as well as the gradient in concentration between each interface. The liquid layer as well as the rubber-like layer have comparable thicknesses, while the hard swollen layer is significantly thinner than both. At the boundary between the swollen layer that has become rubbery and toughened, there is a sudden rise in the concentration gradient. When dissolution temperatures are increased, the step that controls the rate may be the movement of solvated polymers into the liquid stage of the solvent that coexists. The movement of solvent molecules, as discussed previously (130,133,135,137) governs the polymer kinetics within a rigid polymer specimen.

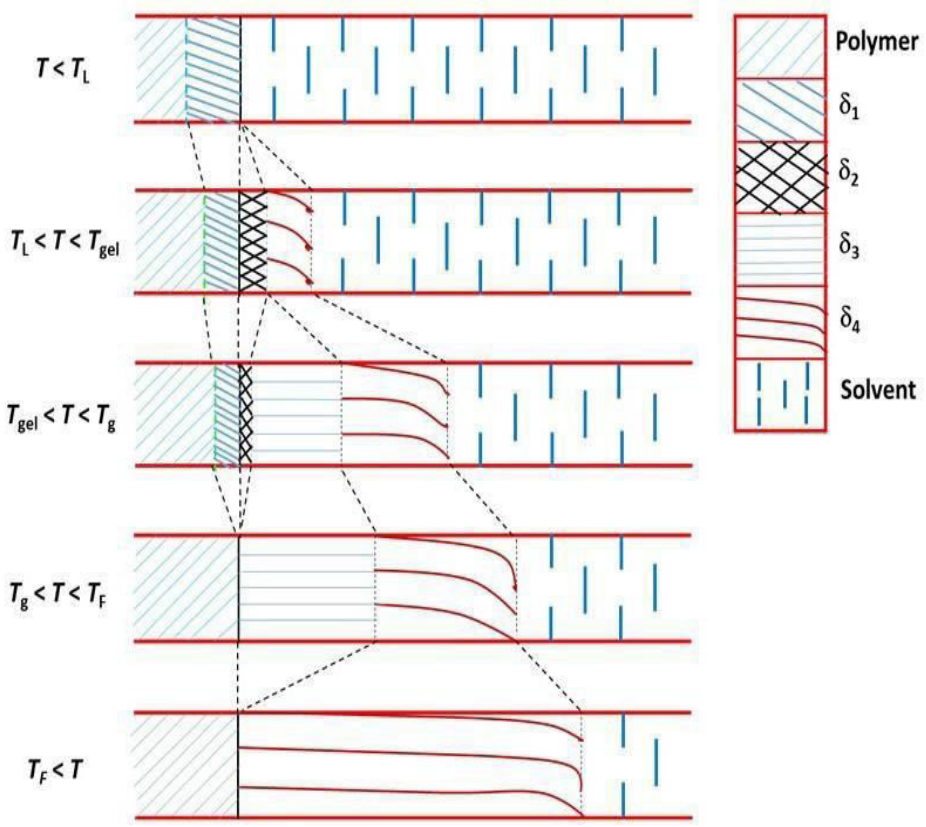

Figure 8. *Ueberreuter K. and F. Asmussen provide an account of the structure of the swollen outermost layer and a list of terms and their corresponding definitions, δ_1 refers to the liquid layer δ_2 refers to the rubber-like layer δ_3 refers to the gel-like layer, and δ_4 refers to the permeation layer. T represents the temperature at which sloughing occurs, T_L represents the temperature of the solvent's phase transition, T_{gel} represents the temperature at which gelling occurs, T_g represents the glass transition temperature of the polymer, and T_F represents the melting temperature of the polymer. These definitions were reproduced from references (130, 133, and 135).*

10.3 The kinetics study of swelling and dissolution of CMC and HEC

The swelling and dissolution of HEC and CMC is not uniform because of their intricate and multi-layered structures, which leads to the creation of structures resembling balloons. The swelling happens in specific areas of the fiber where there are differences in the structure of the walls, resulting in an expansion like a balloon. The biopolymer is in a swollen state with each balloon referring to a swollen state. The quality of the solvent (Figure 9) influences the process of swelling and dissolution (129). The ability of cellulose structures to swell and break down (i.e., dissolution) differs depending on their length, ranging from large molecules to the walls of fibers.

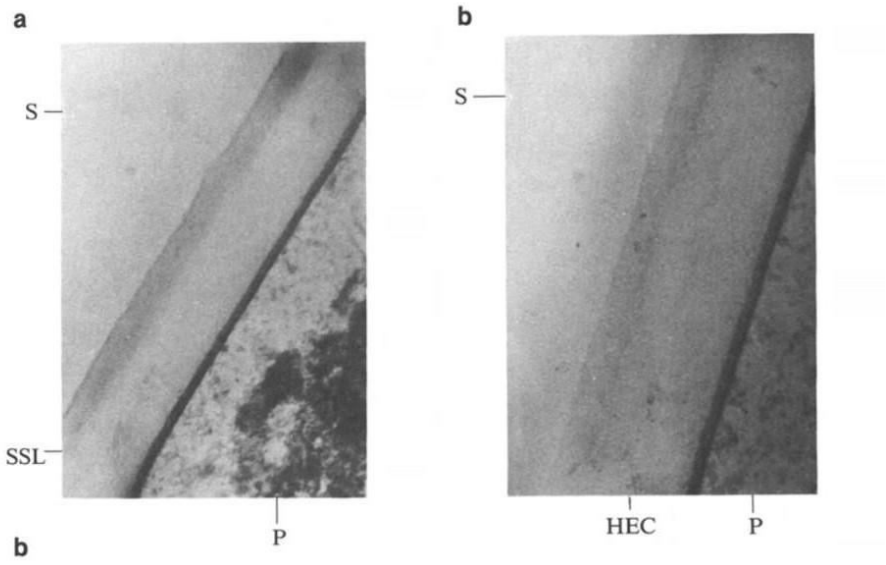

Figure 9. *Images of the swollen layer for CMC and HEC, with sizes ranging from 1cm to 0.1mm, were depicted in the study. These images had been obtained with authorization from Springer Nature under license number 5274210286515 and have been reproduced from reference 129.*

10.4 Kinetics of swelling

In real-world scenarios, it is advantageous to possess absorbents that exhibit a greater ability to swell and absorb. The swelling process is heavily impacted by a few factors including the ability to swell, the range of particle sizes, the surface area, and the composition of the polymer as shown in (Figures 10 and 11) and (Table 5) (141-143). The impact of these factors on the ability to swell has been examined by numerous researchers (144,145). For example, Metz and colleagues. (146) conducted a study on superabsorbent polymers to examine how particle size affects their ability to absorb water. The results showed that as the particle size increased, the rate of water absorption also increased. One possible explanation is that tiny particles offer a greater surface area for water to be absorbed (147).

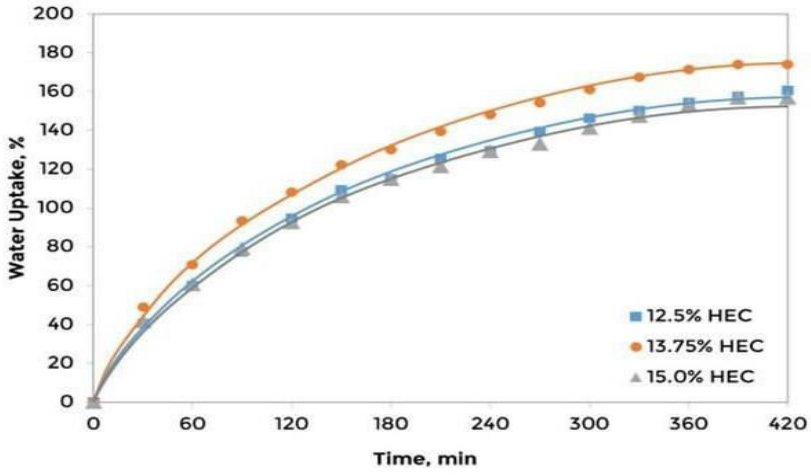

Figure 10. *The HEC hydrogel patterns' capacity to absorb water over time is depicted in the image reproduced from reference 141, with the consent of Trans Tech Publications Ltd. Demand ID 600074454.*

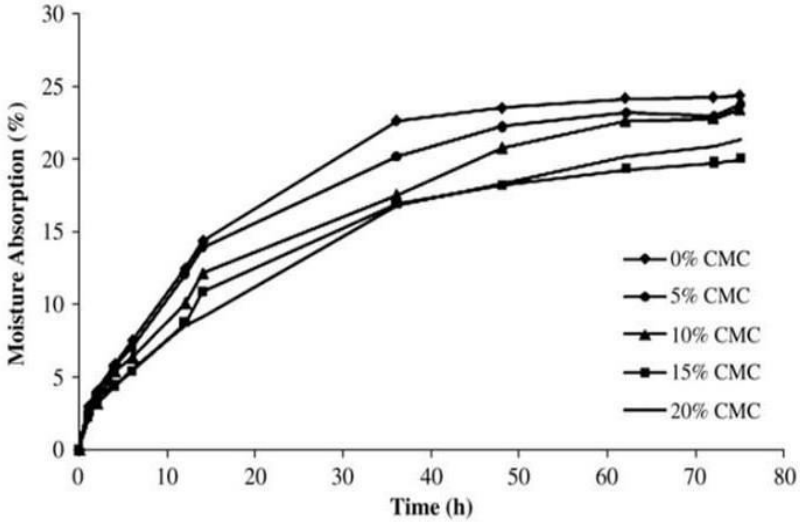

Figure 11. *The concentration of CMC determines just how much moisture starch films are able to absorb. (Reproduced from the reference. 142). Elsevier has been given permission with license number 5274220418935.*

	12.5% HEC	**13.75% HEC**	**15.0 % HEC**
% Maximum Water Uptake	160.5	173.8	156.9

Table 5. *The highest amount of water intake by hydrogels from reference 142, Trans Tech Publications Ltd. is mentioned with ID number 600074454 has been requested.*

The aim of the study was to examine the creation of a hydrogel made from CMC-N-isoPropylacrylamide and the rate of its swell ability by the time. The consider research confirmed that the swelling kinetics are impacted by the size of the particles. (Figure 12) illustrates that water absorption increased dramatically and then stabilized as demonstrated in the (Figure 12). (147).

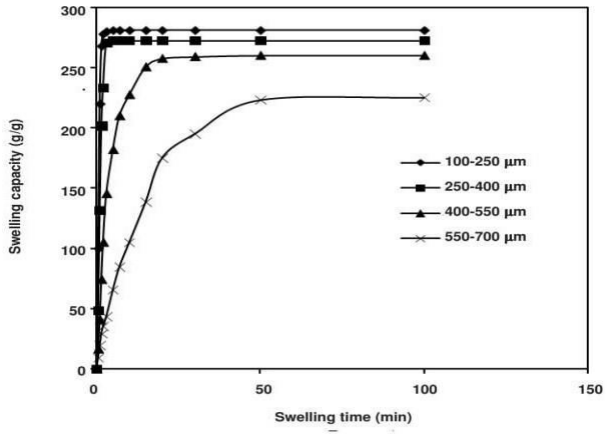

Figure 12. *The swelling kinetics of the CMC-g-PMAAm-coPNIPAAm over-absorbent hydrogel, which comes in different particle sizes, is demonstrated in the image (Reproduced from ref.147) with the consent of Asian Publication Corporation.*

Presuming that swelling follows second-order kinetics, we can mathematically express the speed of swelling at any time.

$$\frac{dW}{dt} = K\,(W_\infty - W)^2 \tag{8}$$

In this context, W represents the amount of water present in the superabsorbent material at a specific time t. W∞ refers to the initial amount of water content before reaching equilibrium, and K is a constant. Rewriting the equation by rearranging it after replacing Equation (8) with t = 0 and W = 0 to W:

$$\frac{t}{W} = \frac{1}{KW_\infty^2} + \frac{1}{W_\infty}t \tag{9}$$

The composites with high absorbency rates show expansion that follows second-order kinetics, as shown in Figure 13 (143-147).

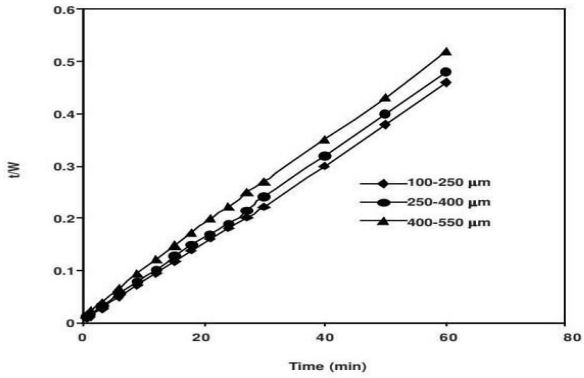

Figure 13. *In order to analyze second-order kinetics, create a graph of t /W against time using superabsorbent hydrogels with varying particle sizes in accordance with Equation (9). (From ref. 147). Authorized by the Asian Publication Corporation.*

Hydrogels produced from HEC (148) exhibited comparable outcomes. Co-polymerization of HEC, sodium acrylate and medicinal stone (MS) led to the creation of composite hydrogels in this particular study. In order to examine how MS, particle size, and saline solution influence the kinetics of swelling, the analysis of (Figure 14) (148) was focused on kinetic swelling.

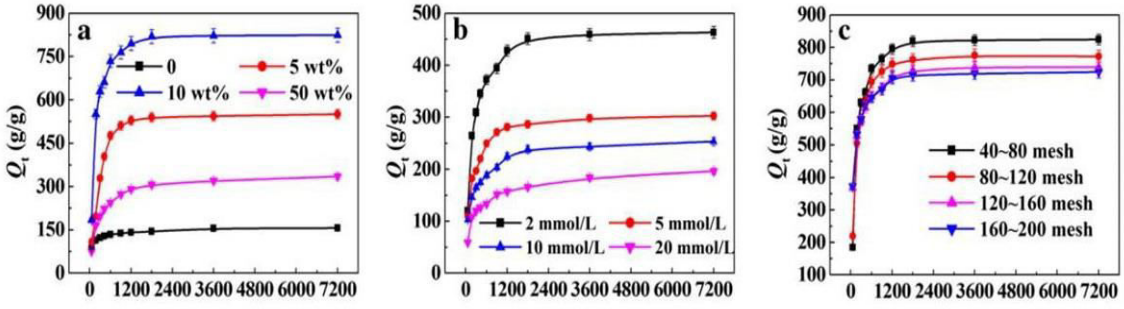

Figure 14. *(a) The changes in swelling kinetics of the hydrogels in pure water (with different MS dosages of 0, 5, 10, in addition to 50 wt.%), (b) the influence of saline solution with different levels on the swelling kinetics of the composite hydrogel (with an MS dosage of 10 wt.%), and (c) the effect of particle size on the swelling kinetics of the composite hydrogel (with an MS dosage of 10 wt.%) were investigated (Reference number 148). Request ID 600074472 from Elsevier.*

According to the findings, the rate of swelling was quicker in the initial 600 seconds and subsequently declined until it leveled off. To assess how hydrogels swell kinetically, the Schott Equation (10) was utilized, which is a second order swelling kinetic model as described in reference (149).

$$\frac{t}{Q_t} = \frac{1}{K_{is}} + \frac{1}{Q_\infty} t \qquad (10)$$

In this context, Q_t represents the swelling amplitude of the hydrogel at a specific time t in grams per gram, Q_∞ refers to the theoretical equilibrium swelling amplitude also in grams per gram, and K_{is} is represents the initial swelling rate constant measured in grams per gram per second.

10.5 Kinetics of dissolution

Different factors have an impact on the breakdown and dissolve of polymeric substances, but the speed at which they permeate the polymer matrix is the primary determinant. The speed at which diffusion occurs is influenced by several factors including the polymer's chemical structure, the solvent used, and the functional groups attached to the polymer chain. These factors include the density of cohesive energy, the size of the solvent molecules, the temperature at which dissolution occurs, the molecular mass of the polymer, and the arrangement of its structure. When the solvent meets the polymer, its molecules spread and diffuse throughout the polymer matrix, leading to the creation of the Solvent-Solid Layer (SSL). The thickness of this layer can differ depending on factors such as the temperature at which dissolution occurs, how quickly the mixture is stirred, the polymer's molecular weight, the solvent's thermodynamic and kinetic activity, and the thermal background of the polymers (131,132,150-153). According to Asmussen and Ueberrreiter, the swollen layer present on a polymer's surface has a complicated structure that is influenced by the dissolution temperature. This layer acts as a distinct interfacial resistance which governs the movement of molecules in both directions across the interface (150). When the dissolution temperature (T) is within the range of the gel point temperature (T_{gel}) along with the glass transition temperature (T_g), where ($T_{gel}<T<T_g$), the polymer surface layer exhibits a complicated composition comprising liquid (δ_1), rubber-like (δ_2), rigid swollen (δ_3), and permeation (δ_4) layers. The swollen polymer layer's thickness and layer distribution are illustrated in (Figure 15), which is also (150).

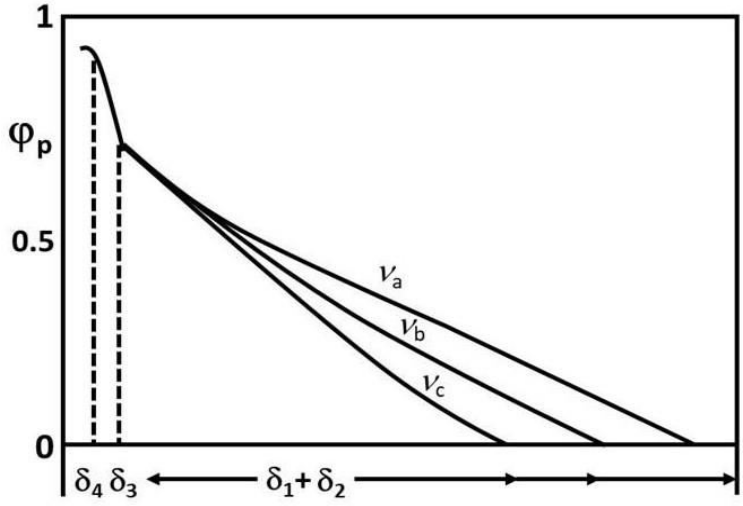

Figure 15. *The spread of the polymer focuses on the swollen layer, which is made up of four layers: (δ_1-liquid, δ_2-rubber-like, δ_3-rigid swollen, and δ_4-permeation layers), varies depending on the mixing rates (with v_2 being the highest, followed by v_1, and $v_{0=0}$ being the lowest). The volume fraction (φ-volume) of the polymer is also a factor in this distribution. This information was obtained (Courtesy of a ref.150).*

10.6 Cross-linkers for creating gel-polymer

The gel is made up of interconnected and cross-linked net structures of hydrophilic polymers that are soluble in water and can expand and swell when they absorb water. Mechanical and physical cross-linking techniques can be used to create hydrogels from natural polymers (154). The arrangement of polymeric networks relies entirely on the presence of either covalent bonds or physical interactions among separate macromolecules. Nevertheless, a sequential secondary linearly chains interfere with each junction of the entire polymeric system net, leading to break alternatively and diffuse based on the chemical composition and length of the polymer chains and cause forming flexible and elastic substances. On the other hand, inflexible secondary chains lead to the formation of stiff and brittle substances. Stable elastomeric networks possess the distinctive quality of being able to swell when exposed to compatible solvent systems. The volume has the capability to be raised up to a thousand percent (155). The creation of cross-links can be made easier through chemical reactions that are activated by pressure, radiation, heat, and alterations in pH values (156). Cross-linking may be accomplished by means of chemical reactions like polycondensation or polyaddition, or through the physical intertwining of macromolecular chains. The process of helix-coil transition involves the tangling and untangling of large molecular chains in a polymer solution due to changes in pH and temperature, as stated in ref. (157.158). Cross-links were generated by combining particular chemical substances, such as cross-linking agents, with resin that was either partially polymerized or not polymerized at all (159). The improvement of starch performance in different uses is frequently achieved through cross-linking (160). A number of substances, including sodium trimetaphosphate, phosphorus oxychloride, epichlorohydrin, citric acid, diphenyl sulphone, anthracene endo-peroxide (161-163), sodium tripolyphosphate, and 1,2,3,4 diepoxybutane, are used to enhance the physical characteristics of materials and the resistance to water of starch-based products (154). The chemical modifier Divinyl sulfone (DVS), which has a length greater than zero, has been extensively used to enhance the mechanical properties and performance of polymers through chemical modification (Figure 16). The pharmaceutical industry has extensively utilized it in addition to cellulose and its derivatives. The rheological advantages of a biopolymer are directly related to its concentration of DVS. Research has discovered that increased levels of DVS lead to an elevation in viscosity, which suggests a greater degree of cross-linking within the biopolymer (164).

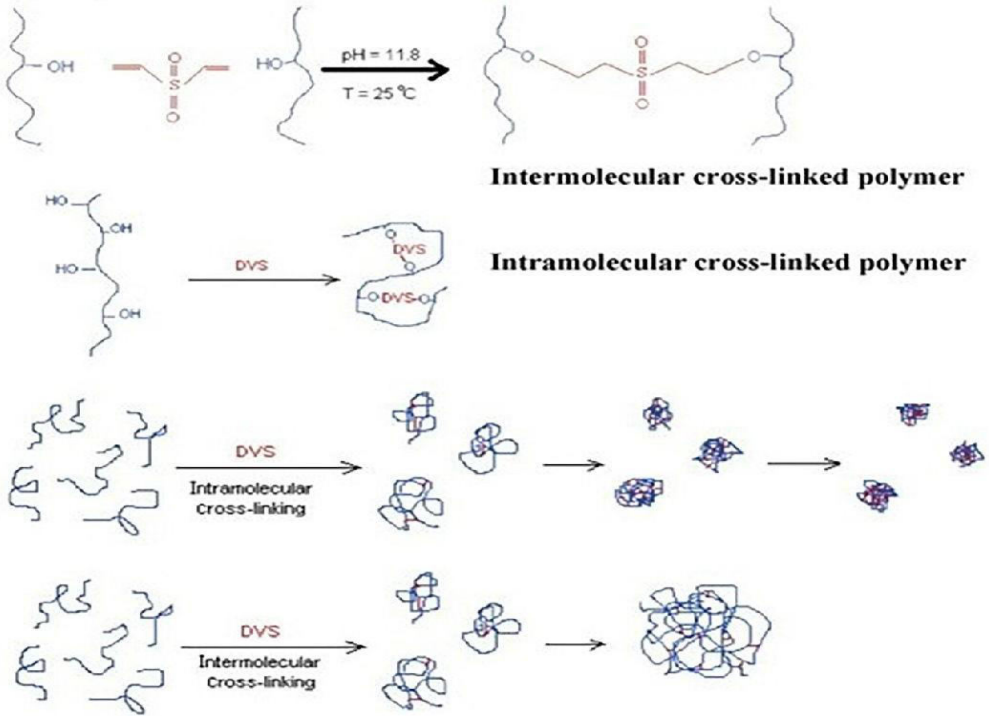

Figure 16. *The process by which the cross-linker reaction occurs and a visual depiction of the cross-linking within and between polymer chains are shown in a figure (164) Reprinted with permission from Atoosa Maleki, Anna-Lena Kjøniksen, Bo Nyström: "Effect of shear on intramolecular and intermolecular association through cross-linking of Hydroxyethylcellulose in the dilution aqueous solutions"; The Journal of Physical Chemistry B, 109 (Jun 1) 12329–12336 (2005). Copyright 2005 American Chemical Society.*

Micelles and polymers can supply the fundamental ingredients for bigger structures as aggregate co-polymers. Whenever surface-active agents are present these micelles can arrange themselves and create liquid crystalline systems (165).

11. Conclusion

The applications potential, natural breakdown, and distinctive characteristics of biopolymers have drawn significant interest in recent years across various industries. The dissertation examined several biopolymers (cellulose derivatives, starch, chitosan, and protein-based biopolymers). Biopolymers possess broader structures, slim films, and flexibility enabling a variety of smart uses. The evaluated biopolymers hold great possibility for constructing novel high-tech coatings for biomedical and non-biomedical applications. The biomedical uses of cellulose derivatives depend upon their lightweight features and compatibility with living organisms. Cross-linked starches are being studied for their unusual mechanical strength and water resistance. The dissertation thus gives a promising starting spot for scientists to investigate the uses of biopolymers in different areas. While biopolymers are analyzed a lot more profoundly, specialists are wanting to produce more advanced as well as substantial elements, opening the door for natural biopolymer coatings to correspond to the environment and operator requirements far more closely.

*****

12. Projects

12.1 Study of the material engineering properties of high-density poly(ethylene)/perlite nanocomposite materials

Our published research paper B focused on the effect of perlite mineral as being a nanofiller in polymer nanocomposites for exclusive needs. Re-search demonstrated that the thermal and mechanical characteristics of HDPE compounds had been considerably influenced by the perlite nanofiller concentration. An important finding was that Young 's modulus of elasticity increased as the amount of the filler increased. It means that the stiffness of the HDPE composites was improved with the inclusion of perlite. This outcome was backed by both destructive uniaxial tensile mechanical strength and nondestructive vibrator mechanical dynamic testing, which measured via displacement transmissibility working with excitation forced oscillation damped a single-degree-of-freedom (SDOF) technique followed by thermal analysis as well. Nevertheless, the study as well observed a decreasing trend in fracture toughness strength as the perlite concentration increased. This implies that the presence of perlite resulted in a weak fracture (brittle fracture) conduct in the HDPE composites. Furthermore, SEM examination proved that ductile fracture processes occurred at climbing filler concentrations. This suggests that the composites exhibited both ductile and brittle fracture surfaces, based on the perlite concentration. Additionally, SEM imaging demonstrated that the filler particles and polymer chains had comparatively strong bonds. This implies great interfacial interaction and adhesion between the HDPE matrix as well as the perlite filler. Overall, the study demonstrated the substantial impact of perlite as a nano filler on the thermal and mechanical properties of HDPE composites, with improved stiffness along with an intricate fracture behavior (i.e., ductile and brittle) based on the perlite concentration. The solid bonding between the polymer chains as well as the filler particles further highlights the possibility for perlite to improve the functionality of polymer nanocomposites in specialized aims.

12.1.1 Materials

White pellets with lot number 1I19091333 of HDPE type 25055E on the Dow chemical company from (USA) have been utilized. The inorganic volcanic glass mineral perlite (Supreme Perlite Company, USA), with a d50 diameter of 447 nm along with a density of 1.10 g/m^3, continues to be used as filler particles (166). Perlite filler moisture content was 0.1 wt.%. 150 composite specimens of perlite/HDPE composites with inorganic filler percentages of five, ten, in addition to fifteen wt.% were made (dog bone design for tensile evaluation, Charpy's pendulum, and then damping dynamic vibrator examination). On the (German Arburg Allrounder) type 420 injection molding machine, composite specimens were made utilizing the injection molding technique. Applied processing temperature ranged from 190 to 220°C, mold temperature 30°C, injection pressure sixty MPa, and also injection rate 20 mm/s (167). Extrusion machine Scientific was used for composite and virgin samples extrusion at the handling ranging from 136 to 174°C, L/D = 40.

12.1.2 Methodology

12.1.2.1 Scanning electron microscopy

Images from an SEM were taken with a Hitachi SU 6600 (Japan) SEM. The Schottky cathode serves as the electron's origin. This microscope has a resolution in secondary electron mode (SE) of 1.3 nm and in backscattered electrons (BSE) of 3 nm. For these pictures, the SE and an accelerating voltage of 5 kV were employed. There was a 6 mm gap between the specimen and the sensor. Studied materials were placed on double-sided carbon tape on an aluminum holder.

12.1.2.2 Thermal analysis

Virgin HDPE thermogravimetry as well as DTA studies were carried out for perlite/HDPE nanocomposites using a concurrent DTA-TG device (Shimadzu DTG 60, Japan). Observations were made between 30 and 550°C at a heat flow rate of 10°C/min in an evolving nitrogen environment (50 ml/min). The crystallinity (Wc) of the nanocomposites was calculated according to the Formula (11) (168,169):

$$W_C = \frac{\Delta H_m}{\Delta H_m^0} \times 100 \tag{11}$$

Here: ΔH_m^0 = 293 J/g is the heating of fusion for 100% crystalline material HDPE, warmed at a speed of 10°C/min (168-170), and ΔH_m J/g is calculated heat of fusion.

12.1.2.3 Uniaxial tensile testing

Injection-molded specimens had been mechanically tensile tried on a Zwick 1456 multifunctional tester (Germany). The measurements had been recognized according to CSN EN ISO 527 1 and CSN EN ISO 527 2 standards (171). Samples have been strained at ambient temperature up to fracture point at the test speeds of 50, 100, and 200 mm/min. Young 's modulus of elasticity and elongation at break happen to be computed from the stress strain correlations. Each experiment was repeated10 times at the surrounding temperature of 22°C, along with average values and standard faults have been calculated.

12.1.2.4 Charpy impact testing

With a fall energy of 25 J, impact testing was performed on the (German made) Zwick 513 pendulum impact tester according to CSN EN ISO 179 2 standards.

12.1.2.5 Displacement transmissibility measurement

The displacement transmissibility T_d (Equation 12), that will be denoted through the system (172,173), talks about the component 's capability to control dynamic mechanical damped vibrations which is excited harmonically induced in single-degree-of-freedom systems:

$$T_d = \frac{y_2}{y_1} = \frac{a_2}{a_1}, \tag{12}$$

Where y_1 is the displacement capacity on the examined specimen input side and y_2 represents the displacement amplitude over the specimen output side, a_1 is the speed amplitude over the input side with the tested sample and a_2 is the acceleration amplitude over the output side with the examined sample. Based on the magnitude of the displacement transmissibility, there are

generally 3 major types of dynamic vibrations: resonance (T_d>1), undamped (T_d=1), and as well damped T_d(-) or (T_d<1) vibration (173). The consequent Formula (13) (172-174) provides the displacement transmissibility of a spring mass damper process, that is represented through the spring 's stiffness (k), damper's damping coefficient (c), and the mass (m):

$$T_d = \sqrt{\frac{k^2+(c\times\omega)^2}{(k-m\times\omega^2)^2+(c\times\omega)^2}} = \sqrt{\frac{1+(2\zeta\times r)^2}{(1-r^2)^2+(2\zeta\times r)^2}} \quad (13)$$

Where exactly the coming equations (14) and (15) (175,176) are used to explain the damping proportion ζ along with the frequency proportion, respectively:

$$\zeta = \frac{c}{2\sqrt{k\times m}}, \quad (14)$$

$$r = \frac{\omega}{\omega_n} = \frac{\omega}{\sqrt{k/m}}, \quad (15)$$

where ω_n is the purely natural frequency plus would be the oscillation frequency (177,178), And finding the frequency ratio r_0 where displacement transmissibility reaches its greatest point (172) is possible if dT_d/d_r = zero in Equation (13):

$$r_0 = \frac{\sqrt{\sqrt{1+8\zeta^2}-1}}{2\zeta} \quad (16)$$

Formula (16) makes it very clear that with a much better damping ratio ζ the regional maximum of the displacement transmissibility is normally transferred to lower amounts because of the frequency ratio r (or with the reducing material stiffness k). The area extrema (i.e., Equation 16) results probably the highest amount with the displacement transmissibility $T_{d\ (max)}$ in the frequency ratio r_0 . The forced oscillation technique was utilized to estimate the values under investigation for dynamic vibration damping. At frequencies between 2 to 3,200 Hz, the T_d was driven using the BK 4810 vibrator along with a BK 3560-B-030 signal pulse multi analyzer and also a BK 2706 power amplifier. Employing BK 4393 accelerometers (Brüel & Kjaer, Nrum, Denmark), the acceleration intensities (a_1 and a_2) on the input and output sides of the considered samples were measured 3 featured inertial masses of bandwidth 0, 90, and 500 g - that were set on top of the periodically evaluated specimens were used to define the displacement transmissibility. The studied block item dimensions were (60 × 60 × 3) mm (length × width × thickness). Each measurement was placed five times at a temperature of 23°C.

\

12.1.3 Results and discussion

As reported in earlier studies (171), inorganic nano/microparticles are used as functional fillers to alter the elastic plastic aspects of polymer composites. It was discovered that the key drivers of the adjusted react structures of these supplies tend to be the physicochemical attributes of the polymer matrix, LLDPE, LDPE, and HDPE alongside the properties of the filler particles (like morphology, diameter, shape, and functionalization of the surface chemistry). The ratio alongside the polymer matrix's amorphous to crystalline regions and the effectiveness of the interface adhesion between the filler molecules as well as the polymer matrix are two extra essential details which should be taken into our consideration (179). SEM pictures of the perlite micro/nano filler particles are shown below in (Figure 17a and 17b).

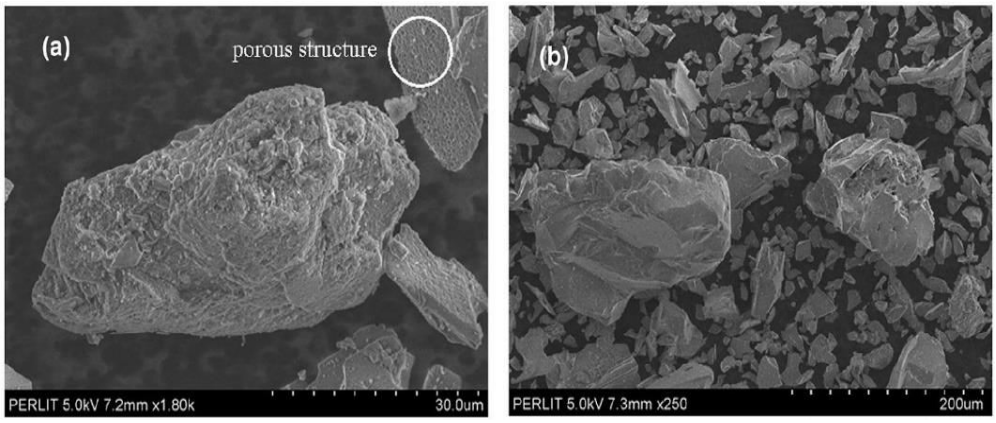

Figure 17. *The perlite micro/nano-filler is depicted in an SEM image.*

There is evidence confirming their permeable (porous) inner composition is supported by proof (Figure 17a). It is generally understood from a variety of sources (166,180,181) that the sound absorption, vibration damping, and dynamic mechanical characteristics of fillers or entire composites are directly influenced by their porous micro/nanostructures (167,182,183). The concentration of filler has a noticeable impact on the Young's modulus of elasticity (E) in the perlite/HDPE composites tested, as shown in (Figure 18).

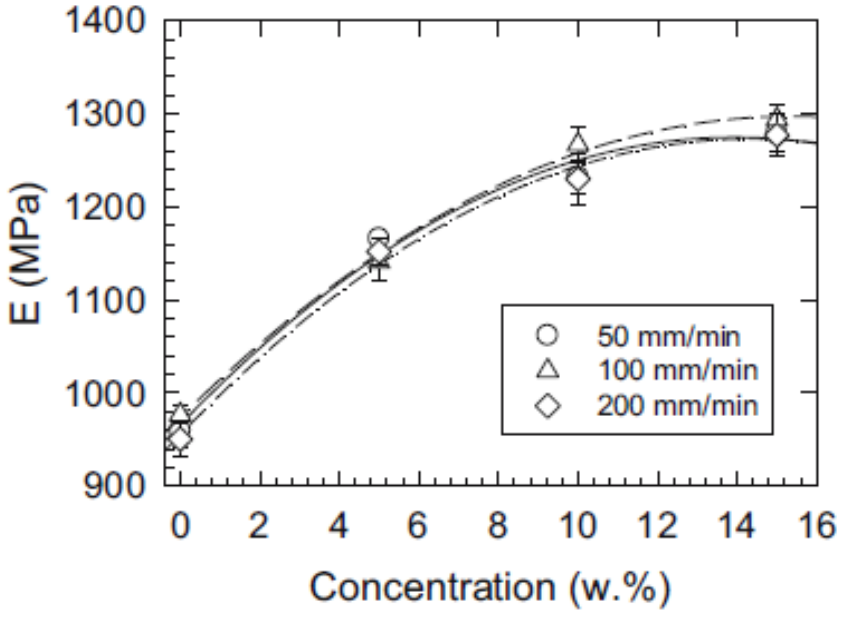

Figure 18. *The relationship between the concentration of inorganic perlite fillers and the modulus of elasticity (E) of Young's approach. Inset: Rates of deformation applied.*

The steady increase in E with greater perlite content was characterized by deformation rates of 50, 100 as well as 200 mm for all research. A 37% increased E was observed for HDPE samples that contain 15 wt.% perlite, which is the same as the E value of pure HDPE. This led to a significant increase in the stiffness of the materials. As illustrated in (Figure 19), there had been a gradual decrease in the elongation at break observed with increasing filler content, following an exponential pattern.

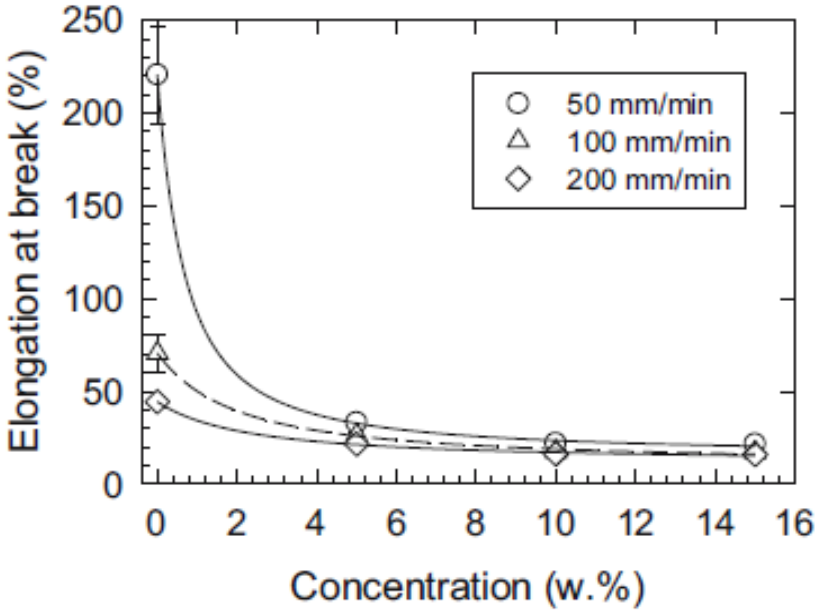

Figure 19. *Perlite filler concentration vs elongation at break. Inset: Rates of strains applied.*

The (Figure 20) indicated the consequences of fracture toughness evaluation was done.

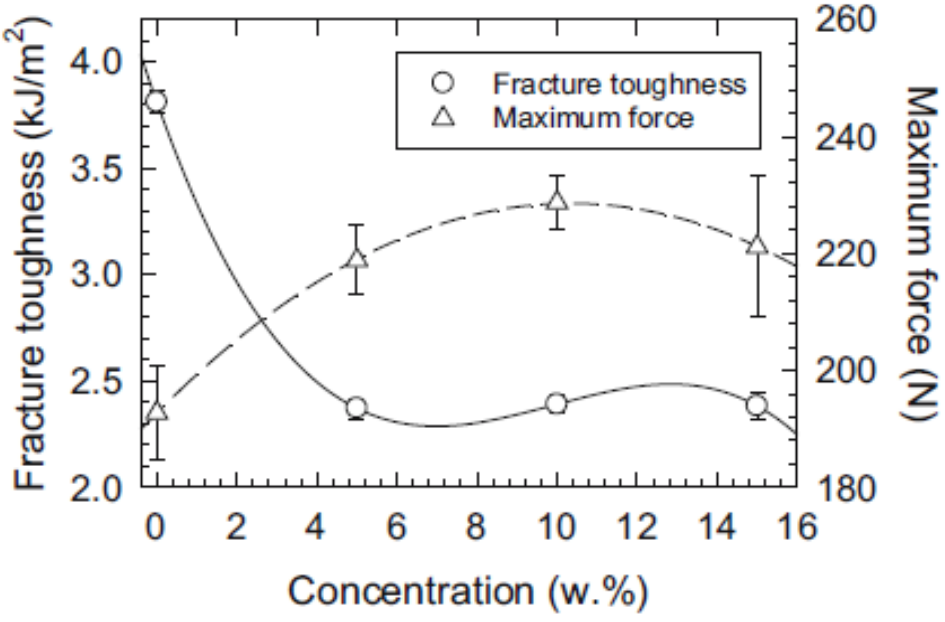

Figure 20. *The correlation between the concentration of inorganic perlite fillers as well as the maximum force and fracture toughness is interdependent.*

The fracture toughness of perlite/HDPE composites showed a substantial decrease, going from 3.8 kJ/m^2 (for pure HDPE) to 2.4 kJ/m^2 within the perlite concentration range of 5 to 15 wt.%. The addition of the mineral filler increased the stiffness of the composite material, as demonstrated during the previous uniaxial tensile testing. This was evident in the increasing modulus (E) as the concentration of filler increased. The Charpy pendulum was utilized to confirm the impact strength during the assessment of fracture (Figure 20) because of the rise in both the maximum force as well as the filler content concerning. The suggested mechanism for transferring mechanical energy, it is apparent from the scanning electron microscope pictures (Figure 21) that there are distinct areas of brittle fracture, as seen in (Figures 21a and 21b), as well as polymer regions that have undergone plastic deformation, characterized by the presence of spurs and deformation shear bands, which are typical of ductile fracture interfaces.

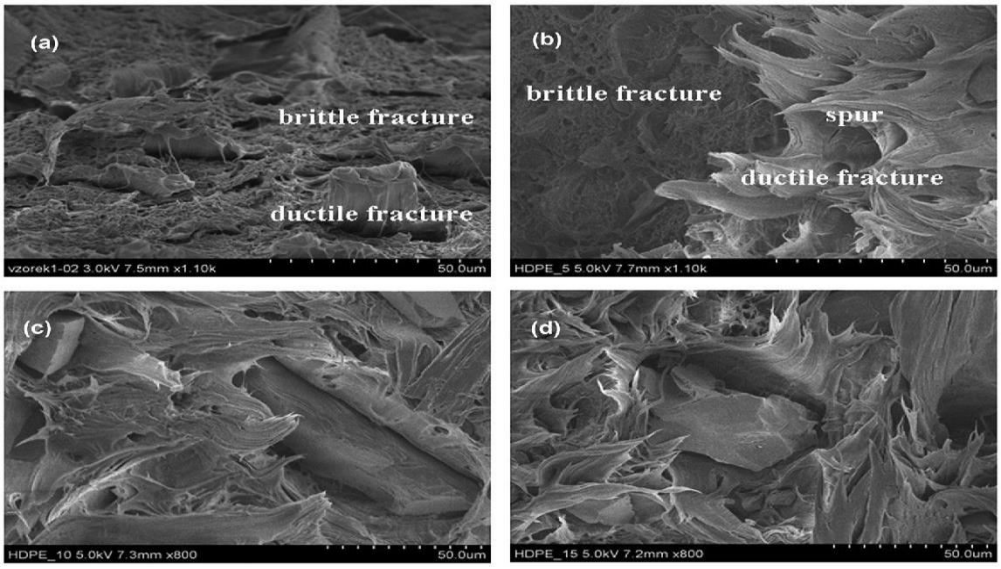

Figure 21. *Scanning electron microscope (SEM) images of the fractured surface were observed after conducting mechanical tensile tests on the samples. HDPE composites with perlite content of 5%, 10%, along with 15% by weight. (Applied deformation rate: (50 mm/min).*

The investigation of the frequency's correlation to the displacement transmissibility which was used to determine the dynamic mechanical vibrations aspects of the composite materials being undergone the examination are displayed in (Figures 22 as well as Figure 23).

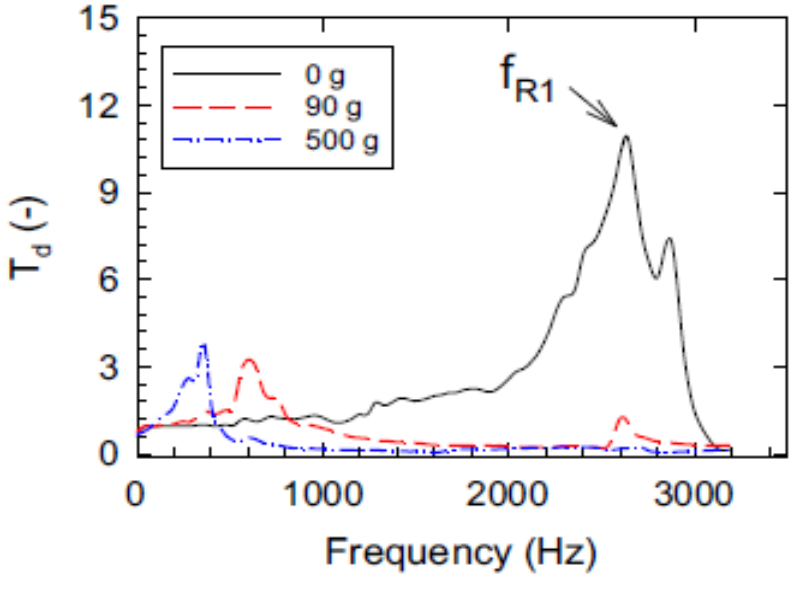

Figure 22. *Relationship between displacement transmission frequency and tested perlite/HDPE composites). The concentration of perlite without any inertial mass is zero.*

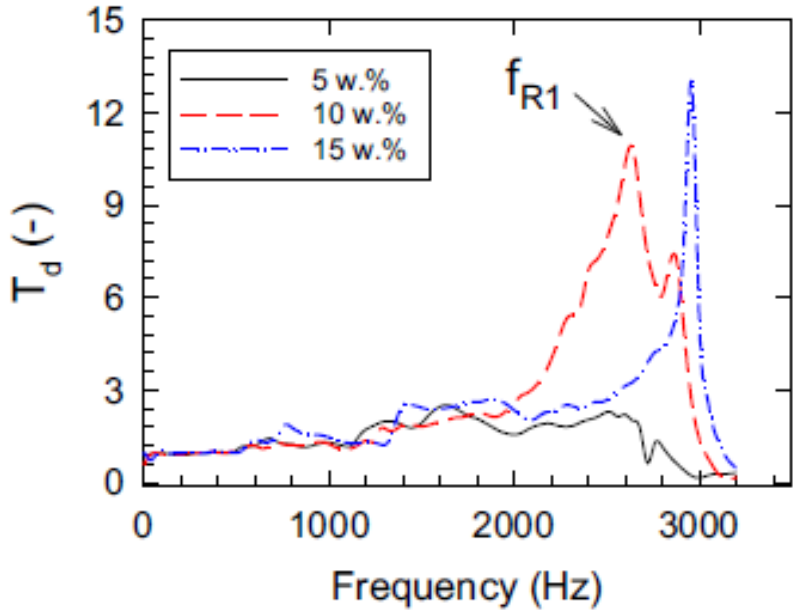

Figure 23. *The displacement transmissibility of the perlite/HDPE polymer nanocomposites under examination was frequency dependent. The inertial mass contains 10 weight percent of perlite.*

The position of the first resonance frequency peak (f_{R1}) in (Table 6) suggests that there is increased stiffness in materials with higher filler concentrations. This is in line with the displacement transmissibility frequency patterns revealed in (Figures 22 as well as 23).

c [wt%]	**Quantity**	**Inertial mass (g)**		
		0	90	500
5	f_{R1} [Hz]	1,614 ± 72	593 ± 26	341 ± 15
	T_{dmax} [–]	2.5 ± 0.2	3.1 ± 0.2	3.7 ± 0.3
10	f_{R1} [Hz]	2,627 ± 112	603 ± 25	346 ± 16
	T_{dmax} [–]	12.1 ± 0.9	3.3 ± 0.2	4.5 ± 0.4
15	f_{R1} [Hz]	2,944 ± 129	626 ± 28	396 ± 17
	T_{dmax} [–]	14.2 ± 1.1	4.6 ± 0.3	4.8 ± 0.4

Table 6. *The composites that were examined were subjected to harmonically induced vibrations in order to ascertain their initial resonance frequency, f_{R1}, and their maximum displacement transmissibility $T_{d\,(max)}$ that could be accommodated. the concentration of c-perlite.*

Equation (16) was evaluated for accuracy, and the results demonstrated that the f_{R1} peak position moves towards higher excitation frequencies as stiffness increases (or damping ratio decreases). The results of the mechanical tensile testing, which included measuring the concentration of perlite within the polymer composite matrix, were in complete agreement

with the resulting dynamic mechanical vibrations behavior, while conducting vibrational tests, it was noticed that an increase in inertial mass caused a shift of f_{R1} towards lower frequencies of excitation harmonically. The observation that the normal frequency decreases with an increase in inertial mass (m) is supported by Equation (14), which in turn results in an alongside decrease in f_{R1}. The vibration damping method enables the evaluation of stiffness of polymer nanocomposites without causing any harm or destructive, unlike the damaging or destructive tensile or fracture assessments. The thermal analyses are presented in (Table 7) and (Figure 24).

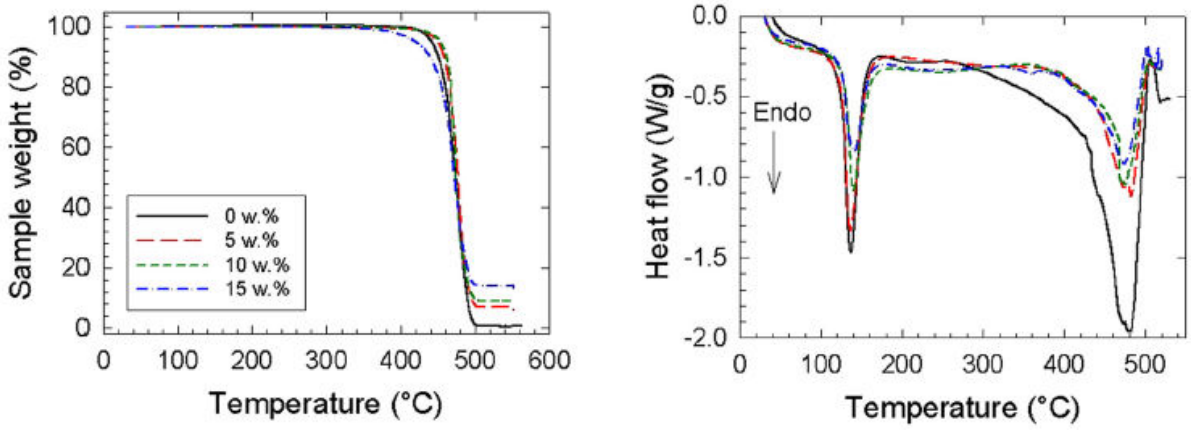

Figure 24. *The TG-DTA thermal examination results for the perlite/HDPE polymer nanocomposites have been determined. Inset: Concentration of perlite.*

c [wt%]	T_m [°C]	ΔH_m [J g^{-1}]	w_C [%]	T_A [°C]	T_D [°C]	TWL [%]
0	137.4	177.7	60.65	455	477.2	100.0
5	136.4	133.9	48.10	463.9	476.1	93.1
10	139.9	92.9	31.44	462.1	474.7	90.0
15	141.6	82.5	28.59	451.3	474.3	86.2

Table 7. *The study examined the thermal properties of both pure HDPE and polymer nanocomposites made with perlite and HDPE. The analysis focused on a number of parameters including the concentration of filler (c), the melting peak point (T_m), the temperature of fusion (H_m), the crystallinity (W_c), the peak of fission in the (DTA) curve (T_D), the initial point (T_A), the total weight loss (TWL), and the endothermic course of action for Hm for each specimen. The temperature range for the analysis was between 95 and 175 degrees.*

12.1.4 Conclusion

The study investigated the influence of perlite mineral filler on the mechanical and thermal properties of HDPE polymer nanocomposites. The findings demonstrated that as filler content increased, Young's modulus of elasticity gradually rose with the decline in elongation at break. At 15 wt.% perlite concentrations, there was a 37% increase in Young's modulus of elasticity compared to the virgin HDPE. Nondestructive dynamic mechanical vibrator testing confirmed the increased stiffness, as indicated by the shift of the first resonance frequency peak position to higher excitation frequencies. However, the fracture toughness showed a decreasing trend with increasing perlite concentration, suggesting brittle fracture occurrence. Regions of ductile fracture processes were observed at higher filler concentrations through SEM images, which were characterized by polymer deformation shear bands and spurs. In the complicated composite matrix, the perlite particles behaved as stress concentrators The research also discovered a little rise in melting temperature with rising filler concentration, suggesting a more solid link between the polymer chains and the filler particles. Ultimately, the findings imply that the thermal and mechanical characteristics of HDPE polymer nanocomposites are considerably influenced by the perlite mineral filler.

*****

12.2 Enhancement of the mechanical properties of HDPE mineral nanocomposites by filler particles modulation of the matrix plastic/elastic behavior

The research paper C investigates the use of two separate mineral fillers at the nanoscale level (nanoclay and nano calcium carbonate) in the production of HDPE materials. The composites that were created were analyzed for their physical and mechanical characteristics. Making use of various techniques such as scanning electron microscopy, transmission electron microscopy, along with energy dispersive spectroscopy, the scientists confirmed that the fillers in the tested samples were evenly distributed. According to the study, the addition of fillers enhanced the mechanical characteristics of polymer composites. Due to the inclusion of additional fillers, there was an increase in both the elastic modulus as well as the indentation modulus. The final composites plastic-elastic mechanical performance was affected by the filler type and concentration used. In summary, the research indicates that incorporating nanosized mineral fillers, like nano calcium carbonate and nanoclay, can enhance the physio-chemical characteristics of HDPE composites. The specific impact varies based on the type and amount of filler used.

12.2.1 Materials

The material utilized in our study was HDPE of HD8100M quality, which was obtained from polymer marketing company limited in (Thailand). The density measurement was 0.952 grams per cubic centimeter, while the melt flow index was 0.25 grams per 10 minutes. The nano calcium carbonate particles referred to as adaCAL-N1-C were procured from Adacal co. located in (Turkey) and underwent stearic acid treatment prior to being processed. The scanning electron microscopy (SEM) confirmed that the particles had an average size of 0.05 m. The nanoclay particles, specifically EsanNANO 1-140, were provided by Eczacbas Esan in (Turkey) and their average size was determined to be 2.7 μm through laser diffractometer measurements. The uniform distribution of nanofillers within the HDPE matrix was verified by TEM and SEM pictures (Figure 25), and this was additionally supported by EDS mapping.

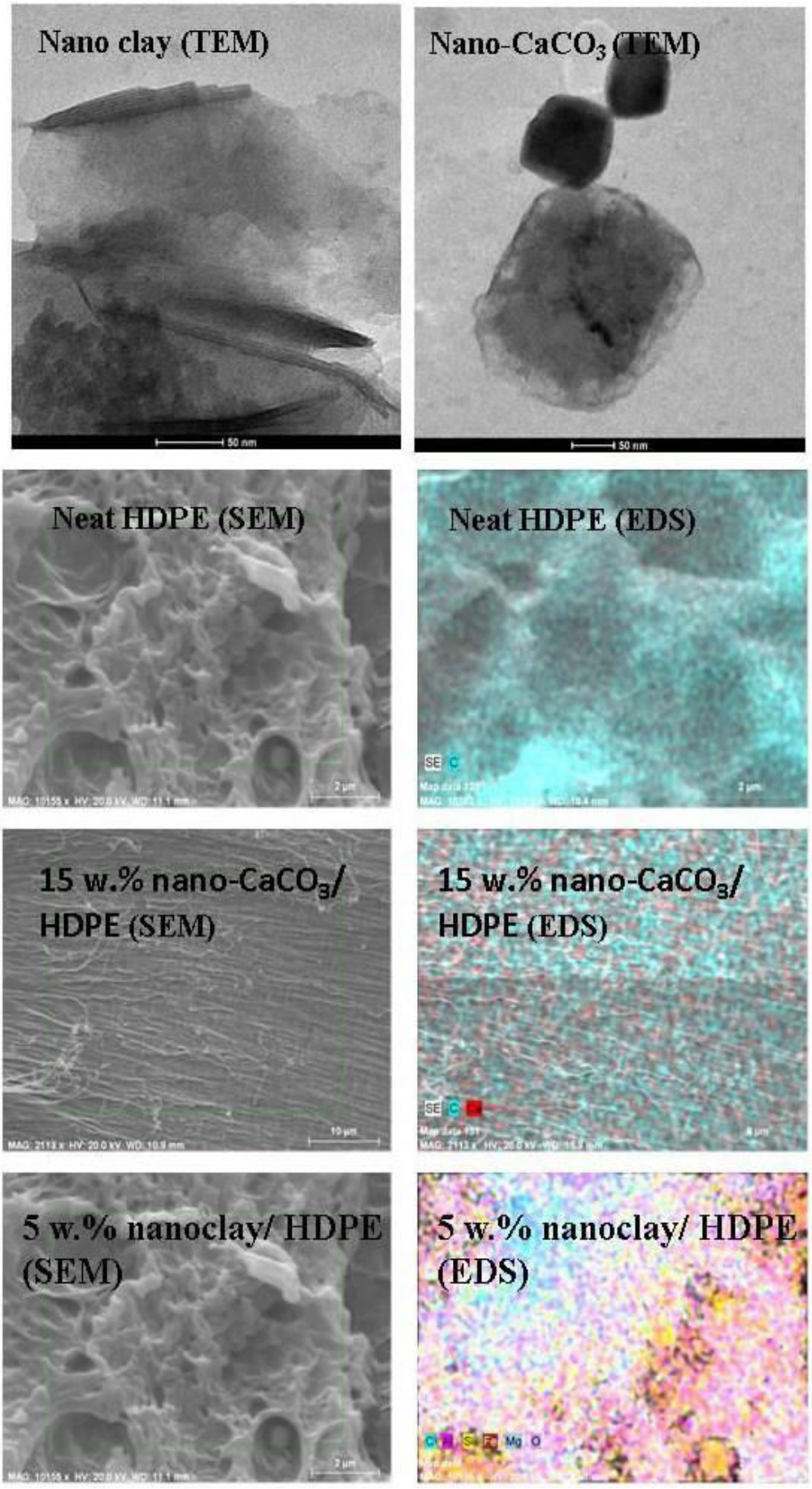

Figure 25. *This research utilized inorganic nanofillers that were pictured on TEM. Nanoclay as well as nano calcium carbonate are additionally found.*

The chemical and physical features of the fillers are given in (Table 8) and are available in refs (184,185).

Filler type	Color	Density (g/cm^3)	Surface area (g/m^2)	Particle size (μm)
Nanoclay	Highly white	1.98	19	2 – 20
Nano-$CaCO_3$	Highly white	2.95	28	0.05 – 0.10

Table 8. *Application of inorganic fillers and physical properties. Nanoclay and nano calcium carbonate are additionally examined.*

Various filler concentrations have been arranged and categorized as CC for nanocalcium carbonate and also NC for nanoclay. A process was conducted to combine nanoclay and HDPE, as well as nano calcium carbonate and HDPE, to create nanocomposites. This was done utilizing a melt blending system that included a Banbury blender, one screw extruder, along with a granule cutting unit. The production rate was 100 kg. The mixer contained a combination of HDPE granules and filler, and also the temperature for processing was maintained at 180°C, which was attained in 15 minutes (186). The extruder screw speed was 330 rpm, and it had a temperature profile consisting of five-barrel temperatures: 200, 190, 190, 190, and 220°C. Afterwards, the nanocomposite blends were separated into small pellets and utilized as experimental specimens for conducting tensile and impact assessments. To obtain the desired results, the PS40E5ASE injection molding equipment was utilized. The equipment had a melt temperature of 210°C, mold temperature of 65°C, and injection pressure of 50 MPa. The wetting liquids used for measuring contact angle were Millipore water from the (USA), which had a conductivity of 0.06 μs/cm, ethylene glycol p.a. from Lach-Ner in (Czechia), and 99% pure diiodomethane of ACS reagent degree from Sigma Aldrich.

12.2.2 Methodology

12.2.2.1 SEM and TEM

To determine the structure along with morphology of the filler particles, TEM (FEI Tecnai G2 Spirit Biotwin model, FEI Company, USA) was employed. The nanofiller specimens were deposited onto a standard 400-grid copper mesh and subsequently scattered in acetone via ultrasonication for 15 minutes. The dispersions were then cast on the copper mesh and air-dried. TEM measurements were conducted at an accelerating voltage of 120 kV. The distribution of nano $CaCO_3$ and nanoclay in the HDPE matrix was analyzed by TEM, wherein an ultra-thin section of approximately 100 nm thickness was obtained from the filled samples using a microtome device (CM1950) from Leica Microsystems Inc. (Buffalo Grove, USA) in a low-temperature environment. To conduct a more comprehensive analysis of the nanofiller distribution, the composites underwent SEM characterization utilizing a (Zeiss EvoLS10) instrument via an energy-dispersive X-ray detector (Germany).

12.2.2.2 Thermal analysis

Differential Scanning Calorimetry (DSC) evaluations were conducted in accordance with ASTM E1356, utilizing a TA Instrument S10 model (Waters, USA) under a nitrogen flow rate of 50 mL/min. The glass transition temperatures (T_g) of both virgin HDPE, as well as its

nanocomposites, were ascertained through DSC curves utilizing the midpoint method at a heating rate of 10°C/min from 30 to 300°C (185-186).

12.2.2.3 Uniaxial tensile testing

Tensile testing of injection-molded specimens was conducted using a universal testing machine autograph AGS-100 Shimadzu from (Japan) and a Zwick 1456 multipurpose tester from (Germany) equipped with a compact thermostatic chamber TCE Series. The data was collected following the CSN EN ISO 527-1 and CSN EN ISO 527-2 norms, utilizing an assessed gauge length of 8 cm. The experiments were carried out at room temperature with deformation rates of 50, 100, and 200 mm/min until the specimens broke. The stress-strain dependence plot was used to obtain the strength at break, Young's modulus, and strain at break. Each study was conducted again 10 times, and the mean values along with standard deviation were computed. The experiments were conducted under laboratory ambient conditions at a temperature of 25°C.

12.2.2.4 Charpy impact testing

The impact tests were conducted by dropping a 25 J energy pendulum using a Zwick 513 Pendulum Impact Tester (Germany) following the CSN EN ISO 179-2 standard. The experiments were repeated 10 times to obtain mean values and standard deviations.

12.2.2.5 Surface free energy (SFE) characterization

The surface free energy (SFE) of both pure HDPE and the researched composites was determined using axisymmetric drop shape assessment, with measurements of the static contact angle of wetting. The measurements were conducted at 23°C using a Krüss DSA 30 (Krüss, Germany), and repeated seven times. To determine the SFE, Owens, Wendt, Rabel, and Kaelble's extension of Fowkes's theory was utilized, which relied on the average static contact angles for water, ethylene glycol, and diiodomethane (188,189).

12.2.2.6 Microhardness

The micro-indentation exams were taken place using a micro combi tester (Anton Paar, Austria) due to the CSN EN ISO 14577 standard. A diamond tip of a cube corner shape (Vickers, Anton Paar, Austria) was used for the measurements. The loading rate (unloading rate) was set at 6 N/min, the maximum load was 3 N, and there was 90s holding time. The depth-sensing indentation procedure was employed for the concurrent measurement of the force on the indentor and the displacement of the indentor's tip. The placement of the indentation hardness (H_{IT}) was studied by carrying out a division of the maximum load (F_{max}) by the projected region of the hardness impression (A_p). The indentation modulus (E_{IT}) was computed by estimating the Poisson's ratio (ν) of the specimens (0.3–0.4) (190,191)) and using the plane strain modulus of elasticity (E*).

$$H_{IT} = \frac{F_{max}}{A_p}, \tag{17}$$

$$E_{IT} = E^{\star}(1 - \nu^2). \tag{18}$$

After conducting the measurements 10 times, the average values and deviations were calculated. The experiments were carried out in a laboratory setting at a temperature of 25°C.

12.2.3 Results and discussion

The findings from the experiments conducted on the composites were condensed in (Figure 26). The obtained deformation curves for stress versus strain displayed the typical patterns of elasticity (up to a 3% strain for minor deformations), a region where elasticity switches to plasticity (up to a 10% strain for minor deformations), in addition to a region where stress remains constant. The above-mentioned occurrence was noticed in composites of HDPE with 5 wt.% nanoclay and 15 wt.% CC, when exposed to strains greater than 18% and 12%, respectively. This observation was reported in reference (192). The curves seen in this particular study were comparable to those found in our earlier research on mineral composites of industrial HDPE under the exact same deformation rate (185-187). Additionally, investigations were conducted on industrial HDPE mineral composites of industrial HDPE under the same deformation rate (185-187). When there was no stress plateau-draw area, the tensile deformation behavior of pure HDPE was more rigid. On the other hand, the 1 wt.% filler concentration in CC/HDPE composites exhibited a greater degree of elastoplastic behavior, as shown in (Figure 26b).

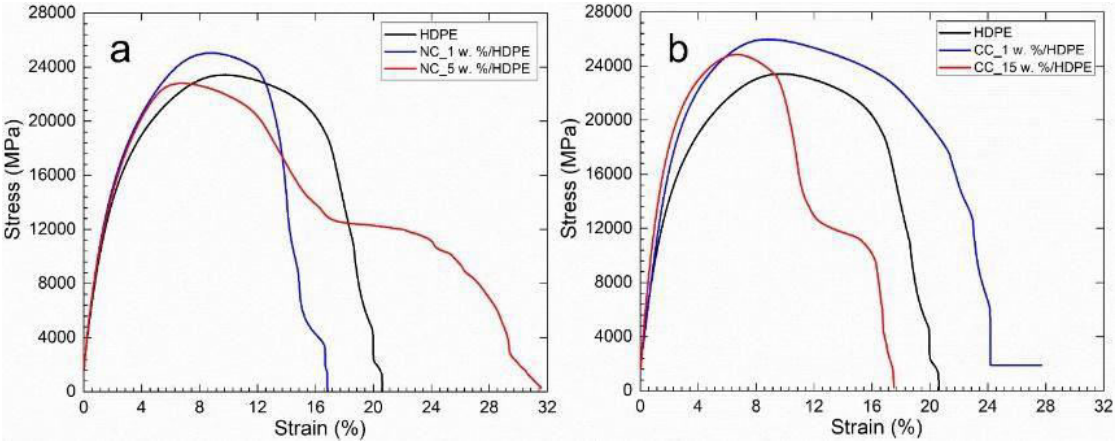

Figure 26. *(a) The overall mechanical performance of NC/HDPE, as well as (b)CC/HDPE composites, was examined by conducting tensile tests at room temperature, with a constant deformation rate of 50 mm/min, while varying the concentration of fillers. The outcomes are displayed as dependencies between strain and stress.*

The behavior of NC/HDPE composites was significantly influenced by the elastic-plastic characteristics. Increasing the concentration of fillers led to improved plastic behavior, as shown in (Figure 27).

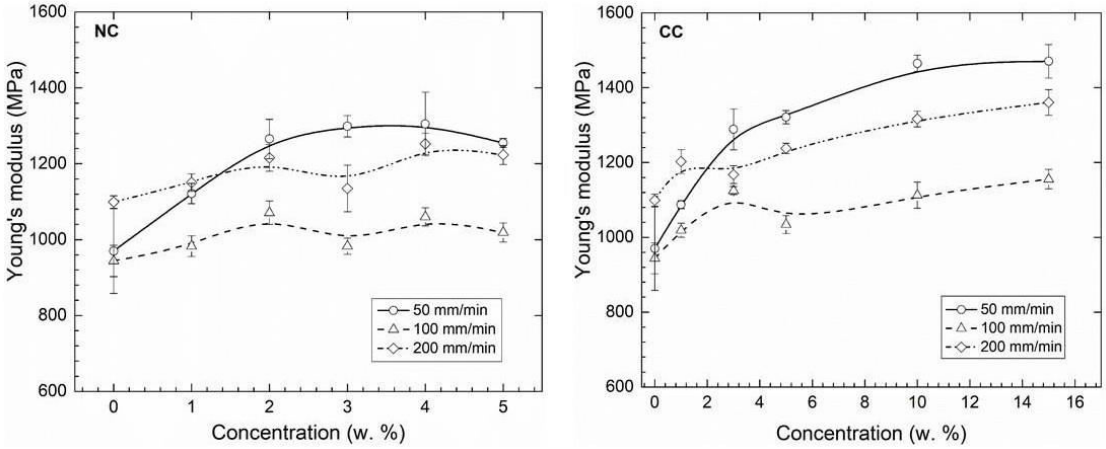

Figure 27. *The relationship between Young's modulus and the amount of filler present in CC/HDPE and NC/HDPE composites was investigated by conducting tensile tests at various deformation.*

This behavior was seen in all rates of deformation as shown in (Table 9). To illustrate, the CC/HDPE composites containing 5 wt.% filler concentrations experienced an increase of approximately 51.5% in the modulus of elasticity from the original HDPE's absolute rate of 970.1 ± 111.7 MPa to 1470.0 ± 54.7 MPa. The addition of 4 wt.% inorganic filler levels resulted in a 34.5% increase in the modulus of elasticity for the NC/HDPE composites, achieving an absolute value of 1304.9 ± 83.7 MPa. The results are consistent with prior data, indicating that the gradual increase in the elasticity modulus of polymer composites as the filler content increases (193,194) may be due to the presence of rigid mineral filler particles.

Sample	Young Modulus (MPa)			Upper Yield (MPa)			Strain at Break (%)			Fracture Toughness (kJ/m^2)
	Rate (mm/min)			Rate (mm/min)			Rate (mm/min)			
	50	100	200	50	100	200	50	100	200	
HDPE	970.1 ± 111.7	943.8 ± 142.2	1099.2 ± 16.2	24.5 ± 1.1	24.8 ± 1.1	25.6 ± 0.4	20.5 ± 0.1	25.8 ± 5.0	16.6 ± 0.6	36.69 ± 5.15
CC_1%	837.5 ± 10.8	648.2 ± 419	1202.7 ± 32.1	25.4± 0.6	24.3 ± 1.1	25.1 ± 0.5	30.8 ± 3.1	33.2 ± 6.7	19.8 ± 0.3	31.48 ± 2.43
CC_3%	1288.9 ± 54.7	1368 ± 2.5	1167.7 ± 23.7	24.4 ± 0.4	25.0 ± 0.2	24.7 ± 0.8	22.0 ± 0.8	19.8 ± 1.0	22.9 ± 1.5	17.26 ± 0.92
CC_5%	1322 ± 10.8	1034.3 ± 299	1237.9 ± 13.7	23.6 ± 0.5	25.4 ± 3.4	25.0 ± 1.1	25.0 ± 3.0	28.5 ± 14.7	17.2 ± 3.1	26.29 ± 1.04
CC_10%	1465.1 ± 12.3	1112.8 ± 273	1316.4 ± 0.4	24.3 ± 1.3	25.2 ± 1.0	26.3 ± 0.7	18.6 ± 2.3	20.5 ± 7.4	14.1 ± 0.4	28.69± 3.4
CC_15%	1470 ± 54.7	1155 ± 255	1360.7 ± 1.7	24.6 ± 0.2	25.3 ± 1.1	28.1 ± 2.8	20.1 ± 2.6	19.7 ± 6.9	11.2 ± 2.2	31.79 ± 3.94
NC_1%	1121.4 ± 26.8	982.9 ± 217	1150.5 ± 23.0	23.6 ± 1.5	26.5 ± 0.5	27.4 ± 2.4	32.8 ± 15.9	19.3 ± 4.6	16.4 ± 6.0	29.21 ± 2.21
NC_2%	1265.4 ± 51.9	1070.9 ± 303	1215.6 ± 48.8	25.8 ± 3.2	27.4 ± 2.2	30.0 ± 2.8	21.2 ± 8.7	20.5 ± 10.5	12.1 ± 0.6	24.37 ± 1.0
NC_3%	1248.7 ± 28.1	982.7 ± 213	1134.9 ± 61.2	27.3 ± 1.9	23.9 ± 1.6	22.4 ± 0.4	19.8 ± 3.2	31.1 ± 11.2	26.6 ± 2.2	28.44 ± 0.09
NC_4%	1304.9 ± 83.7	1060.1 ± 240	1328.3 ± 78.0	23.3 ± 0.1	23.9 ± 0.3	27.9 ± 2.5	27.6 ± 2.2	35.7 ± 7.2	14.4 ± 5.9	23.35 ± 0.27
NC_5%	1255 ± 11.9	1018.8 ± 246	1223.3 ± 25.0	23 ± 0.2	23.5 ± 0.2	24.7 ± 0.2	28.9 ± 2.7	32.88 ± 10	20.5 ± 2.1	22.06 ± 1.42

Table 9. *The research study presents the results of testing the tensile properties of HDPE composites at three different deformation rates: 50, 100, and 200 mm/min. The sample description provides information about the concentrations of fillers, which are expressed as weight percentages.*

(Figure 28) illustrates that both nanoclay and nanocalcium carbonate fillers exhibit nonlinear patterns in terms of their upper yield and filler concentration dependencies in HDPE composites. Nonetheless, the upper yield of CC/HDPE composites did not exhibit notable alterations as the filler concentration increased, except for the composites that contained 4 and 5 wt.% filler concentrations when subjected to a deformation rate of 200 mm/min. In these instances, the initial upper yield values of 25.6 ± 0.4 MPa were increased to 26.3 ± 0.7 MPa and 28.1 ± 2.8 MPa, correspondingly.

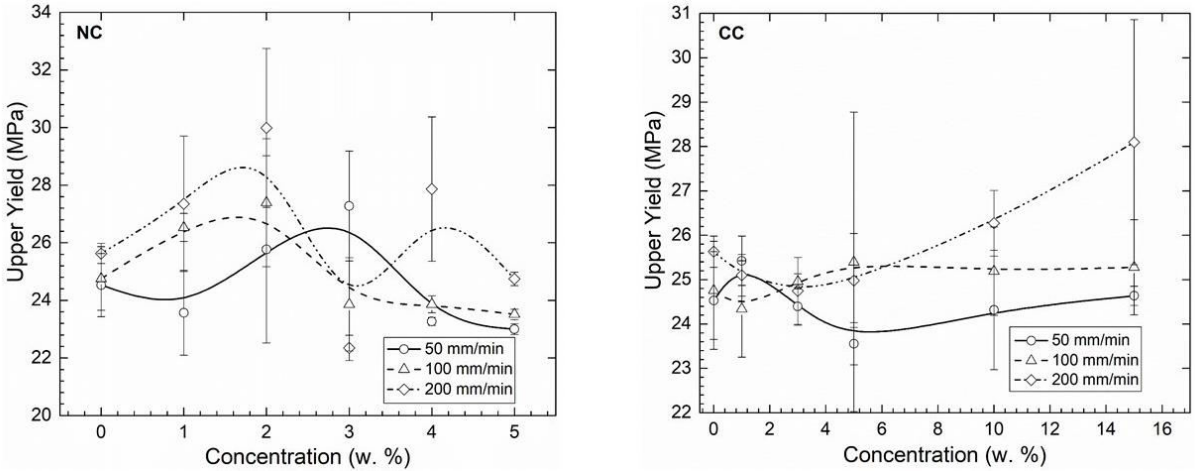

Figure 28. *The CC/HDPE and NC/HDPE composites were found to be dependent on the concentration of inorganic filler and upper yield when subjected to mechanical tensile tests at different strain rates.*

Figure 29 presents the information regarding the relationship between the concentration of fillers and the elongation at break, which has been calculated at various deformation speeds.

The results obtained from the composites made of CC/HDPE showed that as the concentration of filler increased, there was a decrease in the strain at the point of fracture. This implies a decrease in ductility and increased brittle fracture in terms of mechanics models. This supports the well-known principle that polymers with higher crystallinity typically exhibit greater elasticity and stiffness when compared with amorphous methods, which show more plastic behavior. However, in the case of NC/HDPE composites, there was an opposite trend where increasing filler concentration resulted in increased strain before breaking. The reason for this can be explained by how the platelet-shaped nanoclay filler particles align themselves at the interface of the polymer chains during the injection molding process.

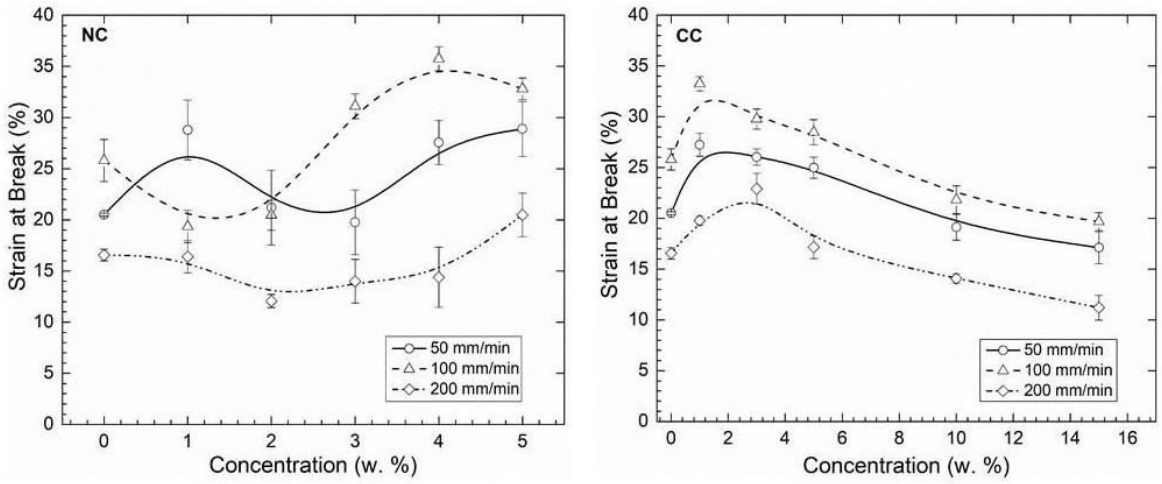

Figure 29. *The mechanical tensile examination of CC/HDPE and NC/HDPE composites at different strain rates determines the elongation at break and nanofiller concentration.*

The analysis of the elongation at break characteristic for 5 wt.% concentrations of nanocomposite fillers, such as nano-clay and nano-calcium carbonate, showed that the composite matrix containing flat-shaped nano clay particles exhibited greater flexibility as compared to the other filler particles at various rates of distortion. The above-mentioned statement is supported by the comparison of the measured values of Young's modulus of elasticity, which demonstrates the CC/HDPE samples had a higher modulus of elasticity than the NC/HDPE samples. Figure 30 illustrates the correlation between the fracture toughness and the concentration of fillers in the composites that were tested. In comparison to the original polymer or virgin one (HDPE), all composite materials exhibited a reduction in fracture toughness. The composite containing 3 wt.% of nano $CaCO_3$ filler had probably the most significant decrease, with a reduction of almost 52.96%. The fracture toughness of NC/HDPE composites was found to be significantly lower, measuring at approximately 22.06 ± 1.42 kJ/m^2.This represents a decrease of about 39.87% in comparison with the original HDPE material. These findings suggest that the composites have an even greater tendency to break easily and exhibit a more brittle behavior when compared with the virgin (Figure 30)

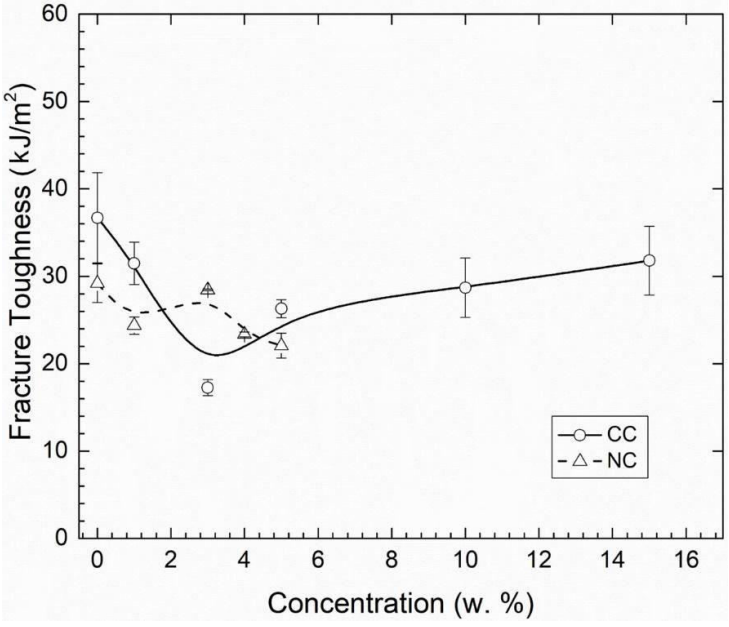

Figure 30. *The Charpy impact test was used to figure out the dependence of fracture toughness and the concentration of fillers in CC/HDPE and NC/HDPE composites.*

The results of the (SFE) calculations are presented in (Table 10), which shows that the addition of $CaCO_3$ and nanoclay fillers brought about a decrease in the initial polarity of the pure HDPE material, making it less polar. The measured increase in the dispersive component of surface free energy (SFE) for composite materials containing 5wt.% CC/HDPE increased from 4.19 ± 0.81 mJ/m^2 (pure HDPE) to 39.51 ± 0.63 mJ/m^2. Similarly, for composite materials containing 3 wt.% NC/HDPE, the dispersive component of SFE increased from 4.19 ± 0.81 mJ/m^2 (pure HDPE) to 39.70 ± 1.09 mJ/m^2. The overall surface free energy (SFE) rose significantly in the 5wt % CC/HDPE composites, going from 19.48 ± 2.91 mJ/m^2 (HDPE in its original state) to 32.95 ± 2.58 mJ/m^2, a rise of approximately 103.8%. In the 3 wt.% NC/HDPE composite, the SFE increased by approximately 69.18% to 32.95 ± 2.58 mJ/m^2. The composite interface is now suited for specialized applications like coating or adhesive joints due to its improved adhesive properties, as evidenced by the observed results.

Sample	Surface free energy [mJ/m^2]		
	Total	Polar	Dispersive
HDPE	19.48 ± 2.91	15.29 ± 2.10	4.19 ± 0.81
CC_1%	36.51 ± 33.80	15.61 ± 14.82	15.61 ± 14.82
CC_3%	36.49 ± 14.86	11.84 ± 7.77	24.65 ± 7.08
CC_5%	39.70 ± 1.09	0.19 ± 0.46	39.51 ± 0.63
CC_10%	23.45 ± 4.41	0.01 ± 0.07	23.44 ± 4.34
CC_15%	26.19 ± 0.05	0.41 ± 0.01	25.78 ± 0.03
NC_1%	30.44 ± 1.04	0.12 ± 0.04	30.32 ± 1.00
NC_2%	30.28 ± 0.92	1.19 ± 0.15	29.09 ± 0.76
NC_3%	32.95 ± 2.58	00.08 ± 0.16	32.86 ± 2.42
NC_4%	29.22 ± 0.66	0.22 ± 0.13	29.00 ± 0.53
NC_5%	23.45 ± 4.41	0.01 ± 0.07	23.44 ± 4.34

Table 10. *The Owens, Wendt, Rabel, and Kaelbe method was used to figure out the total surface free energies, as well as the dispersive and polar components, of the HDPE composites being studied. To obtain these measurements, contact angle measurements were taken using axisymmetric drop shape assessment at a temperature of 23°C.*

The data of the micro-indentation testing on the composite substances are shown in (Figure 31) it illustrates the relationship between the indentation modulus and the amount of the filler, as referred to by the E_{IT} pattern. The results display that as the concentrations of the fillers rise, the indentation also increases, confirming that the fillers boost the mechanical properties of the specimens.

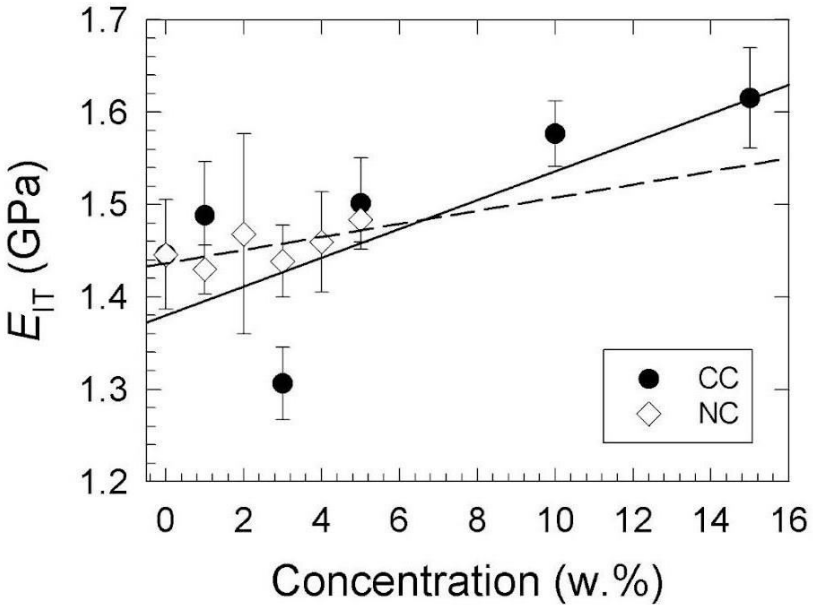

Figure 31. *The relationship between the concentration of fillers and the modulus of indentation (EIT). Type of filler: The Nano CaCO3 has formed a full circle, while the Nanoclay remains empty like a diamond. However, a *Point has been deducted due to the lack of linear regression.*

12.2.4 Conclusion

The research examined the physical and mechanical characteristics of HDPE composites that were produced using two distinct types of nano-sized mineral fillers, which is nanoclay as well as nano $CaCO_3$. The findings demonstrated that the fillers significantly enhanced the mechanical properties of the composites, including an increase in both the elasticity and indentation strength of 170.4 MPa with regard to the modified HDPE. Nano CC/HDPE composites made up of 5% filler concentrations exhibit strength of 54.7 MPa. Both the nature and amount of the filler had an impact on the plastic-elastic aspects. An increase in the stress level that remains constant and a reduction in the amount of ductility before breaking were signs of this. For both kinds of composites, it was determined that the ideal concentration of filler was 5 weight percent. Furthermore, it was observed that both nanocomposites showed enhanced thermal stability when compared to virgin HDPE, suggesting a far more robust bond with the HDPE matrix. These findings indicate that these nanocomposites might be beneficial for incorporating into complex substance designs, as they exhibit a combination of elastic and plastic mechanical properties across various deformation rates, in addition to improved resistance to changes in temperature.

****

12.3 Study of mechanical properties of epoxy/graphene and epoxy/halloysite nanocomposites

The aim of research paper D is to contrast the mechanical characteristics of two distinct nanocomposites. Epoxy/Halloysite and epoxy/graphene. Fillers of graphene nanoplatelets (GnPs) and halloysite nanotubes (HNTs) are utilized in the study at various concentrations and are distributed in epoxy resin matrices. The addition of rubber-modified epoxy resin, particularly carboxyl-terminated-butadiene-acrylonitrile copolymer, enhances the characteristics of nanocomposites. During the process of mechanical evaluation, it was found that the hypothesis of individual GnPs particles sliding within the complex resin nanocomposite matrix was supported by the results. The addition of GnPs nanocomposites resulted in enhanced ductility and plasticity, as demonstrated by a 39% increase in elongation at break, which rose from 0.33 mm in the pure matrix to 0.46 mm. Nevertheless, the utilization of HNTs results in a decline in mechanical rigidity, showing a 20% reduction of Young's modulus of elasticity, declining from 3.4 to 2.7 GPa. The research findings suggest that the behavior of the nanocomposites is intricate, involving both brittle and ductile characteristics. This is supported by the measurements of dynamic stiffness. The research indicates that the mechanical characteristics of epoxy-based nanocomposites can be improved by using fillers in a broad sense.

12.3.1 Materials

The investigation utilized a resin known as DGEBA, which is also called laminating resin MGS L285, along with a hardener known as 3-aminomethyl-3,5,5-trimethyl cyclohexylamine. Hexion, (USA) provided two materials, namely L285, as shown in (Figure 32a). The research utilized liquid rubber made from CTBN copolymer, that had been obtained from Zibo Qilong in China. The liquid rubber had an average of 0.58 - 0.65 carboxyl groups per molecule. The molecular weight of the substance was approximately 3,800 Da and it contained 8-12% acrylonitrile, as shown in (Figure 32c). The CTBN technical information is contained in (Table 11). In (Figure 32), the chemical compositions of CTBN, hardener, and epoxy are depicted. The planar shaped GnPs that were used in this study were not functionalized and had an area of 800 square meters per gram, a thickness ranging from 3 to 7 nanometers, as well as an average width of 1.5 meters. The items purchased from (Nanografi in Ankara, Turkey) were of exceptional quality, and have a purity level of 99.9%. The HNTs that were utilized ($Al_2Si_2O_5(OH)_4$) had a double layer structure that was not cylindrical in form (Esan Eczacibasi, Istanbul, Turkey). The dimensions of the HNTs varied, with an inner diameter ranging from one to 20 nm, an outer diameter ranging from 30 to 50 nm, and a length ranging from 100 to 800 nm.

Parameter	Value
Viscosity (40 °C) (Pa.s)	7 – 12
Carboxyl content (mmol/g)	0.58 – 0.65
Nitrile group content (%)	8.0 – 12.0
Water content (%)	≤ 0.05
Volatile content (%)	≤ 2.0

Table11. *The liquid rubber CTBN used for application has specific properties.*

12.3.1.1 Preparation of nanocomposites and epoxy blends

12.3.1.1.1 CTBN–epoxy blends

The mixture of epoxy resin and 10 wt.% CTBN liquid rubber was put in a beaker and stirred on a warmed plate to solidify the mixture. Afterward, the resulting mixtures underwent ultrasonication for a duration of 15 to 20 minutes to ensure uniformity. Subsequently, they were degassed in a vacuum oven set at 60°C for a period of 1 hour. The amine-based hardener was added by weight in a proportion of 80:20 (epoxy to hardener) with a slight agitation. After that, the mixtures were poured into molds and left to harden at a temperature of 90°C for one hour. This was followed by an additional 3 hours of post-curing at 120°C. (Figure 32) shows the chemical formula for the epoxy blends used.

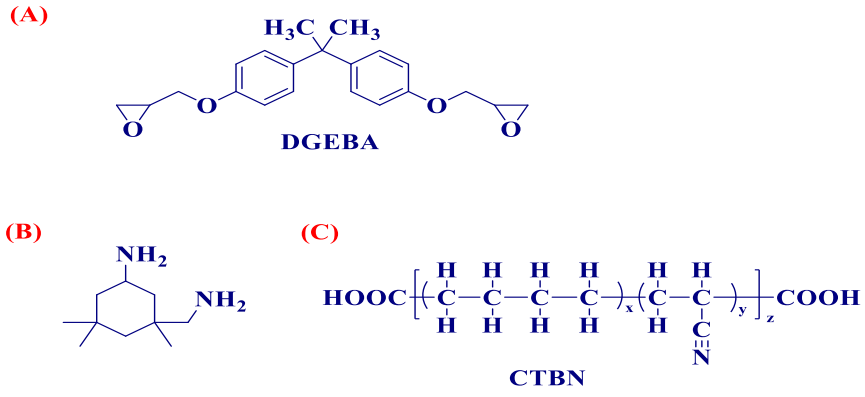

Figure 32. *The build of the substances (a) DGEBA, (b) 3-aminomethyl-3,5,5-trimethylcyclohexylamine, and (c) CTBN as it comes to their chemical composition.*

12.3.1.1.2 CTBN– GnPs–epoxy and CTBN–halloysite–epoxy composites

Previous research determined the nano-reinforcement ratios of epoxy mixtures. A lot of scientists have performed experiments to determine the amount of graphene nanoplatelets (GnPs) and halloysite nanotubes (HNTs) present in the epoxy matrix. The reported concentrations have varied, with GnPs ranging from 0 to 1 weight percent (wt.%) and HNTs

ranging from 0 to 5 (wt.%). The study has checked out how different amounts of fillers affect the tensile, fracture, and flexural properties of the original matrix. To create epoxy mixtures containing HNTs and GnPs, SEM images (Figure 33) have been taken of the epoxy resin with varying concentrations of GnPs (0, 0.125, 0.25, 0.5, 0.75, along with 1 wt.%) and HNTs (0, 1, 2, 4, 5, and 5wt.%) as part of the preparation process. The mixtures were obtained and moved to a RETSCH-PM 100 planetary mill and mixed at a speed of 200 rotations per minute for a duration of 25 hours. The mixing bowls were filled with a combination of epoxy mixtures and balls, resulting in a ratio of 30 balls to every 1 unit of powder. Initially, the mixtures were blended for a period of 30 minutes. After that, they were allowed to rest for ten minutes in order to prevent excessive heating. Following this, the mixtures were blended once again, and this process was repeated until the desired duration of mixing was achieved. Subsequently, a 10 wt.% of CTBN was incorporated into each epoxy mixture, including those containing GnPs and HNTs. This addition resulted in the formation of composite materials known as CTBN-GnPs-epoxy and CTBN-HNTs-epoxy. After that, the prepared mixtures were stirred using ultrasonication for a duration of 25-30 minutes to achieve uniformity. Afterwards, any gases present were removed by placing the mixtures in a vacuum oven at a temperature of 60°C for approximately 1 hour. In addition, the process of curing CTBN-epoxy blends, as pointed out in (Section 12.3.1.1), was utilized to treat the CTBN-GnPs-epoxy and CTBN-HNTs-epoxy composites. It is important to note that all the epoxy/graphene and epoxy/halloysite nanocomposites that were studied had the same amount of CTBN liquid rubber, which was 10% by weight. However, the original epoxy matrix didn't have exactly the same content (195,196-2000).

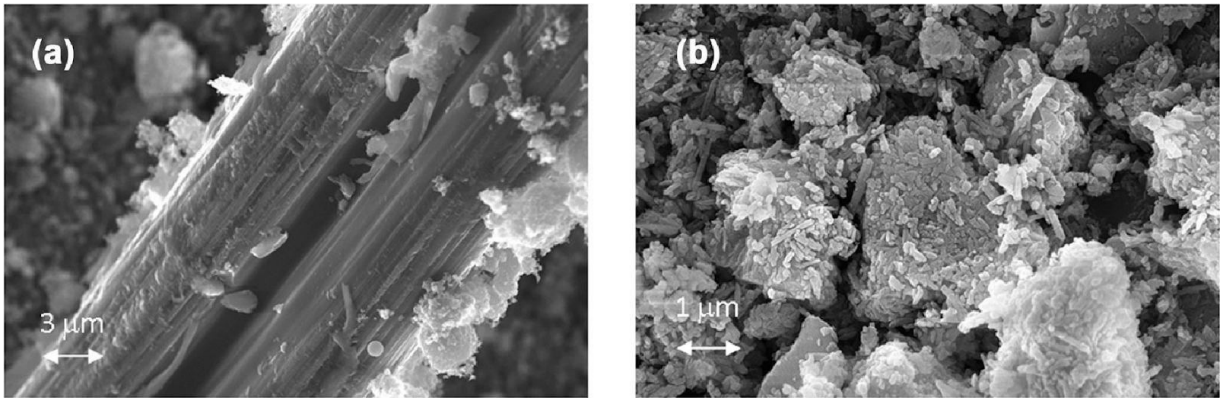

Figure 33. *SEM images displayed the fillers that were analyzed, including GnPs and HNTs.*

12.3.2 Methodology

12.3.2.1 SEM analysis

The examination of SEM was carried out by utilizing a Zeiss EvoLS10 microscope from (Germany) that had an energy dispersive X-ray detector. In order to get the nanofiller samples ready for imaging, the fillers were dispersed in acetone and subjected to ultrasonication for fifteen minutes. The resulting mixture was then poured onto a copper mesh with a regular 400-grid size and left to dry in the air. An accelerating voltage of two kilovolts was utilized to obtain scanning electron microscopy images.

12.3.2.2 Uniaxial tensile testing

The mechanical characteristics of injection-molded samples were evaluated through uniaxial tensile testing, utilizing the universal testing machine Autograph AGS-100 Shimadzu from (Japan) and the Zwick 1456 multipurpose tester from Zwick Roell, Ulm, (Germany). The Compact Thermostatic Chamber TCE Series was incorporated in the Zwick 1456 tester. The tensile test was carried out following the guidelines of' ČSN EN ISO 527-1 and ČSN EN ISO 527-2, with an 80 mm gauge length and a deformation rate of 50 mm/min until the point of fracture. The graphs that depict the relationship between stress and strain were utilized to determine Young's modulus of elasticity and the point of elongation where the material breaks. A total of ten repetitions were carried out for each study, and afterwards, the average values and standard deviations were calculated. The experiments were performed at a consistent temperature of 25°C in the laboratory. Nanofiller specimens were placed on a regular copper mesh with a 400-grid pattern to capture SEM images. SEM analysis has been carried out at 2 kilovolts accelerating voltage with a Zeiss EvoLS10 equipped with an energy dispersive X-Ray detector (Germany). The fillers were mixed with acetone and subjected to ultrasonication for 15 minutes. Afterwards, the mixture was poured onto a copper mesh and then allowed to dry in the air. Finally, the samples were examined using scanning electron microscopy (SEM).

12.3.3.3 Charpy impact testing

The Zwick 513 Pendulum Impact Tester from Zwick Roell in Ulm, Germany was used to carry out impact tests following the guidelines of the ČSN EN ISO 179-2 standard, allowing for a 25 J energy release. The fracture toughness was determined by taking the average and standard deviation of 10 repeated experiments. The experiments were all carried out at the typical temperature of the laboratory, which was 25°C.

12.3.3.4 Microhardness

Micro-indentation tests have been performed in accordance with the SN EN ISO 14577 standard using a micro-indentation tester (micro combi tester, Anton Paar, Austria) to determine micro-hardness. The diamond tip utilized had a cube-corner shape and had been created by Vickers, a company based in Austria. The 3 N was determined as the highest weight allowed, with a loading and unloading speed of 6 N per minute, in addition to a duration of 90 seconds for holding. Tests were carried out using the depth sensing indentation technique, which enables the measurement of both the applied force and displacement of the indentation tip at the same time. The calculation of the indentation modulus was derived from the elastic modulus of the strain at a particular level, using a Poisson's ratio within the range of 0.3-0.4 (201,202).

$$E_{IT} = E^{\star}(1 - v^2). \tag{19}$$

To guarantee accuracy, the indentation modulus was measured multiple times (10 repetitions) as well as the mean values and standard deviations of these measurements were computed. The laboratory conducted the experiments at its normal temperature of 25°C.

12.3.3.5 Uniaxial 3-point bending tests

The Zwick 1456 testing equipment supplied by Zwick Roell GmbH & Co, KG in Ulm, (Germany) was used to carry out a unidirectional, 3-point bending test in accordance with the ČSN EN ISO 14125 standard. The outcomes were evaluated using TestXpert software. The distance between the supports was found to be 64 mm, and both supports and also the load mandrel was found to have a circularity of 5 mm. During the 3-point bending experiment, the speed of deformation was established at 1 millimeter per minute, while the pace of loading was established at 50 millimeters per minute.

12.3.3.6 Displacement transmissibility measurements

The Formula (20) (203) is used to compute displacement transmissibility T_d, which is the measurement of displacement.

$$T_d = \frac{y_2}{y_1} = \frac{a_2}{a_1}, \tag{20}$$

The variables y_1 and y_2 represent the intensity of displacement on the input and output sides of the specimen that was tested. The acceleration amplitude on the input side of the tested sample is denoted by a_1, while on the output side, it is denoted by a_2. Equation (21) (204) offers a solution. The transmissibility of displacement for a system consisting of a mass m, a spring with stiffness k, and a damper with damping coefficient c.

$$T_d = \sqrt{\frac{k^2+(c.\omega)^2}{(k-m.\omega^2)^2+(c.\omega)^2}} = \sqrt{\frac{1+(2.\zeta..r)^2}{(1-r^2)^2+(2.\zeta.r)^2}}. \tag{21}$$

The formula (22) enables the case $dT_d/d_r = 0$ to be met and the frequency ratio r_0 can be determined that corresponds to the greatest amount of displacement transmissibility (205,206):

$$r_0 = \frac{\sqrt{\sqrt{1+8.\zeta^2}-1}}{2.\zeta}. \tag{22}$$

The displacement transmissibility of any framework composed of a spring, mass and damper is governed by the Formula (22). When the physical stiffness of an object decreases or the damping ratio improves, the peak of displacement transmissibility moves towards lower frequency ratios. The Formula (22) calculates the frequency ratio r_0 which produces the maximum displacement transmissibility $T_{(dmax)}$. The vibration-induced tests were carried out using the forced oscillation technique. The experiment involved determining the displacement transmissibility (T_d) within a frequency range of 2 to 3,200 Hz. This was achieved using a BK 4810 vibrator, BK 3560-B-030 signal pulse multi-analyzer, as well as BK 2706 power amplifier. Brüel & Kjaer's BK 4393 accelerometers were used to determine the acceleration amplitudes (a_1 and a_2) at the input and output points of the specimens being measured. The specimens that have been analyzed had three different inertial masses placed on them, which were zero g, 90 g, and 500 g. The transmissibility of displacement was determined for every one of these masses. The dimensions of the tested sample were (60 mm × 60 mm × 3 mm) where a thickness of 3 mm. Five repetitions of all measurements was conducted at a temperature of 22°C, which was the standard.

12.3.4 Results and discussion

Section 12.3.1 demonstrated the typical forms of the nanofillers utilized in this research, as shown in (Figure 33) through SEM analysis. (Figure 33a) shows the GnPs lamellar configuration, which is identifiable by its layer thickness ranging from 3 to 7 nm and a layer width of about 1.5 to 2.0 μm. In contrast, the condensed and aggregation clusters arrangement of HNTs nanotubes (Figure 33b) is made up of separate nanotubes that measure around 30 to 50 nm in diameter and 100 to 800 nm in length. The findings from the tensile-testing trials conducted on the investigated nanocomposites are showcased in (Figure 34) (207). Based on the findings, the Young's modulus of elasticity (E) decreased during uniaxial testing as a result of the rise in the percentage of GnPs filler. The value of the neat matrix dropped from 3.4 GPa to 2.7 GPa with the inclusion of 1 wt.% epoxy and GnPs nanocomposite. The reduction in size was linked to a nonlinear rise in the elongation at the point of fracture, which suggests that the elongation at break increase and consequence the ductility of epoxy/GnPs nanocomposites increased. This phenomenon could be credited for the impact of the GnPs nanofiller molding on the mechanical characteristics of the composite substance. The behavior that was observed was caused by the nanoplatelet sheets sliding into the complex structure of the epoxy/GnP nanocomposite. The reason behind this movement was determined to be due to the bending or turning of cracks, breakage of layers, and the separation or detachment of GnPs layers, as previously mentioned in sources (208,209).

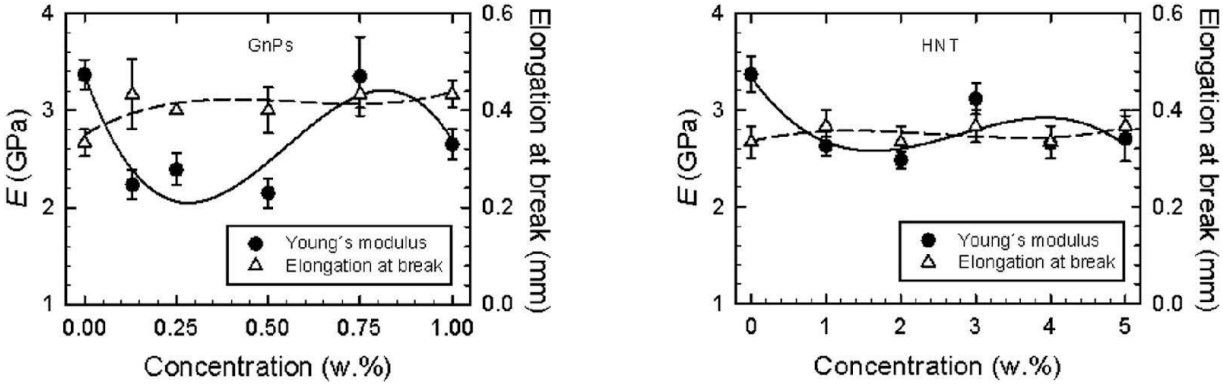

Figure 34. *The connection between Young's modulus of elasticity and also the elongation at break of the investigated nanocomposites containing HNTs and GnPs, taking into account the existence of nanofillers.*

The speed at which the deformation was applied was fifty millimeters every minute. The chart displays a complete line indicating Young's modulus of elasticity, and a broken line representing the elongation at the point of fracture. In comparison, the mechanical stiffness of the elements studied decreased as seen in the (E) for epoxy/HNT nanocomposites which decreased from 3.4 GPa in the pure matrix to 2.7 GPa in the 5 wt.% epoxy/HNTs nanocomposite. The increase in HNTs filler concentration led to an increased stiffness compared to epoxy/GnPs nanocomposites. The results show that there is a constant relationship between elongation at break, which is around 0.36 mm, and the observed results shown in (Figure 35). The composite material was thought to become a lot more brittle fraction following the addition of HNT nanofiller based on the above data. The HNTs nanofillers were prevented from sliding within the composite matrix, which was linked to this. The results of the uniaxial tensile examinations matched the measurements of fracture toughness (207) in a favorable fashion (Figure 35). At a filler concentration of 1 wt.%, the epoxy/HNTs nanocomposites had a higher fracture toughness of 8.2 kJ/m^2 when compared with the epoxy/GnPs nanocomposites that had a fracture toughness of 6.0 kJ/m^2. The fracture toughness showed a gradual decrease that was not linear when more HNTs filler (1-5 w.%) was added.

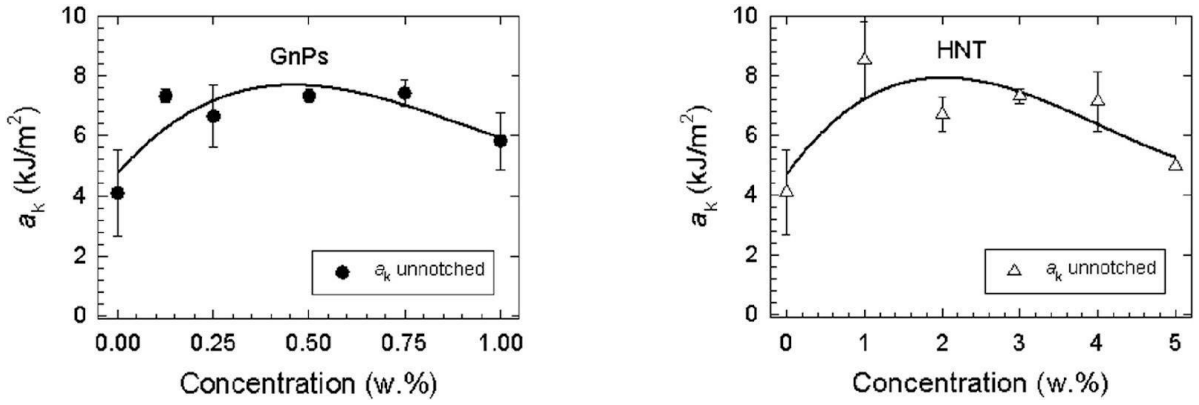

Figure 35. *The dependence of the concentration of the nanofiller on the unnotched fracture hardness of the GnPs and HNTs nanocomposites was investigated.*

The continuous composite matrix was accelerated by CTBN (Figure 32c), which resulted in local deformations in the matrix. The distortion of the matrix mechanisms enabled the spreading of external mechanical energy throughout a significant area, thus hindering the formation of a single brittle crack. To be able to attain the highest level of effectiveness in modifying rubber, specific requirements must be fulfilled, including the establishment of a two-parts structure, sufficient bonding at the interface, and a precise separation distance between adjacent rubber areas (2010). According to (2011), a similar pattern of conduct was noticed in adaptable polymers that contained both soft and hard components, where the hard parts showed increased stiffness, while the soft parts displayed greater elasticity. (Figure 36) depicts the results obtained from the evaluations of micro-hardness versus filler concentration for the two epoxy nanocomposites that were examined. According to the findings, the indentation modulus E_{IT} experiences a non-linear decrease as the concentration of filler decreases. In relation to the epoxy/GnP nanocomposites, it was noticed that the effective elastic modulus E_{IT} of the material decreased from 4.3 GPa (without any GnPs/pure matrix) to 3.4 GPa (with 1 wt.% GnPs nanocomposite). While studying epoxy/HNTs nanocomposites, researchers noted that the material's EIT decreased from 4.3 GPa (in its pure structure) to 3.8 GPa (when a 5 wt.% HNTs nanocomposite was existing). It was believed that the reduction in surface hardness could be attributed to the plasticizing impact of the nanofillers.

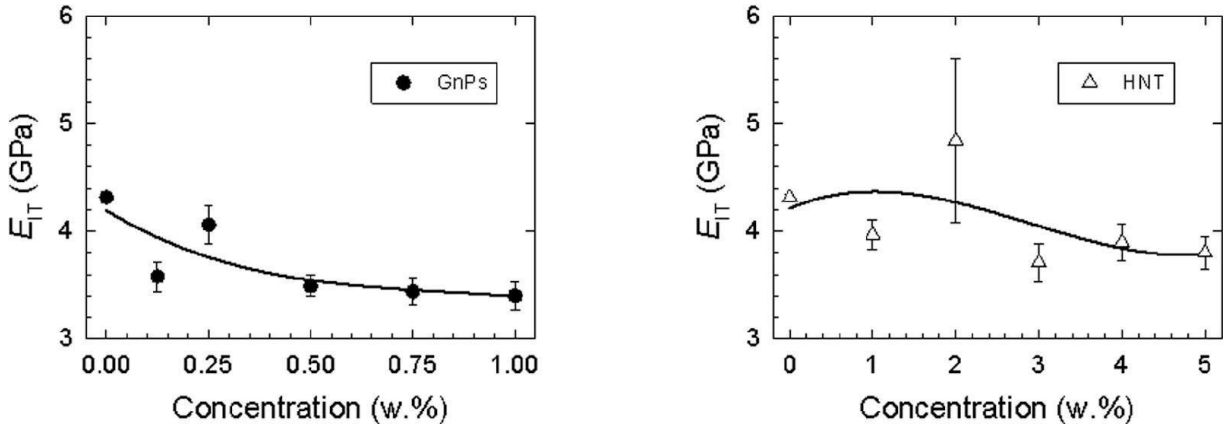

Figure 36. *The relationship between the concentration of nanofillers as well as the indentation modulus of HNTs and GnPs nanocomposites has been examined.*

The results of the 3-point bending tests carried out on the tested nanocomposites are shown in (Figure 37). Brittle materials typically exhibit nonlinear decreasing patterns, which were observed in both nanocomposites under investigation. The research discovered that there was a decrease in the bending modulus (EB) that was not in a straight line as the amount of GnPs filler increased. The bending modulus ranged from 4.3 GPa for the pure matrix to 2.8 GPa for the nanocomposite containing 1 wt.% GnP. The noted occurrence was connected to a consistent and non-linear increase in elongation at the point of fracture, ranging from 5.0 mm (for the pure matrix) to 6.0 mm (for the nanocomposite composed of 1wt.% epoxy and GnPs). The pattern indicates that the composite has increased ductility because of the plasticizing impact of the nanofiller within the prepared epoxy/GnP nanocomposites. On the other hand, the epoxy/HNTs nanocomposites showed a non-linear decrease in EB, going from 4.3 GPa (pure matrix) to 3.0 GPa (in 5wt.% epoxy/HNTs nanocomposites). This indicates that the substances being studied experienced a decrease in their mechanical stiffness. However, there was a small non - linear decrease observed in elongation at break with respect to the amount of HNTs filler present. The break values decreased the elongation from 5.0 mm for pure matrix to 4.1 mm for 5 wt.% epoxy/HNTs nanocomposites. The epoxy/HNTs nanocomposites are found to be more brittle than the epoxy/GnPs nanocomposites, according to the findings.

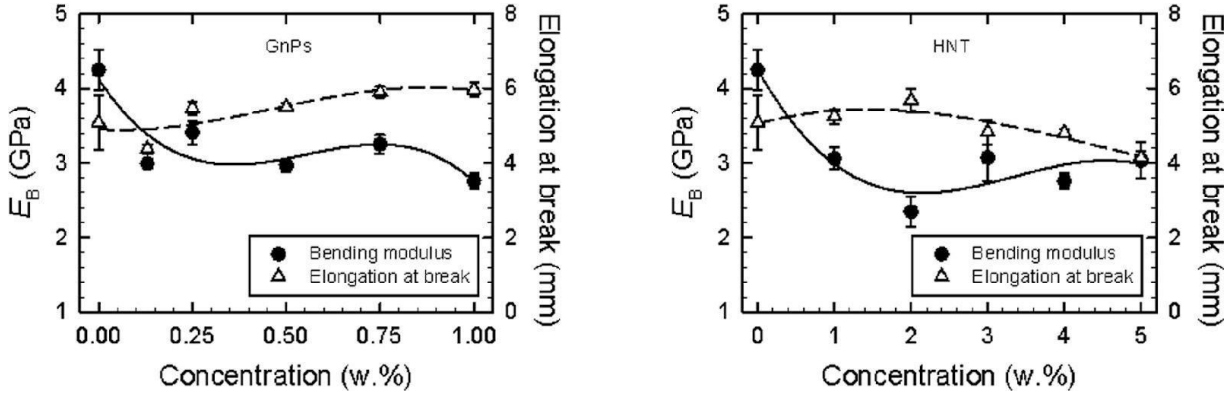

Figure 37. *The concentration of nanofiller was investigated to determine the bending modulus and elongation at the break of HNTs and GnPs nanocomposites. The deformation rate was 50 mm/min. The chart shows two factors, bending modulus, and elongation at break, illustrated by a continuous line and a dotted line, correspondingly.*

The researchers conducted dynamic mechanical evaluations on the nanocomposites being studied, and the results are shown in (Figure 38) and (Figure 39). The frequency connections of displacement transmissibility are depicted in (Figure 38). The results obtained demonstrated a significant degree of similarity with the uniaxial tensile measurements. Figures (38) shows that the displacement of the f_{R1} peak towards higher excitation frequencies is a sign of an increase in material stiffness. A small decrease in the stiffness of the 2nd type was noticed when there were very low amounts of filler present. This was indicated by the minimal shift of f_{R1} towards lower values, as depicted in (Figures 38a) and (Figure 38b). The displacement transmissibility's frequency connections are impacted by the size of the inertial mass, as illustrated in (Figures 38c) and (Figure 38d). According to the research, it was found that an increase in inertial mass resulted in a decrease in the location of the very first resonance frequency peak. As a result, this improved the damping properties of the mechanical vibrations in the components (204).

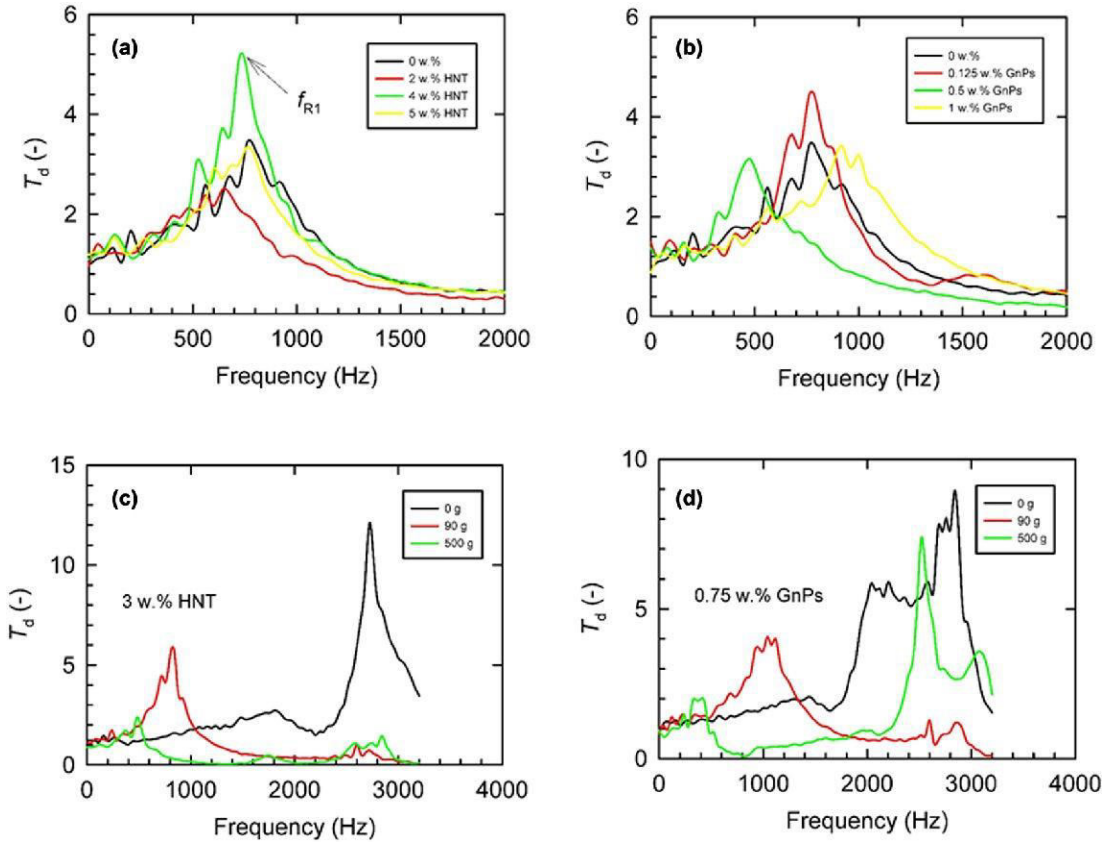

Figure 38. *In order to determine the displacement transmissibility, a comparison was made between the frequency dependencies of the evaluated GnPs and HNTs nanocomposites as shown in the inset a and b. A mass of 90 g inserted in c and d with different concentrations of nanofillers is subjected to inertial forces. The mass that is used in practical applications is related to inertia.*

Furthermore, the rise in f_{R1} with the GnPs concentration validated the enhanced stiffness of the substances, which is consistent with the findings from the prior assessments of the material's tensile strength and fracture toughness as shown in (Figures 34 and 35). The above observations align with the results of the epoxy/GnPs nanocomposite experiment shown in (Figure 39). The experiment demonstrated a clear connection between the concentration of the filler as well as the linear increase of f_{R1} (204). The mechanical stiffness of the epoxy/HNTs nanocomposites decreased as shown by a decrease in f_{R1} and an increase in the concentration of fillers used for the inertial masses, according to (Figure 39b) (204).

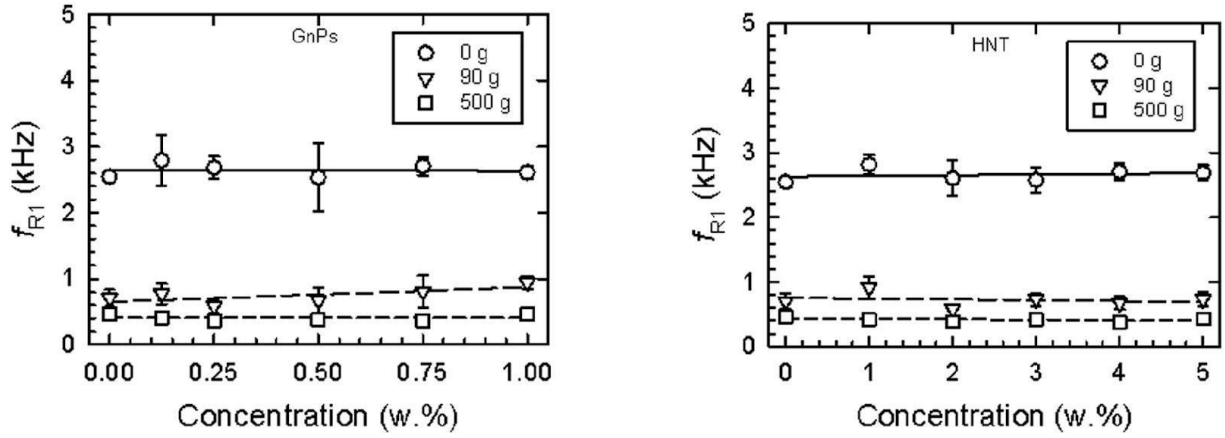

Figure 39. *The concentration dependences of HNTs and GnPs nanocomposites have been compared to their original resonance frequencies. Legend is placed within the graphic.*

12.3.5 Conclusion

The current study has confirmed that it is possible to control the elastic-plastic mechanical properties of complex epoxy resin nanocomposites by using nano-sized GnPs and HNTs fillers. The graph shown in (Figure 34) demonstrates a complex and nonlinear relationship between the concentration of GnPs filler and Young's modulus of elasticity. At exactly the same time, there was an increase in the ductility of the nanocomposites being studied when the concentration of GnPs nanofiller was between 0-1 weight percent. This was demonstrated by the higher elongation at the point of fracture in the specimens, as shown in (Figure 34a). The noted occurrence was ascribed to the interparticle sliding impact demonstrated by the distinct GnPs nanoparticles that dispersed throughout the complex epoxy resin structure. The examination of epoxy/HNTs nanocomposites at concentrations ranging from 1 to 5 wt.% exhibited a steady pattern in Young's modulus of elasticity, with an average value of 2.8 GPa. In addition, (Figure 34) shows that there was a non-linear elongation pattern of approximately 0.35 mm at the point of break. The limited movement of HNTs nanofillers in the matrix is believed to be the root cause of the phenomenon observed during mechanical evaluations. The results of fracture mechanical examinations indicate the rigid epoxy/HNTs nanocomposites tend to be more fracture tough at lower filler concentrations than epoxy/GnPs nanocomposites. This effect can be credited to the GnPs filler's ability to glide and dissipate. The ability of the intricate epoxy/GnPs nanocomposites to change shape and adapt increased as the amount of GnPs filler increased. This was observed through measurements of elongation at break during uniaxial 3-point bending tests. The nanocomposites made of epoxy and HNTs, with a nanofiller concentration of 1 wt.%, exhibited a higher elongation at the point of fracture, measuring 6 mm instead of 5.3 mm. Micro-hardness procedures produced a similar result, with an indentation modulus of 3.4 GPa for epoxy/GnPs nanocomposites compared to 4.0 GPa for epoxy/HNTs nanocomposites (nanofiller concentration 1 wt.%). The epoxy/GnPs nanocomposites appear to have better dissipative mechanical properties, according to this evidence. The previous occurrence was favored to the previously mentioned gliding friction caused by the GnPs nanofiller. The research utilized a distinctive approach to reduce mechanical vibrations, without causing destructive and, by use of forced oscillations. This technique was used to compare the mechanical properties in the low-frequency range of 2-3-200 Hz. The focus was on the location of the initial peak of the resonance frequency. The research verified that epoxy/GnPs nanocomposites exhibited plasticization, as evidenced by a decrease in the position of the very first resonance frequency peak f_{R1} to 2.6 kHz, which was lower than that of epoxy/HNTs nanocomposites, whose f_{R1} magnitude was 2.8 kHz. These two results were acquired when the nanofiller concentration was 1% by weight and there was no inertial mass involved.

*****

12.4 Effect of conditioning on PU foam matrix materials properties

The primary goal of the recently released research article E is to explore the impacts of thermal aging on soft polyurethane foams (PU). Methods including thermal analysis, tensile and compressive testing, and powerful mechanical vibration testing were employed to assess the thermal and mechanical properties. The findings suggest that the physical stiffness of PU foams decreases due to degradation processes caused by an increase in relative humidity in the surrounding atmosphere. The above-mentioned occurrence is credited to the plasticizing of the wall material made of polyurethane foam. As a result, there is a decrease in Young's modulus of elasticity, which leads to an increase in the amount of permanent deformation. The research used a novel approach of vibration damping testing, which does not cause destructive, to confirm the decrease in mechanical stiffness. This decline in stiffness indicates a loss of elasticity due to sample conditioning. The decrease in elastic mechanical performance is further supported by the documented decrease in matrix hardness. The PU foam loses significantly in thermal stability as a result of the conditioning impact.

12.4.1 Materials

The study utilized open-cell soft PU foams that were acquired from a local construction hobby market. The foams had a density of more or less 35.4 grams per cubic centimeter with a tolerance of 0.3 grams per cubic centimeter. Samples of polyurethane, also known as PU, were tested in different shapes and sizes to assess their tensile strength (using dog bone shape), evaluate mechanical vibration, permanent deformation, and measure hardness (using cubic shape). The image depicted in (Figure 40) displays the PU foam utilized in the research. PU foam fragments were utilized for the purpose of thermal analysis. The samples were exposed to various levels of heat (45 and 80°C) and moisture (45 and 80%) for different amounts of time, ranging from 0 to 300 hours, in a controlled environment chamber Discovery 105, angelantoni test technologies, Massa Martana, (Italy).

Figure 40. *The picture below displays the PU foam material that underwent testing.*

12.4.2 Methodology

The uniaxial tensile testing was conducted using the Autograph AGS-X instrument, which is made by Shimadzu in Kyoto, (Japan). The device had been set up making use of the TCE Series compact thermostatic chamber. Tests were conducted in accordance with ČSN EN ISO 527-1 and 527-2 (2012) guidelines, using a deformation rate of 100 mm/min. The study consisted of performing each measurement 10 times and calculating the average results. The research employed a thermal analysis instrument known as SDT 650 Discovery with TRIOS software, which was produced by TA instrument in New Castle, DE, (USA). The instrument was used for conducting DSC/TGA TG and DTA tests simultaneously, and Indium was used as a calibration material for the equipment. Before taking each measurement, the specimens

were placed in an aluminum tray. Consistent observations of weight heat flow and temperature variations were made throughout the experiment. The experiment was carried out in a stationary atmosphere with a heat flow of 10°C a minute, spanning a temperature range of 30 to 300°C. Formula (23) (2013) is used to assess the capability of a material to damping mechanically and symmetrical induced vibrations in single-degree-of-freedom (SDOF) systems, which is measured by the dynamic displacement transmissibility T_d.

$$T_d = \frac{y_2}{y_1} = \frac{a_2}{a_1} = \sqrt{\frac{k^2+(c\cdot\omega)^2}{(k-m\cdot\omega^2)^2+(c\cdot\omega)^2}} \tag{23}$$

where the variables in this equation are known as follows: y_1 represents the displacement amplitude on the start point of the tested sample, y_2 represents the displacement amplitude on the end point, a_1 represents the acceleration amplitude on the start point, a_2 represents the acceleration amplitude on the end point, k represents the stiffness, c represents the damping coefficient, m represents the mass, and w represents the circular frequency (2014,2015). The PU foams being studied were assessed for their dynamic mechanical vibration - damping abilities using the technique of forced oscillation (2016). The degree of permanent deformation has been assessed by adhering to the' ČSN EN ISO 1856 standard. The block being evaluated had dimensions of 50 mm in length, 50 mm in width, and 50 mm in thickness. The displacement transmissibility T_d was evaluated by simulating measurements between the frequency range of 2 Hz and 1000 Hz (2017). This evaluation was conducted using the BK 4810 vibrator along with the BK 3560-B-030 signal pulse multi-function analyzer and the BK 2706 force amplifier. The samples under study were tested for both acceleration amplitudes a_1 and a_2. The assessment was carried out using BK 4393 accelerometers made by Brüel & Kjaer located in Nærum, (Denmark) (2018). The dimensions of the sample being studied were 60 mm in length, 60 mm in width, and 50 mm in thickness. The average displacement-transmissibility was calculated by measuring it three times at a temperature of 25°C, which is considered normal. The indentation method was used to measure the foam hardness using the standard method A of ČSN EN ISO 2439 (645440) for flexible cellular polymeric materials. The samples went through a compression procedure, leading to a 60% decrease in their initial height. After a period of 30 seconds of deformation, the value of force (N) was computed. The samples were measured to be 50 mm in length, 50 mm in width, and 50 mm in thickness. Five measurements were carried out at specific temperatures of 45 as well as 80°C, along with relative humidity levels of 40 and 80%, each measurement was repeated five times in the experiment. The samples went through a 300-hour conditioning procedure where they were subjected to the same temps and relative humidity levels mentioned earlier. After undergoing conditioning, the samples were positioned in the gap of the pressing device and exposed to a pressure that caused their size to decrease by 50 % from the original measurements. This compression process lasted for 30 minutes. After being compressed, the samples were then released and left unrestricted on the flat surface for 30 minutes. The lasting deformation was measured as a ratio to the original size of the sample, and the thickness was reevaluated later.

12.4.3 Result and discussions

The tensile examination of the PU foam components under investigation is shown in (Figure 41). The study revealed that the cellular components improved in mechanical strength and plasticity after 3 hundred hours of conditioning, when subjected to a temperature of 45°C and a relative humidity of 80%, the sample showed an increase in stress at the point of

rupture by 19%, increasing from 155 kPa to 184 kPa. The ductility also rose from 87% under the given conditions of 45°C temperature and 45% humidity to 114% under the given conditions of 80°C temperature and 45% humidity. The conditioning at 80°C exhibited a correlation that remained relatively stable. The durability of the material improved following a 24-hour period of conditioning at a temperature of 45°C and relative humidity of 80%. However, after 48 hours of conditioning, there was a significant drop in mechanical strength. Nevertheless, it was noticed that there was an increase following 3 hundred hours of conditioning. The behavior mentioned previously indicated that significant changes in the structure, which were caused by cross-linking, occurred after 48 hours of exposure to 80% humidity. If the temperature is 80°C and the humidity is relative 45%, then the fracture stress continues to be fairly constant. An increase of around 10% was noticed when the relative humidity was elevated. The information depicted in (Figure 41) displays a noteworthy rise in the ductility of the PU foam material, suggesting that the PU structure has undergone additional plasticization. The improvement in ductility by 19 % from 87% to 114% after subjecting the foam to a 300-hour treatment at 80°C and 45% relative humidity is attributed to changes in the elasticity of the specific cell walls within the foam matrix. The alteration of the foam structure resulted in a modification of the size of each cell, resulting in a rise in the pressure of the air. A change in the shape of individual cellular components is linked to the alteration in magnitude. Cross-linking (2019) and partial hydrolysis (2020) might have affected the viscoplastic and viscoelastic properties of the polyurethane (PU) matrix. It was proposed that the swelling of various parts of the cell walls in PU is a complex reaction of the material. It was hypothesized that the primary ways in which mechanical energy was transferred and dissipated were through viscous friction and the stiffness of the walls (2021).

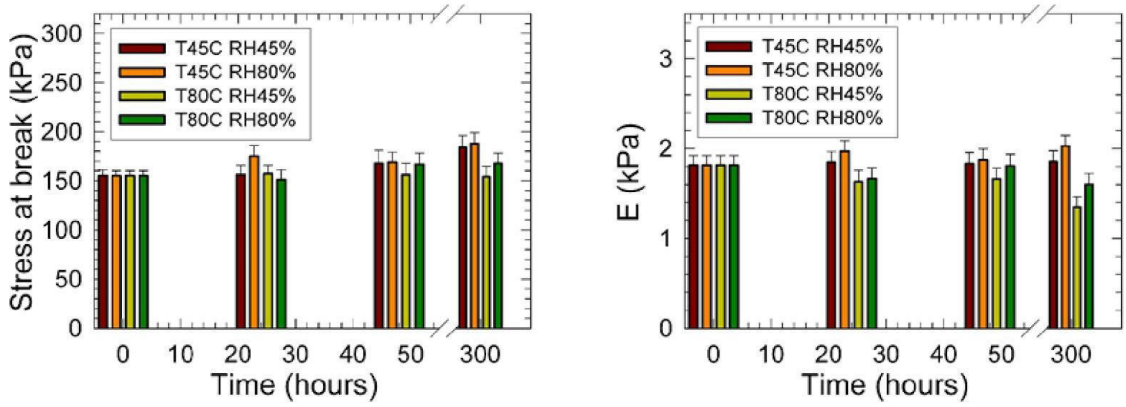

(a) **(b)**

Figure 41. *The results of testing the PU materials being studied through uniaxial tensile evaluation include: (a) determining the stress at which the material breaks and the time it takes to condition at different temperatures and levels of humidity, and (b) determining the elasticity of the material, known as Young's modulus E, while conditioning at different temperatures and levels of humidity. The inset displays the values for T, which represents temperature in degrees Celsius, and RH, which stands for relative humidity in percentage.*

The findings of the research indicate that the increased stress levels observed during the rest of PU samples exposed to 80% relative humidity along with 45°C can be explained by an increase in the stiffness of the structure and the elasticity of Young's modulus. As a result, the brittle pattern of the matrix is enhanced. The research found that signs of matrix hydrolysis were noticed while the conditioning process was carried out at a temperature of 80°C, regardless of the level of relative humidity. The elasticity (E) of the specimen decreased from

1816 Pa (when it was not conditioned) to 1350 Pa (when it had been conditioned at 80°C and 45% relative humidity) and 1600 Pa (when it was conditioned at 80°C and 80% relative humidity). The displacement transmissibility gradually increased with conditioning temperature and relative humidity reaching 80%, according to the results. The PU matrix exhibited greater mechanical stiffness between 250 and 400 Hz, suggesting a higher frequency range. (Figure 42a) illustrates this. A similar result was observed when the conditioning was done at a relative humidity of 40%. According to the hypothesis, the polyurethane matrices that did not react completely underwent a chemical process of cross-linking during the first forty-eight hours of conditioning. This supposition is established by the testing methods used in the past to determine tensile strength. The increased relative humidity as shown in (Figure 42b) resulted in the enhancement of T_d, which made the improvement in mechanical stiffness of the PU matrix even more noticeable. The findings from (Figure 43a) suggest that there is a significant link between the length of time the foams were conditioned and their level of elasticity. The appearance of 2 peaks in the T_d frequencies (occurring at 280 and 430 Hz, with magnitudes of 0.014 and 0.017, respectively) can serve as evidence of this. An increase in stiffness was noticed within the 200 to 600 Hz frequency range, and there have been modifications in mechanical behavior after extended conditioning as shown in (Figure 43b), indicating the presence of plasticity patterns. The foam's elasticity in the frequency range of 200 to 600 Hz was decreased after subjecting it to a 24-hour conditioning period at 80°C and 80% relative humidity, as compared to the initial polyurethane sample. The wall material might have begun to decompose, possibly through hydrolysis.

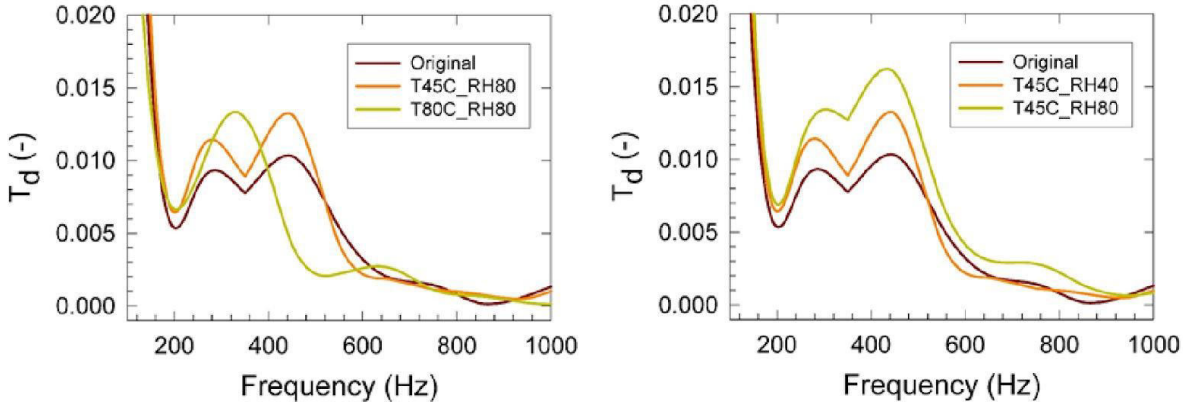

Figure 42. *The relationship between frequency and displacement transmissibility was analyzed using vibration-damping measurements on the PU materials being studied. This was done after a 300-hour conditioning phase, considering the impact of both temperature and humidity conditions. Specifically, the effects of conditioning at 80% relative humidity and below 45°C temperature were examined. The original sample without any conditioning is denoted by the variables T for temperature in degrees Celsius and RH for relative humidity in percentage.*

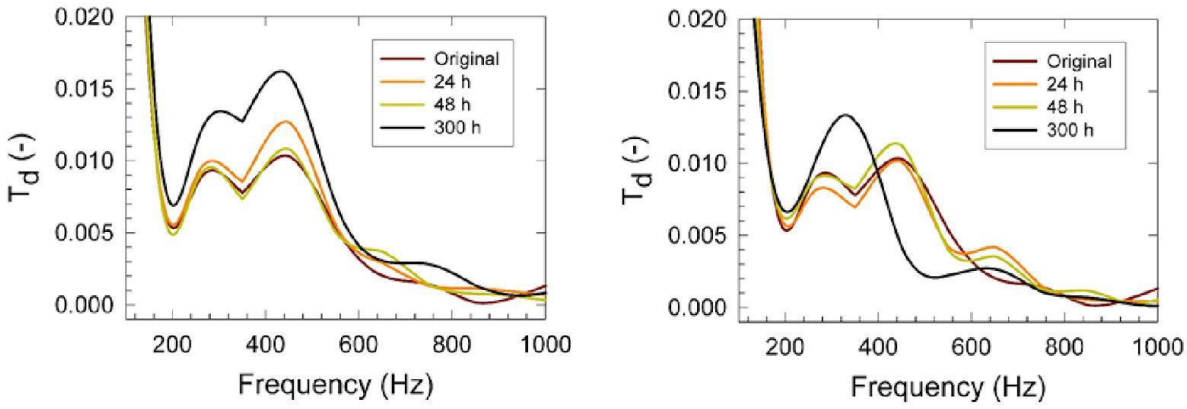

Figure 43. *The examination of the PU substances' oscillation damping demonstrated the correlation between frequency and displacement transmissibility. Figure a display the effects of conditioning time under 45 °C and 80% RH, while Figure b shows the effects of conditioning time under 80°C and 80% RH. The inset indicates the conditioning time in hours, with the original non-conditioned sample.*

The results of sample conditioning on PU foam toughness are shown in (Figure 44). The results indicated that the toughness of all the materials tested decreased, except for those that were subjected to a temperature of 45°C and longer conditioning time. The reduction in hardness observed under the mentioned conditioning details can be attributable to the higher crosslinking density of the PU foam wall matrix. The degree of hardness decreased by 10% to 18% after being conditioned for 300 hours at temperatures between 45°C and 80°C, and with a relative humidity ranging from 45% to 80%. The hardness increased somewhat from 18N to 19 N when relative humidity and the temperature were both 45°C and 45%, respectively. The researchers theorized that the breakdown of PU molecules could be brought on by higher temperatures and increased humidity. Based on Weise et al. (222), crosslinking occurs more frequently in PUs with increased poly(ester) content because ester groups are more prone to hydrolysis than PUs with higher poly(ether) content. The FTIR analysis has confirmed that when ester groups go through hydrolysis, they produce carboxylic acids. These acids then function as unique and non-ductile ionic crosslinks. PU formulations containing only macrodiols experienced a slight rise in mechanical stiffness within the first thousand hours of exposure to weathering. Nevertheless, prolonged contact with weathering led to their eventual deterioration, causing them to weaken to the point of breaking. The results suggest that the deterioration caused a decrease in the mechanical characteristics of poly(ether) type PUs, even though shorter but stiffer crosslinks formed during exposure to weathering.

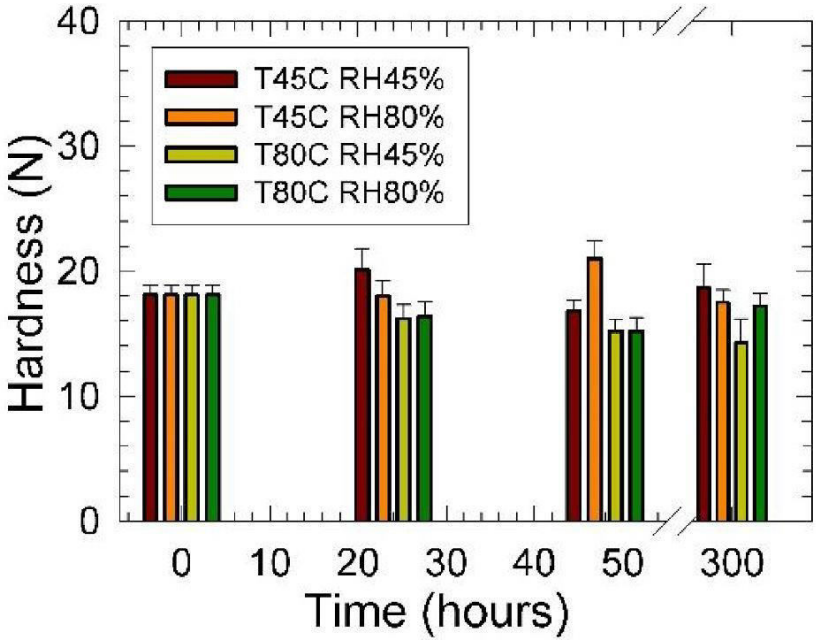

Figure 44. *The correlation between the duration of conditioning and also the level of hardness observed in diverse PU foams under different temperatures and levels of humidity. Inserted: T- represents temperature in degrees Celsius, while RH symbolizes relative humidity in percentage.*

The results shown in (Figure 45) demonstrate that the conditioning temperature plays a significant role in the irreversible deformation of PU foams. In particular, when subjected to a temperature of 45°C during conditioning, there was an increase in elasticity and a decrease in constant deformation when compared with conditioning at higher temperatures. This discovery is in line with the data presented in (Figure 43b), which shows that the Young's modulus of elasticity is greater at lower temperatures of conditioning. The PU foams lasting distortion significantly rose from 18% to 46% as the temperature for conditioning increased from 45°C to 80°C, regardless of the relative humidity. The results showed that the PU foams had a reduced elasticity and an improved plastic mechanical behavior, which were both linked to the reduction in E.

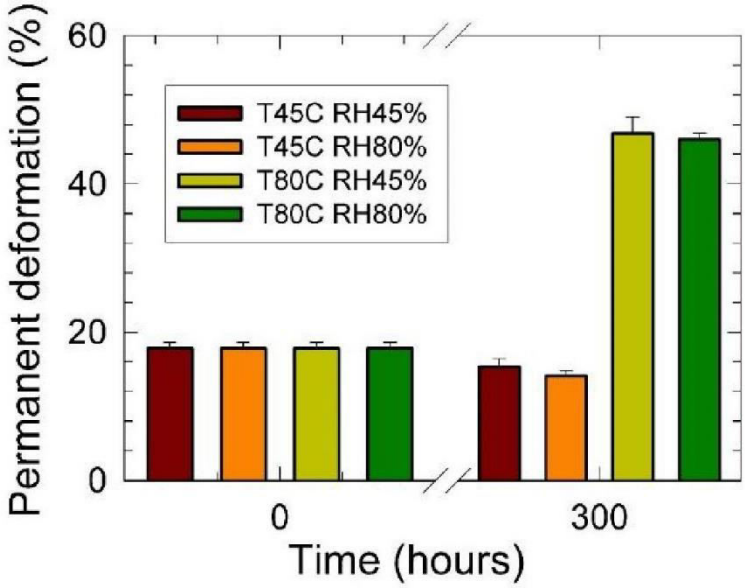

Figure 45. *The relationship between conditioning time and permanent deformation of PU foams is being investigated under different temperature and relative humidity conditions. The inset displays the values for T, which represents temperature in degrees Celsius, and RH, which represents relative humidity in percentage.*

The reference (149) states that single component PUs containing only poly (ester) or poly (ether) macrodiols possess lower mechanical stability than two component PUs containing both macrodiols. The result was a combined effect that resulted in a 24% increase in damping abilities and an 18% enhancement in mechanical strengths after exposure to weather conditions. The enhanced ability of the mixed PUs to absorb vibrations was attributed to a decrease of 15% in the efficiency of the macrodiol chains in packing together, which occurred due to the presence of two different functional groups. The research found that mechanical stabilities increased after weathering, which was due to the combination of the protection and degradation processes of the urethane set by the ester. The degradation structure typically present in the studied polyurethane foams is shown in (Figure 46) and (223,224). The degradation process began at a temperature of 260°C and resulted in a reduction in weight of more or less 86%. Afterwards, there was a release of heat due to the fusion process. The observed deterioration can be explained by the breakdown of the polyurethane material into its individual polyol and also diisocyanate elements. The diisocyanate was then thermally decomposed. The primary substances that were recognized during decomposition were toluene, benzene, phenyl isocyanate, benzonitrile, and methylbenzonitrile. The method of decomposition talked about earlier refers to the process of breaking down diisocyanates and also polyols present in the polyurethane material. This breakdown leads to the emission of carbon dioxide plus hydrogen cyanide gases (225).

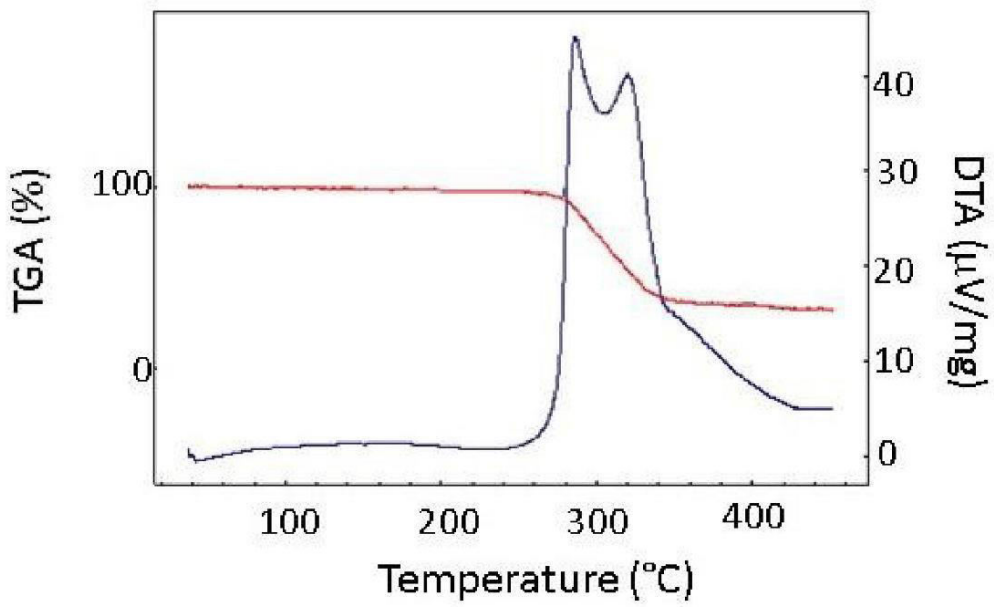

Figure 46. *The red line on the graph signifies the typical thermogravimetric analysis (TGA) pattern observed in the polyurethane foam material. Similarly, the blue line indicates the differential thermal analysis (DTA) pattern observed in the very same material.*

The TGA's evaluation results are briefly summarized in (Figure 47) (215). The empirical evidence suggests that weight loss improves somewhat with increasing conditioning duration, regardless of temperature as well as humidity during conditioning. The alteration in the chemical structure of the polyurethane foam probably resulted in the increase in quantity, perhaps because of the inclusion of unattached isocyanate. The conditioning of PU foam might result in a lessening in its thermal resistance, which is sensible to conclude.

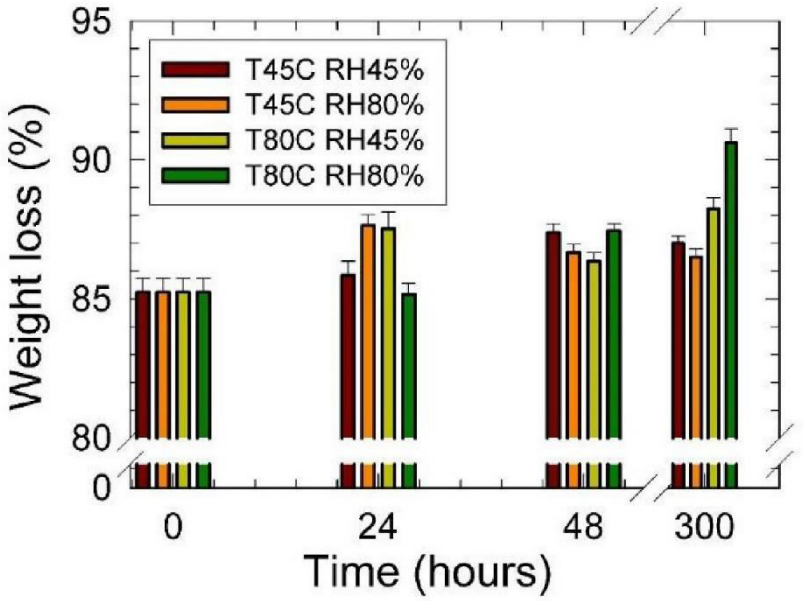

Figure 47. *The PU foams being studied lose weight over time due to conditioning. T-temperature (°C) and RH-relative humidity (%) are shown in the inset.*

12.4.4 Conclusions

The aim of this research was to analyze the physical and chemical characteristics, as well as the mechanical attributes, of commercially available gentle polyurethane foams when subjected to thermal driven degradation. The findings showed that the decline in quality of polyurethane foams began when the temperature and humidity in the surrounding environment increased modulus, the polyurethane foam wall material went through a decrease in stiffnesses due to its plasticization. This was evident from an increment in the constant deformation and dropping in Young's modulus and the elasticity modulus's worth. The phenomenon was even more validated through non - destructive dynamical - mechanical vibration tests, which revealed that the samples exhibited greater vibration damping and reduced elasticity. The decline in the firmness of the matrix was linked to alterations in the mechanical characteristics, suggesting a reduction in the elasticity of the mechanical performance. Moreover, the thermal stability of PU foam was greatly reduced by conditioning.

*****

13. Closing remarks

13.1 Further prospective suggestions for research

The dissertation offers a number of paths for future research and technical progression in the area of polymer nanocomposites. Prospective aspects include the following possibilities:

1) Optimization of filler concentration: Further investigation can focus on enhancing the concentration of fillers in polymer composites to attain the aimed thermal and mechanical features. researchers will be able to gather more comprehensive data and obtain a deeper understanding of the effects of fillers. For specific purposes, it is possible to determine the ideal combination of stiffness, fracture toughness, ductility, along with thermal stability.

2) Investigation of novel fillers: The scope for polymer composites can be expanded by investigating new fillers that possess distinctive characteristics. Scientists could explore how various forms of nanoparticles, fibers, or several other substances added as fillers can enhance specific characteristics or achieve multiple functionalities. Understanding the way in which polymers interact with matrices and how it affects their thermal and mechanical performance is of utmost importance.

3) Advanced techniques for characterization: can offer a more comprehensive understanding of the performance of polymer composites. Advanced microscopy techniques like atomic force microscopy (AFM) and electron microscopy can uncover the microscopic structure and distribution of fillers in the polymer matrix at the nanoscale level. Furthermore, the use of in situ mechanical testing in conjunction with imaging techniques that operate in real-time can enhance comprehension of deformation and failure mechanisms.

4) Fillers that are Sustainable and bio-based: The quest for sustainable and bio-derived substances to use as fillers in polymer composites is gaining greater significance as sustainability becomes a more prominent concern. Investigations can center on the use of fillers obtained from sustainable resources or discarded materials, which can help in the advancement of environmentally friendly and financially feasible composites.

5) Modeling and simulation: Polymer composites and their thermal and mechanical features can be contributed by using modeling and simulation software. By combining empirical data and computer models, the researchers can enhance their understanding of the fundamental behavior of composite materials in different strategies.

6) Application-based research: Prospective research can be driven by specific needs, such as automotive, aerospace, construction, or biomedical sectors. By tailoring the mechanical and thermal aspects of polymer composites to meet the requirements of these applications, researchers can participate in the development of high-performance, and sustainable substances.

13.2 Final conclusion

The objectives of the dissertation are to improve overall understanding and advancements in technology through the following targets:

1) Exploration of the impact of fillers: The main focus of the thesis is to explore how different fillers, including perlite, nano $CaCO_3$, nanoclay, GnPs, and HNTs, impact the thermal and mechanical characteristics of polymer composites, thereby adding to the general comprehension of this topic. The thesis improves our realization of how fillers and polymer matrices interact by looking at the impacts of these fillers.

2) Mechanical property improvement: The technology is advanced through the examination of how mechanical properties in polymer composites can be improved, as explored in the thesis. The study examines the effects of fillers on Young's modulus of suppleness, elongation at break, fracture toughness and plastic elastic behavior. The examination of the mechanical characteristics of composites can assist in developing materials that possess greater strength and longevity, suitable for a range of uses.

3) Nondestructive testing methods: The technology is enhanced by the thesis through the utilization of non-destructive testing methods such as non-destructive vibrator testing along with dynamic mechanical vibration testing. These techniques provide an understanding of the mechanical behavior of polymer composites without causing any damage. The results will aid in evaluating the reliability and excellence of composite materials in practical situations.

4) The fourth aspect is related to the resistance of a substance to heat and its potential breakdown: The research conducted in the thesis adds to the overall understanding of polymer foams and composites by examining their thermal stability and patterns of degradation. This study investigates how variations in temperature and humidity during conditioning affect the mechanical characteristics and thermal endurance of polyurethane foams. To create products that are more durable and dependable, it is necessary to understand the ways in which these materials degrade and behave under different temperatures.

In outline: The dissertation's essential argument sets the stage for future investigations into enhancing the amount of filler used, synthesis of novel types of fillers, improving methods for analysis, and creating patterns that account for multiple measurements. These possible topics have the potential to lead progress in the creation and improvement of polymer composites, resulting in boosting features and expanded uses.

*****

List of publications

A. **Murtaja, Y**., Lapčík, L., Lapčíková, B., Gautam, S., Vašina, M., Spanhel, L., & Vlček, J. (2022). Intelligent high-tech coating of natural biopolymer layers. *Advances in colloid and interface science*, *304*, 102681. https://doi.org/10.1016/j.cis.2022.102681. Impact Factor (IF): 15.6

B. Lapčík, L., Vašina, M., Lapčíková, B., Staněk, M., Ovsík, M. & **Murtaja, Y**. (2020). Study of the material engineering properties of high-density poly(ethylene)/perlite nanocomposite materials. *Nanotechnology Reviews*, *9*(1), 1491-1499. https://doi.org/10.1515/ntrev-2020-0113. Impact Factor (IF): 7.848

C. **Murtaja, Y**., Lapčík, L., Sepetcioglu, H., Vlček, J., Lapčíková, B., Ovsík, M. & Staněk, M. (2022). Enhancement of the mechanical properties of HDPE mineral nanocomposites by filler particles modulation of the matrix plastic/elastic behavior. *Nanotechnology Reviews*, *11*(1), 312-320. https://doi.org/10.1515/ntrev-2022-0023. Impact Factor (IF): 7.14

D. Lapčík, L., Sepetcioğlu, H., **Murtaja, Y**., Lapčíková, B., Vašina, M., Ovsík, M., Staněk, M. & Gautam, S. (2023). Study of mechanical properties of epoxy/graphene and epoxy/halloysite nanocomposites. *Nanotechnology Reviews*, *12*(1), 20220520. https://doi.org/10.1515/ntrev-2022-0520. Impact Factor (IF): 7.14

E. Lapčík, L., Vašina, M., Lapčíková, B., & **Murtaja, Y**., (2021). Effect of Conditioning on PU Foam Matrix Materials Properties. *Materials (Basel, Switzerland)*, *15*(1), 195. https://doi.org/10.3390/ma15010195. Impact Factor (IF): 3.748

Conference presentations

I. **Lapčíková, B.**, Lapčík, L., Murtaja, Y., ″Materials characterization of advanced fillers for composites engineering applications″, Poster 58, e-book of Abstracts of 7th International Conference of Engineering Against Failure, June 21-23, 2023, Spetces Island, Greece. Page 72. Conference co-chairmen: Prof. Spiros Pantelakis (University of Patras, Greece) and Prof. Michael Vormwald (TU Darmstadt, Germany).

II. **Lapčík, L.**, Murtaja, Y., Lapčíková, B., ″Study of mechanical properties of epoxy/graphene and epoxy/halloysite nanocomposites″, Oral presentation 65, e-book of Abstracts of 7th International Conference of Engineering Against Failure, June 21-23, 2023, Spetces Island, Greece. Page 83. Conference co-chairmen: Prof. Spiros Pantelakis (University of Patras, Greece) and Prof. Michael Vormwald (TU Darmstadt, Germany).

III. **Murtaja, Y.**, Lapčík, L., Lapčíková, B., ″Study of the material engineering properties of high-density poly(ethylene)/perlite nanocomposite materials″, Oral presentation 73, e-book of Abstracts of 7th International Conference of Engineering Against Failure, June 21-23, 2023, Spetces Island, Greece. Page 93. Conference co-chairmen: Prof. Spiros Pantelakis (University of Patras, Greece) and Prof. Michael Vormwald (TU Darmstadt, Germany).

References

1. Lapcik L, Lapcikova B, Zboril R. Paper-Based Composite Planar Material, EP3034693B1. Munich: European Patent Office; 2018.

2. Lapcik L, Peterkova Petra, Gheorghiu Mihnea. Method of increasing polypropylene biocompatibility by formation of a structured surface layer based on native or modified collagen. CZ-Patent CZ294386,2004.

3. Lapcik L, Lapcik L, Kubicek P, et al. Study of penetration kinetics of sodium hydroxide aqueous solution into wood samples. BioResources 2014;9:881-93.

4. Marchessault RH. All things cellulose: a personal account of some historic events. Cellulose 2011;18:1377-9.

5. Zhang X, Hikal Walid M, Zhang Yue, et al. Direct laser initiation and improved thermal stability of nitrocellulose/graphene oxide nanocomposites. Appl.Phys. Lett. 2013;102:141905.

6. Li A, Wang Yadong, Deng Lijuan, et al. Use of nitrocellulose membranes as a scaffold in cell culture. Cytotechnology 2013;65:71-81.

7. Gao X, Xu Li-Ping, Xue Zhongxin, et al. Dual-scaled porous nitrocellulose membranes with underwater superoleophobicity for highly efficient oil/water separation. Adv Mater 2014;26:1771-5.

8. Stilwell RL, Marks MG, Saferstein L, Wiseman DM. Oxidized cellulose: chemistry, processing and medical applications. Drug Target Recov Handb Biodegr Polym 1997;7:291-306.

9. Kumar V, Yang Tianrun. HNO_3/H_3PO_4-$NaNO_2$ mediated oxidation of cellulose preparation and characterization of bioabsorbable oxidized celluloses in high yields and with different levels of oxidation. Carbohydr Polym 2002;48:403-12.

10. Bajerová Martina, Krejčová´ Kateřina, Rabišková Miloslava, et al. Oxycellulose beads with drug exhibiting pH-dependent solubility. AAPS PharmSciTech 2011;12: 1348-57.

11. Kanmani P, Rhim Jong-Whan. Properties and characterization of bionanocomposite films prepared with various biopolymers and ZnO nanoparticles. Carbohydr Polym 2014;106:190-9.

12. Noreen A, Zia Khalid Mahmood, Tabasum Shazia, et al. Hydroxyethylcellulose-g- poly (lactic acid) blended polyurethanes: preparation, characterization and biological studies. Int J Biol Macromol 2020;151:993-1003.

13. Alekseeva OV, Rodionova Anna N, Bagrovskaya Nadezhda A, Agafonov Alexandr V, Noskov Andrew V. Effect of the bentonite filler on structure and properties of composites based on hydroxyethyl cellulose. Arab J Chem 2019;12:398-404.

14. Lapcik L, Lapcik L, De Smedt S, Demeester J, Chabrecek P. Hyaluronan: preparation, structure, properties, and applications. Chem Rev 1998;98:2663-84.

15. Uyanga KA, Okpozo Oghenefego P, Onyekwere Okwuchi S, Daoud Walid A. Citric acid crosslinked natural bi-polymer-based composite hydrogels: effect of polymer ratio and beta-cyclodextrin on hydrogel microstructure. React Funct Polym 2020; 154:104682.

16. Kupska I, Lapcik L, Lapcikova B, Zakova K, Jurikova J. The viscometric behaviour of sodium hyaluronate in aqueous and KCl solutions. Colloids Surf A Physicochem Eng Asp 2014;454:32-7.

17. Toledo PV, Limeira Diego PC, Siqueira Nicolas C, Petri Denise FS. Carboxymethyl cellulose/poly (acrylic acid) interpenetrating polymer network hydrogels as multifunctional adsorbents. Cellulose 2019;26:597-615.

18. Raab M. Materiály a člověk: (Materiály a člověk: netradiční úvod do současné materiálové vědy). 1999.

19. Lapcík L, Lapcíkov´a Barbora, Stasko Andrej, EPR study of the thermal decomposition of transannular peroxide of anthracene. Int J Org Chem 2011;1:37.

20. Maleki A, Kjøniksen Anna-Lena, Nyström Bo. Effect of shear on intramolecular and intermolecular association during cross-linking of hydroxyethylcellulose in dilute aqueous solutions. J Phys Chem B 2005;109:12329-36.

21. Lei M, Chen Z, Lu H, Yu K. Recent progress in shape memory polymer composites: methods, properties, applications and prospects. Nanotechnol Rev. 2019 Jan;8(1):327-51.

22. Chamis CC. Polymer composite mechanics review – 1965 to 2006. J Reinf Plast Compos. 2007;26(10):987-1019.

23. Singh P, Magalhães Solange, Alves Luis, et al. Cellulose-based edible films for probiotic entrapment. Food Hydrocoll 2019; 88:68-74.

24. Singh N, Hui D, Singh R, Ahuja IPS, Feo L, Fraternali F. Recycling of plastic solid waste: a state of art review and future applications. Compos Part B Eng. 2017 Apr 15;115:409-22.

25. Recycling of plastic solid waste: a state of art review and future applications. Compos Part B Eng. 2017 Apr 15;115:409-22.

26. Mora A, Verma P, Kumar S. Electrical conductivity of CNT/ polymer composites: 3D printing, measurements and modeling. Compos Part B Eng. 2020 Feb 15;183:107600.

27. Mikula M, Čeppan M, Blecha J, Lapcík L, Kalíšek V. Kinetic dissolution measurement of polymers by solution viscosity recording. Polym Test 1988;8: 339-51.

28. Wang X, Xu P, Han R, Ren J, Li L, Han N, et al. A review on the mechanical properties for thin film and block structure char- acterised by using nanoscratch test. Nanotechnol Rev. 2019 Jan;8(1):628-44.

29. Kenisarin MM, Kenisarina KM. Form-stable phase change materials for thermal energy storage. Renew Sustain Energy Rev. 2012 May;16(4):1999-2040.

30. Beesetty P, Kale A, Patil B, Doddamani M. Mechanical behavior of additively manufactured nanoclay/HDPE nanocomposites. Compos Struct. 2020 Sep 1;247:112442.

31. Lopez-Gonzalez M, Flores A, Marra F, Ellis G, Gomez-Fatou M, Salavagione J, et al. Graphene and polyethylene: a strong combination towards multifunctional nanocomposites. Polymers. 2020 Sep;12(9):2094.

32. Privalko E, Pedosenko A, Privalko V, Walter R, Friedrich K. Composition-dependent properties of Polyethylene Kaolin composites. I. Degree of crystallinity and melting behavior of polyethylene. J Appl Polym Sci. 1999 Aug 15;73(7):1267-71.

33. Da Silva A, Rocha M, Moraes M, Valente C, Coutinho F. Mechanical and rheological properties of composites based on polyolefin and mineral additives. Polym Test. 2002 Feb;21(1):57-60.

34. Zhang Y, Shi J, Zheng J. A method of fracture toughness JIC measurement based on digital image correlation and acoustic emission technique. Mater Des. 2021;197.

35. Gill YQ, Jin J, Song M. Comparative study of carbon-based nanofillers for improving the properties of HDPE for potential applications in food tray packaging. Polym Polym Compos. 2020 Oct;28(8-9):562-71.

36. Lapčík L, Maňas D, Vašina M, Lapčíková B, Řezníček M, Zádrapa P. High density poly(ethylene)/$CaCO_3$ hollow spheres composites for technical applications. Compos Part B Eng. 2017 Mar 15;113:218-24.

37. Ehrenstein GW, Riedel G, Trawiel P. Thermal analysis of plastics: theory and practice. Munich: Carl Hanser Verlag; 2004.

38. Sun X, Zhang J. Displacement transmissibility characteristics of harmonically base excited damper isolators with mixed viscous damping. Shock Vibrat. 2013;20(5):921-31.

39. Tu Z, Shim V, Lim C. Plastic deformation modes in rigid poly-urethane foam under static loading. Int J Solids Struct. 2001 Dec;38(50-51):9267-79.

40. Mishra A, Gangele A. Smart materials for clean and sustainable technology for smart cities. Mater Today Proc 2020;29:338-42.

41. Lv J, Liu Zhuoyu, Zhang Jie, Huo Jizhen, Yu Yingfeng. Bio-based episulfide composed of cardanol/cardol for anti-corrosion coating applications. Polymer 2017;121:286-96.

42. Bourbonnais R, Marchessault Robert H. Application of polyhydroxyalkanoate granules for sizing of paper. Biomacromolecules 2010;11:989-93.

43. Hu B. Biopolymer-based lightweight materials for packaging applications. Light Mater Biopolymers Biofibers 2014:239-55.

44. Nicolson PC, Baron Richard Carlton, Chabrecek Peter, et al. Extended wear ophthalmic lens. In: Official Gazette of the United States Patent and Trademark Office Patents; 2017.

45. Chabrecek P, Lohmann D. Surface modification of extended wear contact lenses by

plasma-induced polymerization of vinyl monomers. Fundam Appl Asp Chemically Modified Surf 1999:223-34.

46. Marchessault RH. All things cellulose: a personal account of some historic events. Cellulose 2011;18:1377-9.

47. Shao ZQ, Wang WJ. Structure and Properties of Cellulose Nitrate. Beijing: National Defense Industry Press; 2011.

48. Zhang Y, Wang Feijun, Gao Kezheng, Liu Yanhua, Shao Ziqiang. Alcogel and aerogel of nitrocellulose formed in nitrocellulose/acetone/ethanol ternary system. Int J Polym Mater Polym Biomater 2016;65:377-83.

49. Tunç S, Duman Osman. Preparation and characterization of biodegradable methyl cellulose/montmorillonite nanocomposite films. Appl Clay Sci 2010;48: 414-24.

50. Mikula M, Čeppan M, Blecha J, Lapcík L, Kalíšek V. Kinetic dissolution measurement of polymers by solution viscosity recording. Polym Test 1988;8: 339-51.

51. Kalisek V, Lapcik L, Mikulaskova B. Evaluation of the fixation of polyester-based textile materials. III. Influence of the fixation conditions on swelling time and degree of fixation. J Polym Mater 1998;15:299-309.

52. Pelikan P, Čeppan Michal, Liška Marek. Applications of numerical methods in molecular spectroscopy. In: Fundamental & Applied Aspects of Chemometrics Book. 1; 2020.

53. LAPČÍK, Lubomír, Michal ČEPPAN a Peter PELIKÁN. Fotochemické procesy. Bratislava: Alfa, 1989. Edícia literatúry pre spotrebný priemysel (Alfa).

54. Gao J H and Xu B Nano Today 2009;4:37.

55. Taniguchi N Ann. CIRF 1983;2:573.

56. Meclean S, Processer E, O'Malley D, Clark N, Ramtoola Z and Brayden D Eur. J. Pharm. Sci. 1998;6:153.

57. Oppenheim R C Int. J. Pharm. 1981;8:217.

58. Kreuter J Pharm. Acta Helv. 1983;58:217.

59. Schafer V, von Briesen H, Andreesen R, Steffan A M, Royer C, Troster S, Kreuter J and Rubsamen-Waigmann H Pharm. Res. 1992;9:541.

60. Narayani R and Rao K P Int. J. Pharm. 1993;95:85.

61. Berthold A, Cremer K and Kreuter J J. Control. Release 1996;39:17.

62. Kreuter J Nanoparticles in Colloidal Drug Delivery Systems (New York: Marcel Dekker) 1994 p 219.

63. Kreuter J J. Drug Target 1995;3:171.

64. Scheffel U, Rhodes B A, Natarajan T K and Wagner H N J. Nucl. Med. 1972;13:498.

65. Birrenbach G and Speiser P J. Pharm. Sci. 1976;65:1763.

66. Kreuter J and Speiser P P Infect. Immun. 1976;13:204.

67. Couvreur P, Kante B, Roland M, Guiot P, Bauduin P and Speiser P J. Pharm. Pharmacol. 1979;31:311.

68. Gurny R Drug Dev. Ind. Pharm. 1981;7:1.

69. Vauthier-Holtzscherer C, Benabbou S, Spenlehauer G, Veillard M and Couvreur P STP Pharm. Sci. 1991;1:109.

70. Allemann E, Leroux J C, Gurny R and Doelker E Pharm. Res. 1993;10:1732.

71. Mathiowitz E et al Nature 1997;386:410.

72. Couvreur P and Vauthier C J. Control. Release 1991;17:187.

73. Couvreur P and Vauthier C Drug Absorption Enhancement Concepts, Limitations and Trends ed A G de Boer (Leiden Amsterdam: Harwood Academic) 1994 p 457.

74. Couvreur P, Dubernet C and Puisieux F Eur. J. Pharm. Biopharm. 1995;41:2.

75. Fattal E, Vauthier C, Aynie I, Nakada Y, Lambert G, Malvy C and Couvreur P J. Control. Release 1998;53:137.

76. Labhasetwar V, Song C and Levy R J Adv. Drug Deliv. Rev. 1997;24:63.

77. Maassen S, Fattal E, Müller R H and Couvreur P STP Pharma. 1993;3:11.

78. Fernandez-Urrusuno R, Fattal E, Porquet D, Feger J and Couvreur P Toxicol. Appl. Pharmacol. 1995;130:272.

79. Emile C, Bazile D, Herman F, Helene C and Veillard M Drug Deliv. 1996;3:187.

80. Rajaonarivony M, Vauthier C, Couarraze G, Puisieux F and Couvreur P J. Pharm. Sci. 1993;82:912.

81. Wang N and Wu X S Pharm. Dev. Technol. 1997;2:135.

82. Calvo P, Remunan-Lopez C, Vila-Jato J L and Alonso M J Pharm. Res. 1997;14:1431.

83. Kumaresh S S, Tejraj M A, Anandrao R K and Walter E R J. Control. Release 2001;70:1.

84. Mua L and Seowc P H Colloids Surf. B 2006;47:90.

85. Couvreur P, Gref R, Andrieux K and Malvy C Prog. Solid State Chem. 2006;34:231.

86. Harito C, Bavykin DV, Yuliarto B, Dipojono HK, Walsh FC Polymer nanocomposites having a high filler content: synthesis, structures, properties, and applications. Nanoscale 2019;11:4653-4682.

87. Hashim AA Polymer thin films. Published by In-Teh In-Teh Olajnica 19/2, 32000 Vukovar, Croatia 2010.

88. Alonso-Redondo E, Belliard L, Rolle K, Graczykowski B, Tremel W, Djafari-Rouhani B, Fytas G Robustness of elastic properties in polymer nanocomposite films examined over the full volume fraction range. Sci Rep 2018; 8:16986.

89. Blattmann CO, Pratsinis SE Single-step fabrication of polymer nanocomposite films. Materials., 2018;11.

90. Begam N, Nimmi Das A, Chandran S, Ibrahim M, Padmanabhan V, Sprung M, Basu JK Nanoparticle-polymer interfacial layer properties tune fragility and dynamic heterogeneity of a thermal polymer nanocomposite films, royal society of chemistry. Soft Matter 2018; 14:8853-8859.

91. Mishra R, Militky J (2019) Nanocomposites. In: Nanotechnology in textiles theory and application. The textile institute book series. pp 263-310, Elsevier.

92. Nanotechnologies-Terminology and definitions for nano-objects-Nanoparticle, nanofibre and nanoplate, ISO/TS 27687:2008. [Accessed March 30,2015]. Iso.org. 26-1-2012. Ref Type: Electronic Citation.

93. Fabbri, P.; Messori, M., Surface Modification of Polymers: Chemical, Physical, and Biological Routes. In Modification of Polymer Properties, Jasso-Gastinel, C. F.; Kenny, J. M., Eds. William Andrew Publishing: 2017; 5:109-130.

94. Liedermann K, Lapčík L, Desmedt S. Study of the Molecular Mobility of Polysaccharide Solid Thin Layers by Dielectric Relaxation Spectroscopy. MRS Online Proceedings Library (OPL); 1997. p. 500.

95. Yu P, Hou Yufeng, Zhang Hongjie, et al. Characterization and solubility effects of the distribution of carboxymethyl substituents along the carboxymethyl cellulose molecular chain. BioResources 2019;14:8923-34.

96. Liedermann K, Lapcik LJ. Dielectric relaxation spectroscopy of some polysaccharides. Chem Pap 1996;50:218-23.

97. Mali KK, Dhawale SC, Dias RJ, Dhane NS, Ghorpade VS. Citric acid crosslinked carboxymethyl cellulose-based composite hydrogel films for drug delivery. Indian J Pharm Sci 2018;80:657-67.

98. Tirpude RN, Puranik Prashant K. Rabeprazole sodium delayed-release multiparticulates: effect of enteric coating layers on product performance. J Adv Pharm Technol Res 2011;2:184.

99. Kausar A. Polymer coating technology for high performance applications: fundamentals and advances. J Macromol Sci A 2018;55:440-8.

100. Choi H, Park Hyungmin, Sagong Woong, Lee Sang-im. Biomimetic flow control based on morphological features of living creatures. Phys Fluids 2012;24:121302.

101. Marcelo G, Saiz Enrique, Pilar Tarazona M. Determination of molecular parameters of hydroxyethyl and hydroxypropyl celluloses by chromatography with dual detection. J Chromatogr A 2007;1165:45-51.

102. Guo J, Skinner GW, Harcum WW, Barnum PE. Pharmaceutical applications of naturally occurring water-soluble polymers. Pharm Sci Technol Today 1998;1: 254-61.

103. Lopez CG, Colby Ralph H, Cabral João T. Electrostatic and hydrophobic interactions in NaCMC aqueous solutions: effect of degree of substitution. Macromolecules 2018;51:3165-75.

104. Barba C, Montan´e Daniel, Farriol Xavier, Desbri`eres Jacques, Rinaudo Marguerite. Synthesis and characterization of carboxymethylcelluloses from non-wood pulps II. Rheological behavior of CMC in aqueous solution. Cellulose 2002;9:327-35.

105. Lopez CG, Richtering Walter. Oscillatory rheology of carboxymethyl cellulose gels: influence of concentration and pH. Carbohydr Polym 2021;267:118117.

106. Liebert TF, Heinze Thomas J. Exploitation of reactivity and selectivity in cellulose functionalization using unconventional media for the design of products showing new superstructures. Biomacromolecules 2001;2:1124-32.

107. Xiquan L, Tingzhu Qu, Shaoqui Qi. Kinetics of the carboxymethylation of cellulose in the isopropyl alcohol system. Acta Polym 1990;41:220-2.

108. Dürig G, Banderet A. Sur la structure des solutions aqueuses de carboxymethylcellulose. Helv Chim Acta 1950;33:1106-18.

109. DeButts EH, Hudy JA, Elliott JH. Rheology of sodium carboxymethylcellulose solutions. Ind Eng Chem 1957;49:94-8.

110. Hermans Jr J. Investigation of the elastic properties of the particle network in gelled solutions of hydrocolloids. I. Carboxymethyl cellulose. J Polym Sci A Gen Pap 1965;3:1859-68.

111. Patruyo LG, Müller AJ, Sa´ez AE. Shear and extensional rheology of solutions of modified hydroxyethyl celluloses and sodium dodecyl sulfate. Polymer 2002;43: 6481-93.

112. Sau AC, Landoll Leo M. Synthesis and Solution Properties of Hydrophobically Modified (Hydroxyethyl) Cellulose. 1989.

113. Tanaka R, Meadows J, Williams PA, Phillips GO. Interaction of hydrophobically modified hydroxyethyl cellulose with various added surfactants. Macromolecules 1992;25:130-10.

114. Kästner U, Hoffmann H, Dönges R, Ehrler R. Hydrophobically and cationically modified hydroxyethyl cellulose and their interactions with surfactants. Colloids Surf A Physicochem Eng Asp 1994;82:279-97.

115. Kästner U, Hoffmann H, Dönges R, Ehrler R. Interactions between modified hydroxyethyl cellulose (HEC) and surfactants. Colloids Surf A Physicochem Eng Asp 1996;112:209-25.

116. Panmai S, homme RK Prud, Peiffer DG, Jockusch S, Turro NJ. Langmuir18; 2002. p. 3860-4.

117. Thuresson K, Nilsson Svante, Lindeman Björn. Influence of cosolutes on phase behavior and viscosity of a nonionic cellulose ether. The effect of hydrophobic modification. Langmuir 1996;12:2412-7.

118. Rachtanapun P, Luangkamin Suwaporn, Tanprasert Krittika, Suriyatem Rungsiri. Carboxymethyl cellulose film from durian rind. LWT- Food Sci Technol 2012;48: 52-8.

119. Wahyuningtyas D, Dinata Arwitra. Combination of Carboxymethyl Cellulose (CMC)-Corn Starch Edible Film and Glycerol Plasticizer as a Delivery System of Diclofenac Sodium1977; 2018. 030032.

120. Lu Z, Huang Jizhen, Songfeng E, et al. All cellulose composites prepared by hydroxyethyl cellulose and cellulose nanocrystals through the crosslink of polyisocyanate. Carbohydr Polym 2020;250:116919.

121. Khan A, Khan Ruhul A, Salmieri Stephane, et al. Mechanical and barrier properties of nanocrystalline cellulose reinforced chitosan-based nanocomposite films. Carbohydr Polym 2012;90:1601-8.

122. Huq T, Salmieri Stephane, Khan Avik, et al. Nanocrystalline cellulose (NCC) reinforced alginate based biodegradable nanocomposite film. Carbohydr Polym 2012;90:1757-63.

123. Kassem I, Kassab Zineb, Khouloud Mehdi, et al. Phosphoric acid-mediated green preparation of regenerated cellulose spheres and their use for all-cellulose cross- linked superabsorbent hydrogels. Int J Biol Macromol 2020;162:136-49.

124. Kirsch M, Birnstein Luise, Pepelanova Iliyana, et al. Gelatin-methacryloyl (GelMA) formulated with human platelet lysate supports mesenchymal stem cell proliferation and differentiation and enhances the hydrogel's mechanical properties. Bioengineering 2019;6:76.

125.Barrer RM. Some properties of diffusion coefficients in polymers. J Phys Chem 1957;61:178-89.

126. Mourougou-Candoni N, Prunet-Foch B, Legay F, Vignes-Adler M, Wong K. Influence of dynamic surface tension on the spreading of surfactant solution droplets impacting onto a low-surface-energy solid substrate. J Colloid Interface Sci 1997;192:129-41.

127. Thompson RL. Solvent-free polymer lithography via the Kirkendall effect. Nucl Instrum Methods Phys Res Sect B 2010;268:2181-4.

128. Abou-Yousef H, Kamel Samir. High efficiency antimicrobial cellulose-based nanocomposite hydrogels. J Appl Polym Sci 2015:132.

129. Lapčík, L., Valko, L., Mikula, M., Jančovičová, V., Panák, J. (1988). Kinetics of swollen

surface layer formation in the diffusion process of polymer dissolution. In: Hummel, K., Schurz, J. (eds) Dispersed Systems. Progress in Colloid & Polymer Science, vol 77. Steinkopff. https://doi.org/10.1007/BFb0116788.

130. Layer Formation in the Diffusion Process of Polymer Dissolution. 1988. p. 221-6. Ueberreiter K, Asmussen UF. J Polym Sci A 1957;23:75.

131. Ueberreiter VK, Asmussen Frithjof. Die auflösungsgeschwindigkeit von polymeren. 1. Formulierung des vorganges und seine temperaturabha¨ngigkeit, Die Makromolekulare Chemie. Macromol Chem Phys 1961;44:324-37.

132. Asmussen VF, Ueberreiter Kurt. Die auflösungsgeschwindigkeit von polymeren, 2. Mitteilung. Untersuchung der stabilit¨at der quellschicht durch konzentrationsund viskosita tsmessungen, Die Makromolekulare Chemie. Macromol Chem Phys 1962;52:164-73.

133. Ueberreiter K, Asmussen Frithjof. Velocity of dissolution of polymers. Part I. J Polym Sci A 1962;57:187-98.

134. Asmussen F, Ueberreiter Kurt. Velocity of dissolution of polymers. Part II. J Polym Sci A 1962;57:199-208.

135. Asmussen F, Ueberreiter Kurt. Die auflösungsgeschwindigkeit von Polymeren. Kolloid-Z Z Polymere 1968;223:6-13-2.

136. Ueberreiter VK, Kirchner Peter. Die auflo¨ auflösungsgeschwindigkeit von polymeren. 4. Mitt. Der einfluß der stro¨mung des lo¨sungsmittels, Die Makromolekulare Chemie. Macromol Chem Phys 1965;87:32-59.

137. Pisarcik M, Mikula M, Mariianiova D, Lapcik L. The influence of hydroxyethylcellulose on the diffusion of acetylsalicylic-acid trihydromagnesium salt in aqueous-solution. Acta Polym 1993;44:92-6. https://doi.org/10.1002/ actp.1993.010440206.

138. Peterkova P, Lapcik L. Determination of the diffusion coefficient of water into atelocollagen type I thin films by attenuated total reflection Fourier transform infrared spectroscopy. Colloid Polym Sci 2000;278:1014-6. https://doi.org/ 10.1007/s003960000366.

139. Xiong RH, Deschout H, Demeester J, De Smedt SC, Braeckmans K. Rectangle FRAP for measuring diffusion with a laser scanning. Microscope 2014;1076: 433-41. https://doi.org/10.1007/978-1-62703-649-8_18; 10.1007/978-1-62703- 649-8.

140. Wu Y, Joseph Sony, Aluru NR. Effect of cross-linking on the diffusion of water, ions, and small molecules in hydrogels. J Phys Chem B 2009;113:3512-20.

141. Jamlang J, Maran˜on Mica Therese, Rigor Girro Jonn, Tumolva Terence. Developing a Physically Cross-Linked Hydroxyethyl Cellulose Hydrogel for Wound Dressing Applications947; 2019. p.3-12.

142. Ghanbarzadeh B, Almasi Hadi, Entezami Ali A. Physical properties of edible modified starch/carboxymethyl cellulose films. Innov Food Sci Emerg Technol 2010;11:697-702.

143. SekiY, Altinisik Aylin, Demircioğlu Bas¸ak, Tetik Caner. Carboxymethylcellulose

(CMC)-hydroxyethylcellulose (HEC) based hydrogels: synthesis and characterization. Cellulose 2014;21:1689-98.

144. Joshi JM, Sinha Vijay Kumar. Graft copolymerization of 2-hydroxyethylmetha- crylate onto carboxymethyl chitosan using CAN as an initiator. Polymer 2006;47: 2198-204.

145. Pandey PK, Srivastava Arti, Tripathy Jasaswini, Behari Kunj. Graft copolymerization of acrylic acid onto guar gum initiated by vanadium (V)-mercaptosuccinic acid redox pair. Carbohydr Polym 2006;65:414-20.

146. Metz SJ, Van de Ven WJC, Jens Potreck MHV, Mulder and Matthias Wessling. Transport of water vapor and inert gas mixtures through highly selective and highly permeable polymer membranes. J Membr Sci 2005;251:29-41.

147. Soleimani F, Sadeghi Hossein, Shahsavari Hadis, Soleimani Arezou, Sadeghi Fatemeh. Studies of swelling kinetics of carboxymethyl cellulose-g-PMAAm-co-PNIPAm superabsorbent hydrogels. Asian J Chem 2013;25:4851.

148. Wang W, Wang Jiang, Kang Yuru, Wang Aiqin. Synthesis, swelling and responsive properties of a new composite hydrogel based on hydroxyethyl cellulose and medicinal stone. Compos Part B Eng 2011;42:809-18.

149. Schott H. Swelling kinetics of polymers. J Macromol Sci B Phys 1992;31:1-9.

150. Kalisek V, Lapcik L, Mikulaskova B. Evaluation of the fixation of polyester-based textile materials. III. Influence of the fixation conditions on swelling time and degree of fixation. J Polym Mater 1998;15:299-309.

151. Mracek A, Benesova K, Minarik A, Urban P, Lapcik L. The diffusion process of sodium hyaluronate (Na-HA) and Na-HA-n-alkyl derivatives films swelling. J Biomed Mater Res A 2007;83A:184-90. https://doi.org/10.1002/jbm.a.31188.

152. Park GS, Crank J. Diffusion in Polymers. London, New York: Academic Press; 1968. ISBN 0121970507-9780121970505.

153. Lapcik L, Machálková A, Minarik A, et al. The internal pressure in thin polymer layers in contact with liquids. In: 41. Mezina´rodní konference o na´t˘erových hmot´ach, KNH 2010; 2010. p. 27-36.

154. Drnovska H, Lapcik Lubomir Jr. Hyaluronate derivatives and their applications. Plasty Kauc 1999;36:291-4.

155. Lapcik L, Lapcik L, De Smedt S, Demeester J, Chabrecek P. Hyaluronan: preparation, structure, properties, and applications. Chem Rev 1998;98:2663-84.

156. Uyanga KA, Okpozo Oghenefego P, Onyekwere Okwuchi S, Daoud Walid A. Citric acid crosslinked natural bi-polymer-based composite hydrogels: effect of polymer ratio and beta-cyclodextrin on hydrogel microstructure. React Funct Polym 2020; 154:104682.

157. Kupska I, Lapcik L, Lapcikova B, Zakova K, Jurikova J. The viscometric behaviour of sodium hyaluronate in aqueous and KCl solutions. Colloids Surf A Physicochem Eng Asp

2014;454:32-7. https://doi.org/10.1016/j.colsurfa.2014.04.018.

158. Lapcikova B, Valenta T, Lapcik L. Rheological properties of food hydrocolloids based on polysaccharides. J Polym Mater 2017;34:631-45.

159. Toledo PV, Limeira Diego PC, Siqueira Nicolas C, Petri Denise FS. Carboxymethyl cellulose/poly (acrylic acid) interpenetrating polymer network hydrogels as multifunctional adsorbents. Cellulose 2019;26:597-615.

160. Raab M. Materiály a člověk: (Materiály a člověk: netradiční úvod do současné materiálové vědy). 1999.

161. Lapcik L, Bakos D, Kello V. Transannular peroxides of anthracene and its derivatives. Preparation, properties, applications. Chem Listy 1990;84:582-605.

162. Stasko A, Blazkova A, Brezova V, Breza M, Lapcik L. Oxygen photosenzitization in the presence of sodium anthracene-1-sulfonate. J Photochem Photobiol A Chem 1993;76:159-65. https://doi.org/10.1016/1010-6030(93)80132-S.

163. Lapcík L, Lapcíkov´a Barbora, Stasko Andrej, EPR study of the thermal decomposition of transannular peroxide of anthracene. Int J Org Chem 2011;1:37.

164. Maleki A, Kjøniksen Anna-Lena, Nyström Bo. Effect of shear on intramolecular and intermolecular association during cross-linking of hydroxyethylcellulose in dilute aqueous solutions. J Phys Chem B 2005;109:12329-36.

165. Lapcik L, Benesova K, Lapcik L, de Smedt S, Lapcikova B. Chemical modification of hyaluronic acid: alkylation. Int J Polym Anal Charact 2010;15:486–96. https:// doi.org/10.1080/1023666X.2010.520904.

166. Lapcik L, Vasina M, Lapcikova B, Hui D, Otyepkova E, Greenwood RW, et al. Materials characterization of advanced fillers for composites engineering applications. Nanotechnol Rev. 2019 Jan;8(1):503-12.

167. Lapčík L, Maňas D, Vašina M, Lapčíková B, Řezníček M, Zádrapa P. High density poly(ethylene)/$CaCO_3$ hollow spheres composites for technical applications. Compos Part B Eng. 2017 Mar 15;113:218-24.

168. Ehrenstein GW, Riedel G, Trawiel P. Thermal analysis of plastics: theory and practice. Munich: Carl Hanser Verlag; 2004.

169. Cuadri AA, Martin-Alfonso JE. The effect of thermal and thermo-oxidative degradation conditions on rheological, chemical and thermal properties of HDPE. Polym Degrad Stab. 2017 Jul;141:11-8.

170. Schawe JEK. Elastomers Vol 1. Mettler-Toledo collected appli- cations. Schwerzenbach: Mettler-Toledo; 2002.

171. Lapcik L, Manas D, Lapcikova B, Vasina M, Stanek M, Cepe K, et al. Effect of filler particle shape on plastic-elastic mechan- ical behavior of high-density poly(ethylene)/mica and poly (ethylene)/wollastonite composites. Compos Part B Eng. 2018 May 15;141:92-9.

172. Rao SS. Mechanical vibrations, 5th edn. Upper Saddle River, USA: Prentice Hall; 2010.

173. Carrella A, Brennan MJ, Waters TP, Lopes V. Force and dis- placement transmissibility of a nonlinear isolator with high- static-low-dynamic-stiffness. Int J Mech Sci. 2012 Feb;55(1):22-9.

174. Ab Latif N, Rus AZM. Vibration transmissibility study of high-density solid waste biopolymer foam. J Mech Eng Sci. 2014;6:772-81.

175. Liu K, Liu J. The damped dynamic vibration absorbers: revisited and new result. J Sound Vibrat. 2005 Jun 21;284(3–5):1181-9.

176. Hadas Z, Ondrusek C. Nonlinear spring-less electromagnetic vibration energy harvesting system. Eur Phys J Spec Top. 2015 Nov;224(14–15):2881-96.

177. Sun X, Zhang J. Displacement transmissibility characteristics of harmonically base excited damper isolators with mixed viscous damping. Shock Vibrat. 2013;20(5):921-31.

178. Tang B, Brennan MJ. A comparison of two nonlinear damping mechanisms in a vibration isolator. J Sound Vibrat. 2013 Feb 4;332(3):510-20.

179. Krasny I, Lapcik L, Lapcikova B, Greenwood RW, Safarova K, Rowson NA. The effect of low temperature air plasma treat- ment on physico-chemical properties of kaolinite/polyethy- lene composites. Compos Part B Eng. 2014 Mar;59:293-9.

180. Lapcik L, Cetkovsky V, Lapcikova B, Vasut S. Materials for noise and vibration attenuation. Chem Listy. 2000;94(2):117-22.

181.Vasina M, Hughes DC, Horoshenkov KV, Lapcik L. The acoustical properties of consolidated expanded clay granulate. Appl Acoust. 2006 Aug;67(8):787-96.

182. Tu Z, Shim V, Lim C. Plastic deformation modes in rigid polyurethane foam under static loading. Int J Solids Struct. 2001 Dec;38(50–51):9267-79.

183. Bernardo V, Laguna-Gutierrez E, Lopez-Gil A, Angel Rodriguez-Perez M. Highly anisotropic crosslinked HDPE foams with a controlled anisotropy ratio: production and characterization of the cellular structure and mechanical properties. Mater Des. 2017 Jan 15;114:83–91.

184. Sepet H, Aydemir B, Tarakcioglu N. Evaluation of mechanical and thermal properties and creep behavior of micro-and nano- $CaCO_3$ particle-filled HDPE nano- and microcomposites produced in large scale. Polym Bull. 2020;77:3677–95.

185. Se pet H, Tarakcioglu N, Misra RDK. Investigation of mechan- ical, thermal and surface properties of nanoclay/HDPE nano- composites produced industrially by melt mixing approach. J Composite Mater. 2016;50:3105-16.

186. Sepetcioglu H. The effect of nanoclay on the nonlinear vis- coelastic behavior of high-density polyethylene. Polym Compos. 2021;42:3481.

187. Sepet H, Tarakcioglu N, Misra RDK. Determination of the mechanical, thermal and physical properties of nano-$CaCO_3$ filled high-density polyethylene nanocomposites produced in an industrial scale. J Composite Mater. 2016;50:3445-56.

188. Kwok D. The usefulness of the Lifshitz-van der Waals/acid- based approach for surface tension components and interfacial tensions. Colloid Surf A-Physicochem Eng Asp. 1999;156:191-200.

189. Gajdosikova R, Lapcikova B, Lapcik L. Surface phenomena and wetting of porous solids. Phys Chem: Indian J. 2011;6:146-62.

190. Oliver W, Pharr G. Measurement of hardness and elastic modulus by instrumented indentation: advances in under- standing and refinements to methodology. J Mater Res. 2004;19:3-20.

191. Manas D, Mizera A, Manas M, Ovsik M, Hylova L, Sehnalek S, et al. Mechanical properties changes of irradiated thermo- plastic elastomer. Polymers. 2018;10:87.

192. Lapcik L, Manas D, Lapcikova B, Vasina M, Stanek M, Cepe K, et al. Effect of filler particle shape on plastic-elastic mechan- ical behavior of high-density poly(ethylene)/mica and poly (ethylene)/wollastonite composites. Compos Pt B-Eng. 2018;141:92-9.

193. Lapčík L, Maňas D, Vašina M, Lapčíková B, Řezníček M, Zádrapa P. High density poly(ethylene)/$CaCO_3$ hollow spheres composites for technical applications. Compos Pt B-Eng. 2017;113:218-24.

194. Bucknall CB. Toughened plastics. Dordrecht: Springer Science + Business Media, B.V.; 1977.

195. Hashmi MA. Enhancement of mechanical properties of epoxy/halloysite nanotube (HNT) nanocomposites. SN Appl Sci. 2019;1(4):1-8.

196. Srivastava S, Pandey A. Mechanical behavior and thermal stability of ultrasonically synthesized halloysite-epoxy composite. Compos Commun. 2019 Feb;11:39-44.

197. Alexopoulos ND, Paragkamian Z, Poulin P, Kourkoulis SK. Fracture related mechanical properties of low and high gra- phene reinforcement of epoxy nanocomposites. Compos Sci Technol. 2017 Sep 29;150:194-204.

198. Wei JC, Atif R, Vo T, Inam F. Graphene nanoplatelets in epoxy system: Dispersion, reaggregation, and mechanical properties of nanocomposites. J Nanomater. 2015;2015:(3):1-12.

199. Chatterjee S, Nafezarefi F, Tai NH, Schlagenhauf L, Nuesch FA, Chu B. Size and synergy effects of nanofiller hybrids including graphene nanoplatelets and carbon nanotubes in mechanical properties of epoxy composites. Carbon. 2012 Dec;50(15):5380-6.

200. Alamri H, Low IM. Microstructural, mechanical, and thermal characteristics of recycled cellulose fiber-halloysite-epoxy hybrid nanocomposites. Polym Compos. 2012 Apr;33(4):589-600.

201. Oliver WC, Pharr GM. Measurement of hardness and elastic modulus by instrumented indentation: Advances in under- standing and refinements to methodology. J Mater Res. 2004 Jan;19(1):3-20.

202. Manas D, Mizera A, Manas M, Ovsik M, Hylova L, Sehnalek S, et al. Mechanical properties changes of irradiated thermo- plastic elastomer. Polymers. 2018 Jan;10(1):87.

203. Rao SS. Mechanical vibrations. 5th edn. Upper Saddle River, USA: Prentice Hall; 2010.

204. Lapcik L, Vasina M, Lapcikova B, Stanek M, Ovsik M, Murtaja Y. Study of the material engineering properties of high-density poly(ethylene)/perlite nanocomposite materials. Nanotechnol Rev. 2020 Jan;9(1):1491-9.

205. Carrella A, Brennan MJ, Waters TP, Lopes V, Jr. Force and displacement transmissibility of a nonlinear isolator with high-static-low-dynamic-stiffness. Int J Mech Sci. 2012;55(1):22-9.

206. Ab Latif N, Rus AZM. Vibration transmissibility study of high-density solid waste biopolymer foam. J Mech Eng Sci. 2014;6:772-81.

207. Murtaja Y, Lapcik L, Sepetcioglu H, Vlcek J, Lapcikova B, Ovsik M, et al. Enhancement of the mechanical properties of HDPE mineral nanocomposites by filler particles modulation of the matrix plastic/elastic behavior. Nanotechnol Rev. 2022 Jan 5;11(1):312-20.

208. Vijayan PP, George JS, Thomas S. The effect of polymeric inclusions and nanofillers on cure kinetics of epoxy resin: A review. Polym Sci Ser A. 2021 Nov;63(6):637-51.

209. Wang FZ, Drzal LT, Qin Y, Huang ZX. Enhancement of fracture toughness, mechanical and thermal properties of rubber/ epoxy composites by incorporation of graphene nanoplatelets. Compos Part A Appl Sci Manuf. 2016 August;87:10-22.

210. Lapcik L, Raab M. Materials Science II. Textbook. 2nd edn. Zlin: Tomas Bata University in Zlin; 2004.

211. Chen FX, Fan JT, Hui DV, Wang C, Yuan FP, Wu XL. Mechanisms of the improved stiffness of flexible polymers under impact loading. Nanotechnol Rev. 2022 Dec 16;11(1):3281-91.

212. Lapcik, L.; Manas, D.; Lapcikova, B.; Vasina, M.; Stanek, M.; Cepe, K.; Vlcek, J.; Waters, K.E.; Greenwood, R.W.; Rowson, N.A. Effect of filler particle shape on plastic-elastic mechanical behavior of high density poly(ethylene)/mica and poly(ethylene)/wollastonite composites. Compos. Part B Eng. 2018, 141, 92-99.

213. Rao, S.S. Mechanical Vibrations, 5th ed.; Prentice Hall: Upper Saddle River, NJ, USA, 2010; p. 1105.

214. Liu, K.; Liu, J. The damped dynamic vibration absorbers: Revisited and new result. J. Sound Vib. 2005, 284, 1181-1189.

215. Hadas, Z.; Ondrusek, C. Nonlinear spring-less electromagnetic vibration energy harvesting system. Eur. Phys. J.-Spec. Top. 2015,224,2881-2896.

216. Carrella, A.; Brennan, M.J.; Waters, T.P.; Lopes, V., Jr. Force and displacement transmissibility of a nonlinear isolator with high-static-low-dynamic-stiffness. Int. J. Mech. Sci. 2012,55,22-29.

217. Dupuis, R.; Duboeuf, O.; Kirtz, B.; Aubry, E. Characterization of Vibrational Mechanical Properties of Polyurethane Foam. Dyn. Behav. Mater. 2016, 1, 123-128.

218. Lapcik, L.; Vasina, M.; Lapcikova, B.; Stanek, M.; Ovsik, M.; Murtaja, Y. Study of the material engineering properties of high-density poly(ethylene)/perlite nanocomposite materials. Nanotechnol. Rev. 2020,9,1491-1499.

219. Platonova, E.; Chechenov, I.; Pavlov, A.; Solodilov, V.; Afanasyev, E.; Shapagin, A.; Polezhaev, A. Thermally Remendable Polyurethane Network Cross-Linked via Reversible Diels-Alder Reaction. Polymers 2021,13,1935.

220. Nemade, A.M.; Mishra, S.; Zope, V.S. Kinetics and Thermodynamics of Neutral Hydrolytic Depolymerization of Polyurethane Foam Waste Using Different Catalysts at Higher Temperature and Autogenious Pressures. Polym. Plast. Technol. Eng. 2010,49,83-89.

221. Casati, F.; Herrington, R.; Broos, R.; Miyazaki, Y. Tailoring the performance of molded flexible polyurethane foams for car seats (Reprinted from Polyurethanes World Congress ′97, 29 September–1 October 1997). J. Cell. Plast. 1998,34,430-466.

222. Weise, N.K.; Bertocchi, M.J.; Wynne, J.H.; Long, I.; Mera, A.E. High performance vibrational damping poly(urethane) coatings: Blending ‘soft’ macrodiols for improved mechanical stability under weathering. Prog. Org. Coat. 2019,136,105240.

223. Gaboriaud, F.; Vantelon, J.P. Thermal-Degradation of Polyurethane Based on Mdi and Propoxylated Trimethylol Propane. J. Polym. Sci. Part A Polym. Chem. 1981,19,139-150.

224. Ballistreri, A.; Foti, S.; Maravigna, P.; Montaudo, G.; Scamporrino, E. Mechanism of Thermal-Degradation of Polyurethanes Investigated by Direct Pyrolysis in the Mass-Spectrometer. J. Polym. Sci. Part A Polym. Chem. 1980, 18, 1923-1931.

225. Tomin, M.; Kmetty, A. Polymer foams as advanced energy absorbing materials for sports applications-A review. J. Appl. Polym. Sci. 2022,139,51714.

Appendix A-E

A. Intelligent high-tech coating of natural biopolymer layers.

B. Study of the material engineering properties of high-density poly(ethylene)/perlite nanocomposite materials.

C. Enhancement of the mechanical properties of HDPE mineral nanocomposites by filler particles modulation of the matrix plastic/elastic behavior.

D. Study of mechanical properties of epoxy/ graphene and epoxy/halloysite nanocomposites.

E. Effect of Conditioning on PU Foam Matrix Materials Properties.

Advances in Colloid and Interface Science 304 (2022) 102681

Contents lists available at ScienceDirect

Advances in Colloid and Interface Science

journal homepage: www.elsevier.com/locate/cis

Historical Perspective

Intelligent high-tech coating of natural biopolymer layers

Yousef Murtaja [a], Lubomir Lapčík [a,b,*,1], Barbora Lapčíková [a,b], Shweta Gautam [b,1], Martin Vašina [b,c], Lubomir Spanhel [d], Jakub Vlček [a]

[a] Palacky University in Olomouc, Department of Physical Chemistry, Faculty of Science, 17. Listopadu 12, 771 46 Olomouc, Czech Republic
[b] Tomas Bata University in Zlin, Department of Foodstuff Technology, Faculty of Technology, Nam. T.G. Masaryka 275, 762 72 Zlin, Czech Republic
[c] Department of Hydromechanics and Hydraulic Equipment, Faculty of Mechanical Engineering, VSB-Technical University of Ostrava, 17. Listopadu 15/2172, Ostrava-Poruba, 708 33 Ostrava, Czech Republic
[d] Institute of Chemical Sciences Rennes, UMR CNRS 6226, University of Rennes 1, Campus Beaulieu, Rennes, France

ARTICLE INFO

Keywords:
Biopolymers
Crosslinking
Diffusion coefficient
Hydrogel swelling
Thermodynamics

ABSTRACT

Polymeric materials play a vital role in our daily life, but the growing concern for the environment demands economical and natural biopolymers that can be cross-linked to create technologically innovative lightweight materials. Their cellular matrix with extreme flexibility makes them highly acceptable for application prospects in material science, engineering, and biomedical applications. Furthermore, their biocompatibility, mechanical properties, and structural diversity provide a gateway to research them to form technologically important materials. In the light of the same, the review covers cellulose derivatives. The first section of the study covers the general properties and applications of cellulose and its derivatives. Then, the biopolymers are characterised based on their dielectric properties, crystallinity, rheology, and mechanical properties. An in-depth analysis of the diffuse process of swelling and dissolution followed by a brief discussion on diffusion and diffusion of crosslinking has been done. The review also covers a section on swelling and swelling kinetics of carboxymethyl cellulose (CMC) and hydroxyethyl cellulose (HEC). The examination of all the aforementioned parameters gives an insight into the future aspects of the biopolymers. Lastly, the study briefly covers some preferred choices of cross-linking agents and their effect on the biopolymers.

1. Introduction

The technology of intelligent materials paves way for the development of sustainable products via their acute flexibility. Their ability to adapt to environment changes in response to a stimulus, enhances their multi-functionality in daily applications as well as in all the engineering fields, medical, defence, and automobile industries. Some of the examples of intelligent materials include memory alloys, hydrogels, thermochromic pigments, photochromic pigments, biopolymer coatings, shape memory polymer etc. [1]. The structure-property relationships permit the significant variation of important physicochemical and biological properties, which broaden their application prospects in material science, engineering, and industrial sectors. The expeditious growth in the science and engineering sectors demands the development of novel and sustainable materials, thereby placing new requirements on material engineers to prepare highly sophisticated mono and composite systems [2].

In the field of materials, the cost and energy consumption for the preparation and processing of heavyweight building materials (mainly transport systems) is very high, thereby limiting their scope for future applications. To avoid this, a constant search has been focused on development of lightweight polymer composites endowing excellent mechanical properties by using low-cost and straightforward synthesis processes. It is also worth mentioning the increasing demand to reduce the environmental wastage and carbon footprint, particularly in the materials industries. Therefore, it is required by researchers to focus on enhancing the properties and functions of the biopolymers. In the view of the same, significant research has been done to produce biopolymers and bio-composites with comparable properties and functionalities to those of traditional bio-based packaging [3]. Some of the biopolymers that have been studied extensively are: Polylactic acid (PLA), polyhydroxyalkanoates (PHA) [4], starch, cellulose, pectin, chitosan among

* Corresponding author at: Palacky University in Olomouc, Department of Physical Chemistry, Faculty of Science, 17. Listopadu 12, 771 46 Olomouc, Czech Republic
E-mail address: lapcikl@seznam.cz (L. Lapčík).
[1] Authors who equally contributed as the first author.

https://doi.org/10.1016/j.cis.2022.102681
Received 12 January 2022; Received in revised form 29 March 2022; Accepted 18 April 2022
Available online 22 April 2022

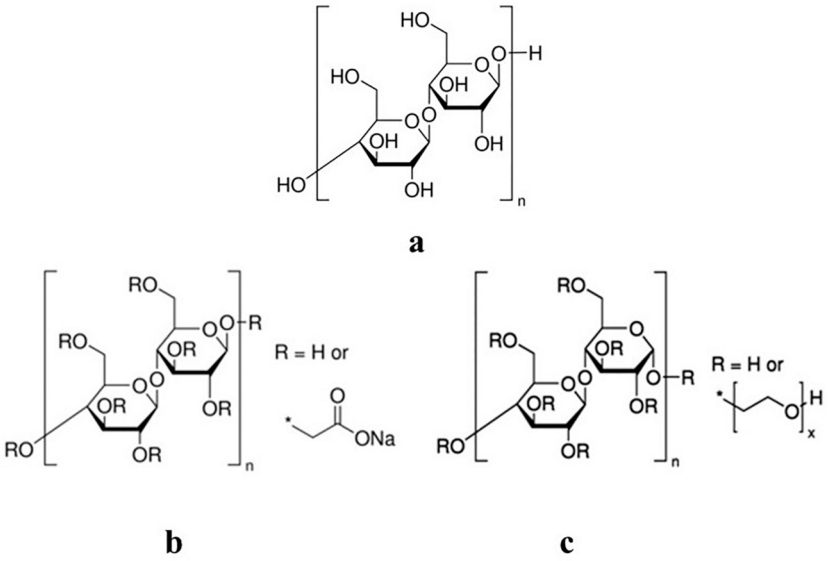

Fig. 1. (a) Chemical structure of cellulose; (b) Chemical structure of carboxymethyl cellulose with its sodium salt; (c) Chemical structure of hydroxyethyl cellulose.

others. It is expected that in the next decade, the weight of cars will reduce to half the original weight owing to the use of lightweight biopolymer composites; consequently, reducing the fuel consumption by 50%. The advantages of lightweight polymer composites and polymer-based ceramics will be applied further to design and manufacture advanced lightweight engines. In this context, natural biopolymers have been drawing more attention because of the following reasons: (i) construction of living organisms' bodies can be done strategically; (ii) different properties in solid, semi-solid, and solution phases; (iii) can be applied directly without requirement of further processing; (iv) permitting the simple design of thin coatings on the surface of solids by the existing methods, which are conventional in printing arts, textile, and packaging material industries [5,6] and thus improving hydrophobicity and hydrophilicity. Cross-linked hydrogel coatings for surface enhancement of contact lenses have also been reported [7,8]. The literature analysis indicates a dominant position of carbon based polymers in the form of nanoscale fibres and dispersions, cyclic fullerenes, alongside silicon and boron polymers. Of the aforementioned biopolymers, the review highlights cellulose and its derivatives viz., oxycellulose, carboxymethyl cellulose, nitrocellulose and hydroxyethyl cellulose.

Cellulose is the most plentiful, renewable, and natural polymer on the planet, with yearly output ranging from 75 to 100 billion tonnes for various industrial and biological uses [9]. It is a glucose-based linear polysaccharide that gives mechanical support to plant cells, bacteria, algae, and fungi (Fig. 1(a)) [10]. Most commercial cellulose fibres are obtained as pulp (natural fibres) or derivative from the natural cellulose of wood, barks, cotton, leaves, and jute. Carboxymethyl cellulose (CMC) was the first cellulose (Fig. 1(b)) to attain commercial and industrial relevance in the 1920s, and it will continue to have a dominant position in the global market. CMC can be easily made via simple processes and low-cost ingredients. The vast market potential of CMC is the main advantage compared to other cellulose derivatives. CMC is used in the paper, textile, pharmaceutical, cosmetic, and food industries, just like cellulose and other cellulose derivatives. Nitrocellulose (NC) is also one of the most commercially relevant and widely utilized natural cellulose derivatives [11]. Its nitrogen content determines the properties and applications of NC. NC with nitrogen content below 12.0 wt% can be used for coatings, printing inks, varnishes, filtration membranes, microfluidic technology, immunoassays, and biochemical analyses [12–14]. The formation of NC aerogel significantly increases NC's surface area and broadens its applications in separations, purification

Table 1
Calculated parameters of measured dielectric spectra of studied polysaccharides (Courtesy of [32]).

Parameter	Compound	
	CMC	HEC
10^3 (ε_s - ε_∞)	37.60	2.28
	2.18	
α	0.0598	0.676
	0.970	
β	1.000	1.000
	1.000	
10^{-3} τ_0/s	68.100	5.120
	3.810	
A'	2.48×10^{-19}	1.08×10^{-18}
n	0.700	0.535

ε_∞ optical permittivity of the sample, ε_s static permittivity of the sample, (ε_s - ε_∞) relaxation strength, τ_0 position of the relaxation on the same axis, α slope of the low – frequency side of the relaxation curve, product $\alpha \times \beta$ describes the slope of the high – frequency side of the relaxation curve, A' is sample surface area, and n is purely D.C. conductivity mechanism.

science, and biomedicine [15]. Oxycellulose (OC) is a semi-synthetic derivative of cellulose that undergoes chemical depolymerization and enzymatic hydrolysis under in vivo conditions [16,17]. It is a non-toxic, biodegradable, biocompatible, and bioresorbable polymer [18,19]. It is a well-established surgical material commercially available as a knitted fabric or staple fibres used to stop bleeding and prevent undesirable tissue adhesion during post operative healing [20]. Hydroxyethyl cellulose (HEC) is non-ionic, hydrophilic, tasteless, and non-toxic cellulose derivative used extensively in pharmaceuticals, cosmetics, and food products (Fig. 1(c)) [21,22]. For instance, HEC cross-linked with citric acid is used as probiotic entrapment material [23]. HEC coatings in combination with other polysaccharides such as chitosan are used and seldom investigated [24]. It has excellent film-forming ability, biocompatibility, and biodegradability, making it suitable for biomedical applications [25]. Composites of natural biopolymers with aluminosilicates are used as packaging materials in the food industry [26].

The primary aim of this review is to characterize the aforementioned biopolymers (particularly CMC and HEC) followed by an extensive evaluation of their diffusion and diffuse process of swelling and dissolution of polymers. The review briefly covers the diffusion and coefficient or cross-linking of biopolymers, followed by a meticulous focus on mechanical properties, surface tension for spreading, diffusion

Table 2
Different characteristics of CMC sample (Reproduced from ref. [33] with the courtesy of BioResources, North Carolina State University).

Degrees of substitution (DS)	Mean length (mm)	Mean width (μm)	Percentage crystallinity (%)	Purity (%)
0.75	2.28	48.1	18.03	95
0.76	2.13	55.7	19.60	95
0.80	1.94	52.8	23.51	95
0.73	1.43	51.7	25.85	95

coefficient, kinetics, and thermodynamics of diffusion, swelling, and dissolution [27]. The review also evaluates the preparation of varieties of industrial auxiliaries for printing arts and textile industries, such as offset print humidifying solutions, offset printing plate's protective solutions, and means for improving colouring of textiles [28–30].

2. Characterisation of biopolymers

The characterisation evaluation of biopolymers (CMC and HEC) was conducted on the basis of crystal/solid-state and liquid/cross-linked state. The dynamics of the macromolecular chain movement was studied by temperature-dependent dielectric spectra in the frequency range of 20 Hz to 1 MHz [31] (Table 1) [32]. The characterisation of CMC with corn starch on the basis of crystallinity, mean length, percent purity and mean width was also reviewed (Table 2) [33]. The data indicates the use of CMC biopolymer as a thickener, emulsion binder, and stabilizer [32,34] in the detergent, cosmetic [35], food, pharmaceutical, drilling, and textile industries [36]. It can also act as a binding granule to form drug tablets in the pharmaceutical industries. The degree of substitution does not affect the percentage of purity. The percentage of crystallinity varies directly with the mean width [37]. HEC is a non-ionic cellulose ether whose water solution properties are very useful in the pharmaceutical, alimentary, and industrial fields [38]. HEC can be used as thickening agent, protective colloid, binder, stabilizer, and suspending agent in a variety of industrial applications including pharmaceuticals, textiles, paper, adhesives, coatings and emulsion polymerization [39].

Sodium salt of carboxymethyl cellulose (NaCMC) is the most extensively used CMC polymer. The rheological analysis for NaCMC indicated that the degree of substitution (DS) affects the flow properties of NaCMC samples. At higher concentration, heterogeneously substituted samples have the ability to form gels [40] and may present thixotropic or shear aging [40,41]. As the DS decreases below a certain threshold (around 0.9), the interchain aggregates and formation of fringed micelles with crystalline core takes place [40,42–44]. These micelles are responsible for the thixotropic and gelling properties of the weakly substituted NaCMC. The rheological properties of the physical gels of CMC without the addition of cross-linking agents depends on hydrophobic interactions between individual macromolecular chains [45–47]. This study revealed that CMC samples with DS ≈ 0.7–0.8 can be separated into two fractions by centrifugation. Fraction A displayed pseudoplastic, non-thixotropic and non-gelling behaviour in salt free aqueous solution whereas fraction B displayed some solubility in water and good solubility in concentrated NaOH. The substituent distribution of fraction B was heterogeneous which led to the formation of thixotropic gel at higher concentration by hydrophobic inter-chain associations. The rheological properties of aqueous solution of HEC can be controlled by modifying the polymer backbone with side chain achievements such as ionic or hydrophobic groups [48]. In hydrophobically modified HEC [49–51], the thickening action is caused by the association of the hydrophobic side chains into an intermolecular transient network. On the other hand, cationically modified HEC tend to behave like typical polyelectrolytes [52]. The viscosity enhancement is due to repulsion of the charged groups along the chain which expands the macromolecule. As the surfactant concentration increases, the number of side chains per micelle decreases to the point that intermolecular associations of

Table 3
Mechanical properties for CMC films synthesized with various NaOH concentrations at 25°C, 75% RH (Reproduced from ref. [55] with the permission of Elsevier. Request ID 60075084).

Types of film	Tensile strength (MPa)	Elongation at break (%)
20 g/100 mL NaOH-CMC	141.16 ± 8.32	2.32 ± 0.26
30 g/100 mL NaOH-CMC	255.54 ± 4.13	2.20 ± 0.81
40 g/100 mL NaOH-CMC	140.77 ± 14.43	2.07 ± 0.50
50 g/100 mL NaOH-CMC	53.42 ± 8.21	2.95 ± 1.13
60 g/100 mL NaOH-CMC	79.62 ± 9.76	2.28 ± 0.98

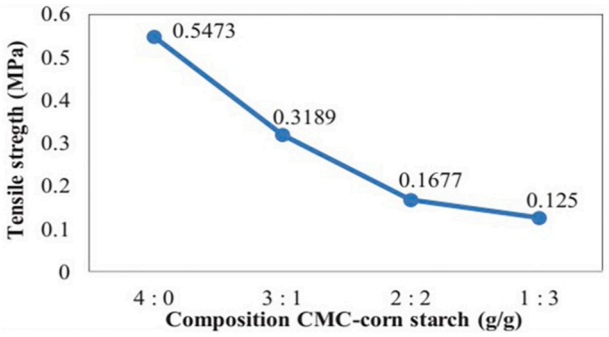

Fig. 2. Analysis of the tensile strength (Reproduced from ref. [57] with the permission of American Institute of Physics licence no. 5270921480448).

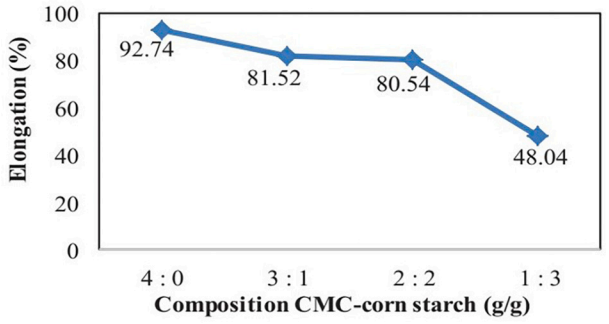

Fig. 3. Analysis of the percentage elongation (Reproduced from ref. [57] with the permission of American Institute of Physics licence no. 5270921480448).

polymer molecules are inhibited due to the electrostatic repulsion between attached micellar aggregates. As a consequence, the shear viscosity of the solution reaches a maximum and then decreases as surfactant concentration is further increased [53,54]. The inhibition of interchain interactions through hydrophobic side chains eventually might lead to a viscosity that is even lower than that of the pure polymer solution.

Tensile strength (TS) is the film's retainable maximum tensile force. It explains the film's maximum force occurring during measurement. Various ratios of CMC produce different tensile strength results. In general, the tensile strength values reduce with the addition of a substrate. In a study conducted on CMC produced by carboxymethylation using sodium monochloroacetate and varying concentrations of sodium hydroxide, it was found that the NaOH concentration affected the TS but not the elongation at break (EB) of the CMC films [55]. TS increased with NaOH concentrations of 20 and 30 g/100 mL (Table 3) [55]. Beyond the 30 g/100 mL concentration, the TS of the films decreased. The more carboxymethyl groups there are, which is directly related to the DS, the more the inter-molecular forces between the polymer chains increased, resulting in a higher TS. Somewhat similar results for TS and EB were recorded in another studies [56,57]. The studies involved the

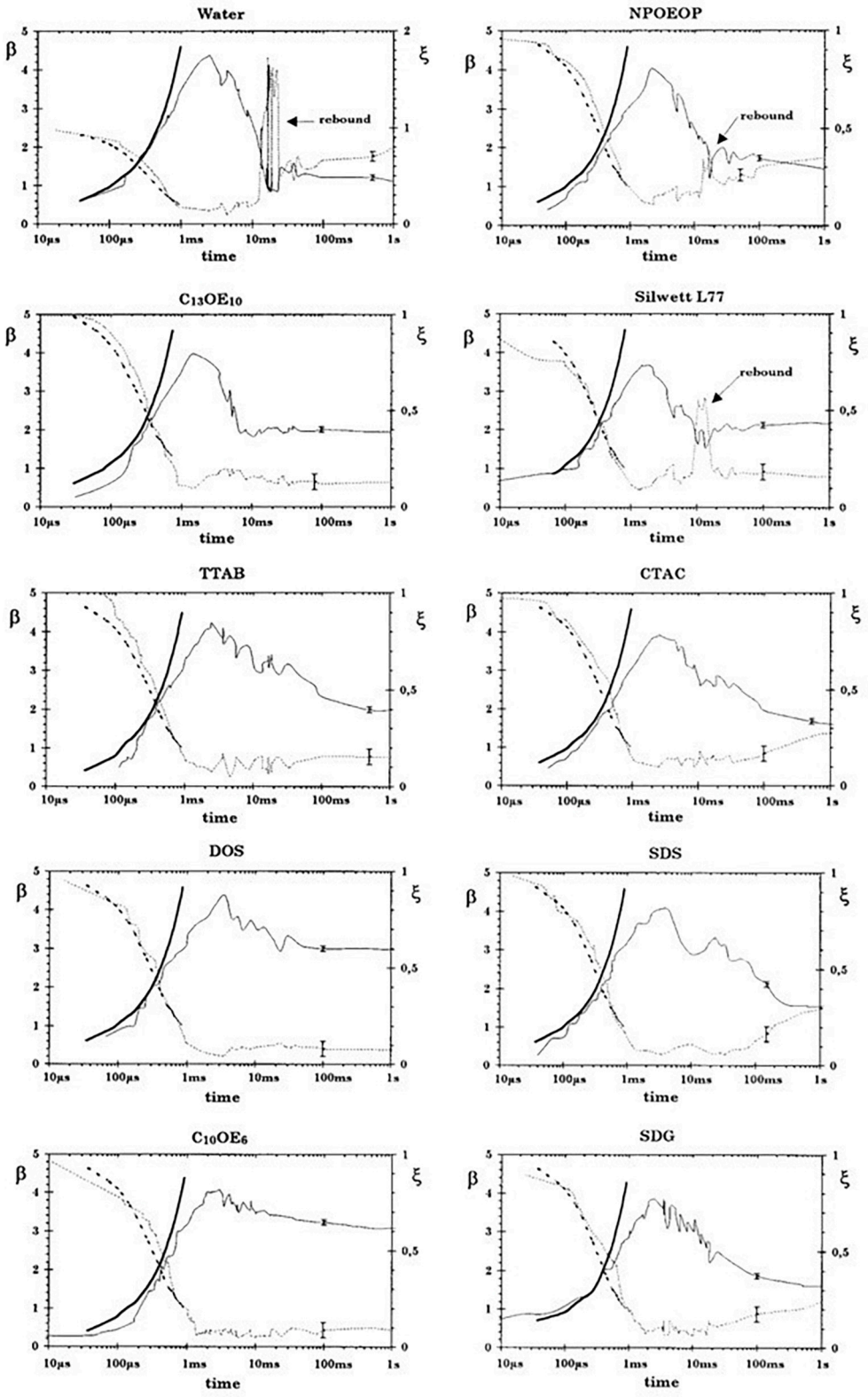

Fig. 4. Spreading factor versus time for water and each surfactant at critical micellar concentration (CM conc × 10) (Reproduced from ref. [64] with the permission of Academic Press, Elsevier Science licence no. 5270931090431).

formation of films with CMC and corn starch. It was found that combining four grams of CMC in the absence of corn starch yielded the highest tensile strength whereas, combination of corn starch with CMC in the ratio of 3:1 yielded the lowest tensile strength (Fig. 2). The percent of elongation increased with a lower concentration of CMC-corn starch (Fig. 3). In general, it was found that the tensile strength reduces with increase in the percentage elongation [57]. Similar results for tensile strength and elongation at break analysis of HEC were studied [58–60]. The study evaluated the tensile strength and elongation at break for pure HEC films vs the films prepared with the addition of cellulose

Table 4
Characteristics of surfactant solutions. Critical micellar concentration (CM conc) and equilibrium surface tension at CM conc × 10. (Reproduced from ref. [64] with the permission of Academic Press, Elsevier Science licence no. 5270931090431).

Surfactant	CMC (g/l)	Equilibrium surface tension at CM conc × 10 (mN/m)
NPOEOP	0.06	36.9
C13OE18	0.08	27.7
Silvett L77	0.10	20.4
C10OE6	0.80	26.1
TTAB	1.18	37.2
CTAC	0.42	34
DOS	0.92	27
SDS	2.38	36.5
SDG	0.60	25

NPOEOP: nonylphenyl polyoxypropylene; C13OE18: isodecyl polyoxyethylene; Silvett L77: trisilioxane oxypropylene polyoxyethylene; C10OE6: isodecyl polyoxyethylene; TTAB: tetradecyl trimethylammonium bromide; CTAC: cetyltrimethylammonium chloride; DOS: sodium dioctyl sulfosuccinate; SDS: sodium dodecyl sulfate; SDG: sodium decylgalacturonate.

nanocrystals (CNC). The addition of 4% of CNC increased the tensile strength by 120.2% but beyond 8%, the addition of CNC did not enhance the tensile strength. The elongation at break reduced by 95.6% in comparison to pure HEC film. The results indicated that the addition of CNC can improve the tensile strength but beyond a threshold value, the elongation at break decreases [58].

3. Diffusion of polymers and surface tension

The term 'diffuse actions' is understood as whole processes that include the transport of substances because of the gradients in chemical potential. Temperature, pressure, electric potential, and magnetic field have significant contributions to chemical potential gradients. Many authors have comprehensively studied this topic [34,61,62].

Two direct relations for explaining the diffusion phenomena are known as Fick's laws. For binary system applying the one-dimensional diffusion Fick's laws:

$$\text{i.Fick's law}: J_i = -D_i\frac{\delta c_i}{\delta x} \tag{1}$$

$$\text{ii.Fick's law}: \frac{\delta c_i}{\delta t} = \frac{\delta}{\delta x}\left(D_i\frac{\delta c_i}{\delta x}\right) \tag{2}$$

where t, x, J_i, D_i, and c_i are time, coordinates, diffusion flow, diffusion coefficient, and concentration of component i, respectively. For known initial and peripheral conditions by solving the given differential equations, the value of diffusion coefficient (D_i) can be determined. For unit concentration gradient, diffusion coefficient determines the flow of a substance per unit area perpendicular to the direction of flow. The values of diffusion coefficient for low molecular weight polymers are within 10^{-5} to 10^{-14} cm^2 s^{-1}. R. M. Barrer et al. [63] divided the systems of polymer-penetrant into four different categories:

$$\text{a)}\ \frac{\partial c}{\partial t} = D\frac{\partial^2 c}{\partial x^2}\ D = \text{const.c} = \text{k.c}^{\cdot} \tag{3}$$

$$\text{b)}\ \frac{\partial c}{\partial t} = \frac{\partial}{\partial x}\left[D(c)\frac{\partial c}{\partial x}\right]\ D = f\ (c)\ c = \text{k.c}^{\cdot} \tag{4}$$

$$\text{c)}\ \frac{\partial c}{\partial t} = \frac{\partial}{\partial x}\left[D(c)\frac{\partial c}{\partial x}\right]\ D = f\ (c)\ c = f\text{`}(c^{\cdot}) \tag{5}$$

$$\text{d)}\ \frac{\partial C}{\partial t} = \frac{\partial}{\partial x}\left[D(c)\frac{\partial C}{\partial x}\right]\ D = f\ (c,t)\ c = f\text{`}(c^{\cdot}) \tag{6}$$

'Category a' is typical for the diffusion of rare and most di-atomic gases in polymers at the viscoelastic state. 'Category b' describes the diffusion in systems of rubber and paraffinic hydrocarbons. 'Category c' is applicable for the diffusion of heavier hydrocarbons in rubber layers. 'Category d' is very common, and the diffusion coefficient depends on concentration and time in this category. Notably, this case involves the strong mutual interactions between chain and penetrant molecules. The mutual interactions usually lead to slow relaxations in the crystalline polymer.

Many technological fields depend on the exact knowledge of the effect of solid/liquid interface interactions on final spreading of liquid drops. The experiment observed the surfactant solutions behaviour at critical micellar concentration (CM conc × 10) (Fig. 4) [64] and water drops from the impact moment to one second after the impact [65]. All the solutions have the same process of spreading (Table 4) [64]. The surface tension is the difference between the foaming medium's surface tension, the defoamer's surface tension, and both substances interfacial tension for the spreading diffusion coefficient (S); thus, mathematically, we can write:

$$S = \sigma_f - \sigma_d - \sigma_{df} \tag{7}$$

where σ_f is the surface tension of the foaming medium, σ_d is the surface tension of the defoamer and σ_{df} is the interfacial tension of both substances.

The defoamer's surface tension reduction causes the spreading coefficient to become increasingly positive. The process shows the defoaming's thermodynamic tendency. Eq. 3 is applicable for insoluble liquid defoamers in bulk. However, deforming effectiveness can be increased by certain dispersed hydrophobic solids. The process of spreading depends mainly on surfactants.

4. Diffuse process of swelling and dissolution of polymers

4.1. Diffuse process of swelling

The conversion of solid polymer in solution at temperatures below the second-order turning point (T_g) usually comprises swelling and dissolution processes. In the swelling process, the solvents come to introduce at the solid polymeric phase and expand the solid surface in the liquid phase. This effect is known as Kirkendahl's effect [66]. It is the impact that leads to loosening of the polymer structure thereby enhancing the movement of macromolecular chain segments, and enhancing the activity of free volume in the system alongside the replacement polymer-polymer contacts by the polymer-solvent contacts. It results in the creation of swollen surface layer with defined thickness and structure [67]. The movement of phase interface, i.e., the interface between swollen layer and the liquid solvent is necessary to understand as its own swelling. The diffusion process of polymer dissolution has been studied in detail by Lapčik and Valko [68]. According to them, the diffusion of liquid solvents into polymer foils can be evaluated on the basis of parameters describing the formation of a surface diffusion layer. Furthermore, the polymer matrix swells due to the solvent effect resulting in the developed surface diffusion layer being donated as a surface swollen layer (SSL) [69]. The swelling process is unsteady in nature resulting formation of the swollen surface layer.

4.2. Swollen surface layer

SSL of polymer represents interphase resistance of a given value influencing the diffusion in both directions from the interface. Ueberreiter K. and Asmussen F. [69–75] reported that SSL comprises complex structures, mostly in temperatures below T_g. Its thickness δ depends primarily on molecular weight, temperature, the kinetic-thermodynamic activity of solvent and minutely on the thermal history of polymer samples. The other four layers within SSL were reported

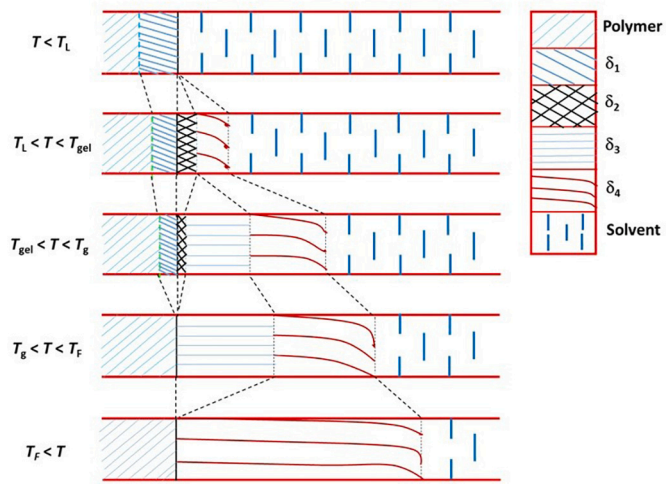

Fig. 5. Structure of the swollen surface layer by Ueberreiter K. and F. Asmussen: δ_1 – liquid layer, δ_2 – rubbery layer, δ_3 – gel layer, δ_4 – infiltration layer, T – temperature of sloughing, T_L – temperature of phase transition of solvent, T_{gel} – gelling temperature, T_g – glass transition temperature, and T_F – melting temperature of polymer (Reproduced from [69,72,74]).

by the authors mentioned (Fig. 5) [69,72,74,76]. If the melting temperature drops below T_{gel}, i.e., $T_L < T < T_{gel}$, the rubbery layer δ_2 disappears and then only layers δ_1 δ_3, and δ_4 are retained. When melting temperature decreases below T_L, i.e., $T < T_L$, layers δ_1 and δ_3 disappear, so the SSL is formed only by layer δ_4. The latter two cases can be well clarified by the following reasons: dissolution in the range of temperatures (T_{gel}) and (T_L), i.e., $T_L < T < T_{gel}$ leads to weakening of the rubbery layer δ_2 to a value that is not visible; it indicates that it cannot affect the swelling process. The transport of solvated polymers into the coexisting liquid phase of the solvent is the rate-determining step at higher dissolution temperatures. The liquid layer consists of solvent molecules accumulated by adsorption on the surface of polymeric substances. Even if the dissolution in flowing solvent is the rate of flowing fluid in this layer virtually zero, the concentration of polymer in this layer grows from almost zero value, which is on the interface with flowing solvent at a value φ_ξ that is on the interface with the rubbery layer. The thickness of this layer depends decisively on the rate of the solvent flow. With increasing rate, the thickness decreases to a certain limit value and does not change anymore. The rubbery layer has the character of a liquid phase with a fixed structure. The content of solvent molecules is large, and the thickness of the layer is comparable with the thickness of the liquid layer. The concentration gradient from one interface to another is almost the same as the liquid layer. A sudden increase in the concentration gradient was observed at the rubbery and tough swollen layer interface. Polymer chains in this layer do not move in the same fashion as in the liquid phase and the thickness of the layer is significantly smaller than in the previous two regions. The system of this layer is composed of the continuous liquid phase, which is continuously permeated by a dispersed polymer (with a gel-like character). The concentration of the solvent is markedly smaller compared to the rubbery phase. The infiltration layer is characteristically different from the previous. The movement of solvent molecules in the direction of concentration gradient takes place in this layer, probably in the exact mechanism as the gas transport through polymeric membrane, i.e., jumping from one vacancy to another without any significant movement of polymer segments. The number of polymer-polymer cross-links is comparable with the number in the original sample. As mentioned before, it is clear that the diffusion of solvent molecules controls the kinetics of polymers into a solid polymer sample.

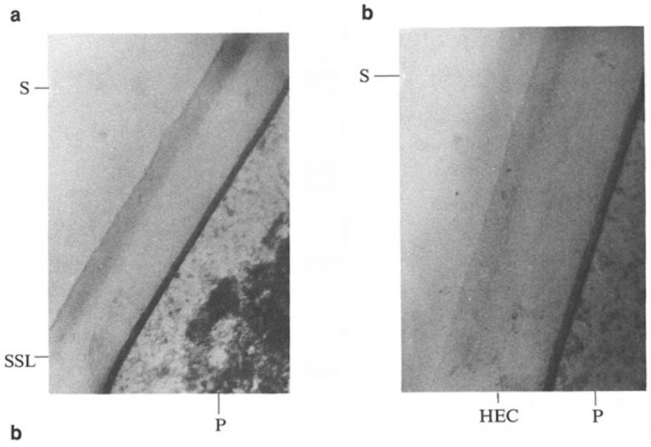

Fig. 6. Surface swollen layer of (a) CMC and (b) HEC (1 cm ~ 0.1 mm) (Reproduced from ref. [68] with the permission of Springer Nature licence no. 5274210286515.

5. Diffusion and diffusion coefficient of cross-linking

Diffusion involves the movement of atoms, molecules, and ions from a higher concentration region to a lower one. The concentration gradient is the major driving force of diffusion. Various fields, such as chemistry, widely use the diffusion concept to characterize swelling kinetics [77] and measurements of diffusion of macromolecules [78]. A mean square displacement's long-time slope gives the diffusion coefficient (D) of cross-linking:

$$D = \frac{1}{6}\mathrm{Iim}_{t\to\infty}\frac{d}{dt}\langle |r(t) - r(0)|^2 \rangle \tag{8}$$

where $r(0)$ and $r(t)$ are the centres of the mass's vectors at time = 0 and t, respectively, in the biopolymer CMC, an increase in the polymer concentration first reduces the diffusion coefficient. However, a larger polymer concentration than a critical value increases the diffusion coefficient [79]. The diffusion coefficient in a CMC relates to the excess mixing volume and biopolymer fraction in the solution. Within the concerned region, the concentration of the solution density is given by the formula:

$$p = p_B^0(1 + aWp) \tag{9}$$

where p_B^0 and aWp are the pure solvent density (0.998 g/cm^3) and the polymer concentration (wt/wt), respectively. For CMC, the value of "a" is 0.0047.

$$\frac{Dg}{D0} = exp\left[-\dot{\pi}\left(\frac{rs + rf}{ksa\varphi^{-0.75C\infty-0.25}(1-2\chi)^{-0.253} + 2rf}\right)^2\right] \tag{10}$$

where a is the equivalent bond length of the monomer, φ is the polymer volume fraction, r_s is the radius of solute, r_f is the radius of polymer chain, C_∞ is the characteristic ratio of polymer, χ is the Flory-Huggins polymer/solvent interaction parameter, D_g is the diffusion coefficient of solute in gel, and D_0 is the diffusion coefficient of solute in water calculated from MD simulation and verified by literature [79]. Since the fitting parameter for the different polymers and solutes considered, Amsden proposed this model as a "universal" model for solute diffusion in hydrogels.

An increase in the cross-linking density causes the diffusion of sodium ions to reduce at 0.5 M. The dynamic and theoretical predictions helped obtain the particles' normalized diffusion [79]. The water content variation also changes the rate of diffusion [57]. There is a need to estimate the Rhodamine's rotational relaxation time to calculate the translational diffusion coefficient [79]. The increase in the cross-linking

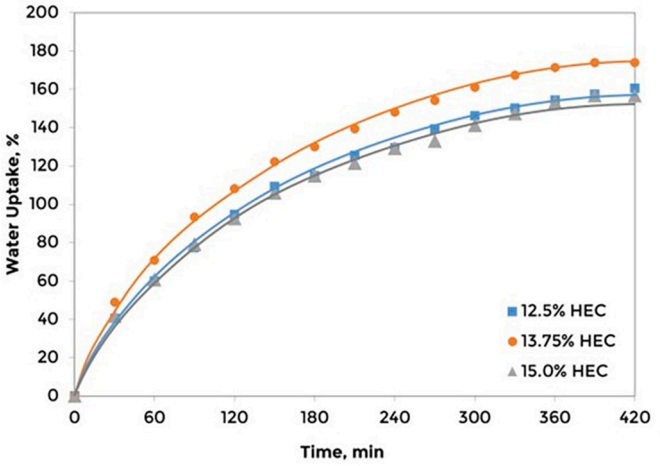

Fig. 7. Water uptake of HEC hydrogel samples with respect to time (Reproduced from ref. [80] with the permission of Trans Tech Publications Ltd. Request ID 600074454).

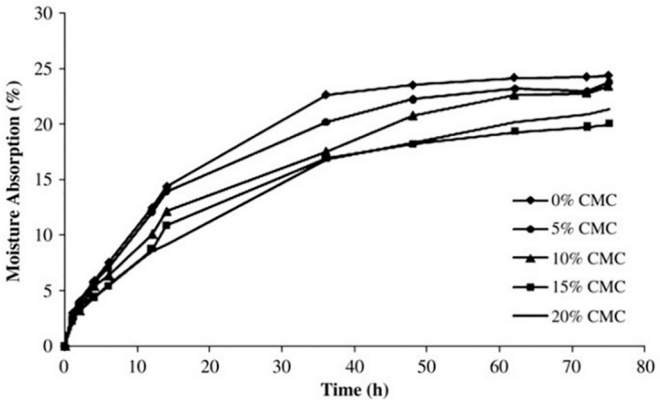

Fig. 8. Moisture absorption of starch films as a function of CMC content (Reproduced from ref. [81] with permission from Elsevier licence no. 5274220418935.

density causes the diffusion coefficient of small. The rise in the relaxation times of the hydrogen bonding correlates with the reduction in water diffusion.

6. The kinetics of swelling and dissolution of CMC and HEC

The swelling and dissolution mechanism for CMC and HEC are not homogeneous because of its multi-scale and complex structures. The ballooning phenomena are the most spectacular effects of the heterogeneous swelling and dissolution. Some selected zones along the fibre provide places for swelling to take place. It is assumed that the structural origins of the ballooning effect relate to the morphological variations among the walls. Each of the balloons presents a swollen state of the biopolymers. The quality of the solvent strongly influences the swelling and dissolution mechanisms (Fig. 6) [68]. The swelling and dissolution characteristics can be revealed at the different cellulose structures' lengths from the macromolecule to the fibre's walls.

6.1. Kinetics of swelling

In practical applications, a higher swelling rate and a higher swelling capacity are required. It is well known that the swelling kinetics for the absorbents is significantly influenced by various factors such as swelling capacity, the size distribution of powder particles, specific size area, and

Table 5
Maximum water uptake of hydrogels (Reproduced from ref. [80] with the permission of Trans Tech Publications Ltd. Request ID 600074454).

	12.5% HEC	13.75% HEC	15.0% HEC
% Maximum water uptake	160.5	173.8	156.9

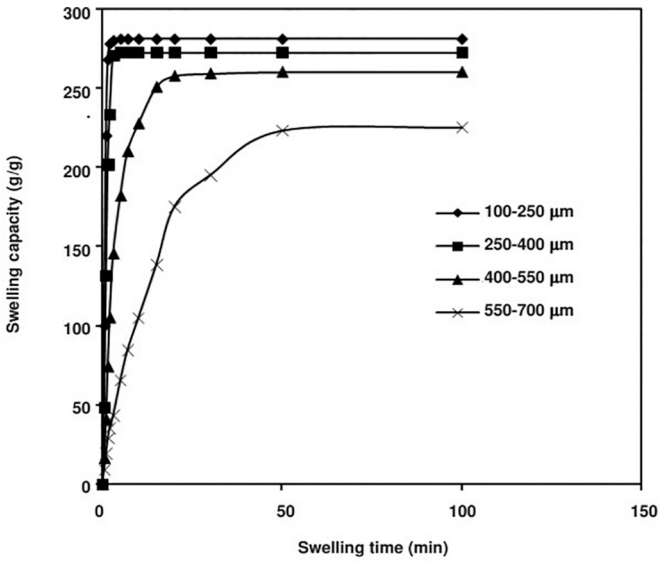

Fig. 9. Representative swelling kinetics of the CMC-g-PMAAm-coPNIPAAm superabsorbent hydrogel with various particle sizes (Reproduced from ref. [86] with the permission of Asian Publication Corporation).

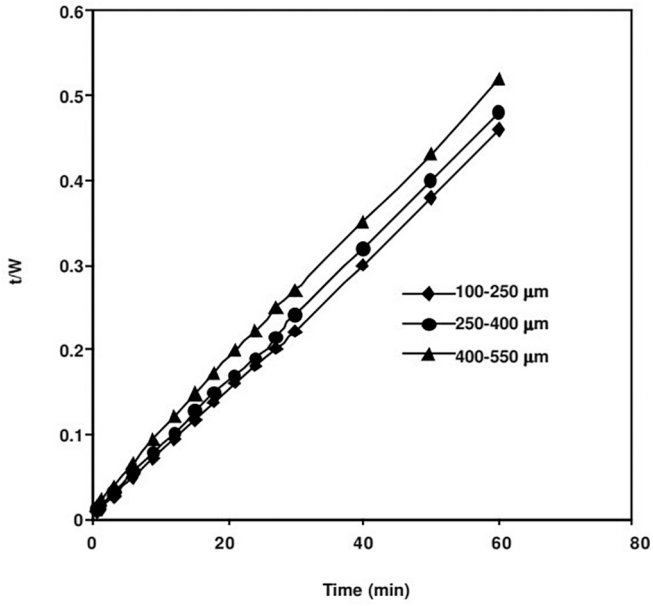

Fig. 10. Plot *t/W* vs. time according to eq. 12 (second-order kinetics) for superabsorbent hydrogels with various particle sizes (Reproduced from ref. [86 with the permission of Asian Publication Corporation]).

composition of the polymer (Figs. 7 and 8, Table 5) [80–82]. Various authors [83,84] have investigated the influence of these parameters on the swelling capacity. For example, Metz et al. [85] analysed the dependency of water absorbency of superabsorbent polymers on particle size. Results indicated that the absorption rate increased as the particle size became smaller. This may be attributed to an increase in surface

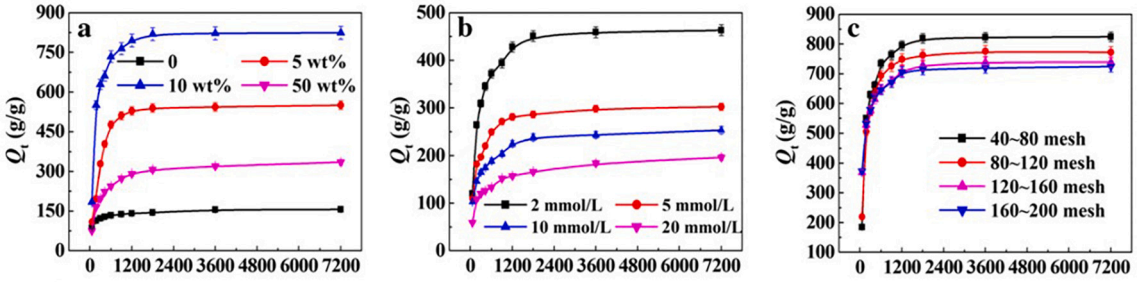

Fig. 11. (a) swelling kinetic curves of the hydrogels (MS dosage, 0, 5, 10 and 50 wt%) in distilled water, (b) effect of the saline solution with various concentration on the kinetic swelling behaviours of the composite hydrogel (MS dosage, 10 wt%), and (c) effect of particle size on the kinetic swelling behaviours of the composite hydrogel (MS dosage, 10 wt%) (Adapted from ref. [87] with request from Elsevier request ID 600074472).

area with decreasing particle size of samples [86].

In a study conducted on the formation and subsequent analysis of swelling kinetics of a CMC-N-isopropylacrylamide based hydrogel, the effect of particle size on the swelling kinetics was confirmed. The rate of water absorbance increased sharply and then began to level-off (Fig. 9) [86]. Considering the second-order kinetics, the swelling rate at any time is expressed as:

$$\frac{d\mathrm{W}}{dt} = K(W_\infty - W)^2 \tag{11}$$

where W is the water content of the superabsorbent at time t, W_∞ is the water content before the equilibrium has been reached and K is the constant. Substituting eq. 11 with limits $t = 0$ and $W = 0$ to W, and rearrangement, the equation can be re-written as:

$$\frac{t}{W} = \frac{1}{KW_\infty^2} + \frac{1}{W_\infty}\, t \tag{12}$$

The swelling of the super-absorbent composites obeys second order kinetics (Fig. 10) [82,86].

Similar results were found for the hydrogels developed from HEC [87]. Composite hydrogels with *co*-polymerization with HEC, sodium acrylate and medicinal stone (MS) were created. The analysis of kinetic swelling (Fig. 11) [87], depicted the effects of MS content, particle size and saline solution on the swelling kinetics. It was found that the swelling rate was faster at initial 600 s. With prolonging swelling time, the swelling rate decreased until a plateau was reached. Schott's second-order swelling kinetics model [88] (eq. 13) was introduced to evaluate the hydrogels' kinetic swelling behaviours.

$$\frac{t}{Q_t} = \frac{1}{K_{is}} + \frac{1}{Q_\infty} t \tag{13}$$

were, Q_t (g/g) is the swelling capacity of the hydrogel at time t (s), Q_∞ (g/g) is the theoretical equilibrium swelling capacity, and K_{is} (g/g s) is the initial swelling rate constant.

6.2. Kinetics of dissolution

The dissolution of polymeric materials has some typical features. The rate of dissolution is controlled by several factors, the determining one is the diffusion rate into the polymer matrix. The diffusion rate depends on the chemical structure of the polymer, solvent and functional groups present on the polymer chain (dissolving parameter density of cohesive energy), solvent molecular volume, dissolution temperature, molecular weight of the polymer, structural ordering of the polymer etc. By getting the polymer into contact with the solvent, the diffusion of solvent molecules into the polymer matrix proceeds, creating thus the SSL (δ) [89,90]. The thickness of this layer depends on the temperature of dissolution, mixing rate, molecular weight of the polymer, kinetic and thermodynamic activity of the solvent, and thermal history of polymers [70,71,91,92].

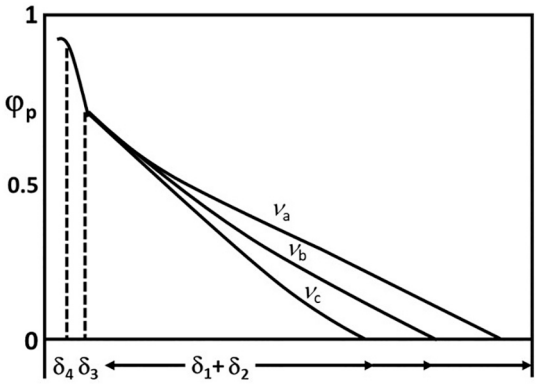

Fig. 12. Distribution of the polymer concentration in the swollen layer δ composed from δ_1 – liquid, δ_2 – rubbery, δ_3 – solid swollen and δ_4 – infiltration layers in a distance from the interface at different mixing rates v_i ($v_2 > v_1 > v_0 = 0$), φ – volume fraction of the polymer (Courtesy of [89]).

Surface swollen layer of a polymer represents interfacial resistance of definite matter, which influences diffusion of molecules in one or another direction from the interface. Ueberrreiter and Asmussen have found that it has a complicated structure with respect to the dissolving temperature [89].

If temperature of dissolution (T) ranges between gel point temperature (T_{gel}) and glass transition temperature (T_g) ($T_{gel} < T < T_g$), then the structure of the surface layer consists of liquid (δ_1), rubbery (δ_2), solid swollen (δ_3), and infiltration layer (δ_4). Thickness and distribution of particular layers in swollen polymer layer are represented in Fig. 12 [89].

7. Cross-linkers for creating gel-polymer

The gel in general is consisted of the cross-linked networks of hydrophilic water-soluble polymers. Gel polymers can swell after absorbing water. It is possible to prepare natural polymer-based hydrogels by mechanical and physical cross-linking [93]. In the case of polymeric networks, their structure is fully dependent on covalent bonds or physical inter-molecular interactions between individual macromolecules. However, each connecting point of the network are mutually separated by a linear secondary chain. In the case when these secondary chains are sufficiently long, and their chemical structure allows adoption of various conformations, these create soft and flexible materials. Contrary to this, rigid secondary chains cause the creation of hard and glassy materials. The characteristic property of the stable elastomeric network is its swelling ability when in contact with proper solvent systems. Therefore, because the polymeric network is, in fact, structuralised solid matter that cannot be dissolved with an exemption of the cases when there is observed loss of their coherent macroscopic

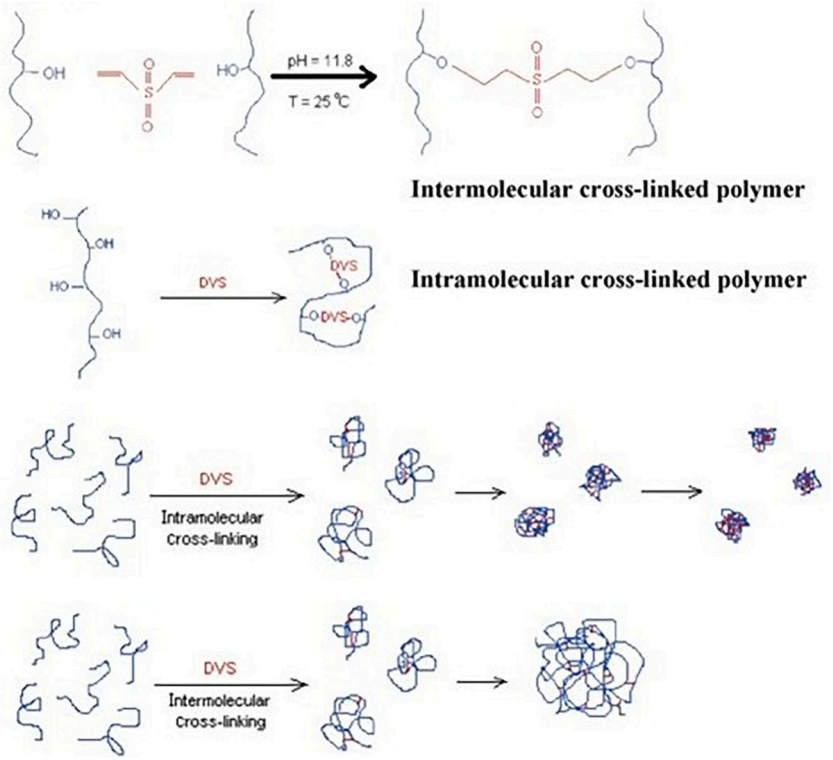

Fig. 13. Mechanism of the cross-linker reaction and schematic representation of intra- and inter-polymer cross-linking [103] Reprinted with permission from Atoosa Maleki, Anna-Lena Kjøniksen, Bo Nyström: "Effect of Shear on Intramolecular and Intermolecular Association during Cross-Linking of Hydroxyethylcellulose in Dilute Aqueous Solutions"; The Journal of Physical Chemistry B, 109 (Jun 1) 12329–12336 (2005). Copyright 2005 American Chemical Society.

structure [65]. Thus, when such cross-linked structure is immersed into the solvent, which is miscible with the polymer chains of the network, the solvent is absorbed, and the network is swollen. The increase of the volume can be up to one thousand percent [94]. Chemical reactions initiated by pressure, heat, irradiation, and change in the pH level can facilitate cross-links formation [95]. The latter cross-linking can be achieved by chemical reactions such as polycondensation, polyaddition or by physical entanglements of macromolecular chains. Physical entanglements and disentanglements of macromolecular chains were reported [96,97] as induced by temperature and pH of the dissolved polymer system known as helix-coil transition. For example, mixing certain chemical agents, such as cross-linking reagents with partially polymerized or unpolymerized resin creates cross-links [98]. Cross-linking is commonly used to improve starch performance for a variety of applications [99]. Cross-linking agents, such as sodium tri metaphosphate, phosphorus oxychloride, epichlorohydrin, citric acid, diphenyl sulphone, anthracene *endo*-peroxide [100–102], sodium tripolyphosphate, and 1,2,3,4-diepoxybutane have been used for the improvement of the materials´ mechanical properties and the starch products´ water stability.

Divinyl sulfone (DVS) is a non-zero length cross-linker that has been widely used to chemically modify polymers to improve the mechanical properties and enhance the performance according to the suitability (Fig. 13) [103]. It has been extensively used in combination with cellulose and its derivatives, especially in the pharmaceutical industries. The concentration of DVS added to the biopolymer directly influences its rheological properties. It has been found that higher concentrations of DVS increases the viscosity thereby indicating a higher cross-linking in the biopolymer [104].

Polymers may act as a basic building component of the larger systems namely of block *co*-polymers and micelles. The latter micelles can be organised in the presence of the surface-active agents to liquid crystalline systems [105].

8. Conclusions

Viewing the state of polymeric materials, the reviewed biopolymers possess enhanced structural diversity, biodegradability, thin coat-forming ability, and diverse flexibility, allowing them to be used in varied application prospects in technologically influential intelligent applications. The lightweight and biocompatibility of cellulose derivatives have been essential in biomedical and non-biomedical fields. The reviewed biopolymers have a high potential in the preparation of intelligent high-tech materials and in unlocking new possibilities for natural biopolymer layers to be better suited to the environment and the needs of end-users. This review provides an attractive route for the scientific community to research the technologically important and intelligent coatings for varied purposes.

Declaration of Competing Interest

The authors declare that they have no known competing financial interests or personal relationships that could have influenced the work reported in this paper.

Acknowledgement

The authors would like to express their gratitude for financing this research by the internal grant of Palacky University in Olomouc (project no. IGA_PrF_2022_020) and to the internal grant of Tomas Bata University in Zlin (project no. IGA/FT/2022/005). Financial support to the author YM by Fischer scholarship of the Faculty of Science, Palacky University in Olomouc in 2021. The authors would also like to express their gratitude to Mgr. Martin Pykala, PhD. (Catrin, Palacky University in Olomouc) for preparation of graphical abstract.

Reference list

[1] Mishra A, Gangele A. Smart materials for clean and sustainable technology for smart cities. Mater Today Proc 2020;29:338–42.
[2] Lv J, Liu Zhuoyu, Zhang Jie, Huo Jizhen, Yu Yingfeng. Bio-based episulfide composed of cardanol/cardol for anti-corrosion coating applications. Polymer 2017;121:286–96.
[3] Hu B. Biopolymer-based lightweight materials for packaging applications. Light Mater Biopolymers Biofibers 2014:239–55.
[4] Bourbonnais R, Marchessault Robert H. Application of polyhydroxyalkanoate granules for sizing of paper. Biomacromolecules 2010;11:989–93.
[5] Lapcik L, Lapcikova B, Zboril R. Paper-Based Composite Planar Material, EP3034693B1. Munich: European Patent Office; 2018.
[6] Lapcik L, Peterkova Petra, Gheorghiu Mihnea. Method of increasing polypropylene biocompatibility by formation of a structured surface layer based on native or modified collagen. CZ-Patent CZ294386, 2004.
[7] Nicolson PC, Baron Richard Carlton, Chabrecek Peter, et al. Extended wear ophthalmic lens. In: Official Gazette of the United States Patent and Trademark Office Patents; 2017.
[8] Chabrecek P, Lohmann D. Surface modification of extended wear contact lenses by plasma-induced polymerization of vinyl monomers. Fundam Appl Asp Chemically Modified Surf 1999:223–34. https://doi.org/10.1533/9781845698591.223.
[9] Lapcik L, Lapcik L, Kubicek P, et al. Study of penetration kinetics of sodium hydroxide aqueous solution into wood samples. BioResources 2014;9:881–93.
[10] Marchessault RH. All things cellulose: a personal account of some historic events. Cellulose 2011;18:1377–9.
[11] Shao ZQ, Wang WJ. Structure and Properties of Cellulose Nitrate. Beijing: National Defense Industry Press; 2011.
[12] Zhang X, Hikal Walid M, Zhang Yue, et al. Direct laser initiation and improved thermal stability of nitrocellulose/graphene oxide nanocomposites. Appl.Phys. Lett. 2013;102:141905.
[13] Li A, Wang Yadong, Deng Lijuan, et al. Use of nitrocellulose membranes as a scaffold in cell culture. Cytotechnology 2013;65:71–81.
[14] Gao X, Xu Li-Ping, Xue Zhongxin, et al. Dual-scaled porous nitrocellulose membranes with underwater superoleophobicity for highly efficient oil/water separation. Adv Mater 2014;26:1771–5.
[15] Zhang Y, Wang Feijun, Gao Kezheng, Liu Yanhua, Shao Ziqiang. Alcogel and aerogel of nitrocellulose formed in nitrocellulose/acetone/ethanol ternary system. Int J Polym Mater Polym Biomater 2016;65:377–83.
[16] Dimitrijevich SD, Tatarko Matthew, Gracy Robert W, Linsky Cary B, Olsen Charles. Biodegradation of oxidized regenerated cellulose. Carbohydr Res 1990;195:247–56.
[17] Dimitrijevich SD, Tatarko Matthew, Gracy Robert W, et al. In vivo degradation of oxidized, regenerated cellulose. Carbohydr Res 1990;198:331–41.
[18] Stilwell RL, Marks MG, Saferstein L, Wiseman DM. Oxidized cellulose: chemistry, processing and medical applications. Drug Target Recov Handb Biodegr Polym 1997;7:291–306.
[19] Kumar V, Yang Tianrun. HNO3/H3PO4–NANO2 mediated oxidation of cellulose—preparation and characterization of bioabsorbable oxidized celluloses in high yields and with different levels of oxidation. Carbohydr Polym 2002;48:403–12.
[20] Bajerová M, Krejčová Kateřina, Rabišková Miloslava, et al. Oxycellulose beads with drug exhibiting pH-dependent solubility. AAPS PharmSciTech 2011;12:1348–57.
[21] Kanmani P, Rhim Jong-Whan. Properties and characterization of bionanocomposite films prepared with various biopolymers and ZnO nanoparticles. Carbohydr Polym 2014;106:190–9.
[22] Noreen A, Zia Khalid Mahmood, Tabasum Shazia, et al. Hydroxyethylcellulose-g-poly (lactic acid) blended polyurethanes: preparation, characterization and biological studies. Int J Biol Macromol 2020;151:993–1003.
[23] Singh P, Magalhães Solange, Alves Luis, et al. Cellulose-based edible films for probiotic entrapment. Food Hydrocoll 2019;88:68–74.
[24] Franca JR, Foureaux Giselle, Fuscaldi Leonardo L, et al. Chitosan/hydroxyethyl cellulose inserts for sustained-release of dorzolamide for glaucoma treatment: in vitro and in vivo evaluation. Int J Pharm 2019;570:118662.
[25] Alekseeva OV, Rodionova Anna N, Bagrovskaya Nadezhda A, Agafonov Alexandr V, Noskov Andrew V. Effect of the bentonite filler on structure and properties of composites based on hydroxyethyl cellulose. Arab J Chem 2019;12:398–404.
[26] Tunç S, Duman Osman. Preparation and characterization of biodegradable methyl cellulose/montmorillonite nanocomposite films. Appl Clay Sci 2010;48:414–24.
[27] Mikula M, Čeppan M, Blecha J, Lapčík L, Kalíšek V. Kinetic dissolution measurement of polymers by solution viscosity recording. Polym Test 1988;8:339–51. https://doi.org/10.1016/0142-9418(88)90051-7.
[28] Kalisek V, Lapcik L, Mikulaskova B. Evaluation of the fixation of polyester based textile materials. III. Influence of the fixation conditions on swelling time and degree of fixation. J Polym Mater 1998;15:299–309.
[29] Pelikan P, Čeppan Michal, Liška Marek. Applications of numerical methods in molecular spectroscopy. In: Fundamental & Applied Aspects of Chemometrics Book. 1; 2020.
[30] Lapčík Ľ. Fotochemické procesy. 1989.
[31] Liedermann K, Lapčík L, Desmedt S. Study of the Molecular Mobility of Polysaccharide Solid Thin Layers by Dielectric Relaxation Spectroscopy. MRS Online Proceedings Library (OPL); 1997. p. 500.
[32] Liedermann K, Lapcik LJ. Dielectric relaxation spectroscopy of some polysaccharides. Chem Pap 1996;50:218–23.
[33] Yu P, Hou Yufeng, Zhang Hongjie, et al. Characterization and solubility effects of the distribution of carboxymethyl substituents along the carboxymethyl cellulose molecular chain. BioResources 2019;14:8923–34.
[34] Mali KK, Dhawale SC, Dias RJ, Dhane NS, Ghorpade VS. Citric acid crosslinked carboxymethyl cellulose-based composite hydrogel films for drug delivery. Indian J Pharm Sci 2018;80:657–67.
[35] Tirpude RN, Puranik Prashant K. Rabeprazole sodium delayed-release multiparticulates: effect of enteric coating layers on product performance. J Adv Pharm Technol Res 2011;2:184.
[36] Kausar A. Polymer coating technology for high performance applications: fundamentals and advances. J Macromol Sci A 2018;55:440–8.
[37] Choi H, Park Hyungmin, Sagong Woong, Lee Sang-im. Biomimetic flow control based on morphological features of living creatures. Phys Fluids 2012;24:121302.
[38] Marcelo G, Saiz Enrique, Pilar Tarazona M. Determination of molecular parameters of hydroxyethyl and hydroxypropyl celluloses by chromatography with dual detection. J Chromatogr A 2007;1165:45–51.
[39] Guo J, Skinner GW, Harcum WW, Barnum PE. Pharmaceutical applications of naturally occurring water-soluble polymers. Pharm Sci Technol Today 1998;1:254–61. https://doi.org/10.1016/S1461-5347(98)00072-8.
[40] Lopez CG, Colby Ralph H, Cabral João T. Electrostatic and hydrophobic interactions in NaCMC aqueous solutions: effect of degree of substitution. Macromolecules 2018;51:3165–75.
[41] Barba C, Montané Daniel, Farriol Xavier, Desbrières Jacques, Rinaudo Marguerite. Synthesis and characterization of carboxymethylcelluloses from non-wood pulps II. Rheological behavior of CMC in aqueous solution. Cellulose 2002;9:327–35.
[42] Lopez CG, Richtering Walter. Oscillatory rheology of carboxymethyl cellulose gels: influence of concentration and pH. Carbohydr Polym 2021;267:118117.
[43] Liebert TF, Heinze Thomas J. Exploitation of reactivity and selectivity in cellulose functionalization using unconventional media for the design of products showing new superstructures. Biomacromolecules 2001;2:1124–32.
[44] Xiquan L, Tingzhu Qu, Shaoqui Qi. Kinetics of the carboxymethylation of cellulose in the isopropyl alcohol system. Acta Polym 1990;41:220–2.
[45] Dürig G, Banderet A. Sur la structure des solutions aqueuses de carboxymethylcellulose. Helv Chim Acta 1950;33:1106–18.
[46] DeButts EH, Hudy JA, Elliott JH. Rheology of sodium carboxymethylcellulose solutions. Ind Eng Chem 1957;49:94–8.
[47] Hermans Jr J. Investigation of the elastic properties of the particle network in gelled solutions of hydrocolloids. I. Carboxymethyl cellulose. J Polym Sci A Gen Pap 1965;3:1859–68.
[48] Patruyo LG, Müller AJ, Sáez AE. Shear and extensional rheology of solutions of modified hydroxyethyl celluloses and sodium dodecyl sulfate. Polymer 2002;43:6481–93.
[49] Sau AC, Landoll Leo M. Synthesis and Solution Properties of Hydrophobically Modified (Hydroxyethyl) Cellulose. 1989.
[50] Tanaka R, Meadows J, Williams PA, Phillips GO. Interaction of hydrophobically modified hydroxyethyl cellulose with various added surfactants. Macromolecules 1992;25:1304–10.
[51] Kästner U, Hoffmann H, Dönges R, Ehrler R. Hydrophobically and cationically modified hydroxyethyl cellulose and their interactions with surfactants. Colloids Surf A Physicochem Eng Asp 1994;82:279–97.
[52] Kästner U, Hoffmann H, Dönges R, Ehrler R. Interactions between modified hydroxyethyl cellulose (HEC) and surfactants. Colloids Surf A Physicochem Eng Asp 1996;112:209–25.
[53] Panmai S, homme RK Prud, Peiffer DG, Jockusch S, Turro NJ. Langmuir18; 2002. p. 3860–4.
[54] Thuresson K, Nilsson Svante, Lindman Björn. Influence of cosolutes on phase behavior and viscosity of a nonionic cellulose ether. The effect of hydrophobic modification. Langmuir 1996;12:2412–7.
[55] Rachtanapun P, Luangkamin Suwaporn, Tanprasert Krittika, Suriyatem Rungsiri. Carboxymethyl cellulose film from durian rind. LWT- Food Sci Technol 2012;48:52–8.
[56] Rachatanapun P, Rattanapanone N. Synthesis and characterization of carboxymethyl cellulose from mimosa Pigra peel. J Appl Polym Sci 2011;122:3218–26.
[57] Wahyuningtyas D, Dinata Arwitra. Combination of Carboxymethyl Cellulose (CMC)-Corn Starch Edible Film and Glycerol Plasticizer as a Delivery System of Diclofenac Sodium1977; 2018. 030032.
[58] Lu Z, Huang Jizhen, Songfeng E, et al. All cellulose composites prepared by hydroxyethyl cellulose and cellulose nanocrystals through the crosslink of polyisocyanate. Carbohydr Polym 2020;250:116919.
[59] Khan A, Khan Ruhul A, Salmieri Stephane, et al. Mechanical and barrier properties of nanocrystalline cellulose reinforced chitosan based nanocomposite films. Carbohydr Polym 2012;90:1601–8.
[60] Huq T, Salmieri Stephane, Khan Avik, et al. Nanocrystalline cellulose (NCC) reinforced alginate based biodegradable nanocomposite film. Carbohydr Polym 2012;90:1757–63.
[61] Kassem I, Kassab Zineb, Khouloud Mehdi, et al. Phosphoric acid-mediated green preparation of regenerated cellulose spheres and their use for all-cellulose cross-linked superabsorbent hydrogels. Int J Biol Macromol 2020;162:136–49.
[62] Kirsch M, Birnstein Luise, Pepelanova Iliyana, et al. Gelatin-methacryloyl (GelMA) formulated with human platelet lysate supports mesenchymal stem cell proliferation and differentiation and enhances the hydrogel's mechanical properties. Bioengineering 2019;6:76.

[63] Barrer RM. Some properties of diffusion coefficients in polymers. J Phys Chem 1957;61:178–89.
[64] Mourougou-Candoni N, Prunet-Foch B, Legay F, Vignes-Adler M, Wong K. Influence of dynamic surface tension on the spreading of surfactant solution droplets impacting onto a low-surface-energy solid substrate. J Colloid Interface Sci 1997;192:129–41.
[65] Lapčík L. Gelová forma hmoty jako základ materiálově-inženýrských prvků : teze přednášky k profesorskému jmenovacímu řízení v oboru Materiálové vědy a inženýrství. 1963. 2002.
[66] Thompson RL. Solvent-free polymer lithography via the Kirkendall effect. Nucl Instrum Methods Phys Res Sect B 2010;268:2181–4.
[67] Abou-Yousef H, Kamel Samir. High efficiency antimicrobial cellulose-based nanocomposite hydrogels. J Appl Polym Sci 2015:132.
[68] Lapčík L, Valko L, Mikula M, Jančovičová V, Panak J. Kinetics of Swollen Surface Layer Formation in the Diffusion Process of Polymer Dissolution. 1988. p. 221–6.
[69] Ueberreiter K, Asmussen UF. J Polym Sci A 1957;23:75.
[70] Ueberreiter VK, Asmussen Frithjof. Die auflösungsgeschwindigkeit von polymeren. 1. Formulierung des vorganges und seine temperaturabhängigkeit, Die Makromolekulare Chemie. Macromol Chem Phys 1961;44:324–37.
[71] Asmussen VF, Ueberreiter Kurt. Die auflösungsgeschwindigkeit von polymeren, 2. Mitteilung. Untersuchung der stabilität der quellschicht durch konzentrationsund viskositätsmessungen, Die Makromolekulare Chemie. Macromol Chem Phys 1962;52:164–73.
[72] Ueberreiter K, Asmussen Frithjof. Velocity of dissolution of polymers. Part I. J Polym Sci A 1962;57:187–98.
[73] Asmussen F, Ueberreiter Kurt. Velocity of dissolution of polymers. Part II. J Polym Sci A 1962;57:199–208.
[74] Asmussen F, Ueberreiter Kurt. Die Auflösungsgeschwindigkeit von Polymeren. Kolloid-Z Z Polymere 1968;223:6–13.
[75] Ueberreiter VK, Kirchner Peter. Die auflösungsgeschwindigkeit von polymeren. 4. Mitt. Der einfluß der strömung des lösungsmittels, Die Makromolekulare Chemie. Macromol Chem Phys 1965;87:32–59.
[76] Pisarcik M, Mikula M, Mariianiova D, Lapcik L. The influence of hydroxyethylcellulose on the diffusion of acetylsalicylic-acid trihydromagnesium salt in aqueous-solution. Acta Polym 1993;44:92–6. https://doi.org/10.1002/actp.1993.010440206.
[77] Peterkova P, Lapcik L. Determination of the diffusion coefficient of water into atelocollagen type I thin films by attenuated total reflection Fourier transform infrared spectroscopy. Colloid Polym Sci 2000;278:1014–6. https://doi.org/10.1007/s003960000366.
[78] Xiong RH, Deschout H, Demeester J, De Smedt SC, Braeckmans K. Rectangle FRAP for measuring diffusion with a laser scanning. Microscope 2014;1076:433–41. https://doi.org/10.1007/978-1-62703-649-8_18; 10.1007/978-1-62703-649-8.
[79] Wu Y, Joseph Sony, Aluru NR. Effect of cross-linking on the diffusion of water, ions, and small molecules in hydrogels. J Phys Chem B 2009;113:3512–20.
[80] Jamlang J, Marañon Mica Therese, Rigor Girro Jonn, Tumolva Terence. Developing a Physically Cross-Linked Hydroxyethyl Cellulose Hydrogel for Wound Dressing Applications947; 2019. p. 3–12.
[81] Ghanbarzadeh B, Almasi Hadi, Entezami Ali A. Physical properties of edible modified starch/carboxymethyl cellulose films. Innov Food Sci Emerg Technol 2010;11:697–702.
[82] Seki Y, Altinisik Aylin, Demircioğlu Başak, Tetik Caner. Carboxymethylcellulose (CMC)–hydroxyethylcellulose (HEC) based hydrogels: synthesis and characterization. Cellulose 2014;21:1689–98.
[83] Joshi JM, Sinha Vijay Kumar. Graft copolymerization of 2-hydroxyethylmethacrylate onto carboxymethyl chitosan using CAN as an initiator. Polymer 2006;47:2198–204.
[84] Pandey PK, Srivastava Arti, Tripathy Jasaswini, Behari Kunj. Graft copolymerization of acrylic acid onto guar gum initiated by vanadium (V)–mercaptosuccinic acid redox pair. Carbohydr Polym 2006;65:414–20.
[85] Metz SJ, Van de Ven WJC, Jens Potreck MHV, Mulder and Matthias Wessling.. Transport of water vapor and inert gas mixtures through highly selective and highly permeable polymer membranes. J Membr Sci 2005;251:29–41.
[86] Soleimani F, Sadeghi Hossein, Shahsavari Hadis, Soleimani Arezou, Sadeghi Fatemeh. Studies of swelling kinetics of carboxymethyl cellulose-g-PMAAm-co-PNIPAm superabsorbent hydrogels. Asian J Chem 2013;25:4851.
[87] Wang W, Wang Jiang, Kang Yuru, Wang Aiqin. Synthesis, swelling and responsive properties of a new composite hydrogel based on hydroxyethyl cellulose and medicinal stone. Compos Part B Eng 2011;42:809–18.
[88] Schott H. Swelling kinetics of polymers. J Macromol Sci B Phys 1992;31:1–9.
[89] Kalisek V, Lapcik L, Mikulaskova B. Evaluation of the fixation of polyester based textile materials. III. Influence of the fixation conditions on swelling time and degree of fixation. J Polym Mater 1998;15:299–309.
[90] Mracek A, Benesova K, Minarik A, Urban P, Lapcik L. The diffusion process of sodium hyaluronate (Na-HA) and Na-HA-n-alkyl derivatives films swelling. J Biomed Mater Res A 2007;83A:184–90. https://doi.org/10.1002/jbm.a.31188.
[91] Park GS, Crank J. Diffusion in Polymers. London, New York: Academic Press; 1968. ISBN 0121970507-9780121970505.
[92] Lapcik L, Machackova A, Minarik A, et al. The internal pressure in thin polymer layers in contact with liquids. In: 41.Mezinárodní konference o nátěrových hmotách, KNH 2010; 2010. p. 27–36.
[93] Drnovska H, Lapcik Lubomir Jr. Hyaluronate derivatives and their applications. Plasty Kauc 1999;36:291–4.
[94] Lapcik L, Lapcik L, De Smedt S, Demeester J, Chabrecek P. Hyaluronan: preparation, structure, properties, and applications. Chem Rev 1998;98:2663–84. https://doi.org/10.1021/cr941199z.
[95] Uyanga KA, Okpozo Oghenefego P, Onyekwere Okwuchi S, Daoud Walid A. Citric acid crosslinked natural bi-polymer-based composite hydrogels: effect of polymer ratio and beta-cyclodextrin on hydrogel microstructure. React Funct Polym 2020;154:104682.
[96] Kupska I, Lapcik L, Lapcikova B, Zakova K, Jurikova J. The viscometric behaviour of sodium hyaluronate in aqueous and KCl solutions. Colloids Surf A Physicochem Eng Asp 2014;454:32–7. https://doi.org/10.1016/j.colsurfa.2014.04.018.
[97] Lapcikova B, Valenta T, Lapcik L. Rheological properties of food hydrocolloids based on polysaccharides. J Polym Mater 2017;34:631–45.
[98] Toledo PV, Limeira Diego PC, Siqueira Nicolas C, Petri Denise FS. Carboxymethyl cellulose/poly (acrylic acid) interpenetrating polymer network hydrogels as multifunctional adsorbents. Cellulose 2019;26:597–615.
[99] Raab M. Materiály a člověk:(netradiční úvod do současné materiálové vědy). 1999.
[100] Lapcik L, Bakos D, Kello V. Transannular peroxides of anthracene and its derivatives. Preparation, properties, applications. Chem Listy 1990;84:582–605.
[101] Stasko A, Blazkova A, Brezova V, Breza M, Lapcik L. Oxygen photosenzitization in the presence of sodium anthracene-1-sulfonate. J Photochem Photobiol A Chem 1993;76:159–65. https://doi.org/10.1016/1010-6030(93)80132-S.
[102] Lapcík L, Lapcíková Barbora, Stasko Andrej, EPR study of the thermal decomposition of transannular peroxide of anthracene. Int J Org Chem 2011;1:37.
[103] Maleki A, Kjøniksen Anna-Lena, Nyström Bo. Effect of shear on intramolecular and intermolecular association during cross-linking of hydroxyethylcellulose in dilute aqueous solutions. J Phys Chem B 2005;109:12329–36.
[104] Maleki A, Kjøniksen Anna-Lena, Nyström Bo. Effect of shear on intramolecular and intermolecular association during cross-linking of hydroxyethylcellulose in dilute aqueous solutions. J Phys Chem B 2005;109:12329–36.
[105] Lapcik L, Benesova K, Lapcik L, de Smedt S, Lapcikova B. Chemical modification of hyaluronic acid: alkylation. Int J Polym Anal Charact 2010;15:486–96. https://doi.org/10.1080/1023666X.2010.520904.

Research Article

Lubomír Lapčík*, Martin Vašina*, Barbora Lapčíková, Michal Staněk, Martin Ovsík, and Yousef Murtaja

Study of the material engineering properties of high-density poly(ethylene)/perlite nanocomposite materials

https://doi.org/10.1515/ntrev-2020-0113
received December 6, 2020; accepted December 19, 2020

Abstract: This paper was focused on application of the perlite mineral as the filler for polymer nanocomposites in technical applications. A strong effect of the perlite nano-filler on high-density poly(ethylene) (HDPE) composites' mechanical and thermal properties was found. Also found was an increase of the Young's modulus of elasticity with the increasing filler concentration. Increased stiffness from the mechanical tensile testing was confirmed by the nondestructive vibrator testing as well. This was based on displacement transmissibility measurements by means of forced oscillation single-degree-of freedom method. Fracture toughness showed a decreasing trend with increasing perlite concentration, suggesting occurrence of the brittle fracture. Furthermore, ductile fracture processes were observed as well at higher filler concentrations by means of SEM analysis. There was also found relatively strong bonding between polymer chains and the filler particles by SEM imagining.

Keywords: perlite fillers, HDPE composites, mechanical testing, vibration damping, thermal analysis

*** Corresponding author: Lubomír Lapčík,** Department of Physical Chemistry, Faculty of Science, Palacky University, 17. Listopadu 12, 771 46, Olomouc, Czech Republic; Faculty of Technology, Tomas Bata University in Zlin, Nam. T.G. Masaryka 275, 760 01, Zlin, Czech Republic, e-mail: lapcikl@seznam.cz
*** Corresponding author: Martin Vašina,** Faculty of Technology, Tomas Bata University in Zlin, Nam. T.G. Masaryka 275, 760 01, Zlin, Czech Republic; VŠB-Technical University of Ostrava, Department of Hydromechanics and Hydraulic Equipment, Faculty of Mechanical Engineering, 17. Listopadu 15/2172, 708 33, Ostrava-Poruba, Czech Republic, e-mail: martin.vasina@vsb.cz
Barbora Lapčíková: Department of Physical Chemistry, Faculty of Science, Palacky University, 17. Listopadu 12, 771 46, Olomouc, Czech Republic; Faculty of Technology, Tomas Bata University in Zlin, Nam. T.G. Masaryka 275, 760 01, Zlin, Czech Republic
Michal Staněk, Martin Ovsík: Faculty of Technology, Tomas Bata University in Zlin, Nam. T.G. Masaryka 275, 760 01, Zlin, Czech Republic
Yousef Murtaja: Department of Physical Chemistry, Faculty of Science, Palacky University, 17. Listopadu 12, 771 46, Olomouc, Czech Republic

1 Introduction

Modification and recycling of polymers is an important part of the polymer research and applications [1–3]. Thermoplastics, such as polyethylene, can offer useful mechanical, chemical, electrical [4], and optical [5] properties, e.g., as the structural supporting components [6] and packaging materials [7]. Due to its low price per unit volume and unique physicochemical properties, it is globally the most used thermoplastic [8]. Poly(ethylene) is a semicrystalline polymer. It is classified based on its density. There are four different groups: high-density polyethylene (HDPE), low-density polyethylene (LDPE), linear low-density polyethylene (LLDPE), and very low-density polyethylene (VLDPE) [9]. Covalent bond between carbon atoms of the poly(ethylene) molecule is extremely stiff and strong similarly as in the diamond. Furthermore, poly(ethylene) chain has the smallest transversal cross-section compared to all polymers [10]. This is due to the lack of the presence of the pendant groups in its macromolecular structure. Therefore, the system of the unidirectional-oriented polyethylene chains has relatively high strong elements available per unit area capable to transmit high mechanical stresses. For this reason, the macroscopic mechanical strength of such structure is very high. Semiempirical estimations of the maximum strength of the polyethylene along its macromolecular chain vary in the range of 16–36 GPa. Theoretical calculations of the modulus of elasticity propose magnitudes from 180 to 340 GPa [10]. However, there was found increased risk of cavities formation at the nano-filler/polymer matrix interface in the HDPE

nanocomposites due to the difference in the Young's modulus of elasticity between the polymer matrix and the filler nanoparticles [11].

Moreover, the tensile properties of polymer fibers might be significantly affected by their fiber structure as found for polyacrylonitrile (PAN) membranes [12]. It was found that these decrease significantly with increasing the fiber orientation angle. The results also showed that the nanofiber membranes exhibited ductile fracture pattern.

The fundamental mechanisms governing the size-dependent mechanical behavior of different crystal structures were described in detail in [13], where the effects of fabrication process and current experimental techniques for micro and nano-compression were investigated as well. The influence of the surface effect on the properties of the nano-scale sample is directly associated with the surface to volume ratio.

Mineral fillers were used as an additive in polymer nanocomposites [14], silicon rubber [15], and in combination with the polyvinyl alcohol fibers/nano-SiO_2 fillers as reinforced cementitious composites [16] in the last decade. At the present, mineral nano-fillers were used as friction reducing additives for improving tribological performance and wear resistance of HDPE [17]. HDPE-nanoclay composites were also used in the additive manufacturing by means of the 3D printing technology, where increase in Young's modulus of elasticity with increasing nanoclay concentration was found [18]. It was found that the net effect of the nano-fillers on the wear resistance was due to the combination of different abilities of the nano-fillers to modify the tensile and compressive mechanical properties of polymers. These were manifested in the observed surface hardness and ductility of the nano-composite, contributed by the nano-fillers to the friction coefficient and the creation of the transfer film [17]. The effect of incorporating nano-fillers into the thermoplastic polymer network results in the improvement of the physicochemical and mechanical characteristics such as low air permeability [19], improved mechanical strength, modulus of elasticity, and stiffness [20–22]. That is why, now, the research focused on composites containing inorganic fillers is important. Perlite powder is an essential material for the application of thermal and acoustic insulation materials [23]. Perlite is the mineral formed by the cooling of volcanic eruptions. It is composed of SiO_2, Al_2O_3, K_2O, Na_2O, and water. Depending on its origin, perlite may contain also TiO_2, CaO, and MgO. When subjected to thermal treatment, natural perlite particles expand up to 20 times in volume, due to the water vaporization [24]. Expanded perlite was also found as an effective sound-absorbing material due to its open pore structure [25]. When sound waves of a certain wavelength enter such pores, they effectively absorb the acoustic energy. Applications of polyethylene prepared with the addition of perlite were reported elsewhere [25]. It was found that perlite enhanced the thermal stability and sound absorption coefficients of polyesters.

Polymer matrix modification, its crystallinity degree, type of reinforcement, filler/matrix adhesion quality [26], filler particles size, etc. influence physicochemical, thermal, and mechanical properties of the final composites [27,28]. That is why, detailed understanding of the effect of the polymer matrix and the filler particles on the overall composite performance in consumer technical products, e.g., at the mechanical deformation loads both static and dynamic, is of scientific and practical importance. For that reason, this paper is focused on combination of the destructive and nondestructive mechanical testing [29] and thermal analysis in combination with SEM imagining for perlite/HDPE composites analysis.

2 Materials

High-density poly(ethylene) (HDPE) type 25055E (The Dow Chemical Company, USA) was used in the form of white pellets (lot. No. 1I19091333). As the filler particles, the inorganic volcanic glass mineral perlite (Supreme Perlite Company, USA) was applied (d_{50} = 447 nm diameter, density 1.10 g/cm^3) [30]. Perlite filler moisture content was 0.1 wt%. There were prepared 150 composites samples (dog bone shape for tensile testing, Charpy's pendulum, and vibrator testing) of virgin HDPE and 5, 10, and 15 wt% of inorganic filler concentrations of perlite/HDPE composites. Composite samples were prepared by means of the injection molding technology on the injection molding machine Arburg Allrounder type 420 C (Germany). Applied processing temperature ranged from 190 to 220°C, mold temperature 30°C, injection pressure 60 MPa, and injection rate 20 mm/s [31]. Extrusion machine Scientific was used for virgin and composite samples extrusion at the processing temperature ranging from 136 to 174°C, L/D = 40.

3 Methods

3.1 Scanning electron microscopy

Scanning electron microscopy (SEM) images were captured using a Scanning Electron Microscope Hitachi SU

6600 (Japan). The source of the electrons is Schottky cathode. This microscope has the resolution in secondary electron mode (SE) 1.3 nm and in back scattered electrons (BSE) 3 nm. For these images, the SE and an accelerating voltage of 5 kV were used. The distance between sample and detector was 6 mm. Studied materials were placed on double-sided carbon tape on aluminium holder.

3.2 Thermal analysis

For perlite/HDPE nanocomposites, virgin HDPE thermogravimetry (TG), and differential thermal analysis (DTA), experiments were performed on a simultaneous DTA-TG apparatus (Shimadzu DTG 60, Japan). Measurements were performed at a heat flow rate of 10°C/min in a dynamic nitrogen atmosphere (50 ml/min) at the temperature range from 30 to 550°C. The crystallinity (w_C) of the nanocomposites was calculated according to the formula (1) [32,33]:

$$w_C = \frac{\Delta H_m}{\Delta H_m^0} \times 100 \tag{1}$$

where: $\Delta H_m^0 = 293\ J\ g^{-1}$ is heat of fusion for 100% crystalline material HDPE, heated at rate of 10°C/min [32,34], and ΔH_m ($J\ g^{-1}$) is measured heat of fusion.

3.3 Uniaxial tensile testing

Tensile testing of injection-molded specimens was performed on a Zwick 1456 multipurpose tester (Germany). The measurements were realized according to CSN EN ISO 527-1 and CSN EN ISO 527-2 standards [35]. Samples were strained at room temperature up to break at the test speeds of 50, 100, and 200 mm/min. From the stress–strain dependencies, Young's modulus of elasticity and elongation at break were calculated. Each experiment was repeated 10× at the ambient temperature of 22°C and average values and standard errors were calculated.

3.4 Charpy impact testing

Impact tests were performed on Zwick 513 Pendulum Impact Tester (Germany) according to the CSN EN ISO 179-2 standard with the drop energy of 25 J.

3.5 Displacement transmissibility measurement

The material's ability to damp harmonically excited mechanical vibration of single-degree-of freedom (SDOF) systems is characterized by the displacement transmissibility T_d, which is expressed by the equation [36,37]:

$$T_d = \frac{y_2}{y_1} = \frac{a_2}{a_1}, \tag{2}$$

where: y_1 is the displacement amplitude on the input side of the tested sample and y_2 is the displacement amplitude on the output side of the tested sample, a_1 is the acceleration amplitude on the input side of the tested sample and a_2 is the acceleration amplitude on the output side of the tested sample.

Generally, there are three different types of mechanical vibration depending on the value of the displacement transmissibility, namely, resonance ($T_d > 1$), undamped ($T_d = 1$), and damped ($T_d < 1$) vibration [37].

The displacement transmissibility of a spring-mass-damper system, which is described by spring (stiffness k), damper (damping coefficient c), and mass m, is given by the following equation [36–38]:

$$T_d = \sqrt{\frac{k^2 + (c \times \omega)^2}{(k - m \times \omega^2)^2 + (c \times \omega)^2}} = \sqrt{\frac{1 + (2\zeta \times r)^2}{(1 - r^2)^2 + (2\zeta \times r)^2}} \tag{3}$$

where: ζ is the damping ratio and r is the frequency ratio, which are expressed by the formulas [39,40]:

$$\zeta = \frac{c}{2\sqrt{k \times m}}, \tag{4}$$

$$r = \frac{\omega}{\omega_n} = \frac{\omega}{\sqrt{k/m}}, \tag{5}$$

where: ω is frequency of oscillation and ω_n is the natural frequency [41,42]. Under the condition $dT_d/dr = 0$ in the equation (3), it is possible to find the frequency ratio r_0, at which the displacement transmissibility has its maximum value [36]:

$$r_0 = \frac{\sqrt{\sqrt{1 + 8\zeta^2} - 1}}{2\zeta}. \tag{6}$$

It is evident from the equation (6) that the local extreme of the displacement transmissibility is generally shifted to lower values of the frequency ratio r with the increasing damping ratio ζ (or with the decreasing material stiffness k). The local extrema (i.e., the maximum

value of the displacement transmissibility T_{dmax}) is obtained at the frequency ratio r_0 from the equation (6).

The mechanical vibration damping testing of the investigated materials was performed by the forced oscillation method. The displacement transmissibility T_d was experimentally measured using the BK 4810 vibrator in combination with a BK 3560-B-030 signal pulse multi-analyzer and a BK 2706 power amplifier at the frequency range from 2 to 3,200 Hz. The acceleration amplitudes a_1 and a_2 on the input and output sides of the investigated specimens were evaluated by means of BK 4393 accelerometers (Brüel & Kjær, Nærum, Denmark). Measurements of the displacement transmissibility were performed for three different inertial masses m (i.e., ranging from 0, 90, and 500 g), which were positioned on the upper side of the periodically tested samples. The tested block article dimensions were (60 × 60 × 3) mm (length × width × thickness). Each measurement was repeated 5 times at an ambient temperature of 23°C.

4 Results and discussion

As known from earlier studies [35], applied inorganic nano/micro particles are used as functional fillers modulating elastoplastic behavior of polymer composites. It was found that dominating factors responsible for controlled mechanical response patterns of the composites are mainly the physicochemical properties of the applied polymer base matrix (e.g., HDPE, low-density poly(ethylene) (LDPE), linear low-density poly(ethylene) (LLDPE), etc.) and the properties of the filler particles (e.g., their uniformity, shape, diameter, and surface chemistry). Other factors, which should be taken into account, are the ratio of the amorphous/crystalline regions of the polymer matrix and the quality of the interface adhesion between filler particles and the polymer matrix [9].

SEM images of the perlite micro/nano-filler particles are shown in Figure 1a and b.

There is an evidence confirming their porous internal structure as shown in Figure 1a. As it is well-known from the literature [30,43,44], the porous micro/nano structures of the fillers or the whole composite articles are directly affecting their sound absorption, vibration damping properties as well as their dynamic mechanical properties [31,45,46].

Typical filler concentration dependencies of the Young's modulus of elasticity (E) of the studied perlite/HDPE composites are shown in Figure 2.

They were characteristic with the gradual increase of the E with the increasing perlite concentration for all deformation rates under study (50, 100, and 200 mm/min). There was observed approximately 37% increase in E for 15 wt% perlite concentration compared to the virgin HDPE. This triggered substantial increase of the materials' stiffness. However, this phenomenon was accompanied with the corresponding exponential decrease of the observed elongation at break with the increasing filler concentration as shown in Figure 3.

There was confirmed increasing stiffness of the composite response to the applied uniaxial deformation with the increasing deformation rate as reflected by original elongation at break for the virgin polymer of 220% (50 mm/min deformation rate) changed to 70% (100 mm/min deformation rate) and to 45% (200 mm/min deformation rate). Interestingly, these differences were not much significant for higher concentrations of the filler exceeding 10 wt% perlite/HDPE composite matrices, suggesting lowered mobility of the poly(ethylene) macromolecular chains.

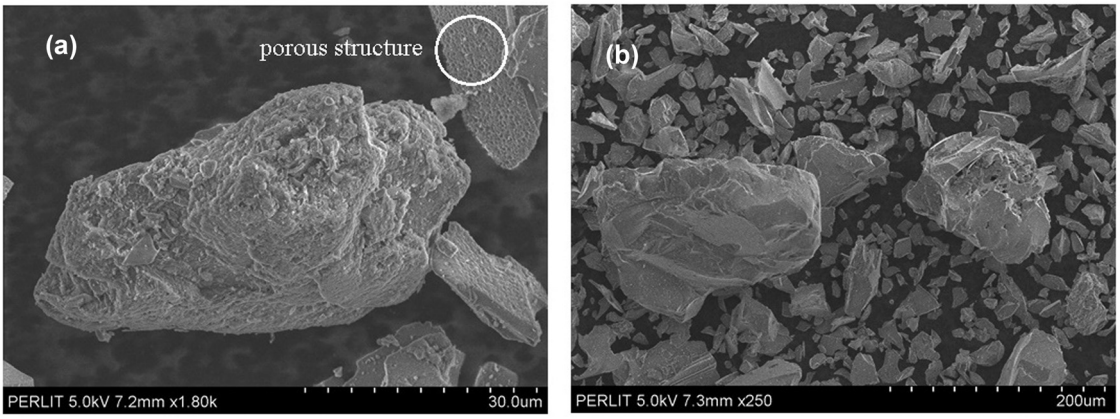

Figure 1: SEM image of the perlite micro/nano-filler.

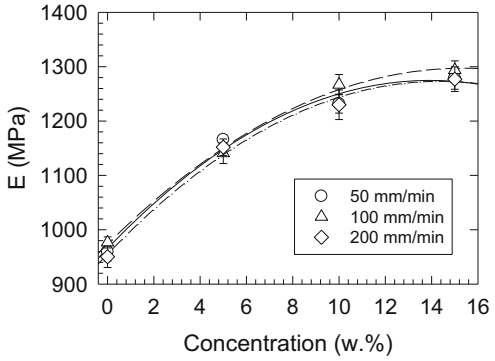

Figure 2: Young's modulus of elasticity (E) vs perlite filler concentration. Inset: applied deformation rates.

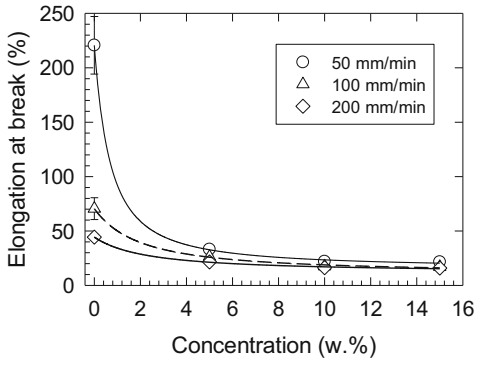

Figure 3: Elongation at break vs perlite filler concentration. Inset: applied deformation rates.

Results of the fracture mechanics measurements of the studied composites are shown in Figure 4.

There was found exponential decrease of the fracture toughness from 3.8 kJ/m^2 (virgin HDPE) to 2.4 kJ/m^2 for perlite/HDPE composites in the perlite concentration range from 5 to 15 wt%. As observed earlier during uniaxial tensile testing, mineral filler brought increase of the material stiffness to the composite matrix as reflected by the increasing modulus E with the increasing filler concentration. Also during impact fracture testing performed on Charpy pendulum, similar effect was confirmed, as reflected in Figure 4, by the increasing maximum force with the increasing filler concentration.

With respect to the proposed mechanical energy transfer mechanism, the SEM images shown in the Figure 5 clearly recognized plastically transformed polymer regions characteristic with the well-developed spurs and deformation bands typical for ductile fracture interface (Figure 5b–d) as well as brittle fracture regions as shown in Figure 5a and b.

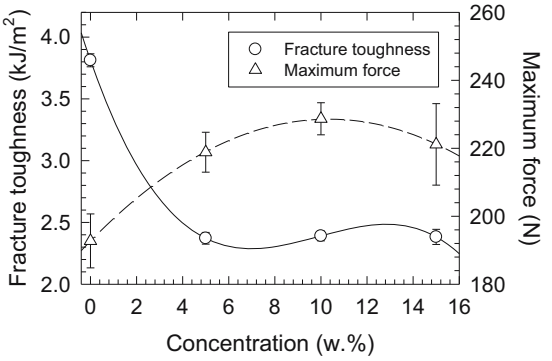

Figure 4: Fracture toughness and maximum force vs perlite filler concentration dependencies.

Results of the dynamic mechanical testing of the studied composites by the forced oscillation method on vibrator device are shown in Figures 6 and 7.

Here (Figure 6), typical frequency dependencies of the displacement transmissibility demonstrated increased material stiffness with the increasing filler concentration as reflected by appearance of the first resonance frequency (f_{R1}) peak position (Table 1).

There was confirmed validity of the formula (6), where with increasing stiffness (or decreasing damping ratio) the f_{R1} peak position was shifted to the higher excitation frequencies. Obtained dynamic mechanical behavior was in excellent agreement with tensile testing measurements, where the E was increased with the increasing perlite concentration in the polymer composite matrix. It was also found that the f_{R1} was shifted to the lower excitation frequencies with the increasing inertial mass applied during vibrational measurements. This fact is in agreement with the formula (4), where the increasing inertial mass m leads to the lower natural frequency ω_n, thus to the lower f_{R1}. From the practical point of view, this method (vibration damping) allows nondestructive evaluation of the stiffness of the polymer nanocomposites in contrary to the destructive tensile or fracture tests.

Results of the thermal analysis are shown in Figure 8a and b and Table 2.

There was found a minor increase of the melting temperature from 137.4°C (virgin HDPE) to 141.6°C (15 wt% perlite/HDPE composite), indicating a stronger bonding between polymer chains and the filler particles. However, the crystallinity was decreased with the increasing perlite concentration from original 60.65 to 28.16%, suggesting perlite had no positive effect on HDPE crystallization as

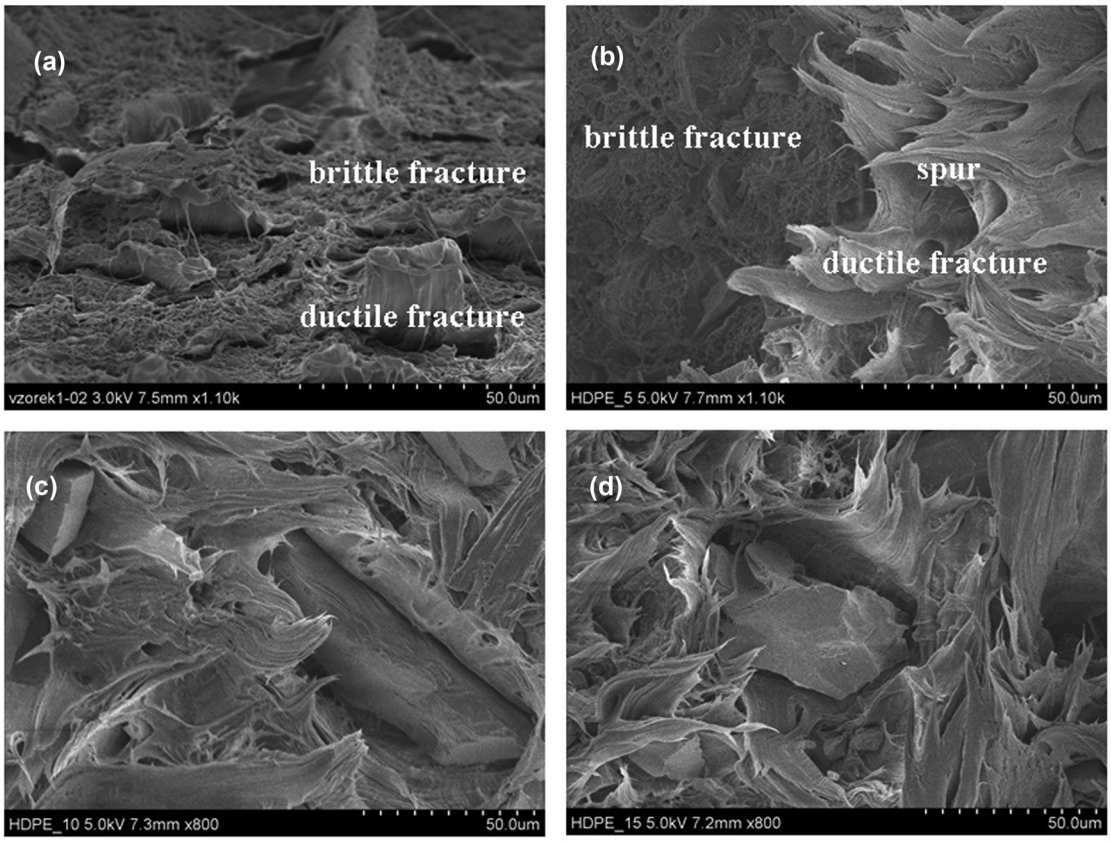

Figure 5: SEM images of the fracture surface after the tensile testing of the samples: (a) virgin HDPE, (b) 5 wt% perlite/HDPE composite, (c) 10 wt% perlite/HDPE composite, (d) 15 wt% perlite/HDPE composite. (50 mm/min applied deformation rate).

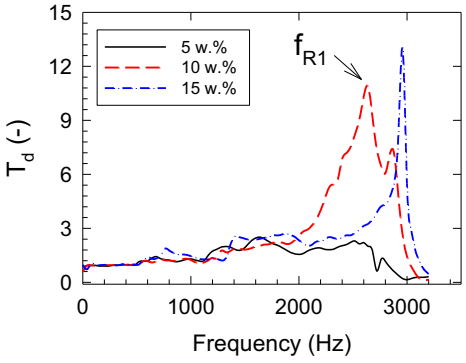

Figure 6: Frequency dependencies of the displacement transmissibility of the tested perlite/HDPE composites (Inset: perlite concentration) without inertial mass (m = 0 g).

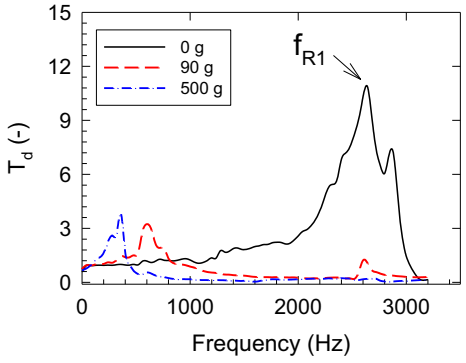

Figure 7: Frequency dependencies of the displacement transmissibility of the tested perlite/HDPE composites (Inset: inertial mass) of 10 wt% perlite concentrations.

was reported, e.g., for halloysite nanotubes filler [47]. It was found (Figure 8a) that the highest degradation rate was observed for 5 wt% composite; however, the lowest degradation rate was found for 15 wt% composite. All curves exhibited one single degradation step attributed to the radical random scission mechanism of polyolefin thermal decomposition [33]. Compared to the virgin HDPE, the onset of the degradation of 15 wt% perlite/HDPE composite was shifted to the lower value, where according to Cuadri *et al.* [33] the predominant chain scission provoked the formation of low-thermal stability compounds. The latter compounds were consecutively eliminated at lower temperatures.

Table 1: First resonance frequency f_{R1} and the corresponding maximum displacement transmissibility T_{dmax} of the investigated composites as induced by harmonically excited vibration; c – perlite concentration

c [wt%]	Quantity	Inertial mass (g)		
		0	90	500
5	f_{R1} [Hz]	1,614 ± 72	593 ± 26	341 ± 15
	T_{dmax} [–]	2.5 ± 0.2	3.1 ± 0.2	3.7 ± 0.3
10	f_{R1} [Hz]	2,627 ± 112	603 ± 25	346 ± 16
	T_{dmax} [–]	12.1 ± 0.9	3.3 ± 0.2	4.5 ± 0.4
15	f_{R1} [Hz]	2,944 ± 129	626 ± 28	396 ± 17
	T_{dmax} [–]	14.2 ± 1.1	4.6 ± 0.3	4.8 ± 0.4

Table 2: Results of the thermal analysis of the virgin HDPE and perlite/HDPE composites

c [wt%]	T_m [°C]	ΔH_m [J g^{-1}]	w_C [%]	T_A [°C]	T_D [°C]	TWL [%]
0	137.4	177.7	60.65	455	477.2	100.0
5	136.4	133.9	48.10	463.9	476.1	93.1
10	139.9	92.9	31.44	462.1	474.7	90.0
15	141.6	82.5	28.59	451.3	474.3	86.2

c – filler concentration, T_m – melting peak temperature, ΔH_m – heat of fusion, w_C – crystallinity, T_D – DTA peak of decomposition, T_A – starting point – intersection of extrapolated staring mass with the tangent applied to the maximum slope of the TG curve (decomposition behavior), TWL – total weight loss, ΔH_m endothermic process detected in the temperature range from 95 to 175°C for all samples.

5 Conclusions

It was found in this study that perlite mineral filler is strongly influencing mechanical and thermal properties of HDPE polymer nanocomposites. There was a confirmed gradual increase of the Young's modulus of elasticity accompanied with the corresponding decrease of the elongation at break with the increasing filler concentration. There was an observed 37% increase in the Young's modulus of elasticity for 15 wt% perlite concentration in comparison with the virgin HDPE. The observed increased stiffness from the tensile testing was confirmed by the nondestructive vibrator testing based on measurement of the displacement transmissibility during forced oscillation measurements. It was reflected by the shift of the first resonance frequency peak position to the higher excitation frequencies. Fracture toughness showed a decreasing trend with the increasing perlite concentration from 4 to 2.3 kJ/m^2, suggesting occurrence of the brittle fracture as well. However, there were observed regions of the ductile fracture processes at higher filler concentrations as found in SEM images. These were characteristic with the observed polymer deformation bands and spurs. It can be concluded that the perlite particles function as the stress concentrators in the complex composite matrix. There was found a minor increase of the melting temperature with the increasing filler concentration, indicating a stronger bonding between polymer chains and the filler particles.

Acknowledgments: This study was supported by the European Regional Development Fund in the Research Centre of Advanced Mechatronic Systems project, project number CZ.02.1.01/0.0/0.0/16_019/0000867. Authors LL and YM would like to express their gratitude for financing this research to the internal grant of Palacky University in Olomouc IGA_PrF_2020_022. Financial support to the author YM by Fischer scholarship of the Faculty of Science, Palacky University in Olomouc in 2020 year, is gratefully acknowledged as well. Special thanks to Dr. K. Čépe for SEM measurements (Palacky University in Olomouc).

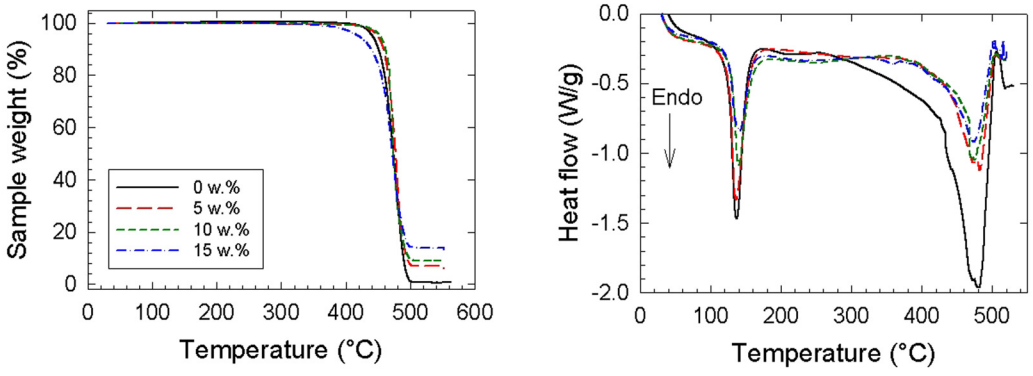

Figure 8: Results of the TGDTA thermal analysis of the studied perlite/HDPE composites. Inset: Perlite concentration.

Conflict of interest: The authors declare no conflict of interest regarding the publication of this paper.

References

[1] Lei M, Chen Z, Lu H, Yu K. Recent progress in shape memory polymer composites: methods, properties, applications and prospects. Nanotechnol Rev. 2019 Jan;8(1):327–51.

[2] Chamis CC. Polymer composite mechanics review – 1965 to 2006. J Reinf Plast Compos. 2007;26(10):987–1019.

[3] Singh N, Hui D, Singh R, Ahuja IPS, Feo L, Fraternali F. Recycling of plastic solid waste: a state of art review and future applications. Compos Part B Eng. 2017 Apr 15;115:409–22.

[4] Mora A, Verma P, Kumar S. Electrical conductivity of CNT/polymer composites: 3D printing, measurements and modeling. Compos Part B Eng. 2020 Feb 15;183:107600.

[5] Wang X, Xu P, Han R, Ren J, Li L, Han N, et al. A review on the mechanical properties for thin film and block structure characterised by using nanoscratch test. Nanotechnol Rev. 2019 Jan;8(1):628–44.

[6] Kenisarin MM, Kenisarina KM. Form-stable phase change materials for thermal energy storage. Renew Sustain Energy Rev. 2012 May;16(4):1999–2040.

[7] Gill YQ, Jin J, Song M. Comparative study of carbon-based nanofillers for improving the properties of HDPE for potential applications in food tray packaging. Polym Polym Compos. 2020 Oct;28(8–9):562–71.

[8] Sauter DW, Taoufik M, Boisson C. Polyolefins, a success story. Polymers. 2017 Jun;9(6):185.

[9] Krasny I, Lapcik L, Lapcikova B, Greenwood RW, Safarova K, Rowson NA. The effect of low temperature air plasma treatment on physico-chemical properties of kaolinite/polyethylene composites. Compos Part B Eng. 2014 Mar;59:293–9.

[10] Lapcik L, Raab M. Materials science II. Textbook. Zlin, Tomas Bata University in Zlin, 2nd edn. Zlin: Tomas Bata University in Zlin; 2004.

[11] Perchacz M, Rozanski A, Kargarzadeh H, Galeski A. Cavitation in high density polyethylene/Al2O3 nanocomposites. Compos Sci Technol. 2020 Oct 20;199:108323.

[12] Liu S, Li D, Yang Y, Jiang L. Fabrication, mechanical properties and failure mechanism of random and aligned nanofiber membrane with different parameters. Nanotechnol Rev. 2019 Jan;8(1):218–26.

[13] Bagheripoor M, Klassen R. Length scale plasticity: a review from the perspective of dislocation nucleation. Rev Adv Mater Sci. 2018;56(1):21–61.

[14] Lapcik L, Jindrova P, Lapcikova B. Effect of talc filler content on poly(propylene) composite mechanical properties. Proceeding paper, engineering against fracture. In: Pantelakis S, Rodopoulos C, (Eds). 1st conference on engineering against fracture conference. Patras, Greece, May 28–30, 2008. Patras: Springer Netherlands; 2009.

[15] Khan H, Amin M, Ahmad A. Characteristics of silicone composites for high voltage insulations. Rev Adv Mater Sci. 2018;56(1):91–123.

[16] Zhang P, Ling Y, Wang J, Shi Y. Bending resistance of PVA fiber reinforced cementitious composites containing nano-SiO2. Nanotechnol Rev. 2019 Jan;8(1):690–8.

[17] Pelto J, Heino V, Karttunen M, Rytoluoto I, Ronkainen H. Tribological performance of high density polyethylene (HDPE) composites with low nanofiller loading. Wear. 2020 Nov 15;460:203451.

[18] Beesetty P, Kale A, Patil B, Doddamani M. Mechanical behavior of additively manufactured nanoclay/HDPE nanocomposites. Compos Struct. 2020 Sep 1;247:112442.

[19] Lopez-Gonzalez M, Flores A, Marra F, Ellis G, Gomez-Fatou M, Salavagione J, et al. Graphene and polyethylene: a strong combination towards multifunctional nanocomposites. Polymers. 2020 Sep;12(9):2094.

[20] Privalko E, Pedosenko A, Privalko V, Walter R, Friedrich K. Composition-dependent properties of Polyethylene Kaolin composites. I. Degree of crystallinity and melting behavior of polyethylene. J Appl Polym Sci. 1999 Aug 15;73(7):1267–71.

[21] Privalko V, Sukhorukov D, Privalko E, Walter R, Friedrich K, Calleja F. Composition-dependent properties of polyethylene Kaolin composites. III. Thermoelastic behavior of injection molded samples. J Appl Polym Sci. 1999 Aug 8;73(6):1041–8.

[22] Privalko V, Korskanov V, Privalko E, Walter R, Friedrich K. Composition-dependent properties of polyethylene/kaolin composites - VI. Thermoelastic behavior in the melt state. J Therm Anal Calorim. 2000;59(1–2):509–16.

[23] Li Y, Sio W, Yang T, Tsai Y. A constitutive model of high-early-strength cement with perlite powder as a thermal-insulating material confined by caron fiber reinforced plastics at elevated temperatures. Polymers. 2020 Oct;12(10):2369.

[24] Celik AG, Kilic AM, Cakal GO. Expanded perlite aggregate characterization for use as a lightweight construction raw material. Phys Chem Probl Miner Process. 2013;49(2):689–700.

[25] Karaca E, Omeroglu S, Akcam O. Investigation of the effects of perlite additive on some comfort and acoustical properties of polyester fabrics. J Appl Polym Sci. 2016 Apr 20;133(16):43128.

[26] Ladeira NE, de Melo Furtado JG, Pacheco EBAV. Thermomorphological analysis of Al2O3/HDPE nanocomposites: one approach in function of the processing and vinyltrimethoxysilane (VTMS) content. Polym Eng Sci. 2019 Jul;59(7):1332–43.

[27] Lapcik L, Jindrova P, Lapcikova B, Tamblyn R, Greenwood R, Rowson N. Effect of the talc filler content on the mechanical properties of polypropylene composites. J Appl Polym Sci. 2008 Dec 5;110(5):2742–7.

[28] da Silva A, Rocha M, Moraes M, Valente C, Coutinho F. Mechanical and rheological properties of composites based on polyolefin and mineral additives. Polym Test. 2002 Feb;21(1):57–60.

[29] Zhang Y, Shi J, Zheng J. A method of fracture toughness JIC measurement based on digital image correlation and acoustic emission technique. Mater Des. 2021;197.

[30] Lapcik L, Vasina M, Lapcikova B, Hui D, Otyepkova E, Greenwood RW, et al. Materials characterization of advanced fillers for composites engineering applications. Nanotechnol Rev. 2019 Jan;8(1):503–12.

[31] Lapčík L, Maňas D, Vašina M, Lapčíková B, Řezníček M, Zádrapa P. High density poly(ethylene)/CaCO3 hollow spheres

composites for technical applications. Compos Part B Eng. 2017 Mar 15;113:218–24.
[32] Ehrenstein GW, Riedel G, Trawiel P. Thermal analysis of plastics: theory and practice. Munich: Carl Hanser Verlag; 2004.
[33] Cuadri AA, Martin-Alfonso JE. The effect of thermal and thermo-oxidative degradation conditions on rheological, chemical and thermal properties of HDPE. Polym Degrad Stab. 2017 Jul;141:11–8.
[34] Schawe JEK. Elastomers Vol 1. Mettler-Toledo collected applications. Schwerzenbach: Mettler-Toledo; 2002.
[35] Lapcik L, Manas D, Lapcikova B, Vasina M, Stanek M, Cepe K, et al. Effect of filler particle shape on plastic-elastic mechanical behavior of high density poly(ethylene)/mica and poly (ethylene)/wollastonite composites. Compos Part B Eng. 2018 May 15;141:92–9.
[36] Rao SS. Mechanical vibrations, 5th edn. Upper Saddle River, USA: Prentice Hall; 2010.
[37] Carrella A, Brennan MJ, Waters TP, Lopes V. Force and displacement transmissibility of a nonlinear isolator with high-static-low-dynamic-stiffness. Int J Mech Sci. 2012 Feb;55(1):22–9.
[38] Ab Latif N, Rus AZM. Vibration transmissibility study of high density solid waste biopolymer foam. J Mech Eng Sci. 2014;6:772–81.
[39] Liu K, Liu J. The damped dynamic vibration absorbers: revisited and new result. J Sound Vibrat. 2005 Jun 21;284(3–5):1181–9.
[40] Hadas Z, Ondrusek C. Nonlinear spring-less electromagnetic vibration energy harvesting system. Eur Phys J Spec Top. 2015 Nov;224(14–15):2881–96.
[41] Sun X, Zhang J. Displacement transmissibility characteristics of harmonically base excited damper isolators with mixed viscous damping. Shock Vibrat. 2013;20(5):921–31.
[42] Tang B, Brennan MJ. A comparison of two nonlinear damping mechanisms in a vibration isolator. J Sound Vibrat. 2013 Feb 4;332(3):510–20.
[43] Lapcik L, Cetkovsky V, Lapcikova B, Vasut S. Materials for noise and vibration attenuation. Chem Listy. 2000;94(2):117–22.
[44] Vasina M, Hughes DC, Horoshenkov KV, Lapcik L. The acoustical properties of consolidated expanded clay granulates. Appl Acoust. 2006 Aug;67(8):787–96.
[45] Tu Z, Shim V, Lim C. Plastic deformation modes in rigid polyurethane foam under static loading. Int J Solids Struct. 2001 Dec;38(50–51):9267–79.
[46] Bernardo V, Laguna-Gutierrez E, Lopez-Gil A, Angel Rodriguez-Perez M. Highly anisotropic crosslinked HDPE foams with a controlled anisotropy ratio: production and characterization of the cellular structure and mechanical properties. Mater Des. 2017 Jan 15;114:83–91.
[47] Ong MY, Chow WS. Kinetics of crystallization for polypropylene/polyethylene/halloysite nanotube nanocomposites. J Thermoplast Compos Mater. 2020 Apr;33(4):451–63.

Research Article

Yousef Murtaja, Lubomír Lapčík*, Harun Sepetcioglu, Jakub Vlček, Barbora Lapčíková, Martin Ovsík, and Michal Staněk

Enhancement of the mechanical properties of HDPE mineral nanocomposites by filler particles modulation of the matrix plastic/elastic behavior

https://doi.org/10.1515/ntrev-2022-0023
received September 20, 2021; accepted November 26, 2021

Abstract: Two different nanosized mineral fillers (nano calcium carbonate and nanoclay) were used in the high density poly(ethylene) (HDPE) composites pilot plant production. Structural and mechanical properties of the prepared composites were examined in this study. The homogenous filler distribution was confirmed in the tested samples by scanning electron microscopy, transmission electron microscopy, and energy dispersive spectroscopy analyses. The fillers' fortifying effect on polymer composites' mechanical performance was confirmed as indicated by the increased elastic modulus and indentation modulus. Additionally, the possible modulation of the plastic-elastic mechanical behavior was confirmed by the type of the filler as well as its concentration used in the final composites testing articles.

Keywords: nanosized mineral fillers, HDPE, composites, mechanical properties

*** Corresponding author: Lubomír Lapčík,** Department of Physical Chemistry, Faculty of Science, Palacky University, 17. Listopadu 12, 771 46 Olomouc, Czech Republic; Department of Food Technology, Faculty of Technology, Tomas Bata University in Zlin, Nam. T.G. Masaryka 275, 760 01 Zlin, Czech Republic,
e-mail: lapcikl@seznam.cz
Yousef Murtaja, Jakub Vlček: Department of Physical Chemistry, Faculty of Science, Palacky University, 17. Listopadu 12, 771 46 Olomouc, Czech Republic
Harun Sepetcioglu: Department of Metallurgy and Materials Engineering, Selçuk University, Faculty of Technology, Konya 42075, Turkey
Barbora Lapčíková: Department of Physical Chemistry, Faculty of Science, Palacky University, 17. Listopadu 12, 771 46 Olomouc, Czech Republic; Department of Food Technology, Faculty of Technology, Tomas Bata University in Zlin, Nam. T.G. Masaryka 275, 760 01 Zlin, Czech Republic
Martin Ovsík, Michal Staněk: Department of Manufacturing Technology, Faculty of Technology, Tomas Bata University in Zlin, Nam. T.G. Masaryka 275, 760 01 Zlin, Czech Republic

1 Introduction

The study of the effect of the nano/microsized mineral fillers blended in the high density poly(ethylene) (HDPE) composite matrix on the mechanical properties of the prepared composites gained excessive attraction in the past 10 years due to their wide application in automotive, aerospace industries [1,2], formulation engineering [3], sound damping materials [4], highly conductive polymeric nanocomposites [5], dielectric material applications [6], etc. Semi-crystalline polymers exhibit, in general, a free-phase continuum system with the crystalline and amorphous phases separated with interphase. The crystalline part is formed with mutually connected spherulites consisting of crystalline lamellae dispersed in the amorphous phase [7]. The type, shape, and size of the mineral filler have a strong impact on the mechanical properties of the thermoplastic-polymer-based composites as well as on their melting behavior and crystallization kinetics [8]. Furthermore, the nature and the quality of the mutual adhesion between the filler and the polymer matrix [9], filler particle size, shape, and particle size distribution have a paramount effect on the final composite application performance [10,11]. This study offers the mechanical testing of the composites prepared from the commercial fillers compounded with HDPE in industrial-scale semi-pilot conditions. The main aim was to confirm the large-scale processability and reproducibility of the manufacturing steps during composites production.

2 Materials

HDPE of HD8100M grade used in our entire experiment was supplied by Polymer Marketing Company Limited (Thailand). The density of the resin was 0.952 g/cm^3 with a melt flow index of 0.25 g/10 min. The nano calcium carbonate ($CaCO_3$) particles, also known as adaCAL-N1-C,

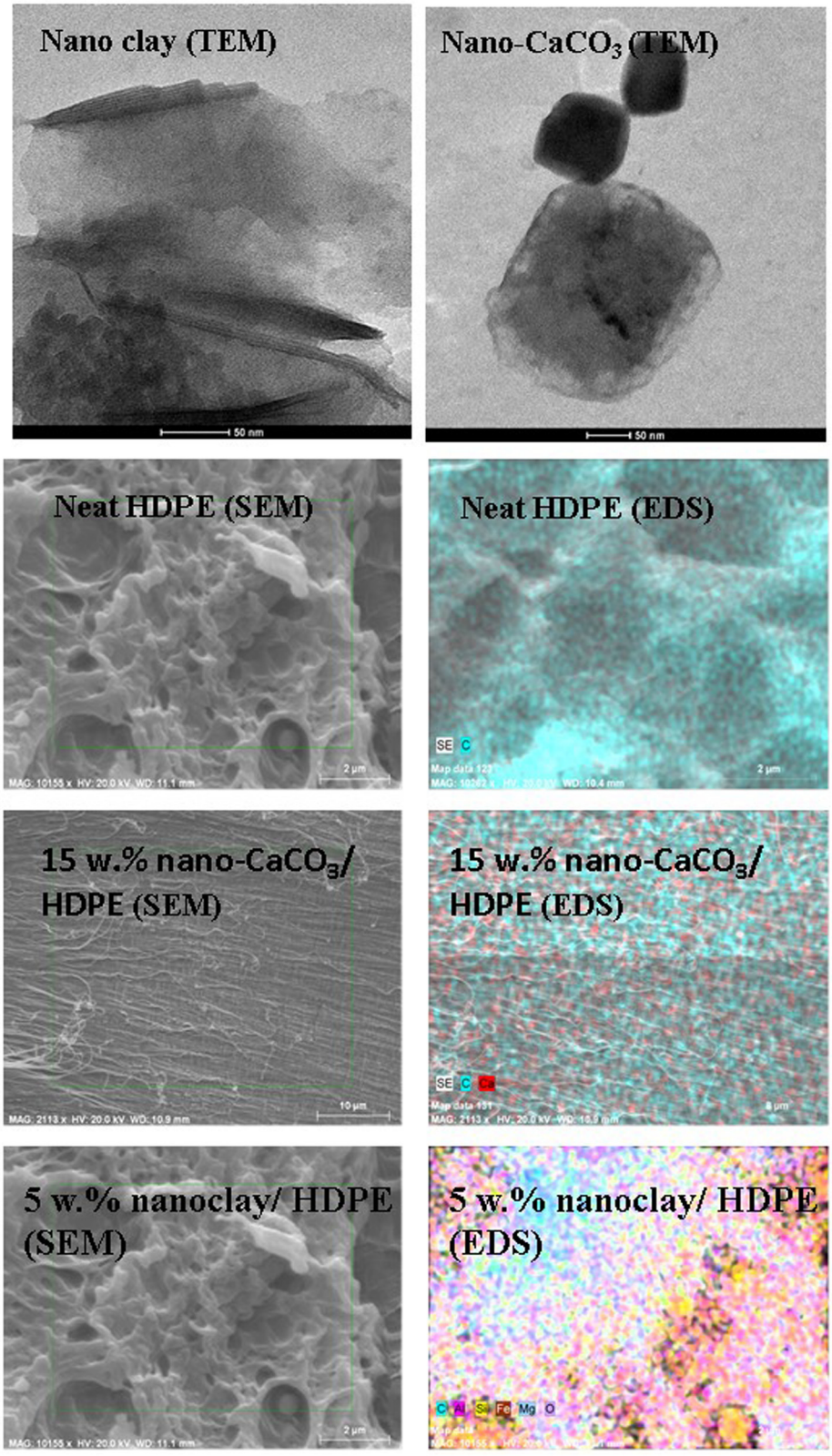

Figure 1: TEM images of the fillers used in this study: Nanoclay and nano $CaCO_3$.

were received from Adacal Co. (Turkey) and were treated with stearic acid prior to further processing. Particles' average size d_{50} was of 0.05 μm as obtained from scanning electron microscopy (SEM) measurements. Nanoclay particles (i.e., EsanNANO 1-140) were supplied by EczacıbasıEsan (Turkey). Particles' average size d_{50} was of 2.7 μm as obtained from laser diffractometer measurements. SEM and transmission electron microscopy (TEM) images of the prepared samples showed that the nanofillers were homogeneously dispersed within the HDPE matrix (Figure 1). This fact was confirmed also by the energy dispersive spectroscopy (EDS) mapping study.

The chemical compositions and physical properties of the used nano calcium carbonate as well as that of the nanoclay are given in Table 1 and are also available in refs [12,13].

Images of both fillers captured by TEM are shown in Figure 1. For testing, the set of samples of different filler concentrations were prepared and labelled as CC for nano calcium carbonate and NC for nanoclay.

Nanoclay/HDPE nanocomposites were prepared by melt mixing system composed of Banbury mixer, single screw extruder, and granule cutting unit allowing semi-pilot production in 100 kg scale. The processing temperature in the mixer was kept at 180°C and the temperature was reached in 15 min after filling the mixer chamber with both the HDPE granules and the filler [14]. The apparatus was then followed by the extruder with a conveyor belt and the cutting unit. Single screw extruder was operating at 330 rpm screw speed with five barrel temperature profiles of 200, 190, 190, 190, and 220°C. Nanoclay/HDPE nanocomposite hot mixtures were cut in water into the shape of granules. Then, they were molded as tensile and impact test specimens using a PS40E5ASE injection molding machine with a melt temperature of 210°C, mold temperature of 65°C, and injection pressure of 50 MPa [14]. Similarly, the nano $CaCO_3$/HDPE nanocomposites were prepared by the melt mixing method as well by use of the same compounder system and the processing parameters as mentioned above in the case of nanoclay/HDPE composites preparation. For both fillers, the weight ratios of the HDPE and the fillers were maintained to obtain the samples of the given filler weight concentration such as 1, 3, 5, 10, and 15 wt% for CC/HDPE composites and 1, 2, 3, 4, and 5 wt% for NC/HDPE composites.

Millipore water (USA) with a conductivity of 0.06 μS/cm, ethylene glycol p.a., (Lach-Ner, Czechia), and 99% pure diiodomethane of ACS reagent grade (Sigma Aldrich, Germany) were used as wetting liquids for contact angle measurements.

3 Methods

3.1 SEM and TEM

TEM (FEI Tecnai G2 Spirit Biotwin model, FEI Company, USA) was used to characterize the shape and morphology of the filler particles. TEM images were taken by placing nanofiller samples on a standard 400 grid copper mesh. Dispersions of acetone fillers were ultrasonicated for 15 min and were casted on the copper mesh and air dried. TEM measurements were performed at 120 kV accelerating voltage. Nano $CaCO_3$ and nanoclay's distributions in HDPE matrix were analyzed by TEM. An ultra-thin section of about 100 nm thickness were cut from filled samples using a microtome device (CM1950) supplied by Leica Microsystems Inc. (Buffalo Grove, USA) in a low-temperature environment. For further examination of the distribution of nanofillers, the composites were characterized by SEM using a Zeiss EvoLS10 equipped with an energy-dispersive X-ray detector (Germany).

3.2 Thermal analysis

Differential scanning calorimetry (DSC) experiments were performed according to ASTM E1356 by using a TA Instrument S10 model (Waters, USA) at a nitrogen flow rate of 50 mL/min. Virgin HDPE and its nanocomposites' glass transition temperatures (T_g) were determined from DSC curves by means of the midpoint method at 10°C/min heating rate from 30 to 300°C [13,15].

3.3 Uniaxial tensile testing

Universal Testing Machine Autograph AGS-100 Shimadzu (Japan) and Zwick 1456 multipurpose tester (Germany) equipped with Compact Thermostatic Chamber TCE Series were used for tensile testing of injection-molded specimens.

Table 1: Physicochemical properties of applied fillers: nanoclay and nano $CaCO_3$

Filler type	Color	Density (g/cm^3)	Surface area (g/m^2)	Particle size (μm)
Nanoclay	Ultra white	1.98	19	2–20
Nano $CaCO_3$	Ultra white	2.95	28	0.05–0.10

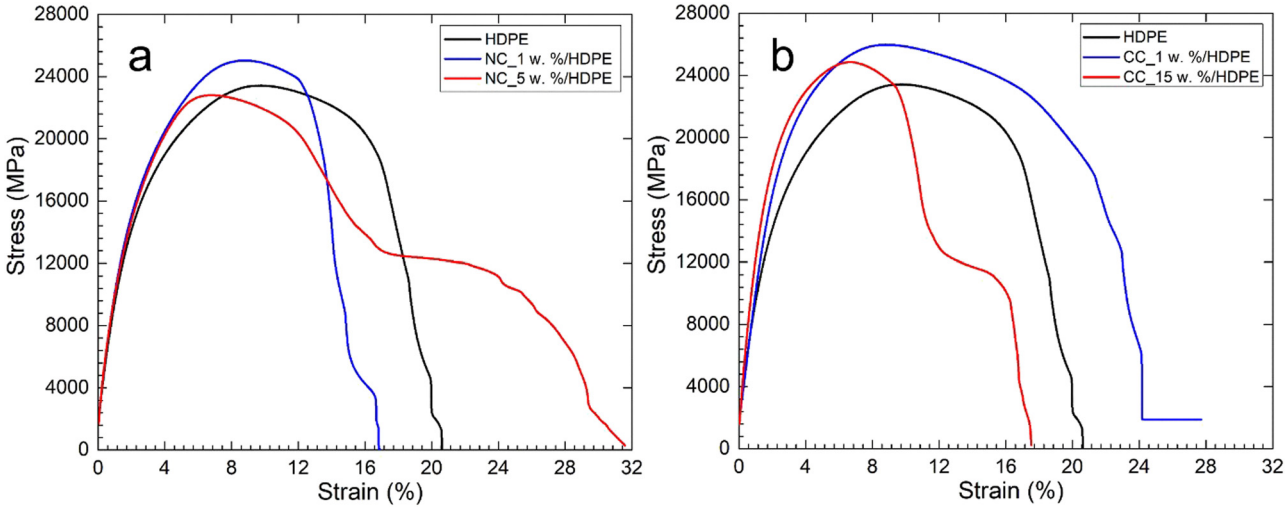

Figure 2: (a) General mechanical behavior of NC/HDPE and (b) CC/HDPE composites with different filler concentrations from tensile testing experiments as obtained for 50 mm/min deformation rates at ambient temperature expressed as stress vs strain dependencies.

All data ptwere recorded as per CSN EN ISO 527-1 and CSN EN ISO 527-2 standards taking the tested gauge length of 8 cm. All experiments were performed at room temperature up to break with 50, 100, and 200 mm/min deformation rates. Strength at break, Young's modulus, and strain at break were obtained from the stress-strain dependence plot(s). Each experiment was repeated 10×, and the mean values and standard deviations were calculated. All experiments were performed at the laboratory ambient conditions of 25°C temperature.

3.4 Charpy impact testing

Impact tests were carried out using Zwick 513 Pendulum Impact Tester (Germany) according to the CSN EN ISO 179-2 standard, allowing 25 J energy drop. Each experiment was repeated 10×, and the mean values and standard deviations were calculated. All experiments were performed at the laboratory ambient conditions of 25°C temperature.

3.5 Surface free energy (SFE) characterization

The SFE of the studied composites and pure HDPE was determined by the static contact angle of wetting measurements based on axisymmetric drop shape analysis. All measurements were performed at 23°C and repeated

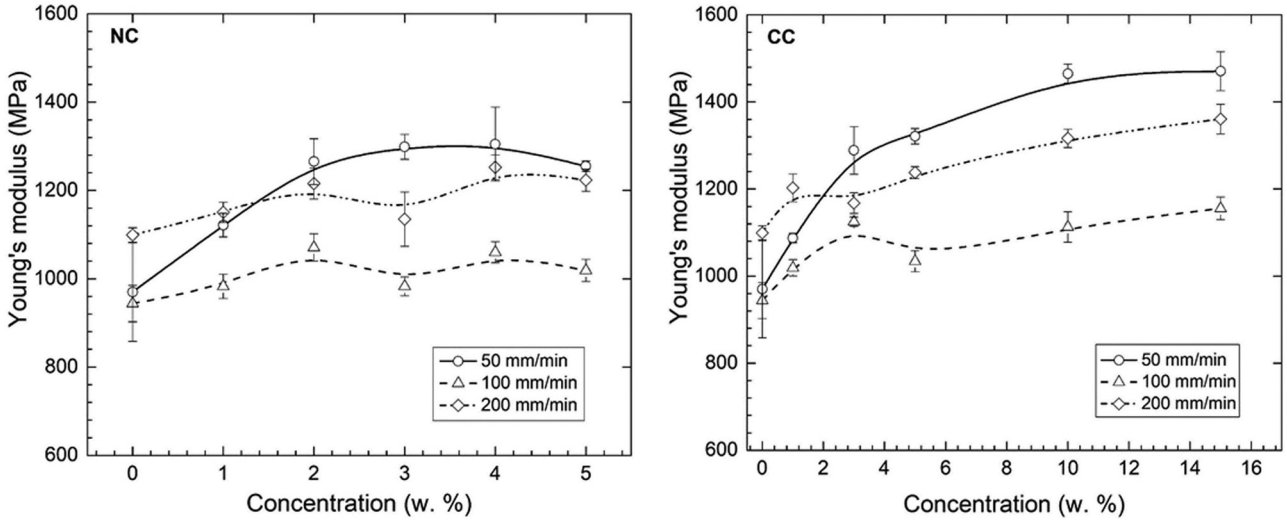

Figure 3: Young's modulus and filler concentration dependencies of the CC/HDPE and NC/HDPE composites obtained with tensile testing experiments for different deformation rates.

Table 2: Results of the tensile testing experiments of the studied HDPE composites at 50, 100, and 200 mm/min deformation rates. Filler concentrations indicated in the sample description are given in wt%

Sample	Young's modulus (MPa)			Upper yield (MPa)			Strain at break (%)			Fracture toughness (kJ/m^2)
	Rate (mm/min)			Rate (mm/min)			Rate (mm/min)			
	50	100	200	50	100	200	50	100	200	
HDPE	970.1 ± 111.7	943.8 ± 142.2	1,099.2 ± 16.2	24.5 ± 1.1	24.8 ± 1.1	25.6 ± 0.4	20.5 ± 0.1	25.8 ± 5.0	16.6 ± 0.6	36.69 ± 5.15
CC_1%	837.5 ± 10.8	648.2 ± 419	1,202.7 ± 32.1	25.4 ± 0.6	24.3 ± 1.1	25.1 ± 0.5	30.8 ± 3.1	33.2 ± 6.7	19.8 ± 0.3	31.48 ± 2.43
CC_3%	1,288.9 ± 54.7	1,368 ± 2.5	1,167.7 ± 23.7	24.4 ± 0.4	25.0 ± 0.2	24.7 ± 0.8	22.0 ± 0.8	19.8 ± 1.0	22.9 ± 1.5	17.26 ± 0.92
CC_5%	1,322 ± 10.8	1,,034.3 ± 299	1,237.9 ± 13.7	23.6 ± 0.5	25.4 ± 3.4	25.0 ± 1.1	25.0 ± 3.0	28.5 ± 14.7	17.2 ± 3.1	26.29 ± 1.04
CC_10%	1,465.1 ± 12.3	1,112.8 ± 273	1,316.4 ± 0.4	24.3 ± 1.3	25.2 ± 1.0	26.3 ± 0.7	18.6 ± 2.3	20.5 ± 7.4	14.1 ± 0.4	28.69 ± 3.4
CC_15%	1,470 ± 54.7	1155 ± 255	1,360.7 ± 1.7	24.6 ± 0.2	25.3 ± 1.1	28.1 ± 2.8	20.1 ± 2.6	19.7 ± 6.9	11.2 ± 2.2	31.79 ± 3.94
NC_1%	1,121.4 ± 26.8	982.9 ± 217	1,150.5 ± 23.0	23.6 ± 1.5	26.5 ± 0.5	27.4 ± 2.4	32.8 ± 15.9	19.3 ± 4.6	16.4 ± 6.0	29.21 ± 2.21
NC_2%	1,265.4 ± 51.9	1,070.9 ± 303	1,215.6 ± 48.8	25.8 ± 3.2	27.4 ± 2.2	30.0 ± 2.8	21.2 ± 8.7	20.5 ± 10.5	12.1 ± 0.6	24.37 ± 1.0
NC_3%	1,248.7 ± 28.1	982.7 ± 213	1,134.9 ± 61.2	27.3 ± 1.9	23.9 ± 1.6	22.4 ± 0.4	19.8 ± 3.2	31.1 ± 11.2	26.6 ± 2.2	28.44 ± 0.09
NC_4%	1,304.9 ± 83.7	1,060.1 ± 240	1,328.3 ± 78.0	23.3 ± 0.1	23.9 ± 0.3	27.9 ± 2.5	27.6 ± 2.2	35.7 ± 7.2	14.4 ± 5.9	23.35 ± 0.27
NC_5%	1,255 ± 11.9	1,018.8 ± 246	1,223.3 ± 25.0	23 ± 0.2	23.5 ± 0.2	24.7 ± 0.2	28.9 ± 2.7	32.88 ± 10	20.5 ± 2.1	22.06 ± 1.42

7× with a Krüss DSA 30 (Krüss, Germany). The Owens, Wendt, Rabel, and Kaelble extended Fowkes theory was used to calculate the SFE of the tested composites and pure HDPE from the average static contact angles for water, ethylene glycol, and diiodomethane [16,17].

3.6 Micro hardness

Micro-indentation tests were performed on a micro-indentation tester (Micro Combi Tester, Anton Paar, Austria), according to the CSN EN ISO 14577 standard. The applied diamond tip was of the cube corner shape (Vickers, Anton Paar, Austria). Measurement parameters were set as follows: maximum load of 3 N, loading rate (unloading rate) of 6 N/min, and holding time of 90 s. All experiments were performed according to the depth-sensing indentation method, allowing simultaneous measurement of the acting force on the indentor and the displacement of the indentor's tip. The indentation hardness (H_{IT}) was calculated as the maximum load (F_{max}) on the projected area of the hardness impression (A_p). Indentation modulus (E_{IT}) was calculated from the plane strain modulus of elasticity (E^*) using an estimated Poisson's ratio (ν) of the samples (0.3–0.4 [18,19]):

$$H_{IT} = \frac{F_{max}}{A_p}, \tag{1}$$

$$E_{IT} = E^*(1 - \nu^2). \tag{2}$$

Each measurement was repeated 10×, and mean values and standard deviations were calculated. All experiments were performed at the laboratory ambient conditions of 25°C temperature.

4 Results and discussion

Results of the tensile testing experiments of the studied composites are shown in Figure 2. Obtained stress vs strain deformation dependencies exhibited typical patterns corresponding to the elastic region (does not exceed 3% strain for small deformations), elastic-plastic transition region (does not exceed 10% strain for small deformations), and the stress plateau draw region occurred for 5 wt% nanoclay/HDPE composites and 15 wt% for CC/HDPE composites at strains exceeding 18% (NC/HDPE composites) and 12% (CC/HDPE composites), respectively [20]. Similar dependencies were found in our previous studies for industrial HDPE mineral composites at the same deformation rate [13,15]. Pure HDPE

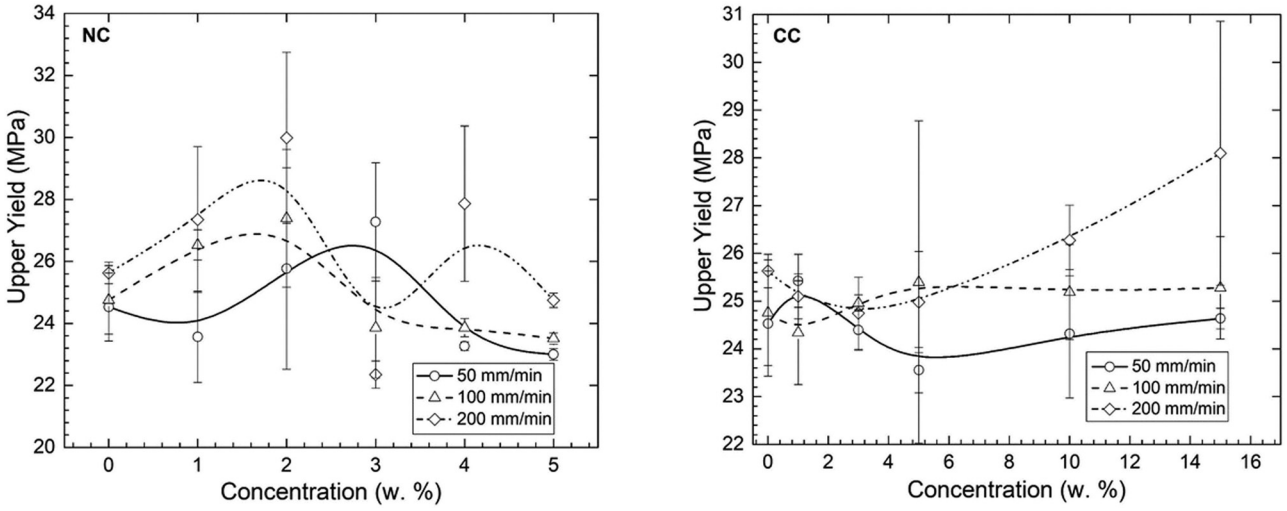

Figure 4: Upper yield and filler concentration dependencies of the CC/HDPE and NC/HDPE composites obtained with tensile testing experiments for different deformation rates.

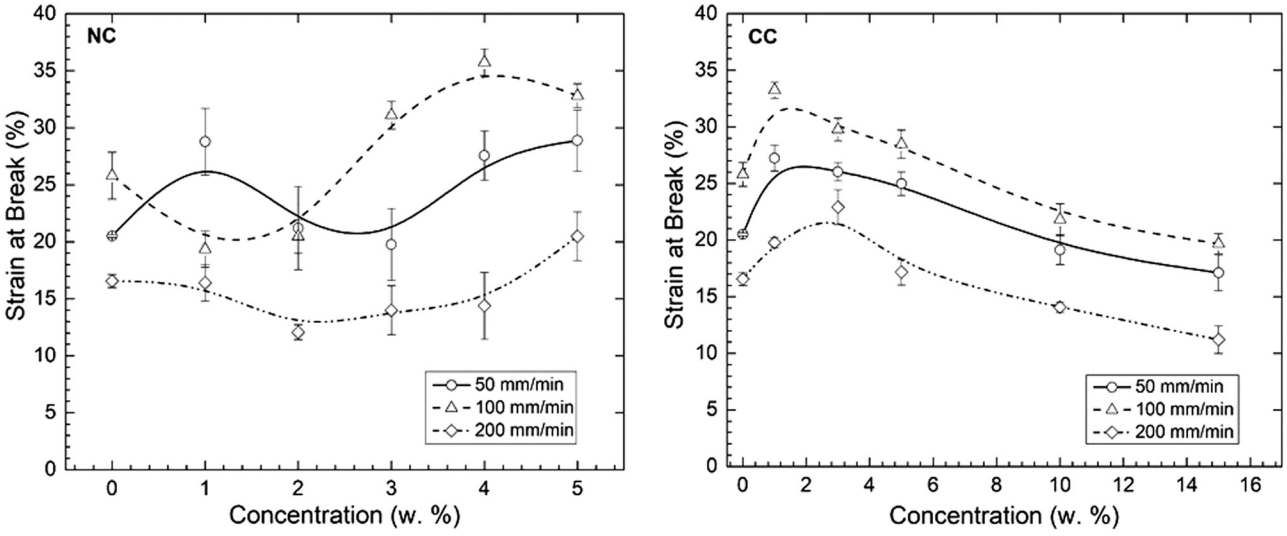

Figure 5: Strain at break and filler concentration dependencies of the CC/HDPE and NC/HDPE composites obtained with tensile testing experiments for different deformation rates.

exhibited more stiff tensile deformation behavior in the absence of the stress plateau draw region. In contrary to that CC/HDPE composites, were characteristic of more elasto-plastic behavior as reflected for 1 wt% filler concentration (Figure 1b). In the case of NC/HDPE composites, there is a significant influence of elastic-plastic properties. With increasing filler concentration, greater plastic behavior was observed, as reflected by the increased stress plateau draw region, as shown in Figure 2b. The abovementioned behavior was also accompanied by the corresponding increase in the Young's modulus of elasticity with increasing filler concentration for both mineral fillers, as shown in Figure 3. Such behavior was confirmed for all applied deformation rates, as given in Table 2. For example, the absolute value of the modulus of elasticity of 970.1 ± 111.7 MPa for original HDPE was increased to 1470.0 ± 54.7 MPa by about 51.5% in the case of CC/HDPE composites with 5 wt% filler concentration. For the NC/HDPE composites, the modulus E was increased by about 34.5% to the absolute value of 1304.9 ± 83.7 MPa with 4 wt% filler concentration. These corresponded very well with previously published data that stiff mineral filler particles were responsible for the observed

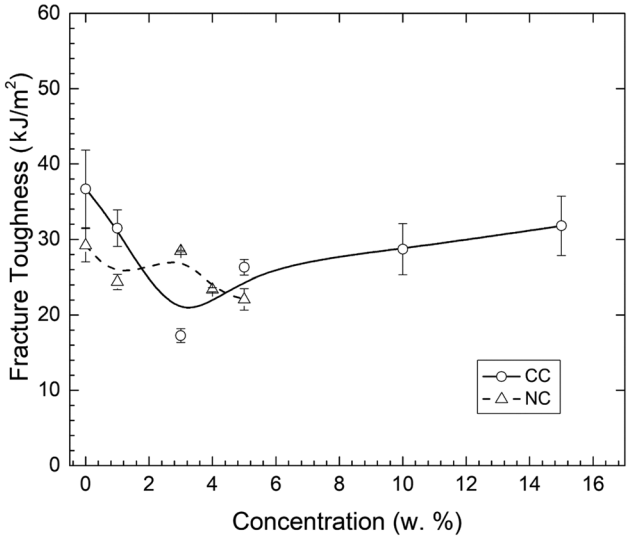

Figure 6: Fracture toughness and filler concentration dependencies of the CC/HDPE and NC/HDPE composites as obtained with Charpy impact testing.

Table 3: Total SFEs and their components (polar and dispersive) of the studied HDPE composites calculated by Owens, Wendt, Rabel, and Kaelble approach from contact angle measurements performed by means of the axisymmetric drop shape analysis (measured at 23°C temperature)

Sample	SFE (mJ/m²)		
	Total	Polar	Dispersive
HDPE	19.48 ± 2.91	15.29 ± 2.10	4.19 ± 0.81
CC_1%	36.51 ± 33.80	15.61 ± 14.82	15.61 ± 14.82
CC_3%	36.49 ± 14.86	11.84 ± 7.77	24.65 ± 7.08
CC_5%	39.70 ± 1.09	0.19 ± 0.46	39.51 ± 0.63
CC_10%	23.45 ± 4.41	0.01 ± 0.07	23.44 ± 4.34
CC_15%	26.19 ± 0.05	0.41 ± 0.01	25.78 ± 0.03
NC_1%	30.44 ± 1.04	0.12 ± 0.04	30.32 ± 1.00
NC_2%	30.28 ± 0.92	1.19 ± 0.15	29.09 ± 0.76
NC_3%	32.95 ± 2.58	00.08 ± 0.16	32.86 ± 2.42
NC_4%	29.22 ± 0.66	0.22 ± 0.13	29.00 ± 0.53
NC_5%	23.45 ± 4.41	0.01 ± 0.07	23.44 ± 4.34

steady increase in the modulus of elasticity of polymer-based composites with increasing filler content [21,22].

Upper yield vs filler concentration dependencies of the HDPE composites are shown in Figure 4. They are typical non-linear patterns for both fillers under study (nanoclay and nano calcium carbonate). However, in the case of CC/HDPE composites, the significant changes in the upper yield with increasing filler concentration were not observed with the exception of the composites with 4 and 5 wt% filler concentration for the 200 mm/min deformation rate, where the original values of 25.6 ± 0.4

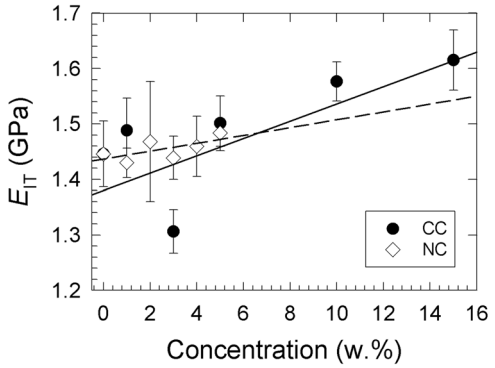

Figure 7: Indentation modulus (EIT) vs filler concentration dependencies. Filler type: full circle – Nano $CaCO_3$ and empty diamond – Nanoclay. *Point omitted for linear regression.

MPa were increasing up to 26.3 ± 0.7 MPa and up to 28.1 ± 2.8 MPa, respectively.

The results of the filler concentration strain at break dependencies measured at different deformation rates are shown in Figure 5. In the case of CC/HDPE composites, observed trend was such that the strain at break was decreased with increasing filler concentration, thus reflecting the loss of plastic behavior, indicating more brittle-like mechanical behavior. This fact fits very well with the well-known theory that polymers with higher crystallinity exhibit higher elastic properties than amorphous systems, which exhibit more plastic behavior [22]. However, the opposite trend was observed for the NC/HDPE composites, where the increased strain at break with increasing filler concentration was found. This was most probably due to the preferential orientation of the individual platelet shape like nanoclay filler particles in the polymer macromolecular chains interphase induced during sample injection molding processing [20]. The comparison of the obtained magnitudes of the elongation at break parameter for 5 wt% nanocomposite filler concentrations (both the nano-clay as well as of the nano-calcium carbonate) confirmed higher plasticity of the composite matrix composed from the nanoclay flat like filler particles for all applied deformation rates. This finding was also in agreement with the mutual comparison of the observed magnitudes of the Young's modulus of elasticity, where the CC/HDPE samples exhibited higher modulus of elasticity than the NC/HDPE samples.

Observed fracture toughness vs filler concentration dependencies of the tested composites are shown in Figure 6. A decrease in the fracture toughness was found for all the composites studied in comparison with the virgin polymer (HDPE). The most significant decrease of about 52.96% was found for the composites containing nano $CaCO_3$ of 3 wt% filler concentration. For NC/HDPE composites, the observed fracture toughness was decreased

to 22.06 ± 1.42 kJ/m^2 magnitude, which was about 39.87% decrease compared to the virgin HDPE. These results clearly demonstrate the higher brittle character of the composites in comparison to the virgin HDPE.

It was found by DSC thermal analysis that the HDPE filled with nano $CaCO_3$ exhibited higher thermal stability in comparison with the virgin HDPE as reflected by increasing T_g from 103.9°C (virgin HDPE) to 126.6°C for 15 wt% CC/HDPE composites. These results were in excellent agreement with the published data of Viljoen and Labuschagné [23]. Similarly, the T_g increased with increasing nano-clay content in the nano-clay/HDPE composites to 128.2°C, thus confirming that the fillers enhanced interaction with the base HDPE matrix.

Results of the SFE calculations are given in Table 3. Obtained results indicated that both fillers ($CaCO_3$ as well as nanoclay) contributed to the observed decrease in the originally more polar character of the virgin HDPE to less polar one as indicated by the observed increase in the dispersive part of SFE from 4.19 ± 0.81 mJ/m^2 (virgin HDPE) to 39.51 ± 0.63 mJ/m^2 (5 wt% CC/HDPE composites) and to 32.86 ± 2.42 mJ/m^2 (3 wt% NC/HDPE composites). The magnitude of the total SFE was increased from 19.48 ± 2.91 mJ/m^2 (virgin HDPE) by about 103.8% up to 39.70 ± 1.09 mJ/m^2 (5 wt% CC/HDPE composites) and by about 69.18% up to 32.95 ± 2.58 mJ/m^2 (3 wt% NC/HDPE composite). Observed results indicate further improvement in the composites interface's adhesive properties, for example, suitable for coating or adhesive joints technical applications.

The composites micro-indentation testing results are shown in Figure 7 where indentation modulus E_{IT} vs filler concentration patterns are shown. These were characteristic with the gradual increase in the indentation modulus with increasing concentrations of both fillers, confirming the fortification effect of the fillers on the mechanical properties of the tested samples.

5 Conclusion

Two different nano-sized mineral fillers (nano $CaCO_3$ and nanoclay) were used in the HDPE composites pilot plant production. The structural as well as mechanical properties of the prepared composites were studied. The fortifying effect of the fillers on the polymer composite's mechanical performance was confirmed as indicated by the increased elastic modulus and the indentation modulus. For example, the absolute value of the modulus of elasticity 970.1 ± 111.7 MPa for original HDPE was increased by about 51.5% to 1470.0 ± 54.7 MPa in the case of nano CC/HDPE composites with 5 wt% filler concentration. For the NC/HDPE composites, the modulus of elasticity was increased by about 34.5% to the absolute value of 1304.9 ± 83.7 MPa with 4 wt% of filler concentration. Additionally, there was confirmed possible modulation of the plastic-elastic mechanical behavior by the type of the filler as well as its concentration used in the final composites testing articles, as confirmed by the increased stress plateau draw region that occurred during the tensile testing and decreased elongation at break with increasing filler concentration. From the practical point of view, the 5 wt% filler concentration seems to be the most favorable one for both CC/HDPE as well as nano-clay/HDPE composites. Simultaneously, the higher thermal stability was found for both nanocomposites in comparison to the virgin HDPE, thus confirming that the fillers enhanced interaction with the HDPE matrix. Based on the abovementioned conclusions, it seems to be advantageous for the application of the latter nanocomposites as the structural elements in the complex product designs offering combined elasto-plastic mechanical behavior in the relatively wide deformation rates regimes accompanied with the higher thermal stability.

Funding information: Financial support from the internal grants of Palacky University in Olomouc (project number IGA_PrF_2021_031) and of Tomas Bata University in Zlin (project numbers IGA/FT/2021/004 and IGA/FT/2021/005) are gratefully acknowledged. Financial support to the author YM by Fischer scholarship of the Faculty of Science, Palacky University in Olomouc in 2021 year is gratefully acknowledged as well.

Author contributions: All authors have accepted responsibility for the entire content of this manuscript and approved its submission.

Conflict of interest: The authors state no conflict of interest.

References

[1] Lapčík L, Ruszala MJA, Vašina M, Lapčíková B, Vlček J, Rowson NA, et al. Hollow spheres as nanocomposite fillers for aerospace and automotive composite materials applications. Compos B Eng. 2016;106:74–80.

[2] Lapcik L, Vasina M, Lapcikova B, Hui D, Otyepkova E, Greenwood RW, et al. Material characterization of advanced fillers for composites engineering applications. Nanotechnol Rev. 2019;8:503–12.

[3] Lapcik L, Vasina M, Lapcikova B, Otyepkova E, Waters KE. Investigation of advanced mica powder nanocomposite filler materials: surface energy analysis, powder rheology and sound absorption performance. Compos B Eng. 2015;77:304–10.
[4] Lapcik L, Vasina M, Lapcikova B, Stanek M, Ovsik M, Murtaja Y. Study of the material engineering properties of high-density poly(ethylene)/perlite nanocomposite materials. Nanotechnol Rev. 2020;9:1491–9.
[5] Huang X, Zeng L, Li R, Xi Z, Li Y. Manipulating conductive network formation via 3D T-ZnO: a facile approach for a CNT-reinforced nanocomposite. Nanotechnol Rev. 2020;9:534–42.
[6] Ali SFA, Elsad RA, Mansour SA. Enhancing the dielectric properties of compatibilized high-density polyethylene/calcium carbonate nanocomposites using high-density polyethylene-g-maleic anhydride. Polym Bull. 2021;78:1393–405.
[7] Drozdov AD, Christiansen Jd. Thermo-viscoelastic and viscoplastic behavior of high-density polyethylene. Int J Solids Struct. 2008;45:4274–88.
[8] Abareshi M, Zebarjad SM, Goharshadi EK. Effect of milling time and clay content on the thermal stability of polyethylene-clay nanocomposite. J Vinyl Addit Technol. 2016;22:285–92.
[9] Said M, Seif S, Challita G. Development of blown film linear low-density polyethylene-clay nanocomposites: Part A: manufacturing process and morphology. J Appl Polym Sci. 2020;137:48589.
[10] Escocio VA, Visconte LLY, da Silva Nazareth AL, de Sousa AMF, Pacheco EB. Permeability, melt flow index, mechanical, and morphological properties of green HDPE composites: effect of mineral fillers. Macromolecular symposia. Vol. 381. Weinheim: Wiley-VCH GmbH; 2018. UNSP 1800127.
[11] Chan JX, Wong JF, Hassan A, Mohamad Z, Othman N. Mechanical properties of wollastonite reinforced thermoplastic composites: a review. Polym Compos. 2020;41:395–429.
[12] Sepet H, Aydemir B, Tarakcioglu N. Evaluation of mechanical and thermal properties and creep behavior of micro-and nano-CaCO(3) particle-filled HDPE nano- and microcomposites produced in large scale. Polym Bull. 2020;77:3677–95.
[13] Se pet H, Tarakcioglu N, Misra RDK. Investigation of mechanical, thermal and surface properties of nanoclay/HDPE nanocomposites produced industrially by melt mixing approach. J Composite Mater. 2016;50:3105–16.
[14] Sepetcioglu H. The effect of nanoclay on the nonlinear viscoelastic behavior of high-density polyethylene. Polym Compos. 2021;42:3481.
[15] Sepet H, Tarakcioglu N, Misra RDK. Determination of the mechanical, thermal and physical properties of nano-$CaCO_3$ filled high-density polyethylene nanocomposites produced in an industrial scale. J Composite Mater. 2016;50:3445–56.
[16] Kwok D. The usefulness of the Lifshitz-van der Waals/acid-base approach for surface tension components and interfacial tensions. Colloid Surf A-Physicochem Eng Asp. 1999;156:191–200.
[17] Gajdosikova R, Lapcikova B, Lapcik L. Surface phenomena and wetting of porous solids. Phys Chem: Indian J. 2011;6:146–62.
[18] Oliver W, Pharr G. Measurement of hardness and elastic modulus by instrumented indentation: advances in understanding and refinements to methodology. J Mater Res. 2004;19:3–20.
[19] Manas D, Mizera A, Manas M, Ovsik M, Hylova L, Sehnalek S, et al. Mechanical properties changes of irradiated thermoplastic elastomer. Polymers. 2018;10:87.
[20] Lapcik L, Manas D, Lapcikova B, Vasina M, Stanek M, Cepe K, et al. Effect of filler particle shape on plastic-elastic mechanical behavior of high density poly(ethylene)/mica and poly (ethylene)/wollastonite composites. Compos Pt B-Eng. 2018;141:92–9.
[21] Lapčík L, Maňas D, Vašina M, Lapčíková B, Řezníček M, Zádrapa P. High density poly(ethylene)/$CaCO_3$ hollow spheres composites for technical applications. Compos Pt B-Eng. 2017;113:218–24.
[22] Bucknall CB. Toughened plastics. Dordrecht: Springer Science + Business Media, B.V.; 1977.
[23] Viljoen WD, Labuschagne FJWJ. The thermal stability of highly filled high-density polyethylene quaternary composites: interactive effects and improved measures. Polym Test. 2020;85:106424.

Research Article

Lubomír Lapčík*, Harun Sepetcioğlu, Yousef Murtaja, Barbora Lapčíková, Martin Vašina, Martin Ovsík, Michal Staněk, and Shweta Gautam

Study of mechanical properties of epoxy/graphene and epoxy/halloysite nanocomposites

https://doi.org/10.1515/ntrev-2022-0520
received October 3, 2022; accepted February 3, 2023

Abstract: This article aimed to compare various mechanical properties of epoxy/graphene and epoxy/halloysite nanocomposites. Graphene nanoplatelets (GnPs) and halloysite nanotubes (HNTs) were used as fillers at different concentrations. The studied fillers were dispersed in the epoxy resin matrices. Elastic–plastic mechanical behavior modulation was observed utilizing the fillers' nanoparticles and carboxyl-terminated butadiene–acrylonitrile copolymer rubber-modified epoxy resin. The hypothesis of the possible preceding inter-particle gliding of the individual GnPs in the complex resin nanocomposite matrix during mechanical testings was also confirmed. Increased ductility (elongation at break increased from 0.33 mm [neat matrix] to 0.46 mm [1 wt% GnPs] [39% increase]) and plasticity of the GnP nanocomposite samples were observed. In contrast, the decreasing mechanical stiffness as reflected in the decreased Young's modulus of elasticity (from 3.4 to 2.7 GPa [20% decrease]) was found for the epoxy/HNT nanocomposites. The obtained dynamic stiffness of the investigated nanocomposites confirmed the complexity of the mechanical response of the studied material systems as a combination of the ductile and brittle phenomena.

Keywords: graphene, halloysite, nanocomposites, epoxy polymer, CTBN rubber, mechanical testing

1 Introduction

Polymeric and resin-based nanocomposites are widely used in material engineering research owing to their capacity to modulate plastic–elastic mechanical performance at static and dynamic mechanical loadings [1]. These nanocomposites are characterized by high mechanical toughness and wear resistance, improved self-lubrication properties, and low friction coefficient [2,3]. Therefore, they have a wide range of application potential in the aerospace [4], automotive [5], chemical, and electronic industries as well as high-voltage outdoor insulation materials [6–8].

The ability of a material to absorb mechanical impact, *i.e.*, its toughness, requires high force resistance and the existence of the deformation mechanisms that absorb and dissipate the applied mechanical energy over a large path, in a large volume, and for a sufficiently long time. Such mechanisms may be inherent in the material due to its specific microstructure but can also be deliberately incorporated into the structure of polymer/epoxy resin composites and blends [9,10]. Such synergistic effect can be obtained by proper selection of the combination of the nanofiller particles' type (graphene nanoplatelets [GnPs], halloysite nanotubes [HNTs], *etc.*), shape, and surface chemistry, by modulating the physicochemical characteristics of the matrix, *etc.*, for example, by adding rubbery plastic components [11,12]. However, literature indicates that relatively few studies have focused on carboxyl-terminated butadiene–acrylonitrile (CTBN) copolymer rubber-modified epoxy

* **Corresponding author: Lubomír Lapčík,** Department of Physical Chemistry, Faculty of Science, Palacky University, 17. Listopadu 12, 771 46 Olomouc, Czech Republic; Faculty of Technology, Tomas Bata University in Zlin, Nam. T.G. Masaryka 275, 760 01 Zlin, Czech Republic, e-mail: lapcikl@seznam.cz
Harun Sepetcioğlu: Department of Metallurgy and Mechanical Engineering, Technology Faculty, Selçuk University, Konya 42075, Turkey
Yousef Murtaja: Department of Physical Chemistry, Faculty of Science, Palacky University, 17. Listopadu 12, 771 46 Olomouc, Czech Republic
Barbora Lapčíková: Department of Physical Chemistry, Faculty of Science, Palacky University, 17. Listopadu 12, 771 46 Olomouc, Czech Republic; Faculty of Technology, Tomas Bata University in Zlin, Nam. T.G. Masaryka 275, 760 01 Zlin, Czech Republic
Martin Vašina: Faculty of Technology, Tomas Bata University in Zlin, Nam. T.G. Masaryka 275, 760 01 Zlin, Czech Republic; Department of Hydromechanics and Hydraulic Equipment, Faculty of Mechanical Engineering, VŠB-Technical University of Ostrava, 17. Listopadu 15/2172, 708 33 Ostrava-Poruba, Czech Republic
Martin Ovsík, Michal Staněk, Shweta Gautam: Faculty of Technology, Tomas Bata University in Zlin, Nam. T.G. Masaryka 275, 760 01 Zlin, Czech Republic

resins filled with GnPs exhibiting the improved fracture toughness [13–16].

Several polymer composites have been reported in recent years, including polyester, polyurethane, epoxy, and phenolics [17,18]. Among these, epoxy polymer composites have gained tremendous attention due to their high mechanical toughness and moisture absorption properties [19]. Additionally, these resins show less shrinkage and less toxic emissions during the curing process [20]. Therefore, epoxy resins are considered high-quality materials on an industrial scale, despite their high cost [21].

In general, the plastic or viscoelastic deformation of materials in front of the crack apex removes part of the crack energy and thus controls its progress within the matrix. Therefore, the difference between brittle and ductile fractures is in their spatial localization and their temporal progression. Most polymer composite materials can break down by either brittle or ductile fractures depending on the external conditions or processes taking place in the material. The transition between ductile and brittle fractures can be temperature dependent, with the temperature regions of the two distinct mechanisms separated by the embrittlement temperature. The latter always lies below the glass-transition temperature. In the same sense, with a drop in temperature, an increase in loading rate can have an effect – although the difference in loading rate must be an order of magnitude greater to have an effect on the nature of the fracture. However, long-term static loading below the yield stress for many polymers also leads to brittle fracture. In this case, the "material self-defence" mechanisms cannot develop sufficiently by creating a plastic zone in front of the crack tip [9].

Tribological properties of resins often indirectly influence their mechanical strength, whereas epoxy resins exhibit limited tribological properties [22]. For example, the service life of pipes made of polymeric composites depends on the effectivity of the energy dissipation during fluid flow, the character of which is dependent on the wall friction of the transported medium. Such pipes are exposed under service conditions to long-term stresses, usually under relatively low temperatures, but sometimes also at the interaction of an active environment. Under these conditions, they cannot properly develop the "self-defense" mechanisms of crack blunting by local plastic deformation, and from the exposed surface small cracks propagate inside the material or even sharp cracks, which eventually lead to brittle fracture [9].

Several methods have been reported to improve these properties, *i.e.*, adding micro- and nano-sized particles as fillers in the resin matrix [23,24]. A large variety of nanofillers, such as SiO_2, MnO_2, TiO_2, Al_2O_3, SiC, Si_3N_4, ZnO, MoS_2, nanoclay, and carbon nanotubes, have been reported in different types of polymeric resins [25–28]. These fillers have demonstrated varying efficiencies with certain limitations, which hinder their practical applications [29].

GnPs, consisting of 30–40 layers of graphene, are widely used nanomaterials due to their high thermal stability and conductivity, high Young's modulus of elasticity, high optical transmittance, high fracture strength, and improved lubrication properties [17,30]. Due to their inherent, intrinsic energy-dissipating mechanisms (sheet bending and sliding), GnPs belong to highly advanced materials used in composite manufacturing [17,31]. However, it is necessary to optimize the content of graphene nanofillers in epoxy resins because higher content leads to nonuniform distribution of graphene in the polymer network [32]. Another challenge is the observed high aggregation rates of graphene arising from the acting Van der Waals interaction forces [33–35]. For this reason, it is necessary to optimize a proper mass ratio of graphene nanofillers to epoxy resin in order to obtain the desired mechanical properties.

Halloysite, an aluminosilicate clay material [36], is another filler commonly used in polymer resins owing to its cylindrical structure, improved mechanical performance, and low cost [37,38]. HNTs exhibit higher dispersion ratio and have surface hydroxyl groups with low density, which results in their smooth diffusion into the polymer matrix, leading to less aggregation [39]. Moreover, due to small basal spacing of crystal planes, the intercalation of HNTs with polymers and additives is difficult [40,41]. However, HNT nanofillers belong to potential functional fillers used in industrial practice [42,43].

Published results confirmed synergistic combination of the plastification effect of the rigid epoxy matrix assigned to the gliding of the individual GnP nanofillers and the stiffening effect of the HNT nanofillers when fracture toughness increased. The latter plastification was also enhanced by the addition of the CTBN polymeric rubber component of the composite epoxy matrix, thus improving material's fracture toughness. A similar effect was also confirmed by molecular dynamics simulations of mono helical soft segments based on Newtonian mechanics theory [44].

In this study, GnPs and HNTs were used separately as fillers to improve the mechanical performance, dispersion, thermal stability, and opto-electronic properties of the epoxy resin composite. A varying mass ratio of both fillers was used in prepared composites, and the effect of the applied nanofillers was evaluated by uniaxial tensile testing, fracture toughness measurements, uniaxial bending testing, indentation micro-hardness measurements, and nondestructive vibration testing.

2 Materials

2.1 Materials

The resin and hardener used in this study were diglycidyl ether of bisphenol A resin (DGEBA) with low viscosity (trade name: laminating resin MGS L285) (Figure 1a) and 3-aminomethyl-3,5,5 trimethylcyclohexylamine (trade name: L285), respectively (both materials were provided from Hexion, USA) (Figure 1b). The liquid rubber used was CTBN copolymer (purchased from Zibo Qilong, China) with an average of 0.58–0.65 carboxyl groups per molecule; its number average molecular weight was about 3,800 Da, and the content of acrylonitrile was of 8–12% (Figure 1c). The technical data of the CTBN are given in Table 1. The chemical structures of epoxy, hardener, and CTBN are shown in Figure 1. Nanofillers used in this study were non-functionalized planar-shaped GnPs of 800 m^2/g specific surface area, layer thickness of 3–7 nm with an average layer width of 1.5 µm, and 99.9% purity (purchased from Nanografi, Ankara, Turkey). The HNTs ($Al_2Si_2O_5(OH)_4$) used had two layers of nanocylindrical structure (Esan Eczacıbası (Istanbul, Turkey)), whose inner diameter, outer diameter, and length were in the range of 1–20, 30–50, and 100–800 nm, respectively.

2.2 Preparation of nanocomposites and epoxy blends

2.2.1 CTBN–epoxy blends

The chemical formulas of the used epoxy blends are shown in Figure 1. For preparing the epoxy blends with CTBN liquid rubber, 10 wt% CTBN was mechanically mixed with epoxy resin in a glass beaker placed on a preheated plate. The blends in the beaker were then stirred by ultrasonication for 15–20 min to obtain homogeneous blends, followed by 1 h of degassing in the vacuum oven at 60°C. The amine-based curing agent was subsequently added at a stoichiometric ratio of 80:20 (epoxy:hardener) by weight at slow stirring. Blends were subsequently cast into molds and cured for 1 h at 90°C, followed by 3 h post-curing at 120°C.

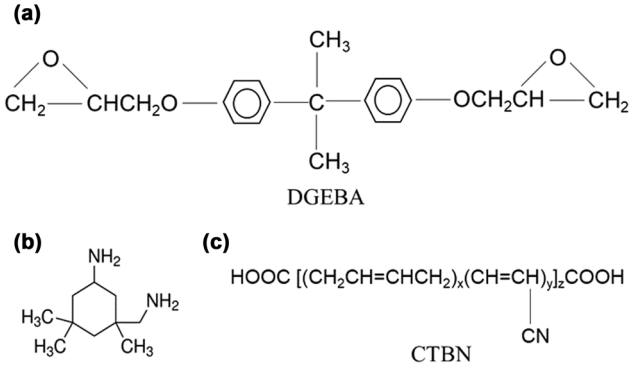

Figure 1: The chemical structure of components (a) DGEBA, (b) 3-aminomethyl-3,5,5-trimethylcyclohexylamine, and (c) CTBN.

Table 1: Properties of the applied CTBN liquid rubber

Parameter	Value
Viscosity (40°C) (Pa s)	7–12
Carboxyl content (mmol/g)	0.58–0.65
Nitrile group content (%)	8.0–12.0
Water content (%)	≤0.05
Volatile content (%)	≤2.0

2.2.2 CTBN– GnPs–epoxy and CTBN–halloysite–epoxy composites

The nano-reinforcement ratios of the epoxy mixtures were created based on the literature. Many authors [43,45–49] have experimentally studied the concentration of GnP and HNTs in the epoxy matrix to be in the range of (0–1) and (0–5) wt%, respectively, and reported the effect of these concentrations on tensile, fracture, and flexural properties of the neat matrix. For preparing the epoxy mixtures with GnPs and HNTs (see Figure 2 for scanning electron microscopy [SEM]), 0, 0.125, 0.25, 0.5, 0.75, and 1 wt% GnPs and 0, 1, 2, 3, 4, and 5 wt% HNTs were added to the epoxy resin, and the obtained mixtures were transferred into a RETSCH-PM 100 planetary mill for mixing at a rotation rate of 200 rpm for 25 h. The epoxy composite mixtures were prepared using 10 mm diameter balls and a bowl made of tungsten carbide as mixing media. The mixing bowls were loaded with the epoxy mixtures and balls, resulting in a ball-to-powder mass ratio of 30:1. First, the mixtures were mixed for 30 min, then rested for 10 min to avoid overheating, then mixed again, and the cycle was continued until the decided mixing time was completed. Subsequently, 10 wt% CTBN was added to each epoxy mixture containing the GnP and HNT reinforcements for preparing the CTBN–GnPs–epoxy and CTBN–HNTs–epoxy composites. The prepared mixtures were stirred using ultrasonication for 25–30 min to obtain the homogeneous mixtures, followed by degassing in a vacuum oven at 60°C for about 1 h. Finally, the curing procedure of CTBN–epoxy blends

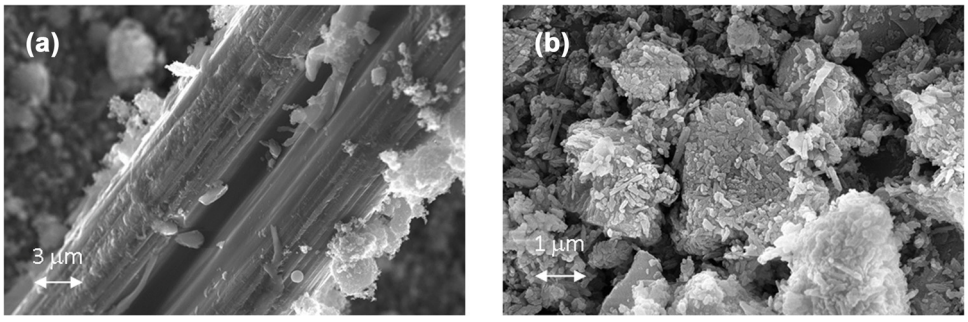

Figure 2: SEM images of the studied fillers: (a) GnPs, (b) HNT.

described in Section 2.2.1 was followed to cure the CTBN–GnPs–epoxy and the CTBN–HNTs–epoxy composites. The same CTBN liquid rubber concentration of 10 wt% was used in all of the investigated epoxy/graphene and epoxy/halloysite nanocomposites; the virgin epoxy matrix prepared was without CTBN liquid rubber.

3 Methods

3.1 SEM analysis

Zeiss EvoLS10 equipped with an energy-dispersive X-ray detector (Germany) was used for SEM analysis. SEM images were taken by depositing nanofiller samples on a standard 400-grid copper mesh. Fillers' acetone dispersions were ultrasonicated for 15 min, cast on the copper mesh, and air dried. SEM measurements were performed at an accelerating voltage of 2 kV.

3.2 Uniaxial tensile testing

Universal Testing Machine Autograph AGS-100 Shimadzu (Japan) and Zwick 1456 multipurpose tester (Zwick Roell, Ulm, Germany) equipped with Compact Thermostatic Chamber TCE Series were used for tensile testing of injection-molded specimens. All data were recorded as per ČSN EN ISO 527-1 and ČSN EN ISO 527-2 standards for the tested gauge length of 80 mm. All experiments were performed at room temperature up to break with a 50 mm/min deformation rate. Young's modulus of elasticity and elongation at break were obtained from the stress–strain dependency plots. Each experiment was repeated 10×, and mean values and standard deviations of the measured quantities were subsequently calculated. All experiments were performed at the ambient laboratory temperature of 25°C.

3.3 Charpy impact testing

Impact tests were carried out using Zwick 513 Pendulum Impact Tester (Zwick Roell, Ulm, Germany) according to the ČSN EN ISO 179-2 standard, allowing a 25 J energy drop. Each experiment was repeated 10× and mean values and standard deviations of the fracture toughness were calculated. All experiments were performed at the ambient laboratory temperature of 25°C.

3.4 Micro-hardness

Micro-indentation tests were performed on a micro-indentation tester (Micro Combi Tester, Anton Paar, Austria), according to the ČSN EN ISO 14577 standard. The applied diamond tip was cube-corner shaped (Vickers, Anton Paar, Austria). Measurement parameters were set as follows: the maximum load of 3 N, loading rate (unloading rate) of 6 N/min, and holding time of 90 s. All experiments were performed according to the depth-sensing indentation method, allowing simultaneous measurement of the acting force on the indenter and the displacement of the indenter's tip. The indentation modulus (E_{IT}) was calculated from the plane strain modulus of elasticity (E^*) using an estimated Poisson's ratio (ν) of the samples (0.3–0.4 [50,51]):

$$E_{IT} = E^*(1 - \nu^2). \quad (1)$$

Each measurement was repeated 10×, and mean values and standard deviations of the indentation modulus were calculated. All experiments were performed at the ambient laboratory temperature of 25°C.

3.5 Uniaxial three-point bending tests

The uniaxial three-point bending test was carried out on a Zwick 1456 testing machine (Zwick Roell GmbH &Co. KG, Ulm, Germany) according to the ČSN EN ISO 14125 standard. The results were evaluated using the TestXpert software. The distance between the supports was set to 64 mm, and the roundness of the supports and the load mandrel was 5 mm. The deformation rate during the three-point bending test was 1 mm/min, and the loading velocity was 50 mm/min.

3.6 Displacement transmissibility measurements

Displacement transmissibility T_d is expressed by the following equation [52]:

$$T_d = \frac{y_2}{y_1} = \frac{a_2}{a_1}, \tag{2}$$

where y_1 is the displacement amplitude on the input side of the tested sample, y_2 is the displacement amplitude on the output side of the tested sample, a_1 is the acceleration amplitude on the input side of the tested sample, and a_2 is the acceleration amplitude on the output side of the tested sample. The displacement transmissibility of a spring–mass–damper system, which is described by spring (stiffness k), damper (damping coefficient c), and mass m, is given by the following equation [53]:

$$T_d = \sqrt{\frac{k^2 + (c \bullet \omega)^2}{(k - m \bullet \omega^2)^2 + (c \bullet \omega)^2}} = \sqrt{\frac{1 + (2 \bullet \zeta \bullet r)^2}{(1 - r^2)^2 + (2 \bullet \zeta \bullet r)^2}}. \tag{3}$$

Under the condition $dT_d/dr = 0$ in equation (3), it is possible to obtain the frequency ratio r_0 at which the displacement transmissibility reaches its maximum value [54,55]:

$$r_0 = \frac{\sqrt{\sqrt{1 + 8 \bullet \zeta^2} - 1}}{2 \bullet \zeta}. \tag{4}$$

It is evident from equation (4) that the local extreme of the displacement transmissibility is generally shifted to lower values of the frequency ratio r with increasing damping ratio ζ (or with decreasing material mechanical stiffness k). The local extrema (*i.e.*, the maximum value of the displacement transmissibility T_{dmax}) is found at the frequency ratio r_0 from equation (4). The mechanical vibration tests were performed by forced oscillation method. The displacement transmissibility T_d was experimentally measured using the BK 4810 vibrator in combination with a BK 3560-B-030 signal pulse multi-analyzer and a BK 2706 power amplifier at the frequency range from 2 to 3,200 Hz. The acceleration amplitudes a_1 and a_2 on the input and output sides of the investigated samples were recorded by BK 4393 accelerometers (Brüel & Kjær, Nærum, Denmark). Measurements of the displacement transmissibility were done for three different inertial masses m (for 0, 90, and 500 g), which were placed on the top side of the tested samples. The dimensions of the tested specimen were 60 mm × 60 mm × 3 mm (length × width × thickness). Each measurement was repeated 5× at an ambient temperature of 22°C.

4 Results and discussion

A typical shape of the used nanofillers, as observed by SEM analysis, is shown in Figure 2. Here the GnP lamellar structure was clearly visible in Figure 2a with a layer thickness of about 3–7 nm and an average layer width of 1.5–2.0 µm. In contrast, the HNT nanotubes exhibited a compact coagulated structure composed of individual nanotubes of approximately 30–50 nm diameter and 100–800 nm length (Figure 2b).

Results of the tensile-testing experiments of the studied nanocomposites are shown in Figure 3. There was a decrease of the Young's modulus of elasticity (E) during uniaxial testing from 3.4 GPa (neat matrix) to 2.7 GPa (for 1 wt% epoxy/GnP nanocomposite) with increasing GnP filler concentration [56]. This effect was accompanied by the increasing nonlinear trend of the obtained magnitudes of the elongation at break, indicating increasing ductility and plasticizing effect of the GnP nanofiller on the mechanical behavior of the prepared epoxy/GnP nanocomposites. Based on the literature [11], it was assumed that this behavior was ascribed to the gliding of the individual nanoplatelet sheets within complex epoxy/GnP nanocomposite matrix accompanied by the crack deflection, layer breakage, and separation/delamination of GnP layers [13]. However, the opposite effect was found in the case of the epoxy/HNT nanocomposites, where the E decreased from 3.4 GPa (neat matrix) to 2.7 GPa (for 5 wt% epoxy/HNT nanocomposite), thus indicating the decreasing mechanical stiffness of the studied materials. Simultaneously, in contrast to the epoxy/GnP nanocomposites, a more brittle behavior with increasing HNT filler concentration was observed. These observations were demonstrated by constant elongation at break (about 0.36 mm) dependency as shown in Figure 3.

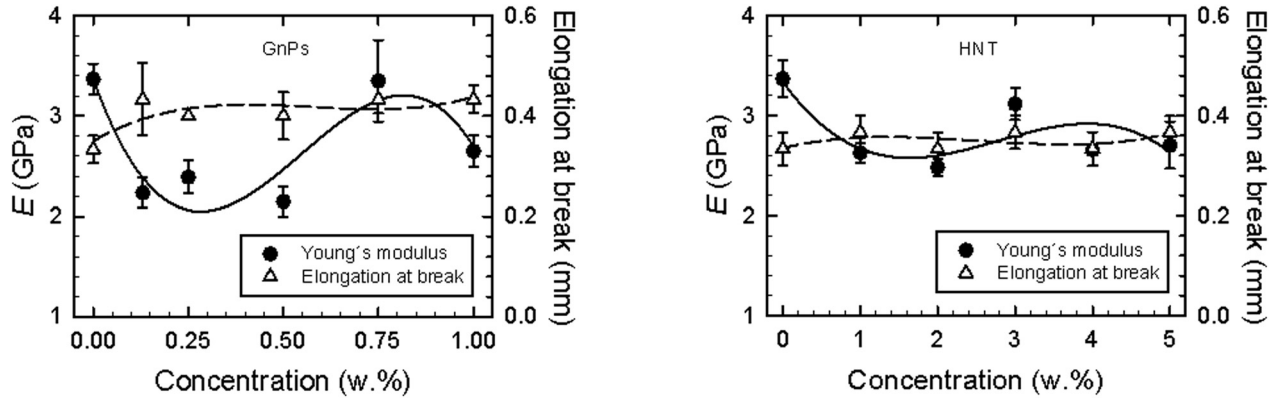

Figure 3: Nanofiller concentration dependencies of the Young's modulus of elasticity and the elongation at break of the studied GnPs and HNT nanocomposites. Applied deformation rate was of 50 mm/min. Continuous line – Young's modulus of elasticity, dashed line – elongation at break.

Based on the aforementioned facts, it was assumed that the HNT nanofiller increased the brittleness of the composite due to the limited movement of the stiffened HNT nanotubes resulting in the hindered gliding of the HNT nanofillers within the composite matrix.

The above-mentioned results of the uniaxial tensile tests were in excellent agreement with the observed fracture toughness measurements (Figure 4), where higher fracture toughness of 8.2 kJ/m^2 of epoxy/HNT nanocomposites was found compared to the 6.0 kJ/m^2 of epoxy/GnP nanocomposites (both at 1 wt% filler concentration). At higher HNT filler concentrations (in the concentration range of 1–5 w%) nonlinear decreasing trend of fracture toughness was observed (Figure 4).

In addition, the presence of CTBN (Figure 1c) acted on the continuous composite matrix as a kind of accelerator, which forces it to develop local deformations. The deformation mechanisms in the matrix then dissipate the external mechanical energy over a large volume, thus preventing the development of a single brittle crack. Optimal performance of rubber modification requires several conditions to be met, namely the establishment of a two-phase morphology, the provision of satisfactory interfacial adhesion, and the establishment of a certain critical distance between adjacent rubber domains [9]. Analogous behavior was observed for multi-phase hard and soft segmental flexible polymers, where hard phases served as stiffening element and the soft phases provided elasticity [44].

Results of the micro-hardness *vs* filler concentration measurements of both the studied epoxy nanocomposites are shown in Figure 5. A nonlinear decreasing trend of the indentation modulus E_{IT} with increasing filler concentration was observed. In the case of the epoxy/GnP nanocomposites, E_{IT} decreased from 4.3 GPa (neat matrix) to 3.4 GPa (for 1 wt% GnP nanocomposite). Similarly, in the case of the epoxy/HNT nanocomposites, E_{IT} decreased from 4.3 GPa (neat matrix) to 3.8 GPa (for 5 wt% HNT

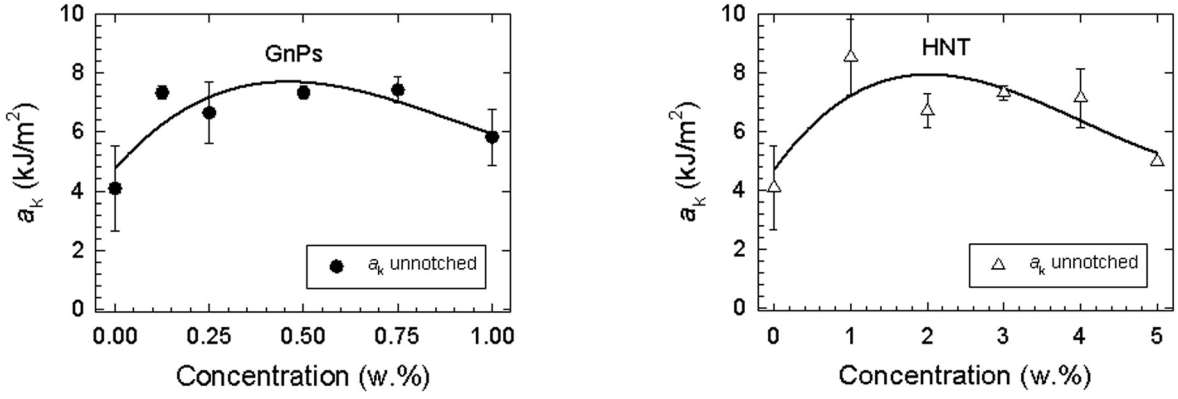

Figure 4: Nanofiller concentration dependencies of the unnotched fracture toughness of the studied GnPs and HNT nanocomposites.

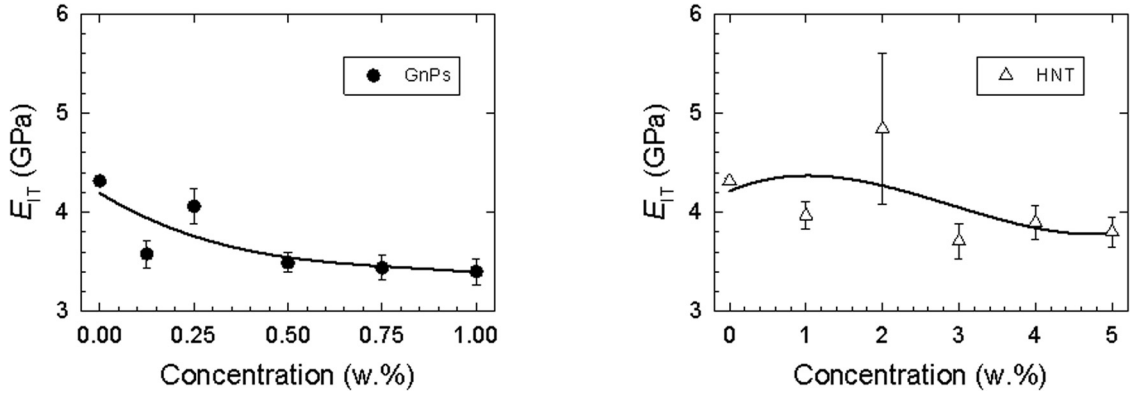

Figure 5: Nanofiller concentration dependencies of the indentation modulus of the studied GnPs and HNT nanocomposites.

nanocomposite). The plasticizing effect of the applied nanofillers was assumed as the most probable cause of this decrease of surface hardness.

Results of the uniaxial three-point bending tests of the studied nanocomposites are shown in Figure 6. Here, nonlinear decreasing patterns were found for both the studied nanocomposites. Such behavior is typical for brittle materials. A nonlinear decrease of the bending modulus (E_B) from 4.3 GPa (neat matrix) to 2.8 GPa (for 1 wt% GnP nanocomposite) with increasing GnP filler concentration was found. This effect was accompanied by the increasing gradual nonlinear trend of the obtained magnitudes of the elongation at break (from 5.0 mm [neat matrix]) to 6.0 mm (for 1 wt% epoxy/GnP nanocomposite), indicating increasing composite ductility due to the plasticizing effect of the nanofiller of the prepared epoxy/GnP nanocomposites. In the case of the epoxy/HNT nanocomposites, E_B nonlinearly decreased from 4.3 GPa (neat matrix) to 3.0 GPa (for 5 wt% epoxy/HNT nanocomposites), indicating decreasing mechanical stiffness of the studied materials. However, the opposite, a minor decreasing nonlinear trend of the elongation at break *vs* HNT filler concentration, was found, where the elongation at break decreased from 5.0 mm (neat matrix) to 4.1 mm (for 5 wt% epoxy/HNT nanocomposites). These results indicated higher brittleness of the epoxy/HNT nanocomposites compared to the epoxy/GnP nanocomposites.

Results of the dynamic mechanical tests of the studied nanocomposites are shown in Figures 7 and 8. Typical frequency dependencies of displacement transmissibility are depicted in Figure 7. The obtained results were in excellent agreement with the uniaxial tensile measurements, indicating increased material stiffness based on the f_{R1} peak position shift to the higher excitation frequencies according to equation (4). However, a minor decrease of the latter stiffness was found for low filler concentrations, as indicated by the negligible shift of the f_{R1} to the lower magnitudes (Figure 7a and b). The effect of the inertial mass magnitudes on the frequency dependencies of the displacement transmissibility is demonstrated

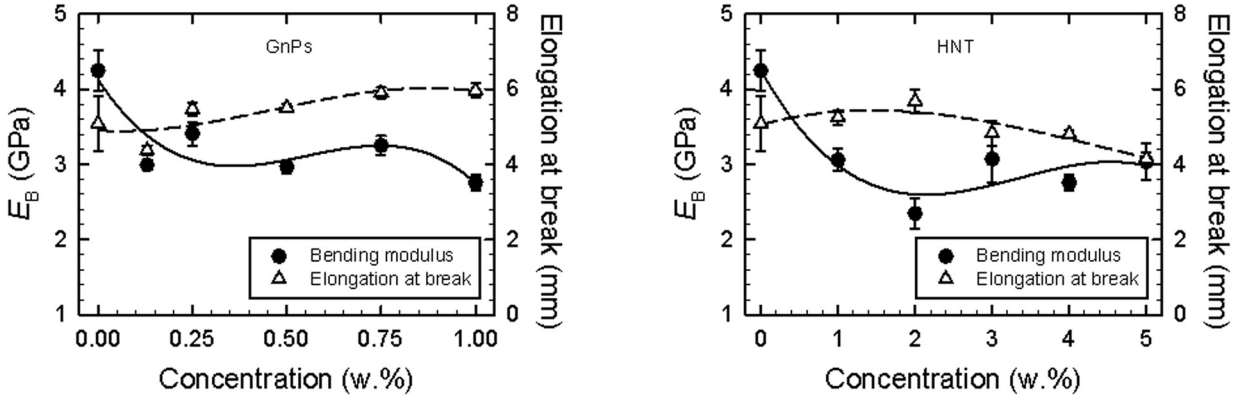

Figure 6: Nanofiller concentration dependencies of the bending modulus and the elongation at break of the studied GnPs and HNT nanocomposites. Applied deformation rate was of 50 mm/min. Continuous line – bending modulus, dashed line – elongation at break.

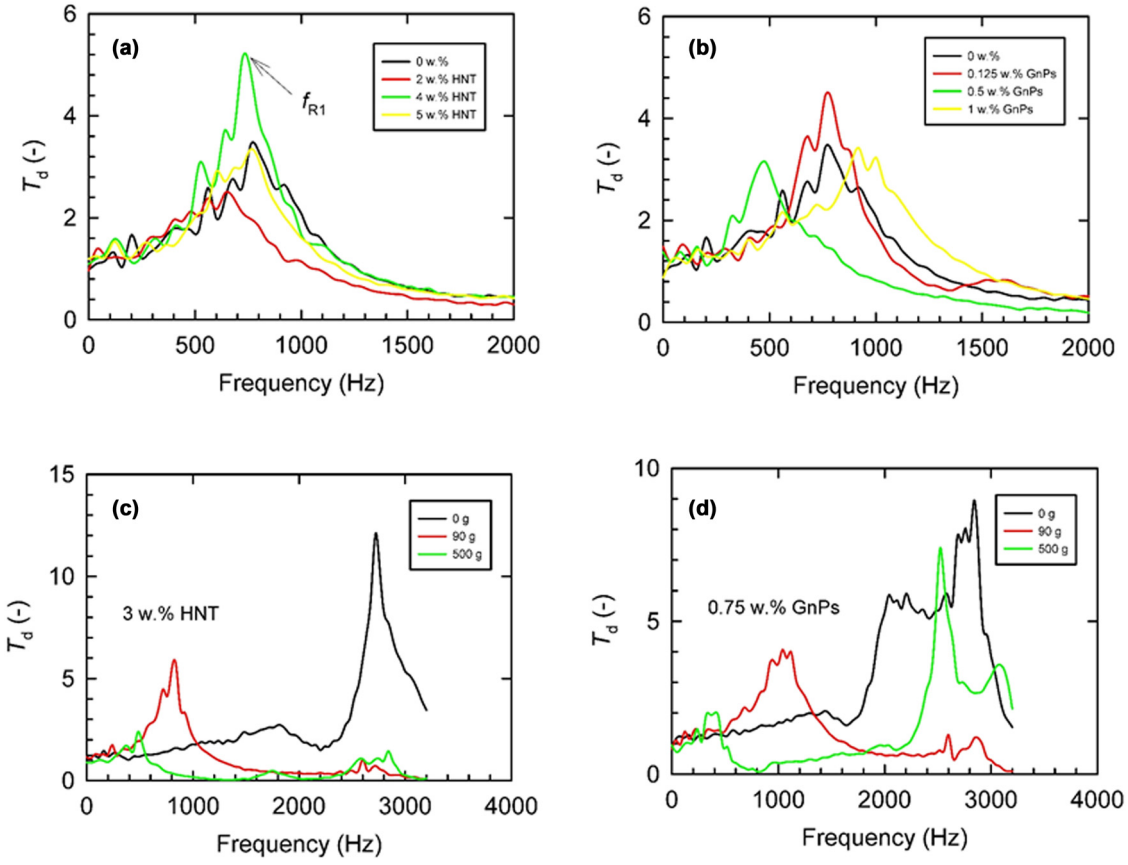

Figure 7: Frequency dependencies of the displacement transmissibility of the tested GnPs and HNT nanocomposites (Inset in a and b: nanofillers concentrations) with applied inertial mass of 90 g (inset in c and d: applied inertial masses).

in Figure 7c and d. It was found that the increasing inertial mass led to the decrease of the first resonance frequency peak position, thereby resulting in the improved materials' mechanical vibration-damping properties [53]. In addition, the obtained increasing f_{R1} with GnP concentration again confirmed materials' increasing stiffness, similar to the case of the previous tensile and fracture toughness measurements (Figures 3 and 4). The latter findings fit very well with the epoxy/GnP nanocomposite results shown in Figure 8, where the linear increase of the f_{R1} with the filler concentration was observed. In contrast, obtained results for the epoxy/HNT nanocomposites exhibited decreased

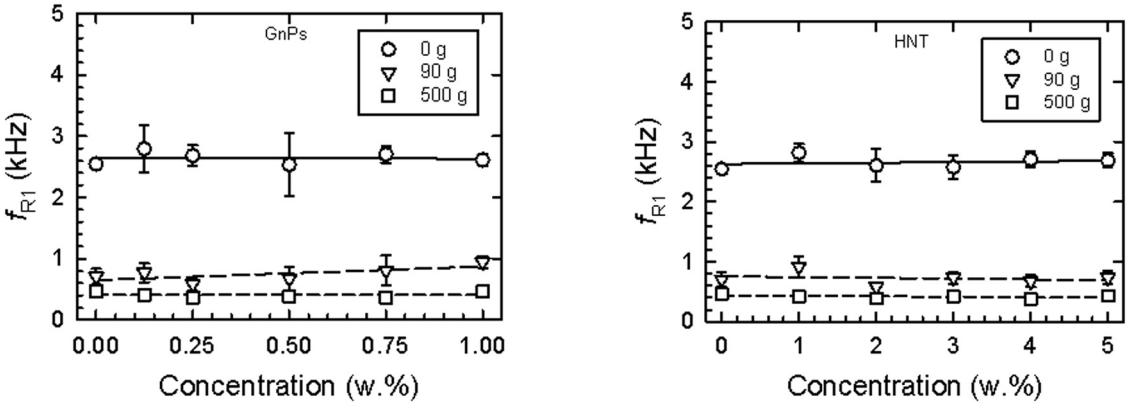

Figure 8: Concentration dependencies of the first resonance frequencies of the studied GnPs and HNT nanocomposites. Inset legend: inertial mass used.

mechanical stiffness as indicated by decreasing f_{R1} with increasing filler concentration for the applied inertial masses.

5 Conclusions

The possibility of elastic–plastic mechanical behavior modulation by means of the application of nanosized GnPs and HNT fillers in the complex epoxy resin-based nanocomposites was confirmed in this study. A complex nonlinear pattern of Young's modulus of elasticity with increasing GnP filler concentration was found. Simultaneously, in the concentration range of 0–1 wt% GnP nanofiller concentration, an increasing ductility of the studied nanocomposites was found, as reflected in the samples' increased elongation at break. This kind of behavior was interpreted by the interparticle gliding effect of the individual GnP nanoparticles dispersed in the complex epoxy resin matrix. A relatively constant trend of Young's modulus of elasticity (approximately of about 2.8 GPa) accompanied by the similar nonlinear pattern of elongation at break (approximately of 0.35 mm) for the studied epoxy/HNT nanocomposites in the concentration range of 1–5 wt% was also found. It was attributed to the hindered local movement of the HNT nanofillers in the matrix during mechanical tests. Fracture mechanical tests confirmed that the fracture toughness obtained at low filler concentrations was higher in the case of the stiff epoxy/HNT nanocomposites compared to the epoxy/GnP nanocomposites due to the GnP filler's gliding-dissipative effect. As obtained by the uniaxial three-point bending tests, the elongation at break measurements confirmed the enhanced plasticity and ductility with increasing GnP filler concentration of the complex epoxy/GnP nanocomposites. This was reflected in the exceeding magnitude of the elongation at break of 6 mm compared to 5.3 mm of the epoxy/HNT nanocomposites (both at 1 wt% nanofiller concentration). A similar effect was also confirmed by micro-hardness tests, where the observed indentation modulus of 3.4 GPa of epoxy/GnP nanocomposites was lower compared to 4.0 GPa of epoxy/HNT nanocomposites (both at 1 wt% nanofiller concentration), thus indicating more dissipative mechanical behavior of the epoxy/GnP nanocomposites. The latter we ascribed to the above-mentioned GnP nanofiller gliding friction. As a novel approach, the nondestructive mechanical vibration damping method of forced oscillations was applied in the low-frequency region of 2–3,200 Hz for the comparison of mechanical properties based on the first resonance frequency peak position. The plastification effect of the epoxy/GnP nanocomposites was confirmed by the lower magnitude of the first resonance frequency peak position of 2.6 kHz compared to the observed magnitude of the f_{R1} of 2.8 kHz for epoxy/HNT nanocomposites (both results obtained at 1 wt% nanofiller concentration and zero inertial mass).

Funding information: This study was supported by the European Regional Development Fund in the Research Centre of Advanced Mechatronic Systems project, project number CZ.02.1.01/0.0/0.0/16_019/0000867. LL and YM would like to express their gratitude for financing this research by the internal grants of Palacky University in Olomouc IGA_PrF_2022_020, IGA_PrF_2023_024 and to Tomas Bata University in Zlin (project nos IGA/FT/2022/005 and IGA/FT/2023/007). Financial support to YM by Fischer scholarship of the Faculty of Science, Palacky University in Olomouc, in the year 2022/2023, is also gratefully acknowledged.

Author contributions: All authors have accepted responsibility for the entire content of this manuscript and approved its submission.

Conflict of interest: The authors state no conflict of interest.

References

[1] Lapcik L, Jindrova P, Lapcikova B, Tamblyn R, Greenwood R, Rowson N. Effect of the talc filler content on the mechanical properties of polypropylene composites. J Appl Polym Sci. 2008 Dec 5;110(5):2742–7.
[2] Bheemappa S, Gurumurthy H. Recent advances in fabrication and characterization of nanofiller filled epoxy nanocomposites. Trends Fabr Polym Polym Compos. 2022;2022:1–40.
[3] Ogbonna VE, Popoola A, Popoola OM, Adeosun SO. A review on the recent advances on improving the properties of epoxy nanocomposites for thermal, mechanical, and tribological applications: challenges and recommendations. Polym Technol Mater. 2022;61(2):176–95.
[4] Krasny I, Lapcik L, Lapcikova B, Greenwood RW, Safarova K, Rowson NA. The effect of low temperature air plasma treatment on physico-chemical properties of kaolinite/polyethylene composites. Compos Part B Eng. 2014 Mar;59:293–9.
[5] Lapcik L, Jindrova P, Lapcikova B. Effect of talc filler content on poly(propylene) composite mechanical properties. Eng Fract. 2009;1:73–80.
[6] Chen X, Li Y, Wang Y, Song D, Zhou Z, Hui D. An approach to effectively improve the interfacial bonding of nano-perfused composites by in situ growth of CNTs. Nanotechnol Rev. 2021;10(1):282–91.
[7] Gouda K, Bhowmik S, Das B. A review on allotropes of carbon and natural filler-reinforced thermomechanical properties of

upgraded epoxy hybrid composite. Rev Adv Mater Sci. 2021 jan;60(1):237–75.
[8] Amin M, Ali M. Polymer nanocomposites for high voltage outdoor insulation applications. Rev Adv Mater Sci. 2015 jun;40(3):276–94.
[9] Lapcik L, Raab M. Materials Science II. Textbook. 2nd edn. Zlin: Tomas Bata University in Zlin; 2004.
[10] Lapcik L', Jancar J, Stasko A, Sáha P. Electron paramagnetic resonance study of free-radical kinetics in ultraviolet-light cured dimethacrylate copolymers. J Mater Sci Mater Med. 1998;9(5):257–62.
[11] Vijayan PP, George JS, Thomas S. The effect of polymeric inclusions and nanofillers on cure kinetics of epoxy resin: A review. Polym Sci Ser A. 2021 Nov;63(6):637–51.
[12] Ouyang CF, Geo Q, Shi YT, Li WT. Effect of CTBN on properties of oxide graphene/epoxy resin composites. Chin Ceram Commun II. 2012;412:393.
[13] Wang FZ, Drzal LT, Qin Y, Huang ZX. Enhancement of fracture toughness, mechanical and thermal properties of rubber/epoxy composites by incorporation of graphene nanoplatelets. Compos Part A Appl Sci Manuf. 2016 August;87:10–22.
[14] Lim YJ, Carolan D, Taylor AC. Simultaneously tough and conductive rubber-graphene-epoxy nanocomposites. J Mater Sci. 2016 Sep;51(18):8631–44.
[15] Xie C, Li Y, Han Y. Fabrication and properties of CTBN/Si3N4/Cyanate ester nanocomposites. Polym Compos. 2016 August;37(8):2522–6.
[16] Konnola R, Joji J, Parameswaranpillai J, Joseph K. Structure and thermo-mechanical properties of CTBN-grafted-GO modified epoxy/DDS composites. RSC Adv. 2015;5(76):61775–86.
[17] Hashim UR, Jumahat A, Jawaid M. Mechanical properties of hybrid graphene nanoplatelet-nanosilica filled unidirectional basalt fibre composites. Nanomaterials. 2021;11(6):1468.
[18] Lapcik L, Manas D, Vasina M, Lapcikova B, Reznicek M, Zadrapa P. High density poly(ethylene)/CaCO3 hollow spheres composites for technical applications. Compos Part B Eng. 2017 Mar 15;113:218–24.
[19] Fiore V, Scalici T, Di Bella G, Valenza A. A review on basalt fibre and its composites. Compos Part B Eng. 2015;74:74–94.
[20] Tarawneh MA, Saraireh SA, Chen RS, Ahmad SH, Al-Tarawni M, Yu LJ, et al. Mechanical reinforcement with enhanced electrical and heat conduction of epoxy resin by polyaniline and graphene nanoplatelets. Nanotechnol Rev. 2020 Jan;9(1):1550–61.
[21] Ma X, Peng C, Zhou D, Wu Z, Li S, Wang J, et al. Synthesis and mechanical properties of the epoxy resin composites filled with sol– gel derived ZrO2 nanoparticles. J Sol Gel Sci Technol. 2018;88(2):442–53.
[22] Sui G, Zhong WH, Liu MC, Wu PH. Enhancing mechanical properties of an epoxy resin using "liquid nano-reinforcements". Mater Sci Eng A. 2009;512(1–2):139–42.
[23] Nath S, Jena H, Sahini D. Analysis of mechanical properties of jute epoxy composite with cenosphere filler. Silicon. 2019;11(2):659–71.
[24] Sim J, Kang Y, Kim BJ, Park YH, Lee YC. Preparation of fly ash/epoxy composites and its effects on mechanical properties. Polymers. 2020;12(1):79.
[25] Kiran MD, Govindaraju HK, Jayaraju T, Kumar N. effect of fillers on mechanical properties of polymer matrix composites. Mater Today Proc. 2018;5(10):22421–4.
[26] Prasob PA, Sasikumar M. Static and dynamic behavior of jute/epoxy composites with ZnO and TiO2 fillers at different temperature conditions. Polym Test. 2018;69:52–62.
[27] Savotchenko S, Kovaleva E, Cherniakov A. The improvement of mechanical properties of repair and construction compositions based on epoxy resin with mineral fillers. J Polym Res. 2022;29(7):1–10.
[28] Zhang HY, Li X, Qian WJ, Zhu JG, Chen BB, Yang J, et al. Characterization of mechanical properties of epoxy/nanohybrid composites by nanoindentation. Nanotechnol Rev. 2020 Jan;9(1):28–40.
[29] Tang L, Wan Y, Yan D, Pei Y, Zhao L, Li Y, et al. The effect of graphene dispersion on the mechanical properties of graphene/epoxy composites. Carbon. 2013;60:16–27.
[30] Ioniţă M, Vlăsceanu GM, Watzlawek AA, Voicu SI, Burns JS, Iovu H. Graphene and functionalized graphene: Extraordinary prospects for nanobiocomposite materials. Compos Part B: Eng. 2017;121:34–57.
[31] Sukur EF, Onal G. Graphene nanoplatelet modified basalt/epoxy multi-scale composites with improved tribological performance. Wear. 2020;460:203481.
[32] Kilic U, Sherif MM, Ozbulut OE. Tensile properties of graphene nanoplatelets/epoxy composites fabricated by various dispersion techniques. Polym Test. 2019;76:181–91.
[33] Wang P, Hsieh T, Chiang C, Shen M. Synergetic effects of mechanical properties on graphene nanoplatelet and multi-walled carbon nanotube hybrids reinforced epoxy/carbon fiber composites. J Nanomater. 2015;2015:1–9.
[34] Mishra BP, Mishra D, Panda P. An experimental investigation of the effects of reinforcement of graphene fillers on mechanical properties of bi-directional glass/epoxy composite. Mater Today Proc. 2020;33:5429–41.
[35] Georgakilas V, Otyepka M, Bourlinos AB, Chandra V, Kim N, Kemp KC, et al. Functionalization of graphene: Covalent and non-covalent approaches, derivatives and applications. Chem Rev. 2012 NOV;112(11):6156–214.
[36] Joussein E, Petit S, Churchman J, Theng B, Righi D, Delvaux B. Halloysite clay minerals - A review. Clay Min. 2005 DEC;40(4):383–426.
[37] Yuan P, Tan D, Annabi-Bergaya F. Properties and applications of halloysite nanotubes: Recent research advances and future prospects. Appl Clay Sci. 2015;112:75–93.
[38] Gaaz TS, Sulong AB, Kadhum AAH, Al-Amiery AA, Nassir MH, Jaaz AH. The impact of halloysite on the thermo-mechanical properties of polymer composites. Molecules. 2017;22(5):838.
[39] Tierrablanca E, Romero-García J, Roman P, Cruz-Silva R. Biomimetic polymerization of aniline using hematin supported on halloysite nanotubes. Appl Catal A: Gen. 2010;381(1–2):267–73.
[40] Kausar A. Review on polymer/halloysite nanotube nanocomposite. Polym Plast Technol Eng. 2018;57(6):548–64.
[41] Kausar A. Polymer coating technology for high performance applications: Fundamentals and advances. J Macromol Sci Part A Pure Appl Chem. 2018;55(5):440–8.
[42] Ghadikolaee MR, Korayem AH, Sharif A, Liu YM. The halloysite nanotube effects on workability, mechanical properties, permeability and microstructure of cementitious mortar. Constr Build Mater. 2021;267:120873.

[43] Hashmi MA. Enhancement of mechanical properties of epoxy/halloysite nanotube (HNT) nanocomposites. SN Appl Sci. 2019;1(4):1–8.
[44] Chen FX, Fan JT, Hui DV, Wang C, Yuan FP, Wu XL. Mechanisms of the improved stiffness of flexible polymers under impact loading. Nanotechnol Rev. 2022 Dec 16;11(1):3281–91.
[45] Srivastava S, Pandey A. Mechanical behavior and thermal stability of ultrasonically synthesized halloysite-epoxy composite. Compos Commun. 2019 Feb;11:39–44.
[46] Alexopoulos ND, Paragkamian Z, Poulin P, Kourkoulis SK. Fracture related mechanical properties of low and high graphene reinforcement of epoxy nanocomposites. Compos Sci Technol. 2017 Sep 29;150:194–204.
[47] Wei JC, Atif R, Vo T, Inam F. Graphene nanoplatelets in epoxy system: Dispersion, reaggregation, and mechanical properties of nanocomposites. J Nanomater. 2015;2015:(3):1–12.
[48] Chatterjee S, Nafezarefi F, Tai NH, Schlagenhauf L, Nuesch FA, Chu B. Size and synergy effects of nanofiller hybrids including graphene nanoplatelets and carbon nanotubes in mechanical properties of epoxy composites. Carbon. 2012 Dec;50(15):5380–6.
[49] Alamri H, Low IM. Microstructural, mechanical, and thermal characteristics of recycled cellulose fiber-halloysite-epoxy hybrid nanocomposites. Polym Compos. 2012 Apr;33(4):589–600.
[50] Oliver WC, Pharr GM. Measurement of hardness and elastic modulus by instrumented indentation: Advances in understanding and refinements to methodology. J Mater Res. 2004 Jan;19(1):3–20.
[51] Manas D, Mizera A, Manas M, Ovsik M, Hylova L, Sehnalek S, et al. Mechanical properties changes of irradiated thermoplastic elastomer. Polymers. 2018 Jan;10(1):87.
[52] Rao SS. Mechanical vibrations. 5th edn. Upper Saddle River, USA: Prentice Hall; 2010.
[53] Lapcik L, Vasina M, Lapcikova B, Stanek M, Ovsik M, Murtaja Y. Study of the material engineering properties of high-density poly(ethylene)/perlite nanocomposite materials. Nanotechnol Rev. 2020 Jan;9(1):1491–9.
[54] Carrella A, Brennan MJ, Waters TP, Lopes V, Jr. Force and displacement transmissibility of a nonlinear isolator with high-static-low-dynamic-stiffness. Int J Mech Sci. 2012;55(1):22–9.
[55] Ab Latif N, Rus AZM. Vibration transmissibility study of high density solid waste biopolymer foam. J Mech Eng Sci. 2014;6:772–81.
[56] Murtaja Y, Lapcik L, Sepetcioglu H, Vlcek J, Lapcikova B, Ovsik M, et al. Enhancement of the mechanical properties of HDPE mineral nanocomposites by filler particles modulation of the matrix plastic/elastic behavior. Nanotechnol Rev. 2022 Jan 5;11(1):312–20.

materials

MDPI

Article

Effect of Conditioning on PU Foam Matrix Materials Properties

Lubomír Lapčík [1,2,*], Martin Vašina [3,*], Barbora Lapčíková [1,2] and Yousef Murtaja [2]

[1] Faculty of Technology, Tomas Bata University in Zlin, Nam. TGM 275, 760 01 Zlin, Czech Republic; lapcikova@utb.cz
[2] Department of Physical Chemistry, Faculty of Science, Palacky University Olomouc, 17. Listopadu 12, 771 46 Olomouc, Czech Republic; yousef.murtaja01@upol.cz
[3] Department of Hydromechanics and Hydraulic Equipment, Faculty of Mechanical Engineering, VSB-Technical University of Ostrava, 17. listopadu 15/2172, Poruba, 708 33 Ostrava, Czech Republic
* Correspondence: lapcikl@seznam.cz (L.L.); martin.vasina@vsb.cz (M.V.)

Abstract: This article deals with the characterization of the thermal-induced aging of soft polyurethane (PU) foams. There are studied thermal and mechanical properties by means of thermal analysis, tensile, compression and dynamic mechanical vibration testing. It was found in this study, that the increasing relative humidity of the surrounding atmosphere leads to the initiation of the degradation processes. This is reflected in the observed decreased mechanical stiffness. It is attributed to the plasticization of the PU foams wall material. It is in agreement with the observed increase of the permanent deformation accompanied simultaneously with the decrease of Young's modulus of elasticity. The latter phenomenon is studied by the novel non-destructive forced oscillations vibration-damping testing, which is confirmed by observed lower mechanical stiffness thus indicating the loss of the elasticity induced by samples conditioning. In parallel, observed decreasing of the matrix hardness is confirming the loss of elastic mechanical performance as well. The effect of conditioning leads to the significant loss of the PU foam's thermal stability.

Keywords: thermal analysis; polyurethanes; open-cell foams; mechanical vibrations; tensile testing; compression testing

Citation: Lapčík, L.; Vašina, M.; Lapčíková, B.; Murtaja, Y. Effect of Conditioning on PU Foam Matrix Materials Properties. *Materials* **2022**, *15*, 195. https://doi.org/10.3390/ma15010195

Academic Editors: Andrea Sorrentino and Halina Kaczmarek

Received: 10 November 2021
Accepted: 24 December 2021
Published: 28 December 2021

1. Introduction

Polyurethanes are a group of polymers formed by the reaction of multifunctional isocyanates with polyalcohols. Polyurethanes (polycarbamates, or PU) are characterized by the (-NH-CO-O-) group [1]. In constitution and properties, they lie between polyureas (-NH-CO-NH-) and polycarbonates (-O-CO-O-). Polyurethane products are very different in nature. The diversity is attributable to the urethane bond's qualities (-NH-C-O-O) and the existence of other groups in the chain, which enable the application of intermolecular forces, cross-linking, and crystallization orientation, flexibility, and chain stiffening [2]. While PU can be synthesized in various methods, it is always based on diisocyanates in practice. Due to the toxicity of isocyanate raw materials and their synthesis method utilizing phosgene, new synthetic routes for polyurethanes without using isocyanates have been developed at present [2].

The study of polymer thermal aging and degradation at specific humidity conditions reached a relatively high importance in technological praxis due to the wide applications of porous polyurethane based materials in automotive, aerospace [3], food packaging [4,5], and consumer products industries [6,7]. In general, polymers are thermally stable until reaching the decomposition threshold [8]. Two main types of polymer thermal decomposition processes are usually recognized for polymer main macromolecular chain: depolymerization and random decomposition. These two processes can occur concurrently or independently. On the other hand, individual polymers are heated in accordance with the specified time-temperature regimes and often experience melting first, followed by

various stages of the thermal degradation process [8]. Temperature changes can stimulate a variety of physical and chemical processes in polymer systems. Important examples of these processes include thermal degradation, cross-linking, crystallization, glass transition, hydrolysis [9] etc.

Authors [10] found that the polyurethane biodegradation is controlled by diffusion of oxygen into the polymer. In PUs, the urethane or carbamate linkage is also susceptible to hydrolysis, as it is an ester linkage of a substituted carbamic acid. However, hydrolytic degradation occurs less readily than with the carboxylic ester linkage. The ultimate strain of the elastomers was decreasing with increasing degradation time.

Changes of the PUs fluorescence mapping signals induced by the weathering indicated degradation process proceeding in the PU matrix, as reflected in the increase in fluorescence intensity over time in the mapped fluorescence signals excited at 470 nm and detected in a wavelength range exceeding 500 nm. These signals revealed as response to the ongoing progress of polymer ageing [11].

Most polyurethanes are derived from three basic building blocks: a polyol (a multifunctional alcohol, usually polymeric, e.g., polybutadiene with hydroxyl-terminated hydroxyls), a diisocyanate, a chain extender (e.g., low molecular weight or polymeric diol or diamine), and a cross-linker (e.g., triol). Two basic procedures are used to synthesize polyurethanes: one-step and two-step, i.e., either a one-step mixing of all components of the reaction mixture or a prepolymer preparation procedure. One-step synthesis of polyurethanes is carried out by simultaneous mixing of polyol, diisocyanate (MDI, TDI), extenders (diols, diamines), and cross-linkers (multifunctional alcohols or amines) [12]. Cross-linking is often carried out with sufficient speed at room temperature and is completed within about a few hours. The reaction time can be shortened as required by adding accelerators (dibutyltindilaurate, stannous octoate, etc.), which are added just before application. The two-step synthesis produces the final polyurethane in two temporally separated reaction steps. In the first stage, the polyol reacts with the diisocyanate to form an intermediate with NCO-terminal groups, the so-called prepolymer. In the second step, the prepolymer reacts with extenders and cross-linkers to form the final product. In general, the prepolymer can be prepared with any excess isocyanate (isocyanate index rNCO/OH > 2). The viscosity of the prepolymer increases strongly (up to 5 times for the original hydroxyl-terminated polybutadiene); the excess liquid isocyanate can prevent or mitigate this increase (dilution effect). The hydroxyl-terminated polybutadiene may be partially replaced by a proportion of polyester diol, polyether diol, or polyol in general. From a homogeneity standpoint, it is frequently preferable to convert these components of the mixture independently into prepolymers before combining. The two-step method improves the characteristics of crosslinked matrices [6].

Presently, the research and development of recyclable and sustainable PU foams are focused on advanced bio-based systems in packaging application, e.g., for refrigerated and frozen foodstuff storage and sale. For this reason, the modern trend in the field is moving towards fully bio-based and compostable foams. However, the direction via partially bio-based PU foams remains the most consistent performer [13]. For example, the application of the algae and algal cellulose added during PU-composite foam production led to the algae base cellulose integration into the PU foam structure and resulted in more open cells and softer foam structure. The PU-composite showed greater shock absorbent capacity in comparison with the usual PU foam suitable for the application in the food packaging industry [14]. Another current trend in PU material development is the non-isocyanate PU foam synthesis [15,16].

According to the structure, soft and rigid PU foams with different specific gravity, porous structure, and mechanical properties are distinguished. The basic components of soft foams are a mixture of 2,4- and 2,6-toluenedioisocyanate and polyols (polyesters-linear or slightly branched, polyethers). The main blowing agent is gaseous carbon dioxide, formed by the reaction of water with the isocyanate group. This reaction produces highly polar groups, forming H-bridges and affecting physical properties. Soft PU foams have a

foam structure with open, interconnected pores. Rigid PU foams are networks with denser interchain bonds or cross-linking sites, and a higher content of rigid urethane sections. The closed pore structure predominates in the foam because the pore walls are more rigid. The mechanical strength of the foam increases with specific gravity. Soft PU rubbers, cross-linked elastomers and soft PU foams have approximately the same chain stiffness. High chain stiffness and intermolecular forces characterize rigid PU foams.

Results of the vibrational dynamical mechanical analysis combined with the FTIR analysis allowed detailed understanding of the induced chemical changes leading to both the crosslinking, as well as degradation processes, in the complex PU matrix [17,18]. The final changes of the mechanical properties were dependent on the type of PU matrix, where poly(ester) based PUs exhibited higher stiffness in comparison with the poly(ether) [19].

The combination of the novel, non-destructive dynamic-mechanical vibrational analysis with the conventional tensile, hardness, and permanent deformation measurements was applied in this study. The latter experimental techniques were combined with the thermal analysis. Studied samples were subjected to varying conditioning times at different temperatures and relative humidity.

2. Materials and Methods

2.1. Materials

Open cell soft PU foams of (35.4 ± 0.3) g/cm^3 density were purchased in the local construction hobby market and studied. PU samples were cut into the required shapes and dimensions of the specimen, e.g., dog bone for tensile, cubic for mechanical vibration analysis, permanent deformation, and hardness testing. A photo of the studied foam is shown in Figure 1. Small bits of the tested PU foams were used for thermal analysis. All materials under study were subjected to the conditioning at two different temperatures of 45 and 80 °C and relative humidity kept at 45 and 80% for different time intervals ranging from 0 to 300 h in the climate chamber Discovery 105 (Angelantoni Test Technologies, Massa Martana, Italy).

Figure 1. Photo of the studied PU foam material.

2.2. Methods

Uniaxial tensile testing was performed on Autograph AGS-X instrument (Shimadzu, Kyoto, Japan) equipped with the Compact Thermostatic Chamber TCE Series. Measurements were performed according to the ČSN EN ISO 527-1, 527-2 standards at 100 mm/min deformation rate [20]. Each measurement was repeated ten times and mean values were calculated.

Thermogravimetry (TG) and differential thermal analysis (DTA) experiments were measured on simultaneous DSC/TGA, SDT 650 Discovery with TRIOS software for thermal analysis (TA Instrument, New Castle, DE, USA). The apparatus was calibrated using indium as a standard. Prior to each measurement, samples were grated into an aluminum pan. Throughout the experiment, the sample temperature and weight-heat flow changes were continuously monitored. The measurements were performed at a heat flow rate of 10 °C/min in a static air atmosphere at the temperature range of 30 to 300 °C.

The material's ability to damp harmonically excited mechanical vibration of single-degree-of-freedom (SDOF) systems is characterized by the displacement transmissibility T_d, which is expressed by the Equation (1) [21]:

$$T_d = \frac{y_2}{y_1} = \frac{a_2}{a_1} = \sqrt{\frac{k^2 + (c \cdot \omega)^2}{(k - m \cdot \omega^2)^2 + (c \cdot \omega)^2}} \quad (1)$$

where y_1 is the displacement amplitude on the input side of the tested sample, y_2 is the displacement amplitude on the output side of the tested sample, a_1 is the acceleration amplitude on the input side of the tested sample, a_2 is the acceleration amplitude on the output side of the tested sample, k is the stiffness, c is the damping coefficient, m is the mass, and ω is the angular frequency [22,23].

The mechanical vibration damping testing of the investigated PU foams was performed by the forced oscillation method [24]. The displacement transmissibility T_d was experimentally measured using the BK 4810 vibrator combined with a BK 3560-B-030 signal pulse multi-analyzer, and a BK 2706 power amplifier at the frequency range from 2 to 1000 Hz [25]. The acceleration amplitudes a_1 and a_2 on the input and output sides of the investigated specimens were evaluated by means of BK 4393 accelerometers (Brüel & Kjær, Nærum, Denmark) [26]. The tested specimen dimensions were (60 × 60 × 50) mm (length × width × thickness). Each measurement was repeated three times at an ambient temperature of 25 °C and mean values of the displacement transmissibility were calculated.

Foam hardness was measured according to ČSN EN ISO 2439 (645440) standard method A "Flexible cellular polymeric materials-Determination of hardness (indentation technique)". During the hardness measurements, the specimens were compressed to 60% of their original height, and the force value (N) was read after 30 s of the deformation. The tested specimen dimensions were (50 × 50 × 50) mm (length × width × thickness). Each measurement was repeated five times at selected conditioning temperatures of 45 and 80 °C and relative humidity of 40 and 80%.

Permanent deformation was measured according to ČSN EN ISO 1856 standard. The tested block specimen dimensions were (50 × 50 × 50) mm (length × width × thickness). Each measurement was repeated five times. Tested samples after conditioning for 300 h at the same temperatures and relative humidity as given in the section above were inserted between the plates of the pressing device compressed to 50% of the original dimensions for 30 min. At the end of the period of compression time, the specimens were released and left lying freely on the table for 30 min. The thickness was then measured again and the permanent deformation expressed as a percentage relative to the original samples dimension was calculated.

3. Results

Results of the tensile testing of the studied PU foam materials are shown in Figure 2. Observed data indicated an increase in mechanical strength and plasticity of the cellular materials after 300 h conditioning as reflected in the increased magnitudes of the stress at break by 19% from 155 kPa to 184 kPa (for sample treated at 45 °C and 80% relative humidity). Simultaneously, the increase in ductility from 87% (at the conditioning temperature of 45 °C and the relative humidity of 45%) to 114% (at the conditioning temperature of 80 °C and the relative humidity of 45%) was observed. For the conditioning temperature of 80 °C, this dependence remained relatively constant. For the relative humidity of 80% and the conditioning temperature of 45 °C, the mechanical strength after 24 h increased, followed by the sharp decline observed after 48 h of conditioning. However, it increased again after 300 h of conditioning. Latter mentioned behavior indicated that at 80% relative humidity, significant structural changes ascribed to the cross-linking were obtained after 48 h of conditioning. At the temperature of 80 °C and a relative humidity of 45%, the stress at break did not change significantly. However, it increased about 10% at the higher relative humidity conditions.

Figure 2 shows that the PU matrix continued to plasticize, as seen by the rise in ductility of the material. We assume that this may be a combination of a change in the elasticity of the individual cell walls of the foam matrix. However, we also have to consider the resulting air pressure increase induced by the change in individual cell volumes during the deformation of the foam structure. The latter change of volume is also associated with a change in the geometry of the individual cells. Simultaneously, the change in the viscoelastic and viscoplastic properties of the PU matrix should be assumed due to the PU

matrix cross-linking [27], and partial hydrolysis [28]. As a complex material response, the varying degrees of swelling of the PU cell walls material were proposed. We assume that the viscous friction and the wall stiffness are the dominant mechanisms of the transferred mechanical energy dissipation [29].

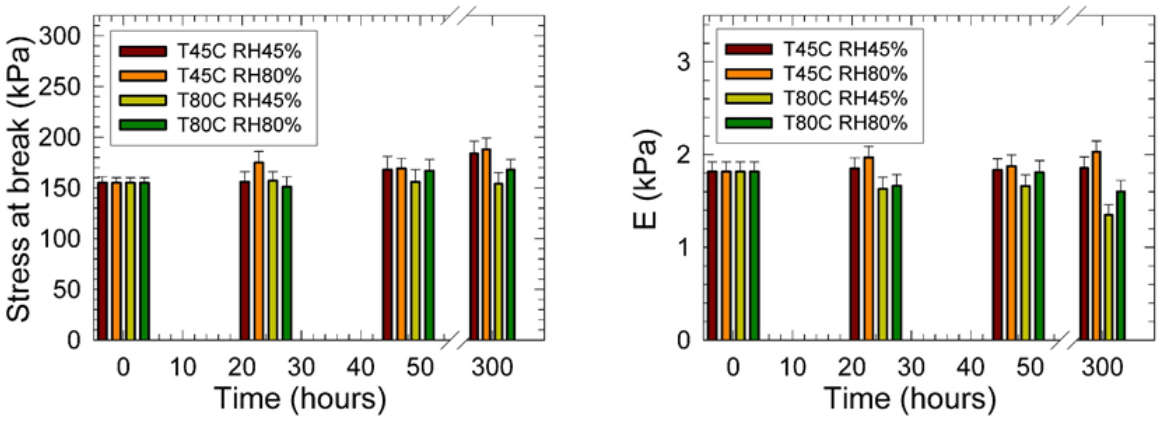

Figure 2. Results of the uniaxial tensile testing of the studied PU materials: (**a**) Stress at break vs. conditioning time at different temperatures and relative humidity; (**b**) Young´s modulus of elasticity (*E*) vs. conditioning time at different temperatures and relative humidity. Inset: T—temperature (°C), RH—relative humidity (%).

The observed increase of the stress at the break for high relative humidity conditioning (80%) at 45 °C indicated an increase of the PU matrix's stiffness, accompanied by the increase of Young´s modulus of elasticity resulting in a simultaneous increase in matrix brittleness. However, signs of matrix hydrolysis were identified at 80 °C conditioning for both relative humidity conditions resulting in the decrease of the *E* from 1816 Pa (original sample without conditioning) to 1350 Pa (conditioned at 80 °C and 45% RH) and to 1600 Pa (conditioned at 80 °C and 80% RH).

Results of the mechanical vibration measurements are summarized in Figures 2 and 3. It was found that the displacement transmissibility gradually increased with the increasing conditioning temperature and high relative humidity of 80% (Figure 3a), indicating higher mechanical stiffness of the PU matrix in the frequency range of 250 to 400 Hz. A similar effect was also found for the 40% relative humidity conditioning. We assume that the chemical cross-linking process of the residual non-reacted PU matrix components proceeded in the time scale of the first 48 h of the conditioning treatment. This hypothesis was also supported by our previous tensile testing measurements discussed above. Simultaneously, the increasing trend of the PU matrix mechanical stiffness was also observed. This was reflected in the increased magnitude of T_d with the increasing relative humidity, as shown in Figure 3b [30]. Results shown in Figure 4a indicated increased elasticity with the increased conditioning time of the studied foams as reflected in the appearance of the two maxima of T_d (at the frequencies of 280 and 430 Hz and magnitudes of 0.014 and 0.017). Observed stiffening appeared in the relatively wide frequency range of 200 to 600 Hz. After prolonged conditioning, plasticization patterns in mechanical behavior were found, as indicated in Figure 4b. After 24 h of conditioning at 80 °C and 80% RH, the foam elasticity was decreased in the frequency range of 200 to 600 Hz in comparison with the virgin PU sample indicating the probable start of the hydrolysis process of the wall material decomposition [31,32].

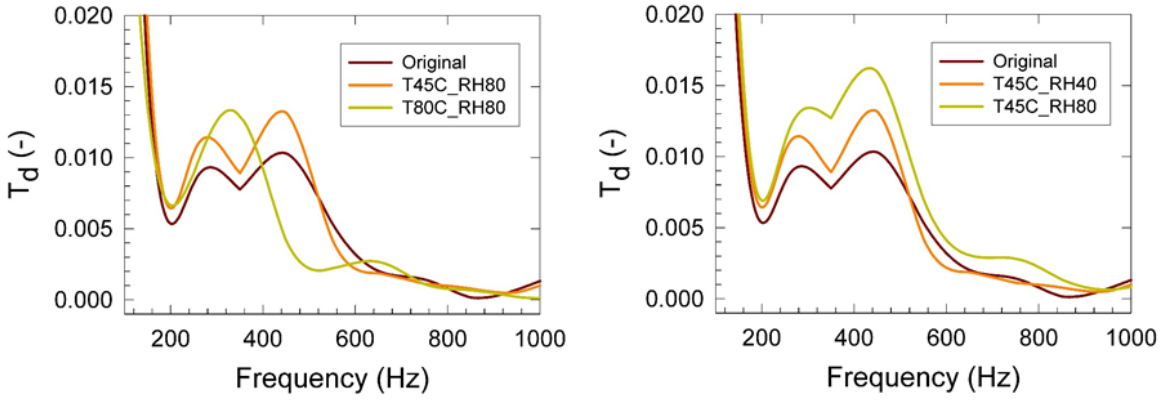

Figure 3. Displacement transmissibility vs. frequency as obtained from the vibration damping measurements of the studied PU materials after 300 h conditioning: (**a**) Effect of the conditioning temperature at 80% RH; (**b**) Effect of the conditioning relative humidity at 45 °C. Inset: T—temperature (°C), RH—relative humidity (%), Original—non-conditioned sample.

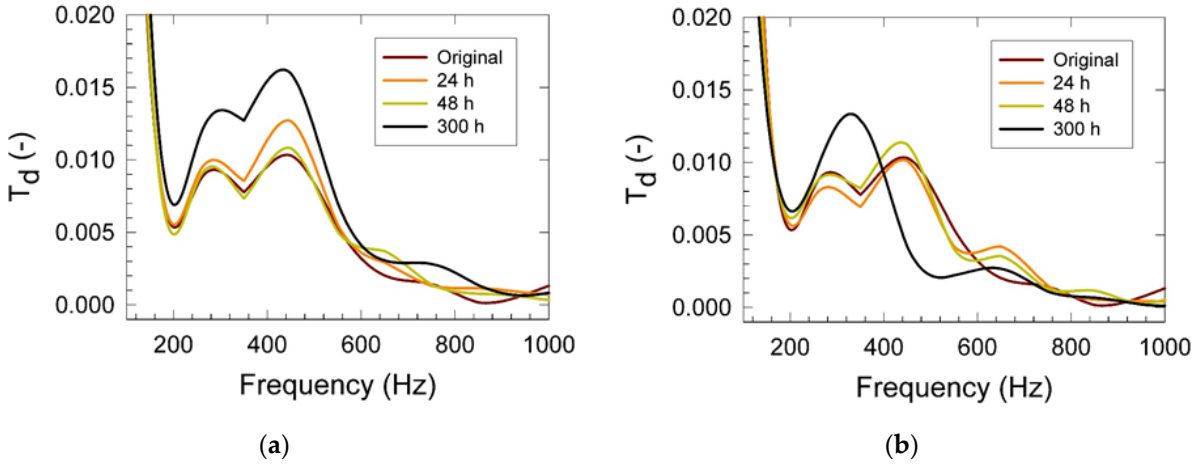

Figure 4. Displacement transmissibility vs. frequency as obtained from the vibration damping measurements of the studied PU materials: (**a**) Effect of the conditioning time at 45 °C and 80% RH; (**b**) Effect of the conditioning time at 80 °C and 80% RH. Inset: Conditioning time (hours), Original—non-conditioned sample.

Results of the effect of the sample conditioning on PU foam hardness are shown in Figure 5. It was found that with increasing conditioning time, the hardness decreased for all tested materials except conditioning at 45 °C. Most probably, this fact was attributed to the increased PU foams wall matrix crosslinking density as obtained at latter mentioned conditioning parameters. After 300 h conditioning in the temperature range of 45 to 80 °C and at the relative humidity of 45 and 80%, the hardness decreased from 10 to 18%. However, at the 45 °C temperature and the relative humidity of 45%, the hardness slightly increased from 18 N to 19 N. We assumed the onset of the PU molecules degradation due to increased temperature and relative humidity. It was found by Weise et al. [19] that crosslinks occur to a greater extent for the PUs containing more poly(ester) because the ester groups can more easily undergo hydrolysis than the PUs containing more poly(ether). It was confirmed by FTIR analysis [19], that the hydrolysis of ester groups yields carboxylic acids, which provide new and rigid ionic crosslinks. In the case of PUs containing only the ether macrodiols, they became slightly more mechanically stiff at the short weathering time less than 1000 h followed by their weakening to the point of fracture after prolonged

weathering. This indicated that although shorter and more ridged crosslinks were formed during weathering, the sum of the degradation ultimately weakened the mechanical properties of poly(ether) type PUs [19].

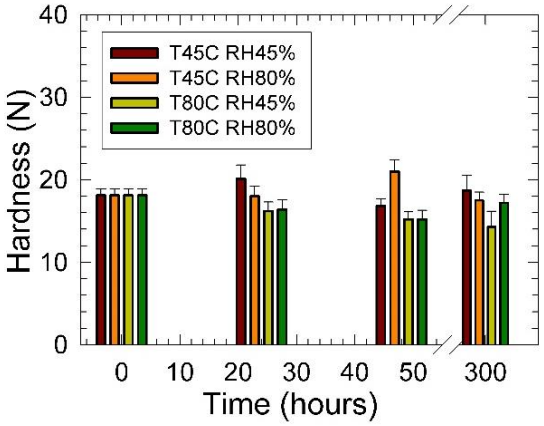

Figure 5. Hardness vs. conditioning time dependencies of studied PU foams at different temperatures and relative humidity. Inset: T—temperature (°C), RH—relative humidity (%).

Results of the permanent deformation measurements are shown in Figure 6. It was found that conditioning at the lower temperature of 45 °C triggered higher elasticity of the PU foams independently of the surrounding atmosphere relative humidity. These results were in excellent agreement with the observed increased Young´s modulus of elasticity, as shown in Figure 2b. With increased conditioning temperature, the permanent deformation vigorously increased from 18% (for the original sample) to 46% after 300 h of conditioning time. The latter permanent deformations were independent of the applied relative humidity. Again, these results agreed with the obtained decrease of the *E* reflecting loss of elasticity and increased plastic mechanical behavior.

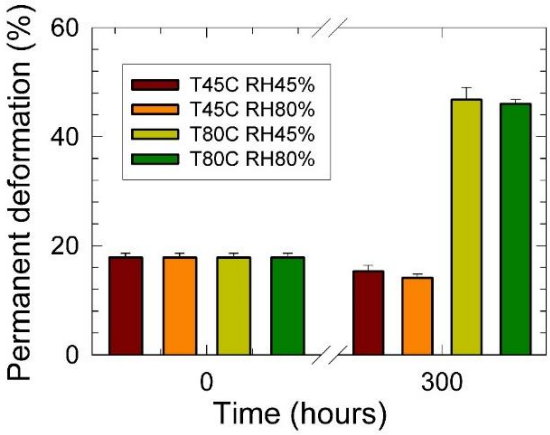

Figure 6. Permanent deformation vs. conditioning time dependencies of studied PU foams at different temperatures and relative humidity. Inset: T—temperature (°C), RH—relative humidity (%).

It was found in the literature [19], that the single component PUs containing either a poly(ester) or poly(ether) macrodiols were mechanically more unstable than the two component PUs containing both macrodiols. This led to a synergistic effect where their damping abilities increased and their mechanical stabilities after weathering increased as well. The increase in the damping abilities of the blended PUs was attributed to a decrease in the packing efficiency of the macrodiols chains by combining the two different functional groups. Furthermore, the increase in the mechanical stabilities after weathering was observed as a result of the competing degradation processes and simultaneous protection of the urethane group by the ester.

A typical degradation pattern of the studied PU foams is shown in Figure 7. The degradation process was started at the temperature of 260 °C with the observed weight loss of about 86%, accompanied by the exothermic heat of fusion. Observed degradation pattern was ascribed to the decomposition of the PU material into the starting polyol and diisocyanate. It was followed by the thermal decomposition of the diisocyanate. Benzonitrile, methylbenzonitrile, phenyl isocyanate, toluene, and benzene were detected as the main decomposition products [33,34]. The latter decomposition process reflected the decomposition of diisocyanates and polyols in the PU matrix accompanied by the evolution of gaseous carbon oxide and hydrogen cyanide [7].

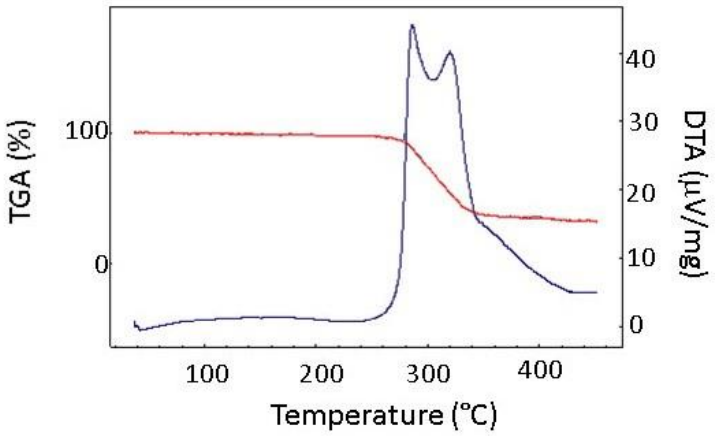

Figure 7. Typical TG DTA pattern of the studied PU foam material: red line—TGA, blue line—DTA.

In Figure 8 results of the TGA analysis are summarized. Observed data shows a minor increase in the weight loss with the increasing conditioning time for both conditioning temperatures and relative humidity. It was ascribed to the change of the chemical composition of the PU foam, most probably due to the addition of the free isocyanate groups. It can be concluded that conditioning led to the loss of the PU foam's thermal stability.

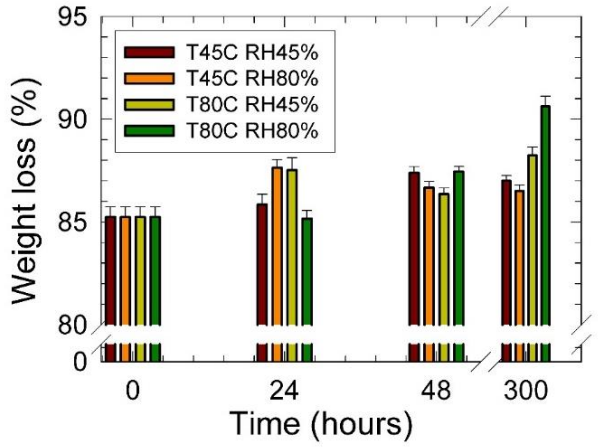

Figure 8. Weight loss vs. conditioning time of the studied PU foams. Inset: T—temperature (°C), RH—relative humidity (%).

4. Conclusions

This study was aimed on the physicochemical and mechanical characterization of the thermal-induced degradation of the commercial soft polyurethane foams. It was found that the increased conditioning temperature and the relative humidity of the surrounding atmosphere led to the initiation of the degradation patterns of the studied PU foams. There was an observed decrease in mechanical stiffness due to the plasticization of the

PU foams wall material, as confirmed by the simultaneous increase of the permanent deformation accompanied by the decrease of the Young's modulus of elasticity. This phenomenon was also confirmed by the nondestructive dynamical-mechanical vibration testing, which confirmed samples´ higher vibration damping, resulting in the loss of elasticity. The last changes of the mechanical behavior agreed with the observed decrease of the matrix hardness, again confirming the loss of elastic mechanical performance. It has been also found that the effect of conditioning led to the significant loss of the PU foam's thermal stability.

Author Contributions: Conceptualization, L.L. and M.V.; methodology, B.L., L.L. and M.V.; investigation, B.L., L.L., Y.M. and M.V.; resources, M.V.; data curation, B.L., L.L., Y.M. and M.V.; writing—original draft preparation, L.L. and M.V.; writing—review and editing, B.L., L.L. and M.V.; visualization, B.L., L.L., Y.M. and M.V.; supervision, L.L.; project administration, M.V.; funding acquisition, M.V. All authors have read and agreed to the published version of the manuscript.

Funding: This study was funded by the European Regional Development Fund in the Research Centre of Advanced Mechatronic Systems project, project number CZ.02.1.01/0.0/0.0/16_019/0000867 within the Operational Programme Research, Development and Education and by Internal Grant of Palacky University in Olomouc, grant number IGA_PrF_2021_031.

Institutional Review Board Statement: Not applicable.

Informed Consent Statement: Not applicable.

Data Availability Statement: Not applicable.

Conflicts of Interest: The authors declare no conflict of interest.

References

1. Krol, P. Polyurethanes—A Review of 60 Years of their Syntheses and Applications. *Polimery* **2009**, *54*, 489–500. [CrossRef]
2. Stachak, P.; Lukaszewska, I.; Hebda, E.; Pielichowski, K. Recent Advances in Fabrication of Non-Isocyanate Polyurethane-Based Composite Materials. *Materials* **2021**, *14*, 3497. [CrossRef] [PubMed]
3. Lapcik, L.; Cetkovsky, V.; Lapcikova, B.; Vasut, S. Materials for noise and vibration attenuation. *Chem. Listy* **2000**, *94*, 117–122.
4. Shaw, S.D.; Harris, J.H.; Berger, M.L.; Subedi, B.; Kannan, K. Brominated Flame Retardants and Their Replacements in Food Packaging and Household Products: Uses, Human Exposure, and Health Effects. In *Toxicants in Food Packaging and Household Plastics: Exposure and Health Risks to Consumers*; Springer: London, UK, 2014; pp. 61–93. [CrossRef]
5. Song, H.Y.; Cheng, X.X.; Chu, L. Effect of Density and Ambient Temperature on Coefficient of Thermal Conductivity of Heat-Insulated EPS and PU Materials for Food Packaging. *Res. Food Packag. Technol.* **2014**, *469*, 152–155. [CrossRef]
6. Volcik, V.; Lapcikova, B.; Lapcik, L.; Asuquo, R. Uses of polyurethane matrixes in the environmental field. *Plasty Kauc.* **2002**, *39*, 164–169.
7. Tomin, M.; Kmetty, A. Polymer foams as advanced energy absorbing materials for sports applications-A review. *J. Appl. Polym. Sci.* **2022**, *139*, 51714. [CrossRef]
8. Lapcikova, B.; Lapcik, L., Jr. TG and DTG Study of Decomposition of Commercial PUR Cellular Materials. *J. Polym. Mater.* **2011**, *28*, 353–366.
9. Scholz, P.; Wachtendorf, V.; Panne, U.; Weidner, S.M. Degradation of MDI-based polyether and polyester-polyurethanes in various environments—Effects on molecular mass and crosslinking. *Polym. Test.* **2019**, *77*, 105881. [CrossRef]
10. Oprea, S.; Oprea, V. Mechanical behavior during different weathering tests of the polyurethane elastomers films. *Eur. Polym. J.* **2002**, *38*, 1205–1210. [CrossRef]
11. Scholz, P.; Wachtendorf, V.; Elert, A.-M.; Falkenhagen, J.; Becker, R.; Hoffmann, K.; Resch-Genger, U.; Tschiche, H.; Reinsch, S.; Weidner, S. Analytical toolset to characterize polyurethanes after exposure to artificial weathering under systematically varied moisture conditions. *Polym. Test.* **2019**, *78*, 105996. Available online: https://www.scopus.com/inward/record.uri?eid=2-s2.0-85069503515&doi=10.1016%2fj.polymertesting.2019.105996&partnerID=40&md5=5d3e6a62259aeed6cdeb3912a2ec95d6 (accessed on 14 December 2021). [CrossRef]
12. Kuranska, M.; Pinto, J.A.; Salach, K.; Barreiro, M.F.; Prociak, A. Synthesis of thermal insulating polyurethane foams from lignin and rapeseed based polyols: A comparative study. *Ind. Crops Prod.* **2020**, *143*, 111882. [CrossRef]
13. Mort, R.; Vorst, K.; Curtzwiler, G.; Jiang, S. Biobased foams for thermal insulation: Material selection, processing, modelling, and performance. *RSC Adv.* **2021**, *11*, 4375–4394. [CrossRef]
14. Jonjaroen, V.; Ummartyotin, S.; Chittapun, S. Algal cellulose as a reinforcement in rigid polyurethane foam. *Algal Res. Biomass Biofuels Bioprod.* **2020**, *51*, 102057. [CrossRef]
15. Cornille, A.; Auvergne, R.; Figovsky, O.; Boutevin, B.; Caillol, S. A perspective approach to sustainable routes for non-isocyanate polyurethanes. *Eur. Polym. J.* **2017**, *87*, 535–552. [CrossRef]

16. Rodrigues, J.D.O.; Andrade, C.K.Z.; Quirino, R.L.; Sales, M.J.A. Non-isocyanate poly(acyl-urethane) obtained from urea and castor (*Ricinus communis* L.) oil. *Prog. Org. Coat.* **2022**, *162*, 106557. [CrossRef]
17. Wilhelm, C.; Rivaton, A.; Gardette, J.-L. Infrared analysis of the photochemical behaviour of segmented polyurethanes: 3. Aromatic diisocyanate based polymers. *Polymer* **1998**, *39*, 1223–1232. Available online: https://www.scopus.com/inward/record.uri?eid=2-s2.0-0032028577&doi=10.1016%2fS0032-3861%2897%2900353-4&partnerID=40&md5=4ffb65e5dd9477d91e7672f4dff2de01 (accessed on 14 December 2021). [CrossRef]
18. Wilhelm, C.; Gardette, J.-L. Infrared analysis of the photochemical behaviour of segmented polyurethanes: Aliphatic poly(ether-urethane)s. *Polymer* **1998**, *39*, 5973–5980. Available online: https://www.scopus.com/inward/record.uri?eid=2-s2.0-0032210353&doi=10.1016%2fS0032-3861%2897%2910065-9&partnerID=40&md5=71595238af20bfe5abd9a439287d94e8 (accessed on 14 December 2021). [CrossRef]
19. Weise, N.K.; Bertocchi, M.J.; Wynne, J.H.; Long, I.; Mera, A.E. High performance vibrational damping poly(urethane) coatings: Blending 'soft' macrodiols for improved mechanical stability under weathering. *Prog. Org. Coat.* **2019**, *136*, 105240. Available online: https://www.scopus.com/inward/record.uri?eid=2-s2.0-85071912699&doi=10.1016%2fj.porgcoat.2019.105240&partnerID=40&md5=aeb9c93665d568497d6faf5157645215 (accessed on 14 December 2021). [CrossRef]
20. Lapcik, L.; Manas, D.; Lapcikova, B.; Vasina, M.; Stanek, M.; Cepe, K.; Vlcek, J.; Waters, K.E.; Greenwood, R.W.; Rowson, N.A. Effect of filler particle shape on plastic-elastic mechanical behavior of high density poly(ethylene)/mica and poly(ethylene)/wollastonite composites. *Compos. Part B Eng.* **2018**, *141*, 92–99. [CrossRef]
21. Rao, S.S. *Mechanical Vibrations*, 5th ed.; Prentice Hall: Upper Saddle River, NJ, USA, 2010; p. 1105.
22. Liu, K.; Liu, J. The damped dynamic vibration absorbers: Revisited and new result. *J. Sound Vib.* **2005**, *284*, 1181–1189. [CrossRef]
23. Hadas, Z.; Ondrusek, C. Nonlinear spring-less electromagnetic vibration energy harvesting system. *Eur. Phys. J.-Spec. Top.* **2015**, *224*, 2881–2896. [CrossRef]
24. Carrella, A.; Brennan, M.J.; Waters, T.P.; Lopes, V., Jr. Force and displacement transmissibility of a nonlinear isolator with high-static-low-dynamic-stiffness. *Int. J. Mech. Sci.* **2012**, *55*, 22–29. [CrossRef]
25. Dupuis, R.; Duboeuf, O.; Kirtz, B.; Aubry, E. Characterization of Vibrational Mechanical Properties of Polyurethane Foam. *Dyn. Behav. Mater.* **2016**, *1*, 123–128. [CrossRef]
26. Lapcik, L.; Vasina, M.; Lapcikova, B.; Stanek, M.; Ovsik, M.; Murtaja, Y. Study of the material engineering properties of high-density poly(ethylene)/perlite nanocomposite materials. *Nanotechnol. Rev.* **2020**, *9*, 1491–1499. [CrossRef]
27. Platonova, E.; Chechenov, I.; Pavlov, A.; Solodilov, V.; Afanasyev, E.; Shapagin, A.; Polezhaev, A. Thermally Remendable Polyurethane Network Cross-Linked via Reversible Diels-Alder Reaction. *Polymers* **2021**, *13*, 1935. [CrossRef] [PubMed]
28. Nemade, A.M.; Mishra, S.; Zope, V.S. Kinetics and Thermodynamics of Neutral Hydrolytic Depolymerization of Polyurethane Foam Waste Using Different Catalysts at Higher Temperature and Autogenious Pressures. *Polym. Plast. Technol. Eng.* **2010**, *49*, 83–89. [CrossRef]
29. Casati, F.; Herrington, R.; Broos, R.; Miyazaki, Y. Tailoring the performance of molded flexible polyurethane foams for car seats (Reprinted from Polyurethanes World Congress '97, 29 September–1 October 1997). *J. Cell. Plast.* **1998**, *34*, 430–466. [CrossRef]
30. Suh, K.; Park, C.; Maurer, M.; Tusim, M.; De Genova, R.; Broos, R.; Sophiea, D. Lightweight cellular plastics. *Adv. Mater.* **2000**, *12*, 1779–1789. [CrossRef]
31. Vakil, A.U.; Petryk, N.M.; Shepherd, E.; Beaman, H.T.; Ganesh, P.S.; Dong, K.S.; Monroe, M.B.B. Shape Memory Polymer Foams with Tunable Degradation Profiles. *ACS Appl. Bio. Mater.* **2021**, *4*, 6769–6779. [CrossRef]
32. Zahedifar, P.; Pazdur, L.; Vande Velde, C.M.L.; Billen, P. Multistage Chemical Recycling of Polyurethanes and Dicarbamates: A Glycolysis-Hydrolysis Demonstration. *Sustainability* **2021**, *13*, 3583. [CrossRef]
33. Gaboriaud, F.; Vantelon, J.P. Thermal-Degradation of Polyurethane Based on Mdi and Propoxylated Trimethylol Propane. *J. Polym. Sci. Part A Polym. Chem.* **1981**, *19*, 139–150. [CrossRef]
34. Ballistreri, A.; Foti, S.; Maravigna, P.; Montaudo, G.; Scamporrino, E. Mechanism of Thermal-Degradation of Polyurethanes Investigated by Direct Pyrolysis in the Mass-Spectrometer. *J. Polym. Sci. Part A Polym. Chem.* **1980**, *18*, 1923–1931. [CrossRef]